

AD-A184 222 HEAT AND MOISTURE TRANSPORT IN THE ATMOSPHERIC BOUNDARY 1/3

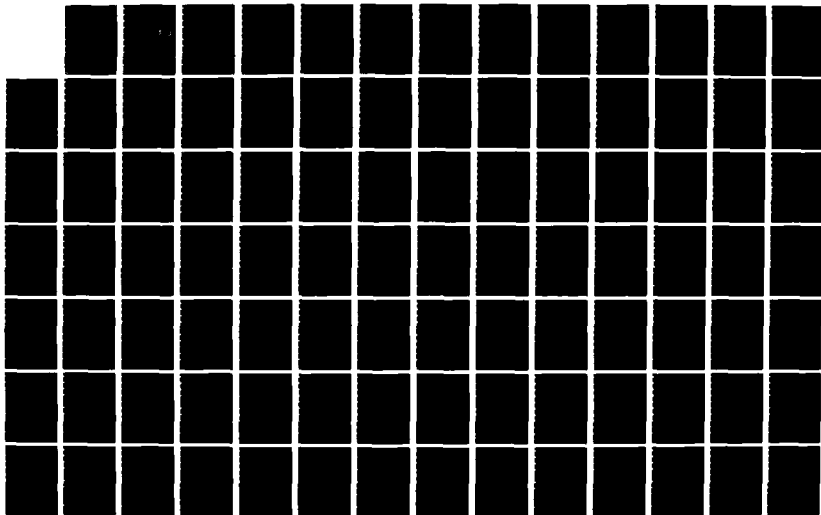
LAYER(U) FLOW ANALYSIS ASSOCIATES ITHACA NY

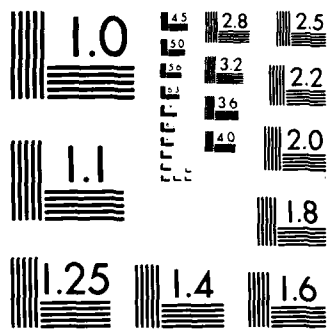
S LEIBOVICH ET AL 85 JAN 87 AFGL-TR-87-0011

UNCLASSIFIED F19628-83-C-0018

F/G 4/2

NL





MICROCOPY RESOLUTION TEST CHART
NATIONAL BUREAU OF STANDARDS 1963-A

AFGL-TR-87-0011

8

Heat and Moisture Transport in the
Atmospheric Boundary Layer

DTIC FILE COPY

Sidney Leibovich
John L. Lumley
J.C.R. Hunt

Flow Analysis Associates
999 Cayuga Heights Rd.
Ithaca, NY 14850

5 January 1987

Final Report
23 January 1983 - 31 December 1986

Approved for public release; distribution unlimited

AIR FORCE GEOPHYSICS LABORATORY
AIR FORCE SYSTEMS COMMAND
UNITED STATES AIR FORCE
HANSCOM AIR FORCE BASE, MASSACHUSETTS 01731

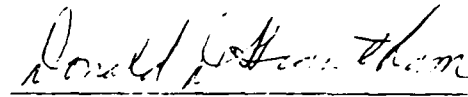
AD-A184 222

DTIC
ELECTE
SEP 01 1987
S D

"This technical report has been reviewed and is approved for publication"

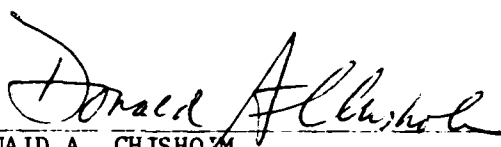


BRUCE A. KUNKEL
Contract Manager



DONALD D. GRANTHAM
Chief, Atmospheric Structure Branch

FOR THE COMMANDER



DONALD A. CHISHOLM
Acting Director, Atmospheric Sciences Division

This report has been reviewed by the ESD Public Affairs Office (PA) and is releasable to the National Technical Information Service (NTIS).

Qualified requestors may obtain additional copies from the Defense Technical Information Center. All others should apply to the National Technical Information Service.

If your address has changed, or if you wish to be removed from the mailing list, or if the addressee is no longer employed by your organization, please notify AFGL/DAA, Hanscom AFB, MA 01731-5000. This will assist us in maintaining a current mailing list.

Do not return copies of this report unless contractual obligations or notices on a specific document requires that it be returned.

Unclassified

SECURITY CLASSIFICATION OF THIS PAGE

AD A184222

REPORT DOCUMENTATION PAGE

1a. REPORT SECURITY CLASSIFICATION Unclassified		1b. RESTRICTIVE MARKINGS			
2a. SECURITY CLASSIFICATION AUTHORITY		3. DISTRIBUTION/AVAILABILITY OF REPORT approved for public release; distribution unlimited			
2b. DECLASSIFICATION/DOWNGRADING SCHEDULE					
4. PERFORMING ORGANIZATION REPORT NUMBER(S)		5. MONITORING ORGANIZATION REPORT NUMBER(S) AFGL-TR-87-0011			
6a. NAME OF PERFORMING ORGANIZATION Flow Analysis Associates	6b. OFFICE SYMBOL (If applicable)	7a. NAME OF MONITORING ORGANIZATION Air Force Gephysics Laboratory			
6c. ADDRESS (City, State and ZIP Code) 999 Cayuga Heights Road Ithaca, N.Y. 14850		7b. ADDRESS (City, State and ZIP Code) Hanscom AFB Massachusetts 01731			
8a. NAME OF FUNDING/SPONSORING ORGANIZATION	8b. OFFICE SYMBOL (If applicable)	9. PROCUREMENT INSTRUMENT IDENTIFICATION NUMBER F19628-83-C-0018			
8c. ADDRESS (City, State and ZIP Code)		10. SOURCE OF FUNDING NOS			
		PROGRAM ELEMENT NO.	PROJECT NO.	TASK NO.	WORK UNIT NO.
		62101F	6670	14	AB
11. TITLE (Include Security Classification) Heat and Moisture Transport in the Atmospheric Boundary Layer					
12. PERSONAL AUTHOR(S) Sidney Leibovich, John L. Lumley, J. C. R. Hunt					
13a. TYPE OF REPORT Final Report	13b. TIME COVERED FROM 1/23/83 TO 12/31/86	14. DATE OF REPORT (Yr., Mo., Day) 1987 January 5		15. PAGE COUNT 292	
16. SUPPLEMENTARY NOTATION					
17. COSATI CODES					
FIELD	GROUP	SUB. GR.			
18. SUBJECT TERMS (Continue on reverse if necessary and identify by block number) Turbulent transport; heat transport; moisture transport; latent heat transport; sensible heat transport; index of refraction fluxuations. ←					
19. ABSTRACT (Continue on reverse if necessary and identify by block number) Development of analytical and computational approaches to turbulent, stratified shear flows and complex terrain, with turbulent transport of latent and sensible heat.					
20. DISTRIBUTION AVAILABILITY OF ABSTRACT UNCLASSIFIED/UNLIMITED <input type="checkbox"/> SAME AS RPT <input checked="" type="checkbox"/> OTIC USERS <input type="checkbox"/>			21. ABSTRACT SECURITY CLASSIFICATION Unclassified		
22a. NAME OF RESPONSIBLE INDIVIDUAL Bruce Funkel		22b. TELEPHONE NUMBER (Include Area Code)		22c. OFFICE SYMBOL AFGL-15A	

DD FORM 1473, 83 APR

EDITION OF 1 JAN 73 IS OBSOLETE

Unclassified

SECURITY CLASSIFICATION OF THIS PAGE

TABLE OF CONTENTS

	<u>Page</u>
Executive Summary	1
Chapter A: Overview of the Modelling of Turbulent Transport Over Complex Terrain	3
Chapter B: Summary and Extension of Analytical Theory of Turbulent Mean Flows over Terrain of Low Slope	29
Chapter C: Stratified Shear Flows Over Low Hills. I. Effects of Upwind Shear	45
Chapter D: Stratified Shear Flows Over Low Hills. II. Stratification Effects in the Outer Flow Region	109
Chapter E: Temperature Field in Turbulent Flow Over Hills	195
Chapter F: Modelling of Turbulent Heat and Moisture Transport in Atmospheric Flows	239
Chapter G: Algorithm Development for Three-Dimensional Second Order Turbulence Model Computations of Flow Over Terrain	275

[illegible]

EXECUTIVE SUMMARY

Objective

The goal of this contract is the establishment of practical methods for the prediction of three-dimensional turbulent atmospheric flow over complex terrain, when environmental conditions at the boundaries of the flow volume are prescribed.

Methods of Approach

The principal approach is turbulence modelling. In particular, we construct a second-order turbulence model, effecting a closure of the hierarchy of Reynolds averaged Navier-Stokes equations with buoyancy effects accounted for in the Boussinesq approximation, and transport of additional scalars, water vapor in particular, included. This model is regarded as the principal product delivered under this contract. To the extent that it is possible, the model is constructed from first principles, and incorporates state-of-the-art concepts in turbulence modelling. It has been constructed to deal with flows of arbitrary complexity, and has been exercised in unsteady one-dimensional computations simulating the growth of the surface mixed layer of the atmosphere, and that of two-dimensional steady boundary layer growth. An efficient numerical algorithm for the implementation of a three-dimensional computation over terrain has been partially developed, but not brought to completion.

A parallel effort has been pursued simultaneously. In it, simple analytical techniques have been developed permitting rapid estimates to be made of basic features of the three-dimensional turbulent flow over terrain of low slope under conditions of arbitrary prescribed shear and atmospheric stability. This effort, which focusses on mean flow quantities, was originally intended to provide an independent, perhaps rough, check of flows calculated by more accurate methods, such as our second-order closure. The method is, however, quite flexible. Together with a complementary theory, described here, which extends rapid distortion theory to temperature fluctuations, it can be used in its

own right to estimate (an inexpensive microcomputer would suffice) terrain-induced distortions of temperature spectra.

Items Delivered

By reference, this report includes those items previously delivered (June 7, 1984) in our *Interim Technical Report*, including computer programs, user's manuals, and theoretical documentation, together with the following additional items which are included as chapters enclosed herewith:

A. Overview of the modelling of turbulent transport over complex terrain, with emphasis on the analytical theory for hills of low slope. (Prepared by J.C.R. Hunt.)

B. Summary and extension of analytical theory of turbulent mean flows over terrain of low slope. (Allows for nearly arbitrary specification of upstream shear and stratification. This is a more general view of item C. Prepared by S. Leibovich.)

C. Stratified shear flows over low hills. I. Effects of upwind shear. (Complete revision of paper included in our *Interim Tech. Report* and including key improvements. This is the basic document underlying the analytical approach and has been submitted for publication. Examples included. Prepared by J.C.R. Hunt, S. Leibovich, and K.J. Richards*.)

D. Stratified shear flows over low hills. II. Stratification effects in the outer flow region. (Continuation of item B. Examples of specific stratification profiles are worked out. To be submitted for publication. By J.C.R. Hunt, K.J. Richards*, and P.W.M. Brighton*.)

E. Temperature field in turbulent flow over hills. (Reviews physical processes entering the problem, discusses mean and fluctuating temperature perturbations induced by flow over terrain of low slope. Prepared by J.C.R. Hunt for Flow Analysis Associates, and based in part on a paper in preparation by W.S. Weng* and J.C.R. Hunt.)

F. Modelling of turbulent heat and moisture transport in atmospheric flows. (Describes the FAA second-order turbulence model, with attention concentrated on developments beyond those described in the *Interim Tech. Report*. Prepared by J.L. Lumley.)

G. Algorithm development for three-dimensional second order turbulence model computations of flow over terrain. (Prepared by J.L. Lumley and P. Mansfield*.)

* Effort not supported by this contract.

Chapter A

**Overview of the modelling of
turbulent transport over complex terrain**

Prepared by
J.C.R. Hunt

Summary

The first part of the report is a review of recent work on the analytical treatment air flow over low hills, in which a framework has been established for studying these problems. The mean flow and the turbulence, in different kinds of stratification in flow over hills are included in the discussion as well as the new problems addressed in this project. In the second part we give a new overview of the physical processes governing the distribution of temperature and humidity over hills, within the same framework that has been established for the flow field. This review lays the foundation for an accompanying report (Chapter E) on new research on the temperature and humidity field.

1. Air flow over hills

1.1 Review of recent work and current concepts

The flow of the turbulent atmospheric boundary layer over a single hill, or groups of hills, is most easily understood by noting the different characteristics of the flow in different region or zones over the hills (see Figure 1). This division is especially appropriate and revealing for understanding how the transport of heat and moisture are affected by or affect the flow over a hill.

1.1.1 Mean velocity and temperature distributions over hills

There are two main regions of the flow, which are sometimes further subdivided. (Hunt & Simpson, 1982, Hunt, Leibovich, Lumley, 1983, referred to hereafter as HLL).

- (i) *The inner region.* This is analogous to the internal boundary layer found on flat terrain downwind of a change in surface roughness, temperature or humidity. The vertical depth of such a layer is determined by the balance between the upward turbulent diffusion of surface vorticity, temperature or humidity and the advection by the mean wind. This means that within such a layer there is a balance between rate of change of mean momentum of the flow and the gradient of shear stress. On flat terrain in a neutral approach flow l is given by

$$(1.1a) \quad l \approx 2k^2x/\ln(l/z_0), \text{ or } l \propto x^{0.8}$$

where z_0 is the roughness length of the surface and k is von Karman's constant ($k = 0.4$).

Over a hill the layer does not grow in a simple way because the flow over the hill sets up an external pressure gradient which changes the surface shear stress. An estimate of l over the top of the hill is

$$(1.1b) \quad l \approx 2k^2L/\ln(l/z_0)$$

where L is the length of the hill from the center line to where it reaches its half height. (Fig. 1). Typically $l \approx L/20$. Thus an important difference between the inner layer associated with roughness changes and that found in flow over a hill is

that in the latter case there is a balance between the rate of change of mean momentum of the flow $U \partial \Delta u / \partial x$, the vertical gradient of the perturbation shear stress $\Delta \tau$ and the pressure gradient Δp . ($U(z)$ is the upwind velocity profile and Δu is the local velocity perturbation over the hill). The governing equation for these inner layers is the following boundary layer equation

$$(1.2) \quad \rho U \partial \Delta u / \partial x + \Delta w \partial U / \partial z = - (1/\rho) \partial \Delta p / \partial x + \partial \Delta \tau / \partial z$$

where ρ is the density, and Δu , Δw are the horizontal and vertical perturbations to the upwind velocity.

An important characteristic of flow in the inner region is that over the hill, if l is given by (1.2), the Lagrangian time scale T_L (or 'turn over' time) of the turbulence, in neutral conditions, is given by $T_L \leq l / 4u^*$. Within the layer T_L is less than the time for the flow to travel along the layer ($= L/U(l)$). Consequently, the turbulence is approximately in equilibrium and the transport processes can be approximately calculated using an eddy viscosity and an eddy diffusivity. This does not mean that the inner layer is similar to the surface layer of the atmosphere where fluxes are approximately constant with height. In fact as shown in Fig. 2, these fluxes must vary rapidly through the layer (as shown in Chapter C). For example, since the shear stress is reduced on the upwind slope of a hill and *increased* over the top, within the inner layer the shear stress must decrease rapidly. Downwind of the hill the inner region merges into the wake of the hill. The mean flow continues to be controlled by a balance between the change of inertia and shear stress, but the pressure gradient becomes much weaker (e.g. - Counihan, Hunt & Jackson, 1974). Consequently in the wake behind a *single hill*, the diffusive action of the turbulence progressively thickens the wake downwind. For a two-dimensional ridge across the flow calculation and observations indicate that if $L/H > 0.2$,

$$l(x)/H \approx K (x/H)^{1/2}$$

where $K \approx 0.1$. But if $L/H < 0.05$, $l(x)$ tends to the form of (1a). (Hunt & Simpson, 1982). Separation of the flow does not appear to be necessary for the transition between these forms for $l(x)$. The value of the coefficient K and the turbulence structure of the wake are largely determined by the flow structure on the lee slope. This is because in the inner region downwind of the hill, unlike over the hill, the time scale of the turbulence is of the same order as the travel time, so that turbulence is not in local equilibrium. However, despite this complexity it is found that the mean velocity and turbulence often has a self-similar structure just like wakes behind obstacles freely suspended in uniform flow. This structure enables analytical models to be developed. There certainly remains more work to do on this aspect of the flow.

If the wake behind one hill impinges onto another hill downwind, then a new pressure gradient develops. It appears that the mean velocity and turbulence over the downwind hill can approximately be described by the theory for the flow over a single hill, but the initial conditions for the second hill are determined by the wake of the upwind hill (Hunt, Leibovich, Lumley, 1983). This concept, however, needs further computational, field and laboratory exploration.

Because it is thin the structure of flow in the inner region is often less affected by buoyancy forces than the flow in the outer region. However little is known about the transition between flow in the inner region driven by upwind conditions but affected by buoyancy forces and local 'anabatic' or 'katabatic' winds driven entirely by the buoyancy forces caused by local warming and cooling of hill slopes. Some new analysis of this problem is presented in Chapter E. See also Fitzjarrald (1983).

(ii) Outer Region

This region extends from just outside the inner region through the boundary layer up to a height of the order L the *length* of the hill. In stable conditons hills can force wave motion many kilometers up into the stably stratified region above the boundary layer.

In *turbulent* flow over a hill of moderate slope (say $L/H < 0.3$) the cross sectional area of any separated regions of flow is small compared to the cross sectional area of the hill. Then the flow in the outer region only depends on the mean velocity and temperature distribution upwind and the shape of the hill. The additional displacement of streamlines by the flow in the inner region is *small* compared with the displacement by the hill. This is not true for *laminar* flows or flow over hills calculated with an assumption of *constant* eddy viscosity (e.g. Sykes 1978), and in those flow the outer and inner regions have to be analyzed together. We have only recently realized that this coupling does not occur in turbulent flow and provides an important simplification to the analysis. (Chapter C, 1986). It means that we can analyze the outer region for a wide range of upwind conditions, without calculating the inner region in each case (Chapter D). (There are of course some important counter examples, as when a separated flow pattern in the wake near the ground collapses with the onset of surface cooling; Scorer 1955).

The other essential simplification of the outer region is that for most atmospheric conditions, it can be divided into two sub-layers: the middle layer in which the flow is controlled by the *shear* in the upwind mean velocity profile, and the *upper layer* in which the flow is governed by inertial and buoyancy forces but in this case it is the upwind temperature profile $\theta_0(z)$ rather than the velocity profile which largely control the flow. (Hunt, Leibovich & Lumley 1983). From the above criterion, the height h_m of the middle layer in neutral or slightly stable flows is given approximately by

$$(3) \quad h_m \approx \min [h, u^*/N(h_m)\ln^{1/2}, L/\ln^{1/2}(h_m/z_0)]$$

where $\min [\]$ means the minimum value. Note N is the buoyancy frequency of the upwind flow. ($N^2 = g d\theta_0/dz/\theta_0(z=0)$).

The analytical work reported in Chapter D has indicated the parameter ranges for studying the effects of stratification on flow over hills. For this brief review we restrict discussion to the situation where the upwind potential temperature increases steadily with height, and the buoyancy frequency $N(z)$ decreases with z .

When $u_* / LN(L) \geq 5$, the upwind velocity profile is effectively neutral, and in the flow over the hill buoyancy forces are negligible. The weak neutral upwind shear amplifies the perturbation Δu to the wind speed over the hill. It is found that, just outside the inner layer,

$$(4) \quad \Delta u / U(l) \approx (H/L) U^2(h_m) / U^2(l),$$

while the perturbation shear stress increases by a larger proportion to

$$(5) \quad \Delta \tau / \tau \approx 2(H/L) [U^2(h_m) / U^2(l)] (1 + 4 / \ln(l/z_0))$$

For example Bradley (1980) has confirmed that the surface shear stress is amplified more than the mean velocity. He found that $\Delta u / U(l) \approx 1$ while $\Delta \tau / \tau \approx 4$. This has important implications for heat and water vapor transport.

When $u_* / NL_1 \approx 1$, but $U(L) / NL > 2$, the temperature gradient is strong enough to affect the turbulence in the approach flow, but too weak for the buoyancy forces to affect the flow over the hill. Because the approach flow has a large distance in which to be affected by the change in turbulence, the upwind velocity gradient is increased. Near the surface the usual Monin-Obukhov scaling can be applied. For example when $u_* / NL \approx 1$, $U(z)$ is approximately described by $U(z) \approx 1/k [u_* \ln(z/z_0) + Nz]$. The important point about this situation is that although the buoyancy forces over the hill are negligible, the fact that the upwind flow has a greater velocity gradient means that the ratio $U(L) / U(l)$ is increased. Therefore from (4), (5) the relative increase of the mean velocity and surface shear stress is *greatly increased*. If the slope of the hill is small, the distribution of Δu and $\Delta \tau$ over the hill is not much changed; only their magnitude. This concept, put forward by Hunt (1981), has been confirmed by Bradley's (1983) recent field measurements over a small escarpment in Australia (Hunt & Richards 1984).

When $U/(NL) \leq 2$, and $U/(NH) > 1$ the buoyancy forces strongly affect the flow over a hill, but they are not strong enough to prevent the flow from passing *over* the hill. However, as $U/(NL)$ decreases, progressively more of the flow passes round 3-dimensional hills (see Chapter D). For $2 \geq U/(NL) \geq 1/2$, the maximum velocity over the hill is less than for neutral flow. For $U/(NL) \leq 1/2$, the maximum velocity perturbation occurs on the lee side of a hill and for uniform stratification a good estimate for a rounded hill is

$$\Delta u_{mx} = U^2(h_m)(H/L)(U/NL)/U(l) ,$$

On the other hand for different kinds of upwind stratification Δu_{mx} can vary considerably from this estimate, and the location of maximum velocity can also vary. Consequently, the distribution of how the surface stress and heat flux also vary in these conditions (Hunt & Richards, 1984).

When $U/(NH) \leq 1$, the kinetic energy of the incident flow is insufficient for all the flow to pass over the top of the hill, and a new flow regime develops. The perturbations to the flow are of the order of $U(H)$, even if the slope $H/L \ll 1$. However when the stratification is strong enough that $U/(NH) \ll 1$ the flow is to first order, a horizontal flow around the hill, or stagnant if the hill is two dimensional. In either case there is region within a distance of U/N the top of the hill where the flow can pass over the top. An approximate analysis for this summit layer was given in HLL.

An important aspect of highly stratified flow is that the horizontal distance around the hill in which the flow is affected is much greater than when $U/NH > 1$. For example around a three dimensional hill when $U/(NH) \ll 1$, Δu decreases in proportion to $(x/L)^{-1}$ outside the wake and to $(x/L)^{-1/2}$ within the wake, whereas when $U/(NH) > 1$, Δu decreases in proportion to $(x/L)^{-2}$ outside the wake and approximately to $(x/L)^{-3/2}$ within the wake. Consequently it is generally more important to consider the interaction of the flow between hills in strongly stratified flow (HLL). This slow decay also means that Coriolis acceleration has a larger time to deviate the flow in very stable conditions, and then

even on scales of the order of 10 to 20km Coriolis effects may be significant (HLL, Merkin, 1975).

Note that when the flow around the hill is approximately horizontal the wake flows are also approximately horizontal. These wake flows behave as if they were generated by cylindrical structures with vertical axes. Turbulence and coherent vortices can develop rather slowly, as satellite photography and many laboratory studies have indicated (e.g. Brighton (1978)). Even in these wake the flow is still controlled by shear stress, so in that sense they are still part of the inner region.

In typical daytime conditions the air flow upwind of a hill is statically unstable, which causes the buoyancy forces to add to the shear turbulence in this case. For weak buoyancy forces ($L/L_{mo} > 1/2$) the gradient of the mean velocity profile is *reduced* and so the relative changes in the wind speed and shear stress are reduced. Bradley's (1983) data agree well into the prediction (4) for this situation. When the buoyancy forces are strong enough that $L/L_{mo} \geq 1$ then the turbulence so mixes the upwind boundary layer that, except within a thin layer ($\sim h/10$), the mean velocity and potential temperature is uniform. So, paradoxically, the unstable buoyancy forces can largely be ignored in the outer region. Figs. 3, 4. Usually in such situations there is a stably stratified region above the mixed layer ($z > h$), which leads to buoyancy forces in the upper layer, but these are *stable* buoyancy forces. (HRB).

1.1.2 *Turbulence structure in the outer region*

The turbulence in the outer region does not affect the mean flow over the hill because generally the hill is not long enough for the turbulent stresses to be comparable with the mean inertial forces. However the changes in the mean velocity, Δu and temperature gradient, $\Delta \theta'$, (or buoyancy frequency ΔN in stable conditions) generally change the turbulence by an amount of the order of $\Delta u/U(z)$ or $\Delta \theta'/\theta'_0(z)$ or $\Delta N/N$.

The kind of distortion the turbulence experiences depends to a large extent on the ratio of the travel time T to the Lagrangian time scale T_L of the turbulence, or in other

words to the relaxation time of the turbulence. This ratio can vary considerably between the inner and outer region and is sensitive to the stratification. If $T_L(z)$ is estimated as usual in terms of the integral scale, then $T_L(z) \sim L_x(w)/\sigma_w$ and $T \sim L/U(z)$. Using published data and also recent measurements of the Boulder Atmosphere Observatory, Hunt, Kaimal & Gaynor (1985) have shown that in most atmospheric conditions

$$(L_x^{(w)})^{-1} \approx A_B/Z + A_S (dU/dz)/(\sigma_w) ,$$

where the blocking coefficient, $A_B \approx 1$ and the shear coefficient $A_S \approx 0.6$. Then in neutral conditions, where $dU/dz = \sigma_w/(0.5z)$, $L_x^{(w)} \approx 0.52$ and therefore $T(\Delta z) < T_L(\Delta z)$ where $\Delta z > L$.

Thus in neutral conditions outside the inner layer, the travel time is less than the Lagrangian time scale and the turbulence is distorted 'rapidly', in a similar way to its behavior in a wind tunnel contraction. The method of rapid distortion analysis can be applied to predict variances and spectral length scales. (Britter, Hunt & Richard, 1981, Bradley 1980).

However, in stable conditions $dU/dz \gg \sigma_w/z$, and often in these conditions $R_i \approx 1/4$ so that $N \approx 1/2 dU/dz$. Then $L_x^{(w)} \sim N(\sigma_w/A_S)/dU/dz \sim \sigma_w/(A_S N)$. Consequently $T/T_L \approx (1/3) LN/U(z) \geq 1$. Therefore, in this situation the relaxation time of the turbulence and the mean flow are in local equilibrium because the mean flow, as already explained, is controlled by inertial and buoyancy forces. Consequently, in the equation for turbulent kinetic energy the advection, the production, the buoyancy flux and the dissipation are all of the same order. (Some preliminary results are presented in Chapter E. Second order modeling (e.g. Zeman & Lumley 1979) should provide the basis for the one-point moments (e.g. of velocity variance, dissipation etc.) which can be combined with the Lagrangian statistical models such as that of Pearson, Puttock and Hunt (1983) to derive integral scales, spectra and correlations.

In convective conditions the Lagrangian time scales are larger than in neutral conditions, so $T < T_L$ and therefore the rapid distortion analysis is appropriate. However in

this case the vertical scales of the turbulent eddies can be so large that a *local* analysis at a given height z may not be appropriate. It is as if the eddies in the wind tunnel were as large as the wind tunnel. This wind tunnel problem has recently been solved with rapid distortion theory by considering the 'image' of the eddies in the boundary (Goldstein & Durbin, 1980). The same techniques could be applied to the problem of calculating convective turbulence over hills. (A statistical theory using the idea of the image eddies has already been developed by Hunt (1984) to analyze the structure of convective turbulence over level ground).

1.2 *Problems examined in this project.*

From previous work the flow over a simple bell shaped hill with well behaved upwind temperature profiles the broad features of the flow in the outer region were reasonably well understood and well validated by computation, and field and laboratory studies. But, this was not the case in the inner region, even when the flow does not separate. The elucidation of the structures of this layer has been a major task of this project and it has been largely completed. However the effects stratification in the inner layer and the effects of different outer layer flows have not yet been examined to date. The effects of stratification on the structure of the inner layer can only be understood when the heat and moisture transfer between the airflow and the hill surface is incorporated into the air flow calculation, because the inner layer is thin enough for turbulence to transport the effects of the surface upwards through the layer. The work done on these problems in this project will be found in this report and in, Hunt & Richards (1984). There have been no successful computations or theories yet for the flow on the lee side of hills for intermediate slopes between say $0.2 \geq H/L_1 \geq 1.0$. Then the slope is large enough that the turbulence structure can no longer be assumed to be a small perturbation of the upwind equilibrium distribution, yet not large enough for a fully separated flow to have developed. Second order modeling (and even $k-\epsilon$) appears to be able to predict many features of these flows

Newley (1985). We have not attempted this problem yet using our sophisticated second order model.

2. *The temperature and humidity field over hills.*

2.1 *Defining the problem*

The temperature and humidity fields over a hill, (denoted by θ and q respectively) are determined by the flow field over the hill and by the distribution upwind of the hill and over the surface of the hill of θ and q . More often the distribution of the *flux* of θ and q over the surface, namely $\langle \theta'w \rangle$, $\langle q'w \rangle$ are known rather than θ and q where θ' and q' are the fluctuations in θ and q . In principle, either $\langle \theta'w \rangle$ or $\langle \theta \rangle + \theta'$ are necessary to specify θ in the interior of the flow. In practice, given the usual assumption about turbulent transport, either $\langle \theta'w \rangle$ or $\langle \theta \rangle$ needs to be specified at about the roughness height, z_0 above the surface.

To calculate certain statistical properties of the fluctuation field of θ' and q' over the hill, it is generally necessary to know or to specify the same statistical properties upwind, for example variances, integral scales, dissipation etc. Of course the longer the hill or chain of hills, the less the correlation between θ' over the hill and upwind and so the less the need to specify θ' upwind. An important point to note is that the time scale of temperature or humidity fluctuation near the surface is usually so small (because $T_L \rightarrow 0$ as $\Delta z \rightarrow 0$), there is no need to specify the fluctuations in θ and q at the surface. However in some convective conditions, θw may vary sufficiently at the surface (if only due to passing clouds) to significantly affect θ' above the surface.

Where the temperature and humidity field over a hill do depend on the structure of θ and q upwind, then it is first necessary to know how to specify the upwind conditions before calculating the change in θ and q over the hill. Recent atmospheric tower measurements over the rolling terrain at Boulder and the flat but rough terrain at Cabauw, Netherlands have compared the turbulence structure there to that obtained in the measurements over Kansas and Minnesota. They have shown that in convective conditions

the turbulence and the temperature fluctuation have a similar and structure distribution in these two situations. In stable conditions, however, there appear to be no universality in the distributions, or the forms of the spectra; in particular large wave motion may or may not occur and these always have a large effect on the spectrum of θ' and it often also has a considerable effect on the spectra of θw and w . (Hunt, Kaimal & Gaynor 1985). In some cases these wave-like motions contributed about 50% of the total variance or covariance. Despite this irregularity in the relation between the turbulence quantities and the overall mean quantities, it was found that the turbulence and temperature fluctuation has some *internal* structure that is rather universal.

It is interesting to note that in stable conditions irregular low frequency wave motion was also observed by Caughey, Wyngaard & Kaimal (1979) over the very flat uninterrupted terrain of Minnesota, but they filtered this component out of their data in order to show the regular structure and regular vertical profiles of the middle to high wave number parts of the spectra.

This filtered component agreed well with a second closure model of Wyngaard's. It is now generally believed that these low frequency motions are associated with the various wave motions which develop on the stable boundary layer and are often stimulated by various scales of topography and by frontal activity some distance from the measurements point. (e.g. Lu Nai-Ping, Neff & Kaimal, 1983).

Consequently the aim of a theoretical or computational model for θ and q over hills ought to be to relate θ and q to arbitrary upwind conditions. This is likely to require a statistical approach. However, as with flow over rough or rolling terrain in stable conditions, the internal structure defining the relations between local turbulence and the temperature fluctuation may, because of their small time scales, continue to be applicable over hills. This provides the basis for analyzing θ and q using second order turbulence models.

2.2 *Defining the transport process and the mathematical models for each region of the flow*

2.2.1 *Inner region*

In this region the temperature, θ , and humidity q , are determined partly by the local heat flux F_θ or water vapor flux F_q from or to the ground, by vertical diffusion of heat and water vapor, and by the advection of heat and water vapor from upwind. Over uniform flat terrain the advection has a negligible affect on the distribution of θ and q . But over non-uniform terrain such as a hill, where the surface fluxes vary with downwind distance, and advection of θ and q affects the vertical distribution of θ and q . Also the convergence and divergence of streamlines and the change in the turbulence over the hill can have comparable effects on $\theta(z)$ and $q(z)$.

A widely accepted model for the 'sensible' heat flux and the water fluxes at the ground, when covered with vegetation, is that developed by Monteith. Its mathematical derivation and implications were nicely discussed by Thom (1975); its use in dispersion modeling was developed by Smith & Blackall (1979). It is convenient to express F_θ and F_q in terms of the net in-coming radiation heat flux R_n and the net heat flux arriving at the surface from the soil G , the Bowen-ratio β , and the latent heat of water, as

$$(2.1) \quad F_\theta = (R_n + F_G) \frac{R\beta}{1+\beta}, \quad F_q = \frac{R}{\lambda(1+\beta)},$$

where the net heat flux from the radiation and soil is $R = R_n + G$. Therefore the relation between F_θ and F_q is

$$(2.2) \quad F_q/F_\theta = 1/(\beta\lambda).$$

The ratio β depends on the shear stress at the ground τ , the roughness z_0 , the local mean temperature θ and water vapor concentration q , and also the *nature* of the vegetation. The lowest value of this ratio is zero, when the winds are moderate, the air is dry and all the energy is used to evaporate water from the vegetation. There is no upper limit of this ratio, if there are few plants or they have a high 'stomatal' resistance.

The changes in F_θ and F_q , denoted by ΔF_θ , ΔF_q , can be expressed in terms of the upwind value of F_θ and F_q , denoted by $F_{\theta 0}$, $F_{q 0}$, and in terms of the changes in R and β .

Thus

$$(2.3) \quad \Delta F_\theta / F_{\theta 0} = \Delta R / R_0 + \delta\beta / [\beta_0(1+\beta_0)]$$

$$(2.4) \quad \Delta F_q / F_{q 0} = \Delta R / R_0 - \delta\beta / (1+\beta_0) .$$

This result shows up the sensitivity of the changes in F_θ and F_q to the value of β_0 .

On more or less sunny days any changes in $(R_n + F_G)$ are mainly caused by changes in the direct solar radiation R_S reaching the surface. Then we can assume that the net radiation and ground heat flux is related to the changes R_S by a relation like

$$(2.5) \quad \Delta R / R_0 \approx \chi_R \Delta R_S / R_{S0} ,$$

where the coefficient χ_R is not equal to 1.0 as supposed by Smith & Blackall (1979), because R_n , the net radiation, is only about 1/3 of the solar radiation reaching a surface. Of course the diffused radiation tends to be concentrated at angles near to the solar elevation ϕ_0 . (Fig. 3). From data quoted by Geiger (1965, p 376) it appears that $\chi_R = 0.7$.

For a slope equal to $(H/L) f$ (x/L), the proportional change

$$(2.6) \quad \Delta R_S / R_{S0} = \cot\phi_0 \cdot (H/L) f$$

Note that $\cot\phi_0$ is smaller in summer than winter. Geiger's data shows that on a south facing slope of 10° , $\Delta R / R_0 = 0.13$ averaged over the whole year, but 0.4 in winter and 0.06 in summer. At $48^\circ N$, $\cot\phi_0 = 2.9$ in winter and .47 in summer, so the predicted variation in $\Delta R / R_0$ from (2.6) would be .5 in winter and .04 in winter. At night or in foggy or overcast conditions R does not depend on the slope (for small slopes).

From Monteith's formula in the appendix we can derive the changes in β caused by changes in θ , q , and τ : β is also changed by variations in the surface vegetation or roughness. We are assuming here that the form of the surface vegetation remains fixed over the hili, and we then have

$$(2.7) \quad \Delta F_\theta / F_{\theta 0} = \Delta R / R_0 + \chi_\tau |\Delta\tau| / \tau + \chi_\theta \Delta\theta / \theta_0 + \chi_q \Delta q / q_0$$

$$(2.8) \quad \Delta F_q/F_0 = \Delta R/R_0 + \psi_\tau |\Delta \tau|/\tau + \psi_\theta \Delta \theta/\theta_0 + \psi_q \Delta q/q_0$$

In sunny conditions (2.5) and (2.6) can be used for the first terms.

As is shown in the appendix χ_τ and ψ_τ can range between about -1/2 and 1/2 in most kinds of condition, when the heat flux is radiation controlled. This is consistent with recent data that gives χ_τ to be about -1/2 in stable conditions, when the heat flux is downwards and the heat transfer is controlled by forced advection over the ground. This is based on a correlation of measurements by Venkatram, (1980). In the former case generally χ_τ depends on the nature and state of the vegetation and the humidity of the air. A range of examples is given in the appendix.

The parameter χ_θ and χ_q depend on the humidity, i.e. the ratio of q_0 to the saturated value of q at the temperature θ_0 if the air is saturated, $\chi_\theta = \chi_q = 0$. But for typical air flow over vegetation in mid-latitudes, a change of -1°C for given q or a doubling of q for given θ produces a similar order of magnitude of increase in F_θ as does a 1 ms^{-1} change in wind speed, i.e. $|\chi_\theta| \sim (1/3)10^{-2}$, $\chi_q \sim 1$.

This provides some framework for considering how the heat and water fluxes can change over a hill. Some results are reported by Hunt & Richards 1984, and a more detailed report is given in Chapter E.

There is some laboratory evidence for the validity of (2.8) when the upwind flow is unsaturated. Dawkins & Davis (1981) measured the change in flux of vapors from a small region on a surface when the same region was located on a hill. They found that the flux increased by about 50% of the increase in $\Delta \tau/\tau$. (That is not how they expressed their result - it is our interpretation.) A similar result was found by Verma & Cermak (1971) in their study of mass transfer over wavy surfaces.

2.2.2 Outer region

In section 1.1.2 the turbulence structure in the outer region was reviewed. We first consider neutral conditions over hills of moderate length ($< 5 \text{ km}$), i.e. not so long that the inner layer thickness is much shallower than the upwind layer. It was shown that in this

case the Lagrangian time scale $T_L(z)$ is greater than the travel time $T(z)$. This implies that the mean temperature and humidity θ and q are not affected by the local turbulence.

The statistics of temperature and humidity fluctuations (θ' and q') depend on their structure upwind of the hill, particularly since they are correlated with their values upwind. The changes in structure of the spectra of θ' and q' depend mainly on the distortion of the mean streamlines. There are also weak effects produced by the changes in the mean temperature gradient over the hill, caused by the convergence and divergence of the mean streamlines, and effects caused on the changes in the turbulence. (Hunt 1984). Although the changes in the turbulence in the outer region can be calculated by the methods of rapid distortion theory (since $T < T_L$), the changes in small scale temperature fluctuations caused by the changes in turbulence, can only be estimated rather approximately.

In stable conditions, it has been shown that in the outer region, the time scales are smaller, i.e. $T > T_L(z)$ so that the turbulence adjusts as it travels over the hill. Therefore the turbulence changes over the hill are controlled by advection, production, buoyancy flux, and dissipation. The mean temperature and water vapor gradients, however, are controlled by the mean flow and their upwind values, *not* by local turbulence. Second order modeling methods can usually work well when the changes are relatively slow. In E, we use the simplest possible approach of assuming local equilibrium for calculating $(\theta')^2$ and $(q')^2$ which is appropriate in strongly stable condition, because large vertical displacements by the fluid elements are not possible. (Hunt 1982, Hunt, Kaimal & Gaynor 1985.)

2.2.3 *Wake region*

The wake is a continuation of the inner region, in that the mean temperature and water vapor concentration are controlled by advection and turbulent diffusion. Therefore the change in surface flux also has been considered, however the largest changes in flux occur over the hill. For example the surface shear stress over a hill with slope of $1/2$ or $H/L = 1$, may be increased by three times, but in the wake the surface shear stress perturbation decreases to less than $1/10$ of this within a distance $2L$ downwind.

Consequently in the wake most of the changes in temperature and water vapor fluctuations are likely to be *advected* from the surface of the hill itself.

There have been some studies of dispersion of heat or other contaminants released on or near bluff bodies in boundary layers. The mean temperature concentration is well described by calculations based on eddy diffusivity models *or* random walk computer simulations. (See review by Hunt 1982b). If such methods work, then the more complex second order change models are likely to be quite satisfactory. The simple turbulence models have the advantage of enabling the computation to be performed more simply or even analytically.

Appendix

Variation of heat and water flux over a surface.

From Monteith's formula, (see Thom, 1975 and Smith & Blackall 1979, F_θ and F_q are given by:

$$F_\theta(z) = \beta R / (1 + \beta), F_q(z) = R / (1 + \beta) \lambda$$

where the Bowen-ratio $\beta(z) = (r_a + r_{st} - r_i) / ((\Delta/\gamma)r_a + r_i)$, R is the *net* surface heat flux, λ is the latent heat of vaporization of liquid water, and the resistances r_a , r_{st} , r_i have the following values:

The aerodynamic resistance $r_a(z) = [1/(ku^*)] \ln((z-d)/z_0/5)$, where d is the displacement height, which is of the order of the vegetation height. $r_a(z)$ is usually defined in terms of the velocity at a particular value of $(z-d)$, eg

$$r_a(z) = 6.25/U(z) \ln((z-d)/z_0) \ln(5(z-d)/z_0) = 2 \times 10^2 / U(z) \text{ for } z_0 \approx 10^{-2} \text{m.}$$

For a typical wind speed of 5ms^{-1} , $r_a \approx 40 \text{ s m}^{-1}$. The stomatal resistance r_{st} is the resistance by the vegetation to evaporation and transpiration. When the plant surfaces are wet $r_{st} \rightarrow 0$, but when the plants transpire very slowly $r_{st} \rightarrow \infty$. In most typical air flows over crops, $r_{st} \approx r_a \approx 40 \text{ s m}^{-1}$. Monteith called r_i the 'isothermal resistance' because if $r_a + r_{st} = r_i$, there can be isothermal flow. Here r_i is defined as:

$$r_i = (\rho c_p / (R\gamma)) (p_{sv} - p_v),$$

where γ is the psychrometric constant $\gamma = \rho c_p / (\lambda \epsilon)$ - (usually in $\text{mb}^\circ\text{C}^{-1}$) and ρ , c_p , ϵ , p are the density, specific heat, ratio of molecular weights of water to air ($=5/8$), and pressure. Further p_{sv} , p_v are the saturated and local vapor pressure, p_{sv} is a function of the temperature θ , $p_v/p = 8/5 q$, where q is the water vapor concentration.

The parameter Δ in the expression for the Bowen ratio is related to r_i :

$$\Delta = 1/2 [(\partial p_{sv}/\partial \theta)(z) + (\partial p_{sv}/\partial \theta)(\theta = 0)]$$

and $\Delta/\gamma(\theta)$ is plotted in Fig. A.1 from Thom (1975).

In order to understand how β varies with perturbation of τ , θ and q , we have to consider various conditions of humidity and plant type.

- (i) In conditions at about 50% humidity over field crops in mid latitudes (Thom, p. 103, 1973) $r_a \approx r_{st} \approx r_i$, $\gamma \approx 0.66 \text{ mb/}^\circ\text{C}$, $R \sim 100 \text{ W/m}^2$. so $\delta\beta \approx 0(-\delta r_a/r_a - \delta r_i/r_i)$. Note that since $2 < \Delta/\gamma < 6$ in these conditions $\partial\beta/\partial r_a < 0$, and $\partial\beta/\partial r_i < 0$.

Thence, since $\partial r_a/\partial \tau \propto -\delta\tau/\tau$, and $\partial r_i/\partial q \propto -\delta q$

$$\delta F_\theta/F_\theta \sim -\delta F_q/F_q = 0(1/2 \delta\tau/\tau, (-\rho c_p/R) (\Delta/r_a) \delta\theta, \delta q/q),$$

depending which term is most significant.

Since $1 \leq \Delta \leq 6 \text{ mb/}^\circ\text{C}$ for $0 < \theta < 40^\circ\text{C}$, $\rho c_p \Delta/(R r_a)$ is of the order of $1 \text{ s m}^{-1} \text{ }^\circ\text{C}^{-1}$.

Then an increase in wind speed reduces the evaporation, and increases the heat flux from the ground.

- (ii) In conditions where there is a strong, dry air flow over irrigated vegetation,

$$r_i \gg r_a, r_i \gg r_{st}, \text{ then } \beta \rightarrow -1$$

so that F_θ/R and F_q/R become indeterminate. But $F_\theta \approx -F_q$

In other words there is a downwards flux of sensible heat.

- (iii) Where there is a strong dry air flow over vegetation which is wet on the surface. then there is no stomatal resistance to transpiration so $r_i \gg r_a \gg r_{st}$. Then $F_q > 0$ and $F_\theta < 0$ because of the evaporation.

In that case $\beta \rightarrow -1 + (\Delta/\gamma + 1)r_a/r_i$ so $F_\theta \approx -[R/((\Delta/\gamma) + 1)]r_i/r_a$, $F_q \approx [R/((\Delta/\gamma) + 1)]r_i/r_a$, and then $\delta F_q/F_q \approx -\delta F_\theta/F_\theta \approx \Delta R/R + (1/2) |\Delta\tau/\tau - \delta r_i/r_i|$

In this case an increase in surface shear decreases the magnitude of F_θ .

- (iv) When the wind is strong, there is some humidity and some transpiration,

$$r_a \gg r_{st}, r_a \gg r_i, \text{ then } \beta \rightarrow 1/(\Delta/\gamma) \approx 1/2 \text{ at } 20^\circ\text{C}.$$

In this case F_q is about twice F_θ ; both are positive if $R > 0$ and both are independent of wind speed.

- (v) When the (stomatal) resistance is high, and the wind speed is moderate so that

$$r_{st} \gg r_a, r_i, \text{ then } \beta \rightarrow r_{st}/((\Delta/\gamma)r_a + r_i) \gg 1. \text{ In this case } F_\theta \approx R \text{ and } F_q \approx (R/r_{st})((\Delta/\gamma)r_a + r_i) \ll R.$$

Here the heat flux is approximately independent of wind speed, but note that F_q increases with r_a , or decreases with wind speed.

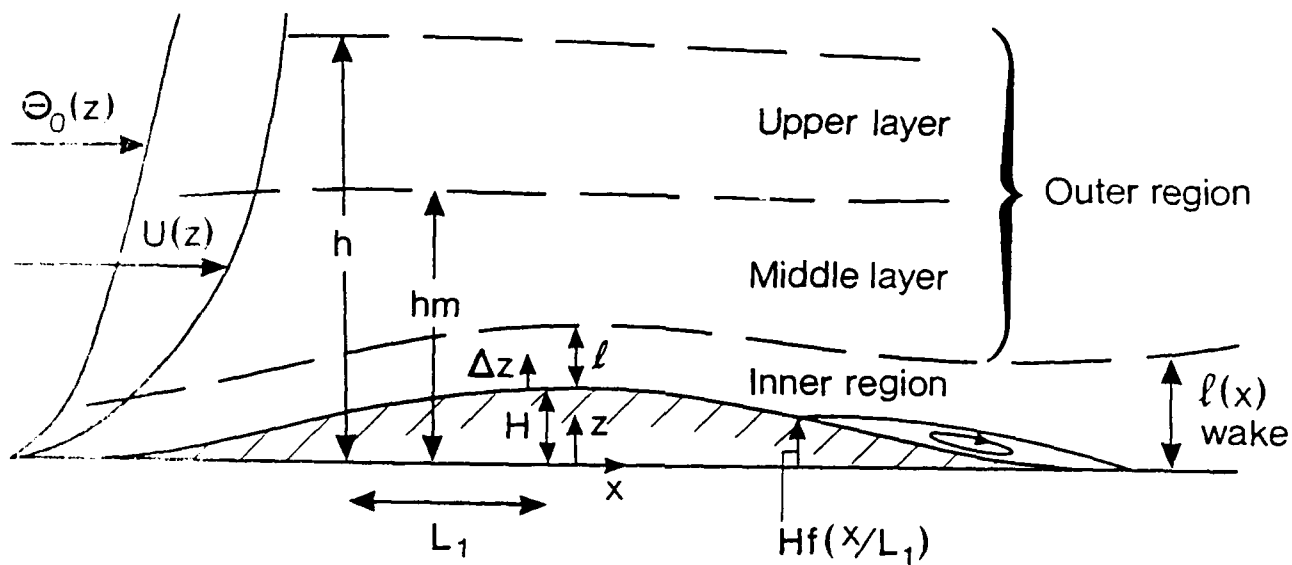


Fig. 1 Schematic diagram (not to scale) of the regions of flow over a hill, and the notation used.

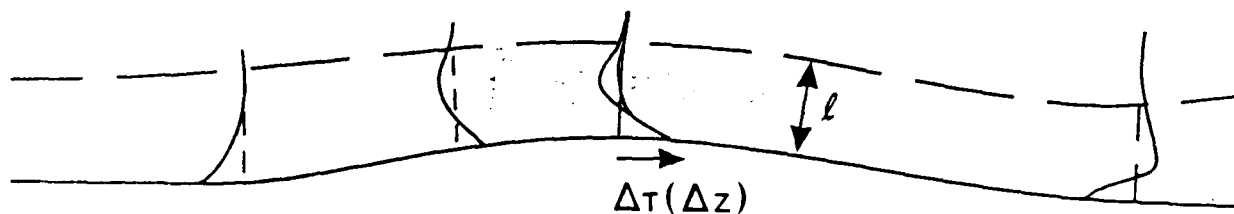


Fig. 2 Typical variations of perturbation shear stress in the inner layer.

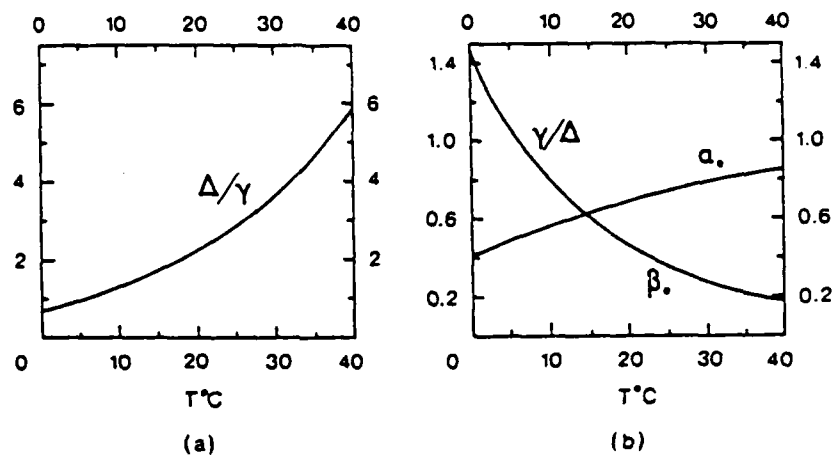


Fig.A.1. Temperature dependence of ratios compounded from Δ , the slope of the saturation vapour pressure versus temperature curve for water, and $\lambda = c_p P / \lambda \epsilon$, the thermodynamic value of the psychrometric constant. The curves are derived from data given by Monteith (1973; Tables A3 and A4) and refer to $p = 1000$ mbar.

References

- Bradley, E.F. (1980) Q.J. Roy. Met. Soc. 106, 101.
- Bradley, E.F. (1983) Proc 6th Int. Wind Engineering Conf. Australia.
- Brighton, P.W.M. (1978) Q.J. Roy. Met. Soc. 179, 189.
- Britter Hunt & Richards (1981) Q.J. Roy. Met. Soc. 107, 91.
- Caughey, S., J. Wyngaard J.C. & Kaimal, J.C. (1979) J. Atmos. Sci. 36, 1041.
- Counihan, J., Hunt, J.C.R., and Jackson, P.S., 1974. Wakes behind two-dimensional surface obstacles in turbulent boundary layers, *J. Fluid Mech.*, 64, 529-563.
- Dawkins, R.A. & Davies D.R. (1981) J. Fluid. 108, 423-442.
- Fitzjarald, D.J. (1983) Katabatic wind in opposing flow NCAR3123-83/1
- Goldstein, M.E. & Durbin, P.A. (1980) J. Fluid Mech. 98, 473.
- Geiger, R. (1965) The Climate near the ground Harvard U.P.
- Hunt, J.C.R. (1981) Proc. Conf. Designing with the wind! CSTB Nantes France.
- Hunt, J.C. R. (1984) J. Fluid Mech. 138, 161-184.
- Hunt, J.C.R. (198a) Atmospheric turbulence and air pollution modelling (Ed Fm Nieuwstadt & H. Van Dop.) Reidel, pp. 231-274.
- Hunt, J.C.R. (1982b) BMFT Colloq. on Exhaust Gas Air Pollution Caused by Motor Vehicle Emission, T. U. V. Cologne, Germany.
- Hunt, J.C.R., Leibovich, S., Richard K. (1986) Stratified shear flows over low hills, I Effects of upwind shear. Submitted to Q.J. Roy. Met. Soc.
- Hunt, J.C.R., Richards, K., Brighton, P.W.M. (1985) Stratified shear flows over low hills II. Stratification effects in the outer flow region. Submitted to Q.J. Roy. Met. Soc.
- Hunt, J.C.R., Leibovich, S., Lumley, J.L. (1983) Report from Flow Analysis Associated to State of Maryland Dept. Nat. Res. Contract P85-81-06, pp. 78.
- Hunt, J.C.R. & Simpson, J.E. (1982) Engineering Meteorology (ed. E.J. Plate), Elsevier Amsterdam, pp. 269-318.
- Hunt, J.C.R., Kaimal, J.C. Gaynor, J. & Korell, A. (1985) Some observations of turbulence structure in stable layer Q.J. Roy. Met. Soc. 111, 793-815.
- Hunt, J.C.R. & Richards K.J. (1984) Boundary Layer Meteorology 30, 223-259.
- Lu Nai-Ping, Neff, W.D., * Kaimal, J.C. (1983) NOAA ERL Rep. No. 4 pp. 53-74. (Ed J.C. Kaimal) U.S. Dept. of Commerce.

- Merkine, L.O. (1975) *J. Atmos. Sci.*, 32, 1887.
- Newley, T.H.J. (1985) Ph.D. Dissertation University of Cambridge.
- Pearson, H.J., Puttock, J.S. & Hunt, J.C.R. (1983) *J. Fluid Mech.* 129, 219.
- Plate, E.J. & Lin C-Y (1965) Colo State University Rep. CER65-EJP14.
- Scorer, R.S., 1955. Theory of air flow over mountains. IV. Separation of flow from the surface. *Q. J. Roy. Met. Soc.* 81, 340.
- Smith, F.B. & Blackall, R.M. (1979) Proc Symp. Math. Models & Turb. Diff. in the Environment, Academic Press.
- Sykes, R.J. (1978) Proc. Roy.Soc. A 351, 225.
- Thom, A. (1975) Vegetation and the Atmosphere) Ed. J.L.Monteith). pp. 57-110.
- Venkatran, A., 1980. *Boundary Layer Met.*, 19, 481.
- Verma, S.B. & Cermak, J.E. (1971) Colo. State Univ. Rep. CER70-71 SBV-JEC-59.
- Zeman, O. & Lumley, J.L. (1979) *Turbulent Shear Flows I*. 295-306; Springer.

Chapter B

Summary and extension of analytical theory of turbulent mean flows over terrain of low slope

**Prepared by
S. Leibovich**

1. Introduction

In this Chapter we survey the analytical theory laid out at somewhat greater length in Chapter C. Here the development is traced from a point of view that differs in the following respects from C:

- (i) the formulation is developed with computer calculations in mind,
- (ii) in view of (i), the analysis is carried out and results presented in Fourier space,
- (iii) the development is three-dimensional throughout,
- (iv) generality of the outer flow is retained, and there is therefore no need for consideration of a "middle layer", and this has the added advantage of a more rigorous matching of the outer region with the inner (two) regions,
- (v) the calculations are done completely in "displaced coordinates", a coordinate system used for only parts of the flow in C.

No attempt is made here to give a self-contained account, and an acquaintance with Sections 1-3 of Item C will be needed in order to understand the developments reported here. Indeed, we will freely refer to equations and arguments in C. Equations cited from C will be identified by appending C to the equation number, e.g., (C3.8.b).

In section 2, we redevelop the theory for the inner and outer layers and match them. In section 3, we summarize the theory by displaying formulas for composite expansions valid throughout both the outer region and the shear stress layer that comprises the bulk of the inner region. In this section, we also lay out a computational strategy permitting this method to be used for arbitrary terrain (of low slope) and upwind conditions.

2. Redevelopment of the theory

We assume we are given a turbulent flow upstream of a hill or series of hills rising out of the plane $z = 0$, with wind speed $U_0 U(z)$ and (potential) temperature $\Delta T_0 \Theta(z)$ (with U_0 and ΔT_0 defined below) specified as functions of elevation. Near the ground, both $U(z)$ and $\Theta(z)$ are assumed to have equilibrium turbulent wall layer structure with roughness length z_0 , so, for example,

$$U(z) \sim (\epsilon/\kappa) \ln(z/z_0) \quad (1)$$

as $z \rightarrow 0$, where κ is the Karman constant, and $\epsilon = u_*' U_0$. In the absence of terrain, these distributions would persist (at least with negligible changes over horizontal distances of order L), and even when perturbed, the near-ground behaviour is assumed to be in wall-layer equilibrium form, but with the local wall stress. The topography is specified by the equation

$$F(x, y, z) = Z = z - \mu f(x, y) = 0,$$

where

$$\mu = H/L,$$

and H is the maximum elevation, and L is a characteristic hill length as defined in C. We assume here (in contrast to C) that all quantities have been made dimensionless, with L as unit of length, and U_0 , the wind speed at large elevations as unit of speed, and some convenient choice, such as the greatest temperature difference (ΔT_0) in the upstream air, as unit for temperature.

Equations (C2.3), when normalized according to the scheme in the preceding paragraph and the Boussinesq density-temperature relationship used, govern the dimensionless mean flow. The diffusive fluxes of momentum and heat are taken in thin-layer form.

The eddy viscosity formulation of C is used, in it, the eddy viscosity is $O(\epsilon)$ and the problem has a boundary layer structure as $\epsilon \rightarrow 0$, with diffusive terms ignorable except in a layer of $O(\epsilon)$ near $Z = 0$. In point of fact, as argued in E, an eddy viscosity-diffusivity

model is not applicable much beyond this layer, and we therefore assume that the eddy viscosity is of smaller order than ϵ above the inner layer. In C, this layer is taken to have a dimensional thickness $l = 2\kappa^2 L / \ln(l/z_0)$, or, in dimensionless terms, its thickness is $2\kappa^2 \delta$, where $\delta = 1/\ln(l/z_0)$ is a small expansion parameter used in the inner layer. The connection between ϵ and δ is through the wall layer behaviour of the upstream (basic) flow, $\epsilon = \kappa \delta U(l)$, so ϵ and δ are of the same order. In this chapter, we use the symbol l to refer to $2\kappa^2 \delta$, that is to the dimensionless version of the length denoted by l in C: in this way, all expansions in the shear stress layer in C can be carried over directly.

With these preliminary remarks, we are led to the following dimensionless system of equations:

$$\mathbf{u} \cdot \nabla \mathbf{u} + \nabla \pi - (g\beta \Delta T_0 L U_0) \theta \mathbf{e}_z = \partial \tau / \partial Z, \quad (2a)$$

$$\mathbf{u} \cdot \nabla \theta + w \Theta'(z) = \partial h / \partial Z, \quad (2b)$$

$$\nabla \cdot \mathbf{u} = 0. \quad (2c)$$

Here θ is the temperature perturbation from $\Theta(z)$, β is the coefficient of thermal expansion, h the heat flux, π is a dimensionless pressure deviation from the hydrostatic pressure in the upstream flow; and the Cartesian (x, y, z) coordinate system (with unit vectors \mathbf{e}_x , \mathbf{e}_y , and \mathbf{e}_z) and mean velocity components (u, v, w) .

The terms on the right in (2) are negligible except in the inner regions where $Z = O(l)$. We assume the inner region is effectively neutral, so that we neglect buoyancy effects in it. Then the "Prandtl transposition theorem" (Rosenhead, sec.V.8, also valid in three dimensions) of laminar boundary layer theory is also applicable to turbulent flows where the mean force from Reynolds stresses involve only derivatives with respect to z or Z , and the pressure (or modified pressure, like π) is a prescribed function of x and y only. This "theorem" says that, if $(u(x, y, z), v(x, y, z), w(x, y, z))$ is a solution to the boundary layer equations, then so is $(u(x, y, Z), v(x, y, Z), w^+(x, y, Z))$, where

$$w^\dagger = w + \mu \mathbf{u} \cdot \nabla f(x, y).$$

Therefore, given a solution $\mathbf{u} = (U(z), 0, 0)$ valid for flow over a plane surface, we have a second solution of the boundary layer equations valid for $Z > 0$, that is, above the surface $F(x, y, z) = 0$, given by

$$\mathbf{u}^\dagger = (U(Z), 0, \mu U(Z) \partial f / \partial x). \quad (3)$$

(Provided temperature perturbations $\theta \ll \Theta$, the same transposition theorem holds for the set (2) without the restriction to neutral conditions in the inner region, but the result is then only approximate, with an error of order $w\theta$.)

While (3) satisfies the differential equations (2) and the boundary conditions as $Z \rightarrow 0$, it fails to satisfy the boundary conditions as $Z/l \rightarrow \infty$, since the vertical component of (3) does not vanish in that limit. This error is of order μ , and to correct it an outer solution is necessary, with $Z = O(1)$, and in the outer region, the right hand sides of (2) are neglected. In the outer region, the flow is a small perturbation to the upwind conditions, so we set

$$\mathbf{u} = (U(z) + \mu u(x, y, z), \mu v(x, y, z), \mu w(x, y, z)), \quad \pi = P + \mu p(x, y, z), \quad (4)$$

insert (4) into the nondiffusive form of (2), linearize, and take Fourier transforms with respect to x and y . Taking the double transform to be of the form

$$w(z, \mathbf{k}) = \int_{-\infty}^{\infty} \int_{-\infty}^{\infty} w(x, y, z) \exp[-i\mathbf{k} \cdot \mathbf{x}] dx dy$$

where

$$\mathbf{k} = k_1 \mathbf{e}_x + k_2 \mathbf{e}_y, \quad \mathbf{x} = x \mathbf{e}_x + y \mathbf{e}_y, \quad (5a)$$

and k_1 and k_2 are the Fourier transform variables or wavenumbers in the x and y directions respectively. We set

$$k = (\mathbf{k} \cdot \mathbf{k})^{1/2} = (k_1^2 + k_2^2)^{1/2}. \quad (5b)$$

Note that we use no special notation to differentiate a variable from its Fourier transform: if it is necessary to avoid confusion, or for emphasis, the distinction is made through the argument list.

The resulting system of ordinary differential equations can be reduced to the following single equation for the double transform $w(z, \mathbf{k})$:

$$w'' + \{\Sigma - k^2\} w = 0 \quad (6a)$$

$$\Sigma = k^2 N^2 / [k_1^2 U^2(z)] - U''(z)/U(z) \quad (6b)$$

$$N^2(z) = (gL/U_0^2) \Theta'(z)/\Theta(0). \quad (6c)$$

Here $()' = d()/dz$, and N is the dimensionless buoyancy frequency or, alternatively, an inverse densimetric Froude number. We observe that one may replace z in equation (6) by the displaced coordinate Z with an error of $O(\mu)$, leading to an overall error of $O(\mu^2)$. As this level of error is neglected throughout the analysis, we assume the replacement has been made and so henceforth $()' = d/dZ$. For future reference, we record here the formulas by which the perturbations u, v , and p may be found from w . These are

$$p(Z, \mathbf{k}) = -i (k_1/k^2) [U(Z)w' - wU'] = -i (k_1/k^2) U^2(Z) (w/U)' \quad (6d)$$

$$v(Z, \mathbf{k}) = - (k_2/k_1) p(Z, \mathbf{k}) / U(Z) \quad (6e)$$

$$u(Z, \mathbf{k}) = i [k_1^2 w' + k_2^2 (U'/U) w] / k_1 k^2 = -p(Z, \mathbf{k}) / U(Z) + i (U'/U) w / k_1. \quad (6f)$$

To match the inner and outer regions to lowest order, we require

$$w(x, y, z) \rightarrow U(z) \partial f / \partial x, \quad (7a)$$

or

$$w(Z, \mathbf{k}) \rightarrow i k_1 U(Z) f(\mathbf{k}) \quad (7b)$$

as $Z \rightarrow 0$. The appropriate boundary condition as $Z \rightarrow \infty$ depends on the stratification in this limit. We assume in all cases that $U(Z) \rightarrow 1$ and $U'(Z) \rightarrow 0$ as $Z \rightarrow \infty$, and we require w to satisfy the radiation condition

$$w(Z,k) \sim C \exp\{-(k/|k_1|)[k^2 - N_0^2]^{1/2} Z\}, \text{ if } |k_1| > N_0, \quad (8a)$$

$$w(Z,k) \sim C \exp\{-i(k/k_1)[N_0^2 - k^2]^{1/2} Z\}, \text{ if } |k_1| < N_0, \quad (8b)$$

if $N \rightarrow N_0$ at great elevations: this reduces to $w \rightarrow 0$ if conditions aloft are neutral. The condition (8) assumes that the buoyancy frequency is real, if conditions are unstable aloft then N_0 will be imaginary, and the appropriate condition then is

$$w(Z,k) \sim C \exp\{-(k/|k_1|)[k^2 + |N_0|^2]^{1/2} Z\}. \quad (9)$$

The outer problem at lowest order is then to solve equation (6) subject to the conditions (7) and either (8) or (9). For general upwind conditions, this must be done numerically, and, for the moment, we assume that this has been done. The relationship of these solutions to those in C, and particularly the "middle layer" solution can be seen as follows. Since U is logarithmic as $Z \rightarrow 0$, the differential equation has an irregular singularity at $Z = 0$. The structure of the solution for small Z is simply found by the method of dominant balance (or can be constructed using the series method for such irregular points as explained in Forsyth, A.R. Theory of differential equations, vol IV, Cambridge, 1900-1902). For very small Z , the function in the brackets in (6a) is dominated by $-U''(Z)/U(Z)$, and so the asymptotic behaviour of the general solution to (6) is, as $Z \rightarrow 0$,

$$w(Z,k) \sim a(k) U(Z) + b(k) U(Z) \int U^{-2}(Z) dZ, \quad (10)$$

which is the same as the solution in the "middle layer", but in the present context has a rigorous mathematical meaning. With $U \sim (\epsilon/\kappa) \ln(Z/z_0)$ as $Z \rightarrow 0$ (where z_0 is the dimensionless roughness length), the second term in (10) vanishes like $Z U(Z) \ln(\ln(Z/z_0))$ and the coefficient of the first term, $a(k)$, is already known from (7). It turns out that the coefficient $b(k)$ is essentially the Fourier transform of the pressure perturbation in the outer flow in the limit $Z \rightarrow 0$, and is of course fixed by the asymptotic boundary condition (8) or (9). That it is the $O(\mu)$ pressure perturbation can be seen since the pressure in the outer flow has Fourier transform

$$p(Z,k) = -i(k_1/k^2)(Uw' - wU') \quad (11)$$

and if this is evaluated from (10) as $Z \rightarrow 0$, we find

$$p(Z, \mathbf{k}) \sim -i(k_1/k^2) b(\mathbf{k}). \quad (12)$$

(That $b(\mathbf{k})$ is determined by the asymptotic conditions (8) or (9) can be seen as follows. Let two independent solutions of (6) be denoted ϕ_1 and ϕ_2 , where $\phi_1 \sim U(Z)$ and $\phi_2 \sim U(Z) \int U^{-2}(Z) dZ$ for small Z . Then necessarily, for Z large, we have

$$\phi_j \sim C_{j1} \exp\{-mZ\} + C_{j2} \exp\{mZ\}, j = 1 \text{ or } 2, \quad (13)$$

where $-m$ is the coefficient multiplying Z in either (8) or (9), whichever of these is appropriate, and the coefficients C_{ij} are determined by the definitions of the ϕ_j . Thus, we have, as $Z \rightarrow \infty$,

$$w(Z, \mathbf{k}) \sim [a(\mathbf{k})C_{11} + b(\mathbf{k})C_{21}]e^{-mZ} + [a(\mathbf{k})C_{12} + b(\mathbf{k})C_{22}]e^{mZ}, \quad (14)$$

so satisfaction of the boundary condition for $Z \rightarrow \infty$ requires

$$b(\mathbf{k}) = -(C_{12}/C_{22})a(\mathbf{k}). \quad (15)$$

This concludes the discussion of the general way $b(\mathbf{k})$ is related to the asymptotic conditions.)

Assuming that a solution for $w(Z, \mathbf{k})$ in the outer region has been found, we have seen that a pressure gradient arises, and this forces a perturbation of the flow in the inner region. Here we consider the shear stress layer, which comprises the bulk of the inner region and in which

$$Z = l\zeta \quad (16a)$$

where ζ is assumed of $O(1)$ and we write

$$\mathbf{u} = (U(l\zeta) + \mu U(l)u_d, \mu U(l)v_d, \mu U(l)w_d) \quad (16b)$$

(see C). The perturbation equations in the shear stress layer are then given by

$$(1 + \delta \ln \zeta)ik_1 u_d(\zeta, \mathbf{k}) + w_d(\zeta, \mathbf{k})/(2\kappa^2 \zeta) = ik_1 \sigma(\mathbf{k}) + (\partial/\partial \zeta)(\zeta \partial u_d/\partial \zeta) \quad (17a)$$

$$(1 + \delta \ln \zeta)ik_1 v_d(\zeta, \mathbf{k}) = ik_2 \sigma(\mathbf{k}) + (1/2)(\partial/\partial \zeta)(\zeta \partial v_d/\partial \zeta) \quad (17b)$$

$$\partial w_d(\zeta, \mathbf{k})/\partial \zeta = -2\kappa^2 \delta i \{k_1 u_d(\zeta, \mathbf{k}) + k_2 v_d(\zeta, \mathbf{k})\} \quad (17c)$$

where $\sigma(\zeta, \mathbf{k})$ is determined from the outer flow pressure according to

$$\sigma(\mathbf{k}) = -p(0, \mathbf{k})/U^2(l), \quad (17d)$$

and the subscript d identifies the perturbations in this (displacement) layer. The factor of one-half in (17b) is explained in Walmsley et al. (1982) (see the references in C).

Now (u_d, v_d, w_d) can be developed as expansions in δ , as done explicitly in C for the two-dimensional case. Writing

$$u_d = u_d^{(0)} + \delta u_d^{(1)} + \dots$$

and similarly for the other variables, we find

$$u_d^{(0)}(\zeta, \mathbf{k}) = \sigma^{(0)}(\mathbf{k}), \quad v_d^{(0)}(\zeta, \mathbf{k}) = (k_2/k_1)\sigma^{(0)}(\mathbf{k}), \quad w_d^{(0)}(\zeta, \mathbf{k}) = 0, \quad (18)$$

and

$$u_d^{(1)}(\zeta, \mathbf{k}) = \{-\ln \zeta + (k^2/k_1^2)\} \sigma^{(0)}(\mathbf{k}) + \sigma^{(1)}(\mathbf{k}) + A(\mathbf{k}) K_0(2(ik_1\zeta)^{1/2}) \quad (19)$$

$$v_d^{(1)}(\zeta, \mathbf{k}) = (k_2/k_1)\sigma^{(1)}(\mathbf{k}) - (k_2/k_1)\sigma^{(0)}(\mathbf{k}) \ln \zeta + B(\mathbf{k}) K_0(2(2ik_1\zeta)^{1/2}) \quad (20)$$

$$w_d^{(1)}(\zeta, \mathbf{k}) = -i (k^2/k_1)(2\kappa^2)\sigma^{(0)}(\mathbf{k}) \zeta, \quad (21)$$

where K_0 is the modified Bessel function, and the constants A and B are determined by application of boundary conditions as $\zeta \rightarrow 0$, and $\sigma^{(1)}$ must be determined by matching with the outer flow. If, as in chapter C, we completely neglect the effects of Reynolds stresses in the outer region, then $\sigma^{(1)} = 0$, and we shall assume this for the present purposes.

As $Z \rightarrow 0$, we require of the full problem that

$$|u| \sim (\epsilon/\kappa) \{[(1 + \mu\tau_{dx})^2 + \mu^2\tau_y^2]^{1/2}\}^{1/2} \ln (Z/z_0) \quad (22)$$

so that

$$\tau_{dx} \sim 2u_d/(1 + \delta \ln \zeta) \quad (23a)$$

and we also have the relation

$$\tau_{dx} = 2U(l)(\kappa/\epsilon) \zeta \partial u_d / \partial \zeta = (2/\delta) \zeta \partial u_d / \partial \zeta. \quad (23b)$$

In terms of the expansion of u_d in the series in δ , equating the expressions in (23a) and (23b) gives, as $\zeta \rightarrow 0$,

$$u_d^{(0)} - \zeta \partial u_d^{(1)} / \partial \zeta \rightarrow 0, \quad (24)$$

and, using the small argument expansions of K_0 , (24) gives

$$A(\mathbf{k}) = -4 \sigma^{(0)}(\mathbf{k}). \quad (25)$$

To find $B(\mathbf{k})$, we note that a similar argument to that above, but carried to the next order, gives

$$\{2[(u_d^{(0)})^2 + (v_d^{(0)})^2]\}^{1/2} - \zeta \partial v_d^{(1)} / \partial \zeta \rightarrow 0, \text{ as } \zeta \rightarrow 0, \quad (26)$$

which fixes $B(\mathbf{k})$ to be

$$B(\mathbf{k}) = -2 \sigma^{(0)}(\mathbf{k}) \{ \sqrt{2} (\mathbf{k}/|\mathbf{k}_1|) + k_2/k_1 \}. \quad (27)$$

3. Composite expansions

If we assume that equation (6) has been solved for w in the outer region, then the results for the mean flow according to the analytic theory can be summarized in a few formulas giving composite results applying throughout the flow, with no distinction as to region. Before displaying these, we look more closely at the way the inner and outer solutions match, and construct the "common parts" in the overlap region.

3.1 *The matching and common parts*

According to the asymptotic matching principle, one rewrites the outer expansion in inner variables, expands and truncates at some prescribed level of approximation, and carries out a similar program on the inner expansion, and agreement between appropriate levels of approximation are required (van Dyke, 1975, Chapter 5). Since we deal throughout with the linear theory (i.e., $O(\mu)$ corrections to the upwind flow), the only small parameter that we need consider is δ (or l).

We observe that, according to (6d-f), all outer variables can be expressed in terms of w , and so we begin by writing w in inner variables, and expanding. Note that what we assume so far to be found is the so-called "one-term outer expansion" for w (and therefore for all outer variables). Set $Z = l\zeta$ in $w(Z, k)$, hold ζ fixed and expand for small l . This gives, from (10) and (1),

$$\begin{aligned} w &\sim a(k)U(l\zeta) + b(k)U(l\zeta)l \int U^{-2}(l\zeta) d\zeta \\ &\sim a(k)U(l)(1 + \delta \ln \zeta) + b(k)U^{-1}(l)l(1 + \delta \ln \zeta) \int (1 + \delta \ln \zeta)^{-2} d\zeta \\ &\sim a(k)U(l)(1 + \delta \ln \zeta) + b(k)U^{-1}(l)2\kappa^2\delta\zeta \end{aligned} \quad (28)$$

where we have truncated the expansion at $O(\delta)$, to give the so-called "2-term inner expansion of the one-term outer expansion", and have used the relation

$$l = 2\kappa^2\delta. \quad (29)$$

According to the asymptotic matching principle (van Dyke, 1975), this must agree with the "one-term outer expansion of the two-term inner expansion". The inner solution available at this stage is

$$\begin{aligned} w &= \mu[ik_1 f(\mathbf{k})U(l\zeta) + w_d] = \mu[ik_1 f(\mathbf{k})U(l\zeta) + \delta U(l)w_d^{(1)}] \\ &= \mu[ik_1 f(\mathbf{k})U(l)(1 + \delta \ln \zeta) + \delta\{-i(k^2/k_1)(2\kappa^2\sigma^{(0)}(\mathbf{k})U(l)\zeta\}] \end{aligned} \quad (30)$$

and this is the one-term outer expansion of the two-term inner expansion. We note that the match is complete provided we take $a(\mathbf{k})$ as already given in (7b), and

$$b(\mathbf{k}) = -i(k^2/k_1)\sigma^{(0)}(\mathbf{k})U^2(l). \quad (31)$$

Using (17d), we can write this in terms of the outer perturbation pressure as

$$b(\mathbf{k}) = i(k^2/k_1)p(0, \mathbf{k}). \quad (32)$$

This is an excellent check on our analysis, by comparison with (12), since as we have already shown, $b(\mathbf{k})$ is completely determined by the outer flow and matching is not required to fix it.

Our analysis shows that the c.p (common part) of the inner and outer expansions for w is the inner expansion itself, so the the outer solution is uniformly valid, and correctly gives w (to order δ) throughout the flow.

To find the appropriate situation for the horizontal velocity components, we expand the inner solution in outer variable by setting $\zeta = Z/l$, and expand holding Z fixed. This gives, for the x -component (of the Fourier transform),

$$\begin{aligned} \mathbf{u} \cdot \mathbf{e}_x &= U(Z) + \mu U(l) [u_d^{(0)}(Z/l, \mathbf{k}) + \delta u_d^{(1)}(Z/l, \mathbf{k}) + O(\delta^2)], \\ &\sim U(Z) + \mu U(l)\sigma^{(0)}(\mathbf{k}) [1 + \delta\{-\ln(Z/l) + (k^2/k_1^2)\} + O(\delta^2)] \end{aligned} \quad (33)$$

and for the y -component

$$\mathbf{u} \cdot \mathbf{e}_y \sim \mu U(l) (k_2/k_1)\sigma^{(0)}(\mathbf{k}) [1 - \delta \ln(Z/l)]. \quad (34)$$

The outer solution for $\mathbf{u} \cdot \mathbf{e}_x$, when written in inner variables and expanded, is (using (6f))

$$\begin{aligned} \mathbf{u} \cdot \mathbf{e}_x &= U(z) + \mu u = U(z) + \mu [-p(Z, \mathbf{k})/U(Z) + i[U'(Z)/U(Z)] [w(Z, \mathbf{k})/k_1]] \\ &\sim U(z) - \mu U'(Z)f(\mathbf{k}) + \mu \sigma U(l) \{1 + \delta[-\ln \zeta + k^2/k_1^2]\}, \end{aligned} \quad (35)$$

where we have used (1), (17d), and (31) in going from the first line to the second. Since $U(z) - \mu U'(Z)f(k) = U(Z)$ in the outer layer with an error of $O(\mu^2)$, we see that the expansion (35) of the outer solution matches precisely with the (33), when the latter is reexpressed in inner variables. Similarly, the outer solution for $u \cdot e_y$, is, from (6e)

$$u \cdot e_y = -\mu(k_2/k_1) p(Z,k)/U(Z)$$

and when expanded in inner variables, this agrees with the outer expansion (34) of the inner solution.

We therefore have shown that the c.p. of the perturbation to $u \cdot e_x$ is

$$\mu \sigma U(l) \left\{ 1 + \delta[-\ln \zeta + k^2/k_1^2] \right\},$$

and that the corresponding c.p. for $u \cdot e_y$ is the right hand side of (34).

3.2 Composite expansions

Additive composite expansions may be obtained by adding the expansions in the inner and outer regions and subtracting the common part, and are uniformly valid throughout the flowfield. The composite expansion for the velocity vector is

$$\begin{aligned} u = & \left\{ U(z) + \mu \left[-p(Z,k)/U(Z) + i[U'(Z)/U(Z)] [w(Z,k)/k_1] + \right. \right. \\ & \left. \left. 4\delta(p(0,k)/U(l))K_0(2(ik_1\zeta)^{1/2}) \right] \right\} e_x \\ & + \left\{ -\mu(k_2/k_1) p(Z,k)/U(Z) + 2\delta(p(0,k)/U(l))(2^{1/2}k/|k_1| + k_2/k_1) K_0(2(2ik_1\zeta)^{1/2}) \right\} e_y + \\ & \mu w(Z,k) e_z \end{aligned} \quad (36)$$

The solution is fully determined provided equation (6) is solved, a task that in general must be carried out numerically.

3.2 Computational strategy

Given an upwind flow, for each wavenumber vector \mathbf{k} , the function Σ is known and the problem (6) for w (and p) is set. In view of the boundary condition (7), it is useful to let

$$w(Z, \mathbf{k}) = ik_1 f(\mathbf{k}) U(Z) Q(Z, \mathbf{k}) \quad (37)$$

in which case $Q(Z, \mathbf{k})$ satisfies the equation

$$Q'' + 2(U'/U)Q' + (k^2/k_1^2)\{N^2/U^2 - k_1^2\}Q = 0 \quad (38)$$

and boundary conditions

$$Q(0, \mathbf{k}) = 1 \quad (39)$$

and the same asymptotic condition ((8) or (9)) satisfied by w . For each wavenumber pair, the problem (38,39) can be solved by any convenient numerical method. Perhaps the easiest is integration by a standard shooting algorithm such as Runge-Kutta. Beginning at a suitable approximation of $Z = \infty$, say a value of Z at which tolerances for $(N^2 - N_0^2)/N_0^2$ and U'' are jointly met, one selects a small value, say 10^{-3} for Q and $-m$ times this value for Q' , where m is the coefficient of Z in the exponential factor of either (8) or (9), and integrates (6) as an initial value problem towards $Z = 0$. If the value obtained at $Z = 0$ is called γ , then the solution to the boundary value problem is $ik_1 f(\mathbf{k})/\gamma$ times the solution generated by the integration procedure. Then w is found from this solution Q from (37) and p may be found from (6d) to be

$$p(Z, \mathbf{k}) = f(\mathbf{k})(k_1^2/k^2)U^2 Q'(Z, \mathbf{k}). \quad (40)$$

A workable computational strategy then begins with a (double) fast Fourier transform of $f(x, y)$ with x and y discretized on a 2D mesh (here we only note that the mesh intervals should be fine enough to resolve the significant features of the terrain, but do not consider the practically important issues of smoothing, etc.). Then Q is found at each \mathbf{k} , w and p are formed from Q , and the composite expansion (36) is constructed (the modified Bessel functions of complex arguments are easily calculated using rational approximations to the Kelvin functions \ker and \kei - see Abramowitz and Stegun, 1965). An inverse

double FFT completes the solution. This procedure can be implemented on a microcomputer in reasonable computational times.

References

- Abramowitz, M. and Stegun, I. 1965. *Handbook of Mathematical Functions*, Dover.
- Forsyth, A.R. 1900. *Theory of Differential Equations*, vol IV, Camb. Univ. Press.
- Rosenhead, L. 1964. *Laminar Boundary Layer Theory*, Oxford Univ. Press, sec. V.8.
- Van Dyke, M. 1975. *Perturbation Methods in Fluid Mechanics*, Parabolic Press.
- Walmsley, J.L., Salmon, J.R., and Taylor, P.A. 1982. On the application of a model of boundary layer flow over low hills to real terrain, *B.L. Met.* **23**,17-46.

Chapter C

**Stratified shear flows over low hills
I. Effects of upwind shear**

Prepared by
J.C.R. Hunt, S. Leibovich, and K.J. Richards

SUMMARY

A general analysis is developed for turbulent shear flows over two- and three-dimensional hills with low slopes which allows for a wide range of upwind conditions, including weak stable or unstable stratification, wakes of upwind hills, or roughness changes. In this paper (part I) the atmosphere is assumed to be neutrally stable and the length of the hills, L , is large compared their heights, H , which is very large compared to the roughness length z_0 . The general structure of the solution is defined by dividing the flow into two regions, each of which is divided into two sublayers: an inviscid outer region composed of an upper layer in which there is potential flow when the atmosphere is neutrally stable, and a middle layer in which the wind shear dominates; and an inner region of thickness $l \ll L$ in which the effects of perturbation shear stresses are confined. Following Sykes (1980), the latter region is divided into two: a shear stress layer where the shear stresses, although weak, determine that the maximum of the perturbation velocity is located in this layer; and an inner surface layer of thickness l_s where the shear stress gradient varies rapidly and the perturbation velocity tends to zero. The details of the middle layer are given here for different kinds of upwind profiles, including logarithmic, 'power law' and linear profiles. It is shown that the analysis can be extended to allow for nonlinear inertial effects in the middle layer. Analytical solutions are derived for the inner region as asymptotic expansions in $\delta = [\ln(l/z_0)]^{-1}$, which is assumed to be small, and this shows that $l_s \sim z_0(l/z_0)^{1/2}$.

The results of the analytical model are compared with our own and with previously published numerical computations of the full equations (applying the same assumptions used for calculating the turbulent shear stresses as used in the analytical work), which have largely been validated against full scale measurements. These results confirm that the relative increase of surface stress is significantly greater than the increase of wind speed

near the surface except when there is no upwind shear (as for example in a logarithmic boundary layer when the roughness length tends to zero - the asymptotic limit studied by Sykes, 1980).

Finally, the paper shows that the outer regions of laminar (or constant eddy viscosity) and of turbulent flows over hills are broadly similar, but that the effects of the flow in the inner region on the outer regions are much smaller in the latter case.

1. INTRODUCTION

There are three main effects to consider in an analysis of stratified or diabatic flows over hills. The first is that of the changes in the vertical profile of the mean velocity upwind of the hill caused by the upwind mean velocity and temperature gradients, and the shear stresses near the surface; the second is that of buoyancy forces associated with the upwind temperature distribution and adiabatic processes along streamlines, and the third is that of buoyancy forces associated with heat transfer from the surface and across streamlines (e.g. the buoyancy forces associated with kata- and anabatic winds).

Our object is to develop general methods for calculating and understanding the airflow and temperature distributions over hills with low slopes when there are significant gradients of velocity and temperature upwind of the hills (see figure 1). If the hill height is H , its length at half-height is $2L$, and the roughness length is z_0 , the situations we consider satisfy the criteria $H/L \ll 1$ and $0 < \ln^{-1}(L/z_0) \ll 1$. This effort is divided into two parts. In this first paper, we concentrate on the first of the above effects, namely, the effect on the flow over hills of different upwind velocity gradients, and of different kinds of flow very close to the surfaces of the hills. The analysis can also be applied to other kinds of complex approach flows, such as may be caused by a turbulent wake from an upwind hill, and in general to any large scale, slow disturbances to turbulent boundary layers.

In the second paper we use the analysis of the present paper to consider the effects of buoyancy forces when the upwind flow is stably or unstably stratified. The approach in these papers is similar to that of Jackson & Hunt (1975) and of Sykes (1980), hereafter known as (JH) and (S) respectively, in that a perturbation analysis is developed and the flow is divided up into an inviscid outer region and a thin inner region where the perturbation shear stresses affect the perturbed flow. In these previous analyses, done for neutral stability, the perturbation flow in the outer region was found to be the same at zero order (in $\ln^{-1}(L/z_0)$) as that of potential flow with a constant velocity upwind. Only at first order in $\ln^{-1}(L/z_0)$ were the effects of shear allowed for, because the only neutral

conditions considered were those where the upwind velocity profile is logarithmic. For this case, Sykes has shown that this potential flow approximation is formally correct only in neutral flows where $\ln^{-1}(L/z_0) \rightarrow 0$ and for hills whose height is much greater than the thickness (l) of the inner region. Jackson (1976) and JH, by an approximate blending of a two-layer description, were able to obtain reasonable estimates of the velocity to be found even when the conditions in S were not satisfied.

It is one of the aims of the present paper to obtain solutions valid over a range of upwind profiles (caused, for example, by values of ϵ , a dimensionless friction velocity, or of the roughness length, z_0 , different from that over the hill or shaped by upwind obstacles), and to show that the matching of solutions between the inner and outer regions can be formally justified only if an intermediate, middle, layer is constructed in the outer region. (In JH, pressure matches but the horizontal perturbation velocity does not; furthermore, the matching turns out to be correct only if the hill height $H \ll l$, which is clearly restrictive.)

Sykes also showed that JH's approximate solution for the inner region, which has a thickness l , is not a mathematically consistent asymptotic analysis (for small values of $\delta = \ln^{-1}(l/z_0)$), because the inner region is actually made up of two layers. The deeper of these inner region layers is where the perturbation shear stress decreases from its large value near the surface, but the perturbation velocity is only affected by the shear stress to first order. This is the *shear stress layer*. Very close to the surface in the *inner surface layer*, the perturbation velocity decreases to zero and is controlled to zero order by the shear stress. Toward the bottom of the shear stress layer, the gradient of the shear stress increases logarithmically. In the inner surface layer this gradient reaches a finite value. The calculation of this transition, which has not previously been analysed, is of practical importance in predicting heat and mass transfer, since the gradient of diffusivity near the surface is effectively determined here. We derive new general solutions for two inner layers which match with each other and with the middle layer.

For neutral conditions there have been several experiments where the basic ideas of JH theory have been tested (Bradley, 1980, 1983; Britter *et al.*, 1981; Mason & King, 1985). The theory has been generalised to three-dimensional hills by Mason & Sykes (1979), and to hills with small-scale undulations (Walmsley *et al.*, 1982). Computations have also been made of the full nonlinear equations using a similar mixing length model for the turbulent shear stress (e.g. Mason & King, 1985; Taylor *et al.*, 1983). The comparisons have shown that the JH theory gives a useful estimate for the perturbation (or speed up), u , in wind speed and in the perturbation surface shear stress, τ' , over hills and for the depth over which the shear stress is significantly increased near the surface. But it does *not* agree with the form of the observed profiles of u or τ' in the inner region, and in particular with the observations that over a hill top, u has a maximum at a height of about $l/3$ and that τ' has a negative value at the top of the inner layer of about the same magnitude as the positive value at the surface (Mason & King, 1985; Taylor *et al.*, 1984).

In order to overcome such shortcomings, Taylor *et al.* (1983) and Mason & King (1985) have made heuristic adjustments to the JH model. These modifications have proved of practical value, but as their authors admit, they are not based on improved solutions to the governing equations and do not indicate how the models might be applied in other conditions when the heuristic adjustments might not be applicable.

The analyses of JH, S, Taylor *et al.* (1983), and Mason & King (1985) are not valid, however, when the upwind flow is strongly sheared, as in stably stratified boundary layers, in wakes, in terrain where the roughness is changing, or when the height of the hill is large compared with the inner region thickness. In parts I and II of this series, the effects of strong shear are accounted for, although the flow is analysed in detail only when the thin inner region of the stratified flow may be considered locally neutral and the significant effects of stratification are confined to the outer region.

One of the major effects of strong shear in the approach flow is the large relative increase in the surface wind speed, even when the slope of the hill is small. In this and in

other cases, ignoring nonlinear inertial effects can lead to errors comparable to those associated with approximations for turbulent shear stresses (Britter *et al.*, 1981). In this paper we show that these nonlinear effects can be estimated so that useful results can be obtained, even for moderate accelerations. The results are similar to those obtained by nonlinear calculation of velocity along the streamlines (Bouwmeester, 1978; Zeman & Jensen, 1987).

Some solutions for stratified flow over hills have been obtained using laminar flow or constant eddy viscosity assumption (e.g. Sykes, 1978). In sections three and five we delineate some of the major differences between laminar and turbulent boundary layer flows, both in terms of the surface shear stress distribution and the effects of the inner region of the outer flow.

2. THE UPWIND FLOW AND THE OUTER REGION

We begin by describing the decomposition of the flow into the two main regions and their sublayers, in which the flow is determined by different physical processes. The flow will be analysed by considering each layer in turn, and then matching the solutions together.

2.1 Normalising the upwind profile

The mean flow in the boundary layer upwind of the hill is taken to be in the x -direction, prescribed as a function $U_B(z)$ of the elevation z above a reference plane. We are interested in the perturbation of this basic flow caused by topography rising above the plane $z = 0$ and extending for horizontal length scales comparable to a distance L .

For simplicity, we are thinking of a single hill with height H and a characteristic length L taken to be the distance between the points corresponding to the half-height of the hill. For some calculations it is more instructive to consider a periodic array of hills of wavelength $(2\pi k)L$, where k is dimensionless. The root-mean-square value of turbulent velocity fluctuations in the basic and perturbed flows are taken to be of the order of u_* , the friction velocity in the unperturbed flow.

Under neutral conditions, the mean profile upwind is characterised by two length scales, the roughness length z_0 and the depth h of the boundary layer, and the velocity levels are characterized by the wind speed U_∞ above the layer. The usual approach is to express U_B in terms of a normalized profile function U_1 as

$$U_B(z) = U_\infty U_1(z/z_0, z/h).$$

This is not adequate, however, if the length L of the hill or surface disturbance is much less than the boundary layer depth, but much greater than z_0 : under these circumstances, the depth over which the flow is disturbed may be significantly less than h . In such cases, the relevant upwind speed is not U_∞ , but the velocity U_0 at a height h_m that is intermediate between L and the height of the hill or (refer to figure 1)

$$U_0 = U_B(h_m).$$

This height (at which the vertical velocity perturbation is *maximum*) defines the depth h_m of the middle layer. In this layer, the velocity field is made up of the upwind boundary layer displaced over the hill plus a velocity perturbation which depends on the slope of the hill. This displaced profile is defined in a normalised form as

$$(2.1) \quad U_B(Z) = U_0 U(Z), \text{ where } Z = z - H f(x/L).$$

This is the relevant choice for the 'base', or unperturbed profile because of the large gradients in the upwind profile near the ground. The definition of h_m depends on the form of the profile $U_B(z)$ and on the length scale L of the hill. (Note that if the hill shape has several scales, the flow can be treated as the superposition of flows over hills of each constituent length, for each of which the definition of h_m is based on the appropriate length. This is the method adopted by Taylor *et al.*, 1983.)

It is assumed that the middle layer is thin compared to the length of the hill, but very deep compared to the roughness length z_0 ,

$$z_0 \ll h_m \ll L.$$

Note that for hills much longer than the boundary layer depth h , no distinction between h and h_m is needed.

The dimensionless function U in (2.1) is assumed to have small variations (on a scale L) for $z/h_m \geq 1$, while near the surface, as $z/h_m \rightarrow 0$, $U \sim (\epsilon/\kappa) \ln(z/z_0)$ for fixed z/z_0 . Here $\epsilon = u_*'/U_\infty$ and we treat ϵ as one of the basic small parameters in the problem. (In most turbulent boundary layers, ϵ is in the range 0.03 to 0.07.) In cases where $U_B(z)$ is the profile of a neutral boundary layer passing over a flat surface, the dimensionless profile function is given by $U = 1 + O(\epsilon)$ as $z/z_0 \rightarrow \infty$. Since we wish to allow for cases where stronger shear may be present in the upwind flow, as may occur if the upwind conditions shaping the flow are more complicated, or if stratification is important, we do *not* assume that $U(Z/z_0, Z/h_m) = 1 + O(\epsilon)$.

The changes forced by the hill arise on horizontal scales of $O(L)$ and on this scale the ratio of Reynolds stress gradients to inertia is $O(\epsilon^2)$, which implies that on this length scale, there is an upper layer (U) in which the mean flow may be treated as inviscid and (because of the assumption on the upstream flow) irrotational.

On length scales of $O(h_m)$, the ratio of Reynolds stress gradients $[O(u^2/h_m)]$ to inertia stresses of $O(U_0^2/L)$ is $O(\epsilon^2 L/h_m)$, which is also assumed to be small enough to be neglected to a first approximation. Thus, the mean flow in this (M) layer may be treated as *inviscid but rotational*. Finally, there must be an inner region (I) extending to a distance l (which must be determined in terms of the other parameters of the problem but which is assumed to be small compared with h_m) above the surface in which changes in the Reynolds stresses are comparable with the perturbation in the inertial and pressure gradient forces (or in the balance between these forces).

The division of the inviscid, or outer, region of the flow into two layers is dictated by the structure of the incident stream. This division is convenient in that it allows us to find the explicit form of the inviscid solutions at their lower levels. In the middle layer (M), extending from a distance of $O(l)$ to a distance of $O(h_m)$ above the hill surface, the upwind velocity gradient is large enough that the horizontal acceleration is determined by the perturbation of the upwind vorticity, which (as §2 shows) implies that

$$L^{-2} \ll |U_B^{-1} d^2 U_B / dz^2| \sim (z^2 \ln(z/z_0))^{-1}$$

for a logarithmic profile.

Thus for very long hills where $L > h$, the above criterion is satisfied for $z < h$ and therefore $h_m = L$. But for shorter hills where $L \ll h$, the middle layer depth is given by

$$h_m \sim L \ln^{-1/2}(h_m/z_0).$$

When $\ln(L/z_0) \gg 1$, h_m can be expressed explicitly by

$$(2.2) \quad h_m \sim L \ln^{-1/2}(L/z_0).$$

For turbulent boundary layers, the middle region over hills has not been properly analysed before, though its importance for disturbances to laminar boundary layers is well known (Stewartson & Williams, 1969; Brighton, 1977). However, the middle layer has been analysed where turbulent boundary layers are perturbed by an external pressure gradient (e.g. Messiter, 1978; Melnik & Chow, 1975.) This region is essential for proper matching of the inner layer (I) and the upper layer (U) (which was not done by JH).

The upper layer begins at distances of $O(h_m)$ from the surface and extends upward through and beyond the incident boundary layer. In this layer, the upwind velocity gradients are negligible, so that

$$L^{-2} \gg |U_B^{-1} d^2 U_B / dz^2|.$$

If one chooses to analyse this problem using formal asymptotic procedures, it is necessary to relate the various length scales to a single length scale (say L), and the asymptotically-small parameter $\epsilon = u^*/U_\infty$. Here we develop a perturbation analysis in the 'engineering' style; this allows us to proceed in a more flexible way with approximate relationships between the variables emerging *a posteriori*, although with the penalty of less definite error estimates. (In appendix B we develop the first three terms of an asymptotic solution for the middle and upper layers.)

2.2 Mathematical statement of the problem

When the upwind conditions are steady in the mean (i.e. steady on a time scale large compared with that of the largest eddies or the time required to pass over the hill), the governing equations for a stratified flow with mean velocity u^* (asterisks will be used to

denote dimensional quantities), the mean pressure p^* and mean density ρ^* are, (in the Boussinesq approximation)

$$(2.3a) \quad (\mathbf{u}^* \cdot \nabla) \mathbf{u}^* = - \frac{1}{\rho_0} \nabla p^* + \frac{1}{\rho_0} \nabla \cdot \boldsymbol{\tau}^* + \mathbf{g}^* \frac{\rho^*}{\rho_0}$$

$$(2.3b) \quad \nabla \cdot \mathbf{u}^* = 0$$

$$(2.3c) \quad (\mathbf{u}^* \cdot \nabla) \rho^* = - \nabla \cdot \mathbf{F}_\rho^*,$$

where ρ_0 is the density at a fixed point, $\boldsymbol{\tau}^*$ is the Reynolds stress tensor, and \mathbf{F}_ρ^* is the mean flux of density. Buoyancy forces are considered in Pt. II; they are not considered further here. The equation relating $\boldsymbol{\tau}^*$ to \mathbf{u}^* is always only approximate, and is discussed in the analysis of the inner region in §3.

The boundary conditions for the analysis are that far from the hill:

$$(2.4a) \quad \mathbf{u}^* \rightarrow U_0(U(z), 0, 0) \text{ and } p^* \rightarrow \rho_0 U_0^2 P(z) \text{ as } (x^2 + y^2 + z^2)/L^2 \rightarrow \infty,$$

while over the surface:

$$(2.4b) \quad \mathbf{u}^* = 0 \text{ on } z = Hf(x/L, y/L) + z_0$$

where z_0 is the very small roughness length. (The analysis in the body of the text is mainly two dimensional, for a three-dimensional hill, see appendix A.) The assumptions of the analysis are that

$$(2.4c) \quad H/L \ll 1 \quad \text{and} \quad \epsilon = u_* / U_0 \ll 1,$$

which implies that $\ln(L/z_0) \gg 1$.

For the upper layer where $z > h_m$, the mean velocity $\mathbf{u}^* = (u^*, v^*, w^*)$ is expressed in terms of the upwind profile $U_B(z)$ and a perturbation, normalized on U_0 as:

$$u^* = U_0(U(z) + u(x, y, z)), \quad v^* = U_0 v$$

$$(2.5a) \quad w^* = U_0 w.$$

The pressure p^* is also normalized on U_0 , so that $p^* = \rho_0 U_0^2 (P+p)$ where ρ_0 is the density in the approach flow. (We shall also use this form of perturbation to analyse the middle layer).

For the middle layer and the inner region, u^* is expressed in terms of the *displaced* upwind profile $U_0 U_d(Z)$ and a perturbation defined in terms of the displaced coordinates (x,y,Z) , where $Z = z - Hf(x/L, y/L)$:

$$u^*(x,y,z) = U_0 u_d^\dagger(x,y,Z), \quad w^* = U_0 w_d^\dagger$$

where

$$\begin{aligned} u_d^\dagger &= U_d(Z) + u_d(x,y,Z) \\ (2.5b) \quad w_d^\dagger &= (U + u_d) (H/L) f'(x/L, y/L) + w_d(x,y,Z) \\ p &= p_d(x,y,Z), \end{aligned}$$

and f' represents a derivative of f with respect to the argument (x/L) . The dagger superscript indicates dimensionless total quantities, that is, the sums of unperturbed and perturbation quantities.

2.3 Analysis of the outer regions, layers (U) and (M)).

Upper layer.

For the upper (and middle) layer u, v, w are determined by the linearized form of the momentum equation (2.3a) (with buoyancy forces omitted and shear stress gradient assumed small, as justified later in this paper- see also JH)

$$(2.6a) \quad U(z) \frac{\partial u}{\partial x} + w \frac{\partial U}{\partial z} = - \frac{\partial p}{\partial x}$$

$$(2.6b) \quad U(z) \frac{\partial v}{\partial x} = - \frac{\partial p}{\partial y}$$

$$(2.6c) \quad U(z) \frac{\partial w}{\partial x} = - \frac{\partial p}{\partial z}$$

$$(2.6d) \quad \frac{\partial u}{\partial x} + \frac{\partial v}{\partial y} + \frac{\partial w}{\partial z} = 0$$

These can be reduced to single equation for w :

$$(2.6e) \quad \left(\frac{\partial^2}{\partial x^2} + \frac{\partial^2}{\partial y^2} + \frac{\partial^2}{\partial z^2} - \frac{d^2 U/dz^2}{U} \right) w = 0 ,$$

which in two-dimensions is further reduced to

$$(2.6f) \quad \left(\frac{\partial^2}{\partial x^2} + \frac{\partial^2}{\partial z^2} - \frac{d^2 U/dz^2}{U} \right) w = 0$$

The terms omitted in this linearization are of $O(w^2/U^2)$.

The upper layer (U) is defined as the layer where the gradients of the upwind velocity profile can be largely ignored to the first order, since

$$(w)^{-1} (\partial^2 w / \partial x^2) \gg U^{-1} \partial^2 U / \partial z^2$$

Where this holds, (2.6) reduces to

$$(2.7) \quad \nabla^2 w = 0.$$

In two dimensions the solution to (2.7) in (U) is

$$(2.8a) \quad w = \frac{1}{\pi} \int_{-\infty}^{\infty} \frac{w^{(MU)}(x') z dx'}{(x-x')^2 + z^2} ,$$

while from continuity

$$(2.8b) \quad u = -p = \frac{1}{\pi} \int_{-\infty}^{\infty} \frac{w^{(MU)}(x') (x-x') dx'}{(x-x')^2 + z^2} ,$$

where $w^{(MU)} = w(z=h_m)$, is the vertical velocity at the interface between the (M) and (U)

layers (see figure 2a). An important parameter for the (M) layer is the pressure field at the

interface $p(z \sim h_m)$, which is expressed in terms of a characteristic magnitude $(-p_0)$ and a normalized function $\sigma(x/L)$ which is $O(1)$. Thus, we write

$$(2.8c) \quad p(z \sim h_m) = p_0 \sigma(x/L).$$

Middle layer.

Given the assumptions of the analysis (2.4), the middle layer for a general three-dimensional hill can be defined to be the layer where $l < z < h_m$ and $h_m \ll L$. Writing the horizontal momentum equation (2.6a) (with no shear-stress terms) in displaced coordinates defined by (2.5b), and neglecting terms in $\partial^2/\partial x^2$ compared with $\partial^2/\partial Z^2$, leads to the ordinary non-linear differential equation for w

$$(2.9a) \quad u_d^\dagger \partial^2 w_d^\dagger / \partial Z^2 - w_d^\dagger \partial^2 u_d^\dagger / \partial Z^2 = 0$$

$$(2.9b) \quad \partial p_d / \partial Z = 0.$$

Note that the leading-order terms omitted in (2.9a) are terms like $u_d^\dagger \partial^2 w_d^\dagger / \partial x^2$ which are of order $U w_d / L^2$. These are smaller than the retained perturbation terms of $O(U w_d / L^2 \times L^2 / h_m^2)$. In (2.9b) the relative error of omitted terms is $O(h_m / L)$ (i.e., $(u_d^\dagger \partial w_d^\dagger / \partial x) / (p_d / h_m) \sim h_m / L$).

The solutions to (2.9) valid for a two-dimensional hill ($z = Hf(x/L)$) are

$$(2.10a) \quad w_d^\dagger = A'(x) u_d^\dagger + B'(x) u_d^\dagger \int_{Z_1}^Z \frac{dZ'}{u_d^\dagger(x, Z')}$$

$$(2.10b) \quad p_d = p_d(x),$$

and the lower limit Z_1 is chosen for convenience to satisfy the criterion

$$l \gg Z_1 \gg z_0,$$

where l is the inner layer thickness. A suitable value for computation is $Z_1 \sim (l z_0)^{1/2}$.

Since (2.3a) can be integrated to Bernoulli's equation in the inviscid middle layer, given $p(x)$, u_d^\dagger can be calculated along a streamline from its upwind height Z_∞ to give

$$(2.10c) \quad u_d^{\dagger 2}(x, Z) = -2p_d(x) + u_d^{\dagger 2}(Z_\infty)$$

where

$$Z_{\infty} = Z - \int_{-\infty}^x \frac{w_d^{\uparrow}}{u_d^{\uparrow}} dx.$$

and the integration is taken along the streamline through (x, Z) .

For low enough values of (H/L) and ϵ the velocity perturbations are small enough that u_d and $w_d \ll 1$. Then (2.10a) reduces to the following expression for the vertical velocity perturbation

$$(2.11a) \quad w_d = [A'(x) - (H/L)f'(x/L)]U_d(Z) + B'(x)Z \{ I(Z)/U_d(Z) \}$$

where

$$I(Z) = 1 + \int_{Z_1}^Z [U_d^2(Z)/Z] \{ U_d^2(Z') - U_d^2(Z) \} dZ'$$

and Z_1 has been introduced already. With w_d given by (2.11a), u_d is determined by continuity to be

$$(2.11b) \quad u_d = - [A(x) - Hf]U_d'(Z) - B(x)J(Z)/U_d(Z)$$

where

$$J(Z) = 1 + U_d U_d' \int_{Z_1}^Z dZ'/U_d^2(Z').$$

The solutions (2.11) extend directly to three dimensions, provided only that f , A , and B are allowed to vary with y . For logarithmic boundary layers, when $Z \gg Z_1$,

$$(2.11c) \quad I(Z) = 1 - 2/\ln(Z/z_0) + O(\epsilon^2)$$

$$J(Z) = 1 + 1/\ln(Z/z_0) + O(\epsilon^2)$$

and so $J(Z)$ decreases slowly with height from its maximum value of $1 + \ln^{-1}(l/z_0)$ at the outer edge of the inner region.

2.4 Matching the (U) , (M) and (I) layers

Matching the linearized solutions for u_d and w_d in the (M) layer (for hills of low enough slope), derived from (2.5) and (2.11), with u_d and w_d in the inner region at $Z \sim l$, and w in the upper layer when $Z \sim h_m$ is performed by matching u and w . This defines the unknown functions $A(x)$, $B(x)$ and $p_d(x)$.

When $Z \sim l$

$$(2.12a) \quad w^{(l)} = U_d(l) (H/L) f' + w_d^{(l)}(x, l); \quad w^{(M)} = A'(x) U_d(l) + B'(x) l U_d^{-1}(l) (1 + O(\epsilon))$$

$$(2.12b) \quad u^{(l)} = U_d(l) + u_d^{(l)}; \quad u^{(M)} = U_d(l) - [A(x) - Hf] U_d'(l) - B(x) J(l) / U_d(l)$$

$$(2.12c) \quad p^{(l)} = p^{(M)}.$$

(Note that these matching criteria are independent of the ratio of l/H , unlike the earlier analysis of JH.)

When $z \sim h_m$, $U_d(Z) = U(z) - HfU'(z)$, so

$$(2.13a) \quad u_d^{(l)}(h_m) = U(h_m) - HfU'(h_m).$$

Also

$$(2.13b) \quad w^{(M)}(x, h_m) = -A'(x) + B'(x) h_m I(h_m) = w^{(MU)}(x),$$

and

$$(2.13c) \quad u^{(M)}(x, h_m) = -A(x)U'(h_m) - B(x)J(h_m) = u^{(MU)}(x) = -p_0\sigma(x).$$

(For logarithmic boundary layer terms of $O(\epsilon)$ are omitted, $U'(h_m) = 0$ and $I(h_m) = J(h_m) = 1$.)

We first match w at the middle layer and inner region interface where $Z \sim l$ using equation (2.12a). We use the fact that $w_d \sim (l/L) u_d$ in the inner layer (by continuity), so that the leading order terms in (2.11a) are $U(l)(H/L)f'$ and $A'(x)U(l)$. Therefore

$$(2.14a) \quad A(x) = Hf(x/L).$$

Matching u at the upper layer and middle layer interface where $Z \sim h_m$, (2.13c) leads to

$$(2.14b) \quad B(x) = [p_0\sigma(x/L) - HfU'(h_m)]/J(h_m)$$

and, using (2.14a),

$$(2.14c) \quad w^{(MU)}(x) = (H/L) f'(x/L) + [p_0\sigma'(x/L) - Hf'(x)U'(h_m)](h_m/L).$$

The leading-order corrections to $w^{(MU)}$ and $B(x)$ are $O(h_m/L)$, which for short hills are of $O(\ln^{-1/2}(L/z_0))$. Therefore from (2.8b), the scale and form of the pressure perturbations can be defined as

$$(2.15) \quad p_0 = -\frac{H}{L}, \quad \sigma(x/L) = \frac{1}{\pi} \int_{-\infty}^{\infty} \frac{f'(x'/L)}{(x-x')} dx'.$$

Substituting the leading terms of these functions back into the general expressions for the displacement velocities in the middle layer in (2.11), we obtain

$$(2.16a) \quad w_d(x, Z) = - (H/L^2) \sigma'(x/L) U_d \int_{Z_1}^Z dZ' / U_d^2(Z')$$

$$(2.16b) \quad u_d(x, Z) = (H/L) \sigma(x/L) J(Z) / U_d(Z)$$

For reference to calculations later, it is convenient to note that these results can be expressed as perturbations relative to the *undisplaced flow*, when $h_m > Z \gg \epsilon H$

$$(2.17a) \quad w(x, z) = H f'(x/L) U(z) - (H/L^2) \sigma'(x/L) U(z) \int_{z_1}^z dz' / U^2(z')$$

$$(2.17b) \quad u(x, z) = - H f(x/L) U'(z) + (H/L) \sigma(x/L) J(z) / U(z).$$

These expressions satisfy (2.6a, c, d) subject to the conditions (2.4c).

From (2.16) the streamline perturbation velocity at the outer edge of the *inner* region is defined by

$$(2.18) \quad u_d^{(l)}(x, Z) \sim (H/L) \sigma(x/L) (1+\epsilon) / U_d(Z)$$

This result (2.18) shows that for $Z \sim l$ the ratio of the perturbation velocity to the upwind velocity, $u_d^{(l)}(Z) / U_d(l)$, is $O[(H/L)(U^2(h_m)/U^2(l))]$. Therefore, even if $H/L \ll 1$ (so that u/U is small in the (U) layer), the shear in the upwind profile may be large enough that $[U(h_m)/U(l)]H/L \sim 1$, so that in (M) the perturbation velocity is of the same order as the upwind velocity. In this case the *non-linear* solution for (M) , (2.10), is applicable at the same time as the *linear* solution in (U) is applicable. And then the *same* functions $A(x)$,

$B(x)$, $p(x)$ obtained in (2.14) from the linear analysis can be used in the non-linear expression (2.10). This is of some practical importance, and is discussed further in §6. (This is the basis of the recent computation by Zeman & Jensen 1987).

Note that the results of the correct matching between the inner and middle layer leads to the similar estimate for u_d in the inner region as the approximate matching between the outer and inner region by JH. Since the pressure is the same in the lower part of the upper layer, and in the inner region, matching p leads to the correct expression for u in the upper layer and for u_d in the inner region; but without an analysis of the middle layer, there could be no proper transition between these layers.

The first-order correction of $O(h_m/L)$ shows how p varies in the upper and middle layers. (see Appendix B and fig. 4). For example, when $L/z_0 = 10^6$ and 10^4 , $h_m/L = 0.26$ and 0.33 respectively.) So that even for hills of moderately large scale ($L \sim 10^3$ m), there are significant variations of pressure within the middle layer (but $\partial p_d/\partial Z$ is still small compared with p_d/h_m , in agreement with (2.9b)). Where a hill has a large curvature near its peak, the decrease in pressure is even more marked, as was found by Bouwmeester (1978) in their wind-tunnel studies of air flow over triangular model hills. The changes in curvature of the p profile in (M) have also been demonstrated by the computations of Newley (1986). In all the subsequent analysis, only the lowest order expression for perturbation pressure p is used.

For short hills where $L < h$, essentially we have solved the equation (2.6f) by assuming $d^2U/dz^2/U$ is discontinuous at $z = h_m$. This leads to a discontinuity in $\partial^2 w/\partial z^2$, but $\partial w/\partial z$ and $\partial u/\partial x$ are continuous across the top of the layer. (Using Fourier transforms and defining h_m for each wavenumber this discontinuity is deferred to third order). In either case, the error is negligible for practical purposes.

2.5 Solution for the upper layer

For a three-dimensional hill, from the straightforward generalization of (2.15) derived in Appendix A, σ is a function of x and y given by

$$(2.19) \quad \sigma(x/L, y/L) = \frac{1}{\pi} \int_{-\infty}^{\infty} \int_{-\infty}^{\infty} \frac{(\partial f / \partial x)(x', y') \bullet (y - y') dx' dy'}{[(x - x')^2 + (y - y')^2]^{3/2}}.$$

Thence from (2.11) and (2.15) the magnitudes for u_d and w_d and p_d in the middle region (M) are determined; v_d in region (M) can be calculated from (A.7c).

In region (U), it is convenient to use the scale L to normalize the magnitude of velocity perturbations on the slope and their distribution so that,

$$\{u^{(U)}, v^{(U)}, w^{(U)}\} = (H/L) \left\{ \sigma(x/L, y/L) G_u(x/L, y/L, z/L), \left(\int_{-\infty}^{\infty} \frac{\partial \sigma}{\partial y} dx \right) G_v\left(\frac{x, y, z}{L}\right), \frac{\partial f}{\partial x}\left(\frac{x, y}{L}\right) G_w\left(\frac{x, y, z}{L}\right) \right\}$$

where the profile functions $G_u, G_v, G_w \rightarrow 1$ as $z/L \rightarrow 0$, and $G_u, G_v, G_w \rightarrow 0$ as $z/L \rightarrow \infty$.

In two-dimensions, ignoring terms of h_m/L or smaller, these distribution functions are

$$(2.20) \quad \left[\sigma G_u, \frac{\partial f}{\partial x} G_w \right] = \frac{1}{\pi} \int_{-\infty}^{\infty} \frac{\frac{\partial f}{\partial x}(x'/L) \bullet [(x - x'), z] dx'}{(x - x')^2 + z^2}$$

and in three-dimensions

$$(2.21) \quad \left[\sigma G_u, \int_{-\infty}^x \frac{\partial \sigma}{\partial y} dx \bullet G_v, \frac{\partial f}{\partial x} G_w \right] \\ = \frac{1}{2\pi} \int_{-\infty}^{\infty} \int_{-\infty}^{\infty} \frac{\frac{\partial f}{\partial x}(x'/L, y'/L) \bullet [(x - x'), (y - y'), z] dx' dy'}{[(x - x')^2 + (y - y')^2 + (z - z')^2]^{3/2}}.$$

3. Inner Region

3.1 Scalings

In the inner region, the velocity perturbations to the displaced upwind profile and pressure perturbations are defined by (2.5b). In addition we now consider Reynolds shear stresses, which are expressed in terms of the upwind values $\rho_0 u_*^2 = \epsilon^2 \rho_0 U_0^2$ as

$$(3.1) \quad \tau = \epsilon^2 \rho_0 U_0^2 [1 + \tau_d(x, Z)]$$

Since the thickness of the inner region l is small compared with the length of the hill L , $\partial/\partial x \ll \partial/\partial Z$, and the linearized momentum equation reduces to

$$(3.2a) \quad U(Z) \frac{\partial u_d}{\partial x} + w_d \frac{\partial U}{\partial Z} = - \frac{\partial p_d}{\partial x} + \epsilon^2 \frac{\partial \tau_d}{\partial Z}.$$

The continuity equation for the inner region is

$$(3.2b) \quad \frac{\partial u_d}{\partial x} + \frac{\partial w_d}{\partial Z} = 0$$

Variations of p_d with Z in the inner layer are negligible, but this may not be so in strongly stratified flows (see Hunt & Richards, (1984)).

Two approaches are possible to determine the thickness l of the inner layer and the order of magnitude of τ_d . By considering the flow very close to the surface, where the velocity profiles is assumed to be logarithmic, u_d , and τ_d are related by

$$U(Z) + u = \epsilon/\kappa (1 + \tau_d/2) \ln (Z/z_0)$$

where

$$(3.3a) \quad U(Z) = (\epsilon/\kappa) \ln (Z/z_0), \quad u_d = (\epsilon \tau_d / 2 \kappa) \ln (Z/z_0).$$

Thence over a small distance above the surface *of the order of* z_0 , it follows that

$$(3.3b) \quad \tau_d = 2u_d/U(Z) = O(\epsilon^{-1} u_d).$$

Alternatively, it can be assumed that the mixing length theory applies approximately through the inner layer (as used by Taylor & Gent 1974; Deaves 1980). In that case for small perturbations (following JH)

$$(3.4a) \quad \epsilon^2 \tau_d = 2\kappa \epsilon Z \partial u_d / \partial Z, \quad \text{or} \quad \tau_d = 2\kappa \epsilon^{-1} Z \partial u_d / \partial Z.$$

Note that (3.4a) includes the effect of a perturbation to the eddy 'viscosity' which exactly equals the contribution from the original eddy viscosity and the perturbation velocity gradient.

Thence, when $\ln(Z/z_0) = O(1)$, we recover the same result as (3.3b).

The magnitude of τ_d can also be expressed in terms of the perturbation velocity at the top of the inner layer, where $Z \sim l$. Since, as we shall show, u_d is proportional to $\ln(Z/z_0)$, it follows that

$$(\partial u_d / \partial Z)(l) \sim u_d(l) / [l \ln(Z/z_0)].$$

Therefore $\partial u_d / \partial Z \ll u_d / l$ and

$$(3.4b) \quad \tau_d(l) = O[\varepsilon^{-1} u_d(l) / \ln(l/z_0)].$$

Substituting (3.4a) into (3.2) yields an equation for the velocity and pressure fields

$$(3.5) \quad (\varepsilon/\kappa) \{ \ln(Z/z_0) \partial u_d / \partial x + w_d / Z \} = - \partial p_d / \partial x + \partial (2\varepsilon \kappa Z \partial u_d / \partial Z) / \partial Z.$$

From the Z-component of momentum, we determine that pressure variations across the inner layer are of $O(\delta^2)$, where $\delta = \ln^{-1}(l/z_0)$. When Z/l is $O(1)$, to leading order in ε the inertial and pressure gradient terms balance (as in the middle layer), so to leading order the shear stresses do not affect the velocity profile. But to the next order, the inertial and shear-stress terms are in balance. Since $\partial/\partial x \sim 1/L$, it follows that the balance of the first order terms leads to an estimate for the thickness of the layer for the first order terms, viz

$$(3.6) \quad l \ln(l/z_0) = 2 \kappa^2 L,$$

following JH and (S) (though by a different argument!). (As we shall see the maximum gradients of u_d occur on a much smaller scale than l .)

3.2 Solution for the shear-stress layer

The solution for u_d to (3.5) when $\ln(l/z_0) \gg 1$ is most easily derived and best understood by dividing the inner region into two layers, a *shear-stress (SS) layer* where $z_0 \ll l_s < Z < l$, and an *inner surface (IS) layer* where $z_0 < Z < l_s \ll l$ (as suggested by Sykes (1980) for a specific scaling of a hill in the limit $\ln(l/z_0) \rightarrow \infty$). The magnitude of l_s/l follows from the detailed analysis (Sykes, 1980 suggested $l_s \sim z_0$; Mason & King, 1986 and Jensen, 1985 have suggested $l_s \sim \delta l$: neither estimate was based on solutions to the equations).

In the shear-stress layer, the natural coordinates are $X = x/L$ and $\zeta = Z/l$ and the asymptotically small parameter is $\delta = \ln^{-1}(l/z_0)$. The variables have the following scaling for the leading-order and first-order terms

$$(3.7a) \quad u_d = - (p_0/U(l)) \{ u_d^{(0)}(X, \zeta) + \delta u_d^{(1)}(X, \zeta) + \dots \}$$

$$(3.7b) \quad w_d = - (p_0/U(l)) \{ \delta w_d^{(1)}(X, \zeta) + \delta^2 w_d^{(2)}(X, \zeta) + \dots \}$$

$$(3.7c) \quad p_d = (p_0/U(l)) \{ \sigma^{(0)}(X) + \delta^2 \sigma^{(2)}(X, \zeta) + \dots \}$$

$$(3.7d) \quad \tau_d = - (2p_0/U^2(l)) \{ \tau_d^{(1)} + \delta \tau_d^{(2)} + \dots \},$$

where the pressure variation with ζ is explicitly indicated to appear only at $O(\delta^2)$.

By noting that $\ln(Z/z_0) = \ln(l/z_0) (1 + \delta \ln \zeta)$, and substituting equation (3.7) into (3.5), the zero and first-order terms of u_d are determined by

$$(3.8a) \quad \partial u_d^{(0)}/\partial X = \partial \sigma^{(0)}/\partial X$$

$$(3.8b) \quad \partial u_d^{(1)}/\partial X + \ln \zeta \partial u_d^{(0)}/\partial X + w_d^{(1)}/2\kappa^2 \zeta = (\partial/\partial \zeta)(\zeta \partial u_d^{(1)}/\partial \zeta).$$

It is convenient now to take the Fourier transforms in X , e.g.

$$u_d^{(1)}(X, \zeta) = \frac{1}{2\pi} \int_{-\infty}^{\infty} u_d^{(1)}(k, \zeta) \exp(ikX) dk.$$

No special symbols are used for the Fourier transforms of variables. Where it may be unclear from the context (or where emphasis is desired) whether a variable being considered is in physical or Fourier space, we indicate this by the argument list; thus $u_d^{(1)}(k, \zeta)$ is the Fourier transform (in X) of $u_d^{(1)}(X, \zeta)$. Then (3.8b) becomes

$$(3.8c) \quad ik(u_d^{(1)}(k, \zeta) + \ln \zeta u_d^{(0)}) + w_d^{(1)}/2\kappa^2 \zeta = (\partial/\partial \zeta)(\zeta \partial u^{(1)}/\partial \zeta),$$

where k is the wavenumber normalized on L . From continuity

$$(3.8d) \quad w_d^{(1)}(k, \zeta) = -ik \int_0^\zeta 2\kappa^2 u_d^{(0)}(k, \zeta) d\zeta.$$

The boundary conditions above the (SS) layer follow from the matching with the (M) layer using the results of (2.14), (2.15), (2.16) and (3.6). Note that (2.16b) can be rewritten as

$$u_d^{(0)}(x, Z) \sim -[p_0 \sigma(X)/U(l)] [1 - \delta \ln(Z/l) + \delta + O(\epsilon^2)].$$

Thus as $\zeta \rightarrow \infty$

$$(3.9a) \quad u_d^{(0)} \sim \sigma(X)$$

$$(3.9b) \quad u_d^{(1)} \sim -\sigma(X)(\ln \zeta - 1)$$

$$(3.9c) \quad w_d^{(1)} \sim -(d\sigma/dX)(2\kappa^2 \zeta),$$

and (3.9b) leads to the stress behaving as

$$(3.9d) \quad \tau_d^{(1)} \sim -\sigma(X).$$

(Note that there is no term in (3.7d) for $\tau_d^{(0)}$ because $\partial u_d^{(0)}/\partial \zeta = 0$.)

The boundary conditions below the (SS) layer as $\zeta \rightarrow 0$ follow from matching with the (IS) layer. Its analysis (which follows) shows that across the thin (IS) layer, the change in shear-stress perturbation $\tau_d^{(1)}$ is of second order, so that from (3.3a), as $\zeta \rightarrow 0$,

$$(3.10a) \quad u_d^{(0)} \sim \tau_d^{(1)}$$

$$(3.10b) \quad u_d^{(1)} \sim \tau_d^{(1)} \ln \zeta + \tau_d^{(2)},$$

$$(3.10c) \quad w_d^{(1)} \rightarrow 0.$$

The solutions to (3.8), subject to (3.9) and (3.10) are

$$(3.11a) \quad u_d^{(0)}(k, \zeta) = \sigma(k)$$

$$(3.11b) \quad u_d^{(1)}(k, \zeta) = \sigma(k)[1 - \ln \zeta - 4K_0(2(ik\zeta)^{1/2})]$$

$$(3.11c) \quad w_d^{(1)}(k, \zeta) = -i2\kappa^2 k \sigma(k) \zeta$$

where $\sigma(k)$ is the Fourier transform of $\sigma(X)$, and K_0 is the modified Bessel function.

From (3.4a) $\tau_d^{(1)}$ can be calculated from $u_d^{(1)}$.

From the solution for $u_d^{(1)}$ the surface perturbation shear stress can be derived using (3.10) as $\zeta \rightarrow 0$, since

$$u_d^{(1)}(k, \zeta) \sim \sigma(k) [\ln \zeta + 2 \ln k + 4\gamma + 1 + i\pi]$$

where γ is Euler's constant; it therefore follows that

$$(3.12a) \quad \tau_d^{(1)}(k, 0) = \sigma(k)$$

$$(3.12b) \quad \tau_d^{(2)}(k, 0) = \sigma(k) [2 \ln k + 4\gamma + 1 + i\pi].$$

3.3 Inner surface layer

When Z is of the order of the roughness height z_0 , then (numerically) $\ln \zeta$ is of the same order as $\ln(l/z_0)$ and the expansion procedure of the (SS) layer is not valid. Since the most significant feature of the (IS) layer is the rapid change in the shear-stress *gradient*, $\partial \tau_d / \partial Z$, we derive an equation for τ_d from (3.2a) and (3.2b) using the mixing-length approximation (3.4a). We find that

$$(3.13) \quad (2\kappa^2 LZ)^{-1} \{ \ln(Z/z_0) \partial \tau_d / \partial X + \partial \langle \tau_d \rangle / \partial X \} = \partial^2 \tau_d / \partial Z^2$$

where $X = x/L$ as before and

$$\langle \tau_d \rangle = \int_{z_0}^Z \tau_d(Z') [(1/Z') - (1/Z)] dZ'.$$

The boundary conditions on τ_d are defined at the surface by (3.2a) and (2.4b), so that at $Z = z_0$,

$$\partial \tau_d / \partial Z = \epsilon^{-2} \partial p / \partial x = \epsilon^{-2} L^{-1} p_0 d\sigma / dX$$

or with Fourier transforms and using the scaling of the expansion (3.7),

$$(3.14) \quad \partial \tau_d(k, \zeta) / \partial Z = 2p_0 l^{-1} U^{-2}(l) ik \sigma(k) \ln(l/z_0)$$

where we have used the relations

$$U(l) = (\epsilon/\kappa) \ln(l/z_0), \quad L = (l/2\kappa^2) \ln(l/z_0).$$

For matching with the (SS) layer scaling (3.7), the outer boundary condition as $Z/z_0 \rightarrow \infty$ is (retaining two terms in the expansion).

$$\tau_d \sim 2p_0 U^{-2}(l) Z \partial(u_d^{(0)} + \delta u_d^{(1)}) / \partial Z,$$

so that from (3.11), the Fourier transform of $\partial \tau_d / \partial Z$ must match

$$(3.15) \quad \partial \tau_d(k, Z) / \partial Z \sim -2ip_0 l^{-1} U^{-2}(l) k \sigma(k) \{2[\ln \zeta + \ln k] + \pi i + 4\gamma\}$$

as $l/z_0 \rightarrow \infty$ and $Z/l \rightarrow 0$. Note that (3.14) shows how at the surface $\partial \tau_d / \partial Z$ is $O(\epsilon^{-1} \tau_d(0)/l)$, i.e. an order of magnitude larger than $\partial \tau_d / \partial Z$ in the (SS) layer.

An analytical solution for τ_d in the (IS) layer can be constructed because, as we shall show, the thickness of this layer, l_s , is much greater than the roughness length but sufficiently thin that

$$(3.16a) \quad z_0 \ll l_s \delta.$$

Thence from (3.14) the change in τ_d across the layer is small compared with $\tau_d(z_0)$ so that

$$(3.16b) \quad |\tau_d(l_s) - \tau_d(z_0)| \ll |\tau_d(l_s)|.$$

Therefore on the left-hand side of (3.13) the variation in the *coefficients* of $\partial \tau_d / \partial x$ are much larger than the variation in $\partial \tau_d / \partial x$ itself, and (3.13) becomes

$$(3.17) \quad ik \delta Z^{-1} l^{-1} \tau_d(k, l_s) \{2 \ln(Z/z_0) + (z_0/Z) - 1\} = \partial^2 \tau_d(k, Z) / \partial Z^2,$$

where,

$$\tau_d(k, l_s) = -2p_0 U^{-2}(l) \sigma(k) [1 + \delta(2 \ln k + 4\gamma - 1 + i\pi)].$$

Integrating (3.17) within the (IS) layer from z_0 to Z , and using (3.14), leads to

$$(3.18) \quad \partial \tau_d(k, Z) = 2ik p_0 \sigma(k) l^{-1} U^{-2}(l) \delta^{-1} \{1 - \delta^2 [1 + \delta(2 \ln k + 4\gamma - 1 + i\pi)] [\ln^2(Z/z_0) - \ln(Z/z_0) - 1 - z_0/Z]\}.$$

If we let $Z = l\zeta$, hold ζ fixed and let $l/z_0 \rightarrow \infty$, the result agrees with (3.15), thus establishing a match to second order in δ between the inner solution (3.18) at the outer edge of the (IS) layer and the (SS) layer. In addition, (3.18) also satisfies (3.14) at $Z = z_0$. Since (3.16b) is satisfied, τ_d is continuous across the (IS) layer, which justifies the surface boundary conditions for the (SS) layer.

The thickness l_s of the (IS) layer cannot be defined any more precisely than by the inequality, (3.16a), but an estimate is made in the next section.

3.4 Discussion of the inner region results

Vertical profiles of the velocity and shear-stress perturbations in the inner region are presented in figure 2. In this case L is taken as a quarter wavelength. In figure 2a the different orders of approximation to u_d are presented schematically. Note the change of $O(h_m/L)$ caused by the acceleration in the middle layer, and the increase of $O(\ln^{-1}(l/z_0))$, caused by the shear in the inner region. In figure 2b the calculation of the real part of the Fourier Transform of $u_d^{(1)}$, from (3.11), is presented from the asymptotic analysis. This would be the profile over the *crests* of a sequence of hills.

The solution for $u_d^{(1)}$ may be compared with the solutions obtained by Jackson & Hunt (1975) to the *approximate* equation

$$(3.19) \quad \partial u_d / \partial X = -U^{-1}(l) \partial p / \partial X + (\partial / \partial \zeta)(\zeta \partial u_d / \partial \zeta)$$

namely (in Fourier transform space)

$$(3.20) \quad u_d(k, Z) = -p_0 \sigma(k) U^{-1}(l) (1 - K_0(2[ik\zeta])^{1/2} / K_0(2[ik(Z_0/l)])^{1/2}).$$

JH neglected (somewhat inconsistently) the velocity shear and the vertical velocity in the inner and outer region; consequently, the perturbation velocity outside the inner layer does not decrease in proportion to $1/U(Z)$, and therefore within the inner layer the perturbation velocity increases *monotonically* with height.

Jensen & Peterson (1978) suggested a simple formula for the inner region, $u_d(Z) = u_d(l) \ln(Z/z_0) / \ln(l/z_0)$, which is also shown on figure 2(b).

When the velocity shear in the middle layer is allowed for in the outer region analysis, the boundary conditions (3.10a,b) imply that u_d should have a maximum value within the inner region. The solution (3.11b) shows that the maximum in u_d occurs at a height

$$Z_{mx}/l = 0.08$$

if we define k as 2π (or the horizontal length scale L as the wavelength of a row of periodic hills), or

$$Z_{mx}/l = 0.3$$

if we define L as the $1/4$ of the wavelength and $k = 2\pi/4 = 1.6$. The second order computations of Newley (1986) and the model of Taylor et al. (1983) shows that Z_{mx}/l decreases as z_0/L decreases. For the smallest value at $z_0/L = 0.5 \times 10^{-4}$, they both compute $Z_{mx}/l \approx 0.3$ for flow over periodic terrain with L equal to the $1/4$ wavelength. [For $z_0/L \approx 0.5 \times 10^{-3}$, Z_{mx}/l has been computed to be about 0.6]

The actual magnitude for the (Fourier transform of the) maximum perturbation velocity in the inner region can also be expressed as

$$(3.21) \quad u_{d:mx} = p_0 \sigma(k) U^{-1}(l) [1 + \beta \delta]$$

where β depends on the value chosen for L . If L is the quarter wavelength for a periodic row of hills, figure 2b shows that $\beta = 1.8$. If L is equal to the wavelength, $\beta = 3.2$ (but (l/z_0) is increased by a factor of about 4, so the net increase is small). The result (3.21), is similar to the suggestion of Newley (1986) that $u_{d:mx} \approx p_0 \sigma(k)/U(Z_{mx})$, this implies $\beta = 1.2$. In JH, $\beta = 0$, and in Sykes' limit of $\ln(l/z_0) \rightarrow \infty$, $U(l) = 1$, and the term involving β again vanishes. Thus, our consideration of shear in the middle layer and in the inner region leads to an *increase* in the predicted speed up, in contrast to previous analytical treatments.

The solution for surface shear stress in (3.12) shows that a phase lead of surface shear stress of $\phi = \tan^{-1}(\pi\delta)$, which is close to values computed from the full governing equations and shear stress closure. In figure 3, we compare our results with computations reported by Richards & Taylor (1980). The approximations of JH lead to a lower value of $\phi = \tan^{-1}(\pi\delta/2)$. Therefore the velocity gradients of the undisturbed flow have an important effect on the shear stress in the inner region. (This agrees qualitatively with the phase lead computed and measured in the laboratory by Thorsness et al (1978) for water flow over smooth wavy walls).

The vertical profile of the first order perturbation shear stress $\tau_d^{(1)}(k, Z)$ is plotted in figure 2(c) and its gradient is plotted in fig. 2(d). The real part, $\tau_d^{(R)}$, gives the component in phase with the zero order perms for p_d , u_d and the surface elevation. This gives the form

of the profile over the crest of a hill, and shows how the gradient of shear stress is zero at the surface and the gradient is maximum at a height of about $l/3$ (for L equal to the quarter length of the hill) where the perturbation velocity is also maximum. The negative perturbation velocity gradient at the top of the inner region leads to the negative real perturbation shear stress at $Z \sim l$.

The imaginary part of $\tau_d^{(1)}(k, Z)$, $\tau_d^{(1)}$, gives the component in phase with the pressure gradient $\partial p_d / \partial x$ and the out-of-phase component of u_d : $\tau_d^{(1)}$ tends to zero above the inner region, as the out-of-phase component of u_d tends to zero. Figure 2(d) shows that towards the surface, as $Z/l \rightarrow 0$, the gradient of $\tau_d^{(1)}$ rapidly increases, but that within the (IS) layer $\partial \tau_d^{(1)} / \partial Z$ tends to a constant value. This graph shows that an appropriate definition for the thickness l_s of the (IS) layer is the height where $\partial \tau_d^{(1)} / \partial Z$ starts decreasing, i.e. where $\partial \tau_d^{(1)} / \partial Z$ in the (SS) layer is equal to the surface value of $\partial \tau_d^{(1)} / \partial Z$ in the (IS) layer. Applying this definition in (3.18) leads to an equation for l_s , namely

$$(3.22a) \quad 2 \ln(l/l_s) \ln(l/z_0) \approx 1,$$

to which the solution is

$$(3.22b) \quad l_s \approx (lz_0)^{1/2}.$$

Note that this estimate for the thickness of the inner surface layer is not an estimate for the height where the shear stress balances the inertial terms, nor is it an estimate for where u_d reaches a maximum. It is useful to define it as the height below which the simple shear stress layer analysis cannot be applied.

Note also that at the top of the inner region and above it, the mixing model of shear stress is quite incorrect because the eddy time scales become comparable with the time of travel of an eddy over the hill. Then the effects of curvature and straining on the turbulence lead to quite different magnitudes and even signs of the Reynolds stresses (Zeman & Jensen, 1987; Newley, 1986). Since we have seen that only the first order correction is affected by the shear stress in the upper part of the shear stress layer, it follows that the overprediction of $(-\partial \tau_d / \partial Z)$ by the mixing length model slightly underpredicts u_d at the top

of a hill. On the downwind slopes the errors associated with this shear stress model are more acute.

Since the roughness height z_0 is always much *smaller* than the height of the roughness elements (typically $1/30$), (3.22) means that the inner surface layer may be partially below the height of the roughness elements. This occurs if $l/z_0 \leq 10^3$, say $l \approx 30\text{m}$ and $z_0 \approx .03\text{m}$ as in fig 2(d). In other words the gradients of shear stress can in practice be greatest at or below the heights of the roughness elements. But since the average force per unit height on roughness elements is equal to $\partial\tau_d/\partial Z$, and since this force may be changed by a perturbation in the local horizontal velocity, this suggests that $\partial\tau_d/\partial Z$ may not reach its theoretical value at the surface in the presence of typical roughness elements (or viscous effects in low Reynolds number laboratory experiments).

4. Structure of the Middle Layer

4.1 Typical upwind velocity profiles

The profiles of the perturbation horizontal and vertical velocities u and w in the middle layer and the upper layer depend on the form of the upwind mean velocity profiles $U(z)$. In this section we consider different forms of $U(z)$ particularly to show when and how large amplifications in u can occur in the middle layer. We assume here that L/h is large enough that $h_m = h$, and consider a special case for which the hill slope need *not* be small.

In neutral and moderately stable conditions, it is useful to consider profiles for which in $0 < z < h$ either

$$(4.1a) \quad U(z) = (z/h)^n,$$

or

$$(4.1b) \quad U(z) = 1 - \Omega + \Omega(z/h),$$

holds, and in $z > h$,

$$(4.1c) \quad U(z) = 1.$$

For neutral and unstable conditions (4.1a) is a suitable approximation when $n \ll 1$ where n increases with the roughness of the terrain (Davenport 1961), and decreases in unstable conditions. In stable conditions (4.1a) is often used to describe the profile over the whole depth of the boundary layer but with exponent n varying with elevation, the values of n lying between 0.4 and 1.0 (e.g. Irwin (1979)). It should be noted, however, that even in stable conditions the velocity profile is approximately logarithmic when z is less than about 1/5 of the Monin-Obukhov length L_{MO} , so that even in stable conditions $n \ll 1$ near the ground. To understand how in moderately stable conditions the shear affects the flow, we consider the linear profile (4.1b) rather than the power-law profile with variable $n(z)$. In this case $U(0)$ is not zero, but should be considered as the extrapolated limit of the profile in the outer part of the boundary layer as $(z/h) \rightarrow 0$ (Fig. 5a).

Because with a linear shear profile the curvature of the profile is confined to a thin layer at the top of the boundary layer, and because the analysis in section 3 of the lower boundary condition for the middle layer is not applicable in an obvious way, the boundary layer with a linear shear profile is analyzed *ab initio* in section 4.2 and the results compared with those found by the general (but weak shear) methods of Section 2.3. In section 4.3 we compare the middle region perturbation velocity profiles for different kinds of upwind mean profile.

4.2 Outer region with a uniform shear profile in the boundary layer

For a specific profile it is convenient to introduce a streamfunction Ψ , to define the scales of the perturbation velocities and streamfunction ψ in terms of the small slope parameter (H/L) and the boundary layer thickness parameter $\mu^{-1} = h/L$, and we scale the coordinates (x, z) with L . Let

$$(4.2) \quad u^* = U_{\infty}(U(z) + (H/L)u) \quad , \quad w^* = U_{\infty}(H/L)w$$

and

$$\Psi = LU_{\infty} \left[\int_0^z U(z') dz' + (H/L) \psi \right] .$$

In this section all distances are made dimensionless with respect to L . (Although we had defined x and z as dimensional variables in the previous section, in this section only, we make the replacements $x/L \rightarrow x$ and $z/L \rightarrow z$.)

Since $d^2U/dz^2 = 0$ in (M) as well as (U) , the governing equation for the (M) and (U) layers is the same as (2.7) which becomes

$$(4.3) \quad \nabla^2 \psi = 0.$$

In contrast to (2.6f) and (2.9), however, (4.3) is not an approximation but is exact in both (U) and (M) . Following § 2.4 the boundary condition ψ at the outer edge of the inner

region is that the flow be parallel to the surface of the hill, (because the displacements of the inner layer are negligible to $O(\delta)$), so on

$$(4.4) \quad z = (H/L) f(x), \quad \psi = 0.$$

By considering the Taylor expansions of $\psi(x, z)$ about $z = 0$, the boundary condition (4.4) becomes

$$(H/L) \left\{ \psi(x, 0) + (H/L) f(x) \partial \psi / \partial z \right\} = - \int_0^{(H/L) f} (1 - \Omega + \Omega \mu z) dz.$$

Retaining terms of $O(H/L)$ and $O(\Omega H/h \times H/L)$ it follows that

$$(4.5) \quad \psi(x, 0) = - [(1 - \Omega) f(x) + \beta f^2(x)]$$

where $\beta = \Omega H / (2h)$. In the upper layer

$$(4.6) \quad u, w \rightarrow 0 \text{ as } x^2 + z^2 \rightarrow \infty.$$

The height of the material line dividing the middle (M) and upper (U) layers is defined by

$$z = Z(x) = \mu^{-1} (1 + (H/L) \zeta(x)).$$

Since z must be the height of a streamline, matching requires

$$(4.7) \quad \mu^{-1} \zeta = - \psi^{(M)} = - \psi^{(U)}.$$

On matching the pressure in the (M) and (U) layers at $z = Z(x)$, and retaining terms only to $O(H/L)$, we find that $\zeta(x)$ is related to $u^{(M)}$ and $u^{(U)}$ by

$$(4.8) \quad \Omega \zeta(x) + u^{(M)}(x, \mu^{-1}) = u^{(U)}(x, \mu^{-1}).$$

Denoting the Fourier transform of ψ by

$$(4.9a) \quad \psi(k, z) = \int_{-\infty}^{\infty} e^{-ikx} \psi(x, z) dx,$$

that of $f(x)$ by $F(k)$, and that of f^2 by $G(k)$, the solution to (4.3) subject to (4.5), (4.6),

(4.7), and (4.8) is

$$(4.9b) \quad \psi^{(M)}(k, z) = C_1 \sinh |k| z + C_2 \cosh |k| z$$

and

$$(4.9c) \quad \psi^{(U)} = C_3 e^{-|k|z}$$

where

$$(4.9d) \quad C_1 = \{(1-\Omega)F(k) + \beta G(k)\} \left[\frac{|k|\mu^{-1} - \Omega + |k|\mu^{-1} \tanh(|k|/\mu)}{(|k|\mu^{-1} - \Omega) \tanh(|k|/\mu) + |k|/\mu} \right]$$

$$(4.9e) \quad C_2 = -[(1-\Omega)F(k) + \beta G(k)]$$

$$(4.9f) \quad C_3 = e^{|k|/\mu} [C_1 \sinh(|k|/\mu) + C_2 \cosh(|k|/\mu)].$$

These solutions can be checked against the potential flow solution where $\Omega = 0$ and the solution for an infinitely thick uniform shear profile where $(L/h) \equiv \mu \rightarrow 0$. In the latter case, reverting now to dimensional coordinates x and z ,

$$(4.10a) \quad C_1 \sim (1-\Omega)F + \beta G, \text{ so } u^{(M)}(x, 0) = (H/L)U'(0)\sigma_s(x/L)$$

where

$$(4.10b) \quad \sigma_s(x/L) = \frac{1}{\pi} \int_{-\infty}^{\infty} \frac{f'_s(x'/L) dx'}{x-x'}$$

and

$$(4.10c) \quad f'_s = f(x/L) \left(1 + \frac{\beta f(x/L)}{1-\Omega} \right) = f(x/L) \left(1 + \frac{dU}{dz} \frac{Hf(x/L)}{2U'(0)} \right).$$

To compare with the general solution of section 2 and 3, we consider the limit where the boundary thickness h is thin compared with the length L of the hill and where the slope (H/L) is small but where the strength of the shear (i.e. β) is arbitrary. In the limit of $\mu \rightarrow \infty$,

$$(4.11a) \quad C_1 \sim \left[(1-\Omega)F + \beta G \right] \left\{ \frac{1}{(1-\Omega^2)} + \frac{\Omega\mu}{k(1-\Omega)} \right\} \\ = \left(F + \frac{\beta G}{1-\Omega} \right) \left(\frac{1}{1-\Omega} + \frac{\Omega\mu}{k} \right) (1 + O(k, \mu))$$

and

$$(4.11b) \quad C_2 = -(1-\Omega)\{F + [\beta/(1-\Omega)]G\}.$$

Thence when terms of $O(h/L)$ are negligible in the middle layer, the perturbation velocity is given by

$$(4.12a) \quad u^{(M)} = \frac{-(H/L)\Omega}{h/L} f_s(x) + \frac{(H/L) \sigma_s(x)}{1 - \Omega}$$

or

$$(4.12b) \quad u^{(M)} = - (dU/dz) H f_s(x) + [1/U(0)](H/L_1) \sigma_s(x/L)$$

where σ_s and f_s are defined in (4.10c).

In the upper layer,

$$(4.13) \quad u^{(U)} = (H/L) \sigma_s(x/L) G_u(x/L, z/L),$$

where G_u is defined in (2.20).

The implication of these results for the flow is discussed in section 4.3. From the point of view of checking the analysis, we note that the expressions for $u^{(M)}$ and $u^{(U)}$ are identical to those obtained from (2.11b) and (2.18). But we note that when there is a *uniform* shear flow in the upwind boundary layer, the values of $A(x)$ and $B(x)$ obtained in section 2.3 are only valid provided that the change in the upwind speed over the height of the hill is negligible compared to the wind speed above the inner region, i.e. $\beta(1-\Omega)^{-1}$ or $\{dU/dz\} H/U(0) \ll 1$. If the shear is large enough at the surface, then we have seen that the outer region analysis can be simply extended by considering the hill has the fictional 'shear' shape $f_s(x)$ given by (4.10c). It is also important to note that the middle layer solution, equation (2.8), is valid even if d^2U/dz^2 is a 'delta' function.

4.3 Typical middle-layer velocity profiles

The results of Section 2.3, for a neutrally-stratified or log profile in the middle layer enable general expressions to be written down for horizontal velocity perturbations relative to the upwind velocity at the same height

$$(4.14a) \quad u^{(M)} = (H/L) \{ -L(dU/dz)f(x) + \sigma(x/L)[U^2(h_m)/U(z)] J(z) \}$$

where

$$(4.14b) \quad J(z) = 1 + U(z)U'(z) \int_z^{\infty} dz/U^2(z)$$

and $\sigma(x/L)$ is given by (2.a,b). Note that the integral for $J(z)$ always converges for turbulent boundary layers where $U(z) \propto \ln(z/z_0)$ and $J = 1$ when $z \geq h_m$.

If the upwind velocity has a log profile

$$(4.15) \quad J(z) = 1 + zU'(z)/U(z) (1 + O(\ln(z/z_0))^{-1}) = 1 + O(\ln(z/z_0))^{-1}$$

and for a 'power-law' profile, as given in (4.1a)

$$(4.16) \quad J = (1-n)/(1-2n).$$

The latter expression cannot be applied when $n = 1/2$ both because the power law is not a uniformly good approximation to $U(z)$ and because the integral for $J(z)$ is singular. So in both these cases

$$(4.17) \quad u^{(M)} = (H/L) \left[-L \frac{dU}{dz} f(x) + \frac{\sigma(x/L)U^2(h_m)}{U(z)} (1 + O(\frac{zU'(z)}{U(z)}) \right].$$

It is also interesting to note that the horizontal velocity displacement perturbation at Z above the surface is given, for these cases, by

$$(4.18) \quad u^{(M)} = (H/L) \left[\frac{\sigma(x/L)U^2(h_m)}{U(Z)} (1 + O(\frac{ZU'(Z)}{U(Z)}) \right].$$

A different result is obtained for a linear profile, as given in (4.1b) and analyzed in Section 4.2. In this case $J(z) = U(z)/U(0)$ and

$$(4.19a) \quad u^{(M)} = (H/L) \left[L(-dU/dz)f(x) + \frac{\sigma(x/L)U^2(h_m)}{U(0)} \right]$$

which can be rewritten

$$u^{(M)} = (H/L) [\sigma(x/L)U(h_m) + dU/dz (h_m\sigma - Lf)]$$

and, for a given displacement Z ,

$$(4.19b) \quad u_d^{(M)} = (H/L) [\sigma(x/L)U^2(h_m)/U(0)].$$

Graphs are shown in Figure 5 of $u(x,z)$ and $u_d(x,Z)$ for the limited cases of upwind log profiles, or power-law profiles where $n \ll 1$, and linear profiles. They show how u and u_d both increase near the ground in the first case, but are nearly constant in the second case. They also demonstrate how the relative speed-up, $u_d(x,Z)/U(Z)$ is much increased by an increase in the exponent n or the velocity gradient of the upwind profile.

To understand how the amplification occurs it is instructive to consider the discontinuity in u at the top of the middle layer. The upward deflection of the vortex lines of the middle layer into the upper layer produced by the upwind profile passing over the hill produces a *negative* perturbation in u equal to $-HfdU/dz$. But the flow over the hill is not a pure upwards displacement; since the flow in the upper layer speeds up over the hill by $(H/L)\sigma U(h_m)$, this produces a *downward* deflection of the streamline relative to the hill surface and of the vortex lines which *increases* the velocity (in displaced coordinates) in the middle layer. (If the velocity gradient is weak enough that $h_m dU/dz \ll U(h_m)$, then the downward deflection is $(H/L)h_m\sigma$ and the accompanying increase in velocity is $(H/L)\sigma h_m dU/dz$.) Thus the increase in u_d , the perturbation velocity at the same displacement Z , is caused by the downward deflection (relative to the hill surface) of the streamlines over the depth of the middle layer. Note that because there are discontinuities in the upwind velocity gradient at $z = h$, u_d and u have discontinuities, denoted by $\langle \rangle$, equal to

$$(4.20a) \quad \langle u \rangle_{z=h} = (H/L) [LfU'(h) + \sigma(1-J)U(h)]$$

$$(4.20b) \quad \langle u_d \rangle_{z=h} = (H/L) \sigma(1-J).$$

For a log or a power-law profile these discontinuities are very small ($O(\ln^{-1}(h/z_0))$ or $O(n)$). For a linear profile

$$(4.21) \quad \langle u \rangle = (H/L)[Lf - \sigma h_m U(h)/U(0)]U'$$

which is generally positive since $h_m \ll L_1$.

It is often of practical interest to be able to estimate the *relative* speed up, S , near the surface of a hill. From (4.14), when $L \gg h_m$ and if the upper layer is neutrally stable, S can

be expressed quite generally in terms of the upwind profile and the hill shape factor $\sigma(x/L)$ as:

$$(4.22a) \quad S = u_d(x, Z)/U(Z) = (H/L) [\sigma(x/L) U^2(h_m)/(U(z)U(Z))] J(z).$$

If the local shear at Z is small enough that $UH/U(z) \ll 1$ this reduces to

$$(4.22b) \quad S(x, Z) = (H/L) [\sigma(x/L) U^2(h_m)/U^2(Z)] J(Z).$$

It is interesting to note that in the lowest part of the middle layer, where $l \leq z \ll h_m$, the factor $J(z)$ is approximately unity for all the profiles considered here log, power law ($n \ll 1$), and linear. Thus the amplification factor $(U(h_m)/U(z))^2$ proposed in JH is of wider validity than just the log profile considered there and in the subsequent papers referenced in Section 1.

If the length of the 'hill' is small enough that $L \gg h_m$, and the upwind profile is linear, then it follows from (4.10a) that, if the variation of wind speed over the hill height is small, i.e.

$$(4.23a) \quad H dU/dz / U(0) \ll 1, \quad S = (H/L) \sigma(x/L).$$

On the other hand, if the variation of the wind speed over the hill height is large,

$$(4.23b) \quad S(x, Z) \sim (H/L) U(H)/U(Z)$$

and the shape factor is no longer the function $\sigma(x/L)$ but depends on the shear profile, as shown in (4.10) of Section 4.2. Note how the amplification of wind speed over the hill is much less in (4.23) compared with (4.22) because there is no net displacement of vorticity into regions of lower vorticity in this case.

5. Defining and Extending the Range of Validity of the Analysis

5.1 Conditions for the linear analysis

From the results for the inner and middle layers, in particular (3.7), (3.11), (3.12) and (4.18), it is now possible to state, *a posteriori*, the conditions under which the linear analysis is valid and, if it is only valid in limited regions of the flow, where those regions are. To linearize the inertial terms in the equations it is assumed that

$$(5.1a) \quad |u_d| \ll U(Z)$$

and to estimate the shear stresses, defined in dimensionless terms by (3.1), it is assumed that

$$(5.1b) \quad |\tau_d| \ll 1.$$

From (3.7) and (2.15), it follows that these conditions are satisfied if

$$(5.2a) \quad u_d/U(l) \sim (H/L)U^2(h_m)/U^2(l) \ll 1.$$

and

$$(5.2b) \quad \ln(l/z_0) \gg 1.$$

Note that (5.2b) is consistent with the initial assumption (2.4c).

To satisfy the criterion (5.2a) for stably stratified boundary layers, or in the wakes of upwind hills, where $U(l)/U(h_m) \ll 1$, the hill slope must be smaller than is required for a logarithmic upwind profile. This condition is essentially the same as that of *laminar* flow over humps. However in laminar flows $U(h_m)/U(l) \sim h_m/l$ so that (when $h \sim L$) even if $H \ll L$, unless the inner region is much thicker than the height of the hill, (i.e. $l \gg H$) then changes in the surface shear stress of $O(1)$ can occur and the flow must separate (Smith *et al.* 1981). In turbulent flows even if $H \gg l$, (5.2a) may be satisfied because $U(h_m)/U(l) \sim 1 + O(\epsilon)$, which is very much less than h_m/l .

5.2 Allowing for non-linear effects

As in the flow of laminar boundary layers over surface humps, the flow of turbulent boundary layers may be such that the slope of the hill is low enough, i.e.

$$(5.3a) \quad H/L \ll 1,$$

for a linear analysis to be valid in the upper layer (U) of the outer region. Yet within the middle layer (M) and within the inner region, the velocity gradient dU/dZ may be so large that the perturbation velocity u_d and shear stress τ_d may increase sufficiently that

$$(5.3b) \quad u_d(Z) \sim U(Z)$$

and

$$(5.3c) \quad \tau_d \sim 1.$$

The condition of flow over a low slope and a large change in surface velocity, i.e. (5.3a,b) can only occur simultaneously if the ratio of wind speed at the top of the inner layer to that at the top of the middle layer is such that

$$(5.3d) \quad H/L \ll 1 \text{ and } U_0^2(l)/U_0^2(h_m) \sim H/L.$$

In this case $u_d(Z)$ in (M) is given in terms of $p(x)$ in the upper layer by Bernoulli's equation along streamlines from (2.10c) and (2.13c)

$$(5.4) \quad U^2(Z) + 2U(Z)u_d(x,Z) + u_d^2(x,Z) = 2(H/L)\sigma(x/L) + U^2(Z_\infty),$$

where $U(Z_\infty)$ is the velocity on the streamline upstream of the hill. Denoting, for the present purposes, the *linear* solution as $u_d^l(x,Z)$, the perturbed velocity u_d in the layer (M) corrected for nonlinear effects is

$$(5.5) \quad \frac{u_d}{U(Z)} = -1 + \left(1 + \frac{2u_d^l(x,Z)}{U(Z)}\right)^{1/2}$$

Here we have neglected the contribution by the second-order correction to $U(Z_\infty)$ which is $O(2u_d^l \ln(Z/z_0))$. This result is also valid for a three-dimensional low hill. The nonlinear correction is of $O(h_m H/L^2)$ if $h_m H \ll U(h_m)U(l)$.

To test the non-linear correction of (5.5) a comparison is made with the results from a nonlinear numerical model for the perturbation velocity at the top of the inner region ($Z \sim l$). The numerical model is similar to that of Taylor (1977) and which has been extended by Richards & Taylor (1980) to allow for steeper topography. The model retains

the nonlinear inertial terms and uses a isotropic eddy viscosity based on a mixing length and the local turbulent kinetic energy. The model is for a deep turbulent neutral boundary layer over a two-dimensional hill where $h \gg L$. It is therefore appropriate to use as the linear solution $u_d^l(Z)$ in (5.5) the outer region solution (2.16b) or that given by Britter, Hunt, and Richards (henceforth BHR) (1981) (their equation (2.4)).

BHR made a detailed comparison between the linear analysis and nonlinear computations of a turbulent boundary layer flowing over a hill with $H/L \sim 0.4$, $L \sim h_m \sim 0.25h$ and $U^2(l)/U^2(h) = 0.25$. The nonlinear computation and measurements for the peak velocity just above the inner region ($Z = l$) at the top of the hill gave a value for $u_d(l)/U(l) = 0.8$, whereas the linear analysis gave a value of about 1.2. The new correction given by equation (5.5) gives a value of 0.84.

The value of $\ln(l/z_0) = 2.7$ for the hill used by BHR was low because of unusually large roughness elements. The value of $u_d(l)/U(l)$ as a function of slope, H/L , given by the nonlinear model at the crest of the hill with a more typical value of $\ln(l/z_0) = 6.4$ and the same shape (that is $f = 1/(1 + (x/L)^2)^{1/2}$) is shown in Figure 6. Also shown is the linear solution and the nonlinear correction. The non-linear correction of the linear model brings the results closer to those of the computations. It was remarked in BHR that this discrepancy was due to the neglect of nonlinear inertial effects: the analysis given here shows this to be the case and also considerably extends the range of applicability of the linear analysis of the upper (U) and middle (M) layers.

A similar non-linear correction has previously been suggested by Bouwmeester (1978), but was not fitted in to the general asymptotic analysis.

5.3 A comparison between turbulent and laminar flows over humps

It is important to note how even in the inviscid outer regions there are significant differences between *laminar flow* over surface humps and turbulent flow over hills. In laminar flows over hills of length $L > h$, and height $H \ll l$, the magnitude of the perturbation

to flow in (M) and (U) is determined by the structure of the inner flow region, where viscous shear stresses balance the acceleration and pressure gradient. In these turbulent flows, when there is no separation, we have shown by matching arguments that the middle and outer layer solutions only depend on the upwind velocity $U(z)$, and the height and shape of the hill.

There is a straightforward explanation for this difference. Consider the vertical flux at a level $l+H$ which lies just above the inner region at the top of a two-dimensional hill.

Then by continuity

$$(5.6) \quad \int_{-\infty}^x w(x, l+H) dx = \int_0^{l+H} U(z) dz - \int_0^l U(Z) dZ - \int_0^l u_d(Z) dZ.$$

The first two terms on the righthand side give the displacement of the upwind profile caused by the hill and the third term is the *downward* displacement caused by the excess perturbation velocity in the inner region.

For the cases of turbulent or laminar boundary layers over a hump, these terms can be estimated in both the cases as

$$(5.7a) \quad \int_{-\infty}^x w(x, l+H) dx < U(l+H) H + l [U(l+H) - U(l) - l u_d(x) Q]$$

where

$$Q = \int_0^1 [u_d(x, \zeta) / u_d(x, l)] d\zeta,$$

and where we have again written $\zeta = Z/l$. Note that $Q = 0(1)$.

Thence

$$(5.7b) \quad \int_{-\infty}^x w(x, l+H) dx < U(l+H) H \left[1 - \frac{l}{H} \frac{u_d(x, l)}{U(l+H)} Q \right].$$

In a neutral turbulent boundary layer, from (4.18)

$$(5.8) \quad \frac{l}{H} \frac{u_d(x, l)}{U(l+H)} \sim \frac{U^2(L)}{U(l)} \frac{(H/L)(l/H)}{U(l+H)} \sim \delta \ll 1.$$

From the expansion of u_d in the inner region (3.7), Q can be written

$$(5.9) \quad Q = \int_0^1 \{ (u_d^{(0)} + \delta u_d^{(1)}) u_d^{(0)}(x, l) \} dz,$$

where solutions for $u_d^{(0)}$ and $u_d^{(1)}$ are given by (3.11).

From (5.7b), (5.8) and (5.9) it follows that, to zero order in $\ln^{-1}(l/z_0)$, the upward flux into the outer region is not affected by the velocity perturbations near the surface. Furthermore, since to leading order the velocity perturbation $u_d^{(0)}$ is not affected by shear stresses in the inner region, to first order, the upward flux is also not affected by the turbulence in the inner region. Therefore, even to $O(\ln^{-1}(l/z_0))$, the perturbed flow in the outer region is only affected by *the shape and height of the hill and the form of the upwind profile*. However the shear stress in the inner region does have an effect on the outer flow at order δ^2 (i.e., $O(\ln^{-2}(l/z_0))$), when the displacement by the first-order perturbation velocity $u_d^{(1)}$ is significant. (This displacement is asymmetric and induces a small change in the phase of the external pressure of $O(\ln^{-2}(l/z_0))$, typically of the order of 1° for l/z_0 of 10^4 (Newley 1986)).

However in a laminar boundary layer flow over a long hill where $L \sim h$ or where $Lh \sim h^2 \gg 1$ (the so-called triple-deck scale),

$$(l/H) [u_d(x, \xi)/U(l)] \sim 1.$$

(In the latter case $u_d \sim (U^2(L)/U(l)) \times (H/L)$, which is the same magnitude as for the turbulent flow (Smith *et al.* 1981)). Therefore the displacement of the upwind profile by the hill is of the same order as the displacement by the perturbed velocity profile.

Consequently, for laminar boundary layers the magnitude of the inviscid flow over a hill or hump is determined by the structure of the inner region flow, and particularly by the velocity reduction in the wake (Smith *et al.* 1981). This means that even in the outer

tion, solutions using a constant viscosity (or eddy viscosity) may not be reliable guides to the behaviour of turbulent flows. The fact that for turbulent flows the outer region flow is largely independent (except in the particular circumstances of separated flows) of the inner region, is a very important result which we make use of in Part II. (For hills which are steep enough to produce separated flows in their wakes, this assumption is not valid; the wakes may significantly affect the outer region flow (e.g. Scorer 1955).)

5.4 Unified expressions

If the layers (U) and (M) within the outer region are distinct, and if the conditions (2.4) are satisfied, a uniformly valid approximation for u, w for both layers is

$$(5.10a) \quad u = U(Z) + \frac{(H/L)\sigma(x/L)G_u(x/L, z/L)J(Z/L)}{U(Z)}$$

$$(5.10b) \quad w = (H/L)(\partial f/\partial(x/L))U(z)G_w(x/L, z/L)(1 + O(h_m/L))$$

where the middle layer function $J(Z/L)$ is given by (2.11b). For a power law velocity profile (5.10a) is the same as the result of Dawkin's & Davies (1981). For logarithmic profiles, these expressions are the same (to first order in $[\ln(L/z_0)]^{-1}$) as those given by Jackson (1976), which compared well with wind-tunnel experimental data (Britter, Hunt & Richards (1981)). If the layer (M) becomes negligibly thin, then these formulae show that the flow becomes simply potential flow above the inner region, without the amplification of u that occurs in (M), (the case is treated by Sykes (1980)). For an approximate correction to (5.10a) to allow for nonlinear effects, (5.5) can be used. If the length of the hill is small compared to the boundary layer height, h , then the second-order terms in appendix B should be used. (See figure 4.)

6. Conclusions.

In this paper we have developed a general analytical method for calculating the mean flow and the shear stress near the surface for two- and three-dimensional turbulent shear flows over hills with *low slopes*. The effects of buoyancy forces on the mean flow

over the hill are assumed to be negligible here, though these forces may be strong enough to affect the upwind profile.

The main conclusions are:

(i) **Flow regions**

The flow can be analyzed in modular form by dividing up the space over the hill into two *flow regions*, the outer and inner regions. The outer region has to be further divided into an upper (*U*) and middle layer (*M*). The inner region is divided into a shear-stress layer (*SS*) and an inner surface layer (*IS*).

(ii) **Outer regions**

In the middle layer the shear of the upwind profile is dominant and the vertical velocity perturbation w (relative to a horizontal surface) induced by the hill *increases* with height (in proportion to $U(z)$) while in the upper layer the velocity and pressure perturbations decay in a potential flow. The depth of the middle layer (*M*) depends on the wind profile and the length of the hill - for a logarithmic profile $h_m \sim L/\ln^{1/2}(L/z_0)$. If, however, the length is greater than the boundary-layer depth (h), then $h_m \sim h$. The upwind velocity at h_m , U_0 determines the magnitude of the pressure perturbations in the flow, and thence the perturbations near the surface. Defining h_m is particularly important when the profile changes due to the action of stable stratification (Hunt & Richards 1984). The horizontal velocity perturbation u is, to second order in $\ln^{-2}(L/z_0)$, in phase with the surface elevation and in the upper layer decreases exponentially over a periodic surface like $u \sim \pi(H/2L)U(h_m)e^{-\pi z/2L}$ while over a single hill $u \sim (H/L)U(h_m)(L^2/z^2)\sigma(x/L)$.

In the middle layer, the horizontal velocity perturbation (in displaced coordinates), u_d , decreases with height more rapidly

$$u_d \sim (H/L) \frac{U^2(h_m)}{U(Z)} \sigma(x/L) (1 - O(h_m/L)),$$

assuming a logarithmic or typical power law profile of the upwind velocity. (For a linear shear profile see §4).

By introduction of a middle layer, inconsistencies in the JH model have been overcome: estimates for the magnitude of the horizontal velocity perturbation near the surface have only been slightly changed. The form of the vertical perturbation w , however, is significantly changed by effects occurring in the middle layer; (w) in fact *increases* with height in the middle layer until $z \sim h_m$, before decreasing in the upper layer.

(iii) *Inner region structure*

To the first approximation (i.e. zeroth order in $\ln^{-1}(l/z_0)$), the horizontal velocity perturbation u_d is not affected by shear stresses in the shear stress layer. In the next approximation, however, there is a balance between the gradients of perturbation shear stresses and the accelerations, and u_d reaches a maximum at a height of about $l/3$, given by

$$(u_d)_{mx} \approx (H/L)[U^2(h_m)/U(l)] (1 + 1.8\delta)$$

where l is the depth of the inner region defined in terms of L , the quarter length of the hill.

In the lower part of the shear stress layer and the surface shear stress layer, the perturbation velocity has a logarithmic profile. The perturbation shear stress layer has its maximum positive values at the surface, but decreases through the shear stress layer to a *negative* value of comparable magnitude.

The significance of the inner surface layer of $O((z_0/l)^{1/2})$ times the thickness of the inner region, is that across it the vertical gradient of the perturbation shear stress increases from its first-order value in the shear stress layer to a zero-order value at the surface where it balances the perturbation pressure gradient.

The phase of the surface shear stress (and of the velocity in the inner surface layer) *leads* the phase of the pressure distribution by an angle that depends on the roughness length (about $\tan^{-1}(\pi/\ln(l/z_0))$). This is in sharp contrast with the phase lead of nearly $\pi/4$ for laminar flows over an undulating surface.

(iv) *Net drag on topography*

The displacement caused by turbulent flow in the inner region of the flow on the outer region is small $O(\ln^{-2}(l/z_0)H/L)$. (By contrast in laminar flows over long surface

humps ($L \sim h$) the displacement by the inner region is comparable with that produced by the hill.) However the significance of this small inner region displacement is that it is slightly *out of phase* with the elevation of the hill, by $O(\ln^{-2}(l/z_0))$. This gives rise to a net drag on the hill (or water surface in the case of waves) of order $H^2 L^{-1} U^2 (h_m) \ln^{-2}(l/z_0)$. For hills of low slope this is a larger effect than that caused by distortion of the approaching turbulence, which conflicts somewhat with previous suggestions by Townsend (1980), Sykes (1980); see also Newley (1986).

(v) *Analysis supercedes Jackson & Hunt*

The analysis here has been developed for a wider range of conditions than in the earlier work of Jackson & Hunt. The depth of the inner region l may be less or greater than the height of the hill H ; corrections have been derived for weak nonlinear effects of accelerations for small but finite hill slope and for the fact that the length of the hill is not very large compared with the depth of the middle layer (i.e. correction of order h_m/L).

(vi) *Comparison with numerical experiments*

These key results of the analysis are consistent with a number of the numerical computations of the full equations including those with slightly different models for the closure relation between shear stresses and velocity gradients. The maximum speed up in the shear stress layer may be slightly dependent on the closure. (Newley 1986). As the slope increases, the velocity and shear stress on the downwind slopes become increasingly sensitive to the closure.

Acknowledgements

JCRH and SL worked on this paper at Flow Analysis Associates, Ithaca, New York with support from the U.S. Air Force Geophysics Laboratory, Hanscom, AFB, Mass. We are grateful for valuable comments by Peter Taylor, John Walmsley, Ian Sykes, and Trevor Newley.

Appendix A. Solution for the middle layer over a three-dimensional hill

We consider flow over a three-dimensional hill defined by $z = Hf(x/L, y/L)$ where $H/L \ll 1$. The governing equations for w in the middle layer where the conditions $\partial/\partial z \gg \partial/\partial x, \partial/\partial y$ are defined to hold in $h_m > Z \gg \epsilon H$, is

$$(A.1) \quad \left(\frac{\partial^2}{\partial z^2} - \frac{U''}{U} \right) w = 0,$$

for a hill with low enough slope.

The solution for w has the same form as (2.17), namely

$$(A.2) \quad w = \frac{\partial A}{\partial x}(x, y) U(z) + \frac{\partial B}{\partial x}(x, y) U(z) \int_{z_1}^z \frac{dz'}{U^2(z')},$$

where $z_0 \ll z \ll L$. The solutions for u can be obtained from the equations (2.6a,b,d) which leads to

$$(A.3) \quad \frac{\partial}{\partial x} \left(\frac{\partial^2}{\partial x^2} + \frac{\partial^2}{\partial y^2} \right) u + \frac{U'}{U} \frac{\partial^2 w}{\partial y^2} + \frac{\partial^3 w}{\partial z \partial x^2} = 0,$$

and v is obtained from (2.6a) and (2.6b).

The solution for u from (A.2) and (A.3) may be written in terms of a function $H(x, y)$ as

$$(A.4) \quad u = -p_0 \left\{ B(x, y) U'(z) \int \frac{dz}{U^2(z)} + \frac{H(x, y)}{U(z)} \right\} - A(x, y) U'(z),$$

where

$$(A.5) \quad \left(\frac{\partial^2}{\partial x^2} + \frac{\partial^2}{\partial y^2} \right) H(x, y) = \frac{\partial^2 B}{\partial x^2}.$$

Substituting (A.4) and (A.5) into (2.6a) yields

$$(A.6a) \quad p = p_0 \times H(x, y) = p_0 \sigma(x, y)$$

so that

$$(A.6b) \quad \frac{\partial^2 B}{\partial x^2} = \left(\frac{\partial^2}{\partial x^2} + \frac{\partial^2}{\partial y^2} \right) \sigma(x,y)$$

and

$$(A.7a) \quad v = \frac{1}{U(z)} \int_{-\infty}^{\infty} \frac{\partial \sigma}{\partial y} (x',y) dx',$$

where $\sigma(x,y)$ is calculated from the upper layer:

$$(A.7b) \quad \sigma(x,y) = \frac{1}{2\pi} \int_{-\infty}^{\infty} \int_{-\infty}^{\infty} \left\{ \frac{\partial f}{\partial x} \cdot \frac{(x-x')}{[(x-x')^2 + (y-y')^2]^{3/2}} \right\} dx' dy'$$

Thence from (A.7), as in the two-dimensional middle layer, u and v can be expressed to leading order (when $\epsilon \ll 1$) as

$$(A.8) \quad u = (\sigma/U(z))(1+O(\epsilon)).$$

Note that v is given by (A.7c), at least to $O(h_m/L)$. Second-order terms in (h_m/L) in the solution for w and u can be calculated from Appendix B. If the height of the hill is comparable with l or larger (as is usually the case), then (A.7a) and (A.8) can be adapted to give $v_d(x,y,Z)$ and $u_d(x,y,Z)$ if $U(Z)$ is substituted for $U(z)$ as shown in §2.

The result (A.8) shows how there is an amplification of u and v in the lower part of the outer region in a three-dimensional flow, i.e. the middle layer, just as over a two-dimensional hill. This justifies the extension of the scaling laws of Jackson & Hunt (1975) for two-dimensional hills to flow over three-dimensional hills. Mason & Sykes (1979) calculated the inner region over such a hill using the same approximate equation as in III (i.e. 3.19) and found in fact that it gave a useful estimate for the wind field.

AD-A184 222

HEAT AND MOISTURE TRANSPORT IN THE ATMOSPHERIC BOUNDARY 2/3

LAYER(U) FLOW ANALYSIS ASSOCIATES ITHACA NY

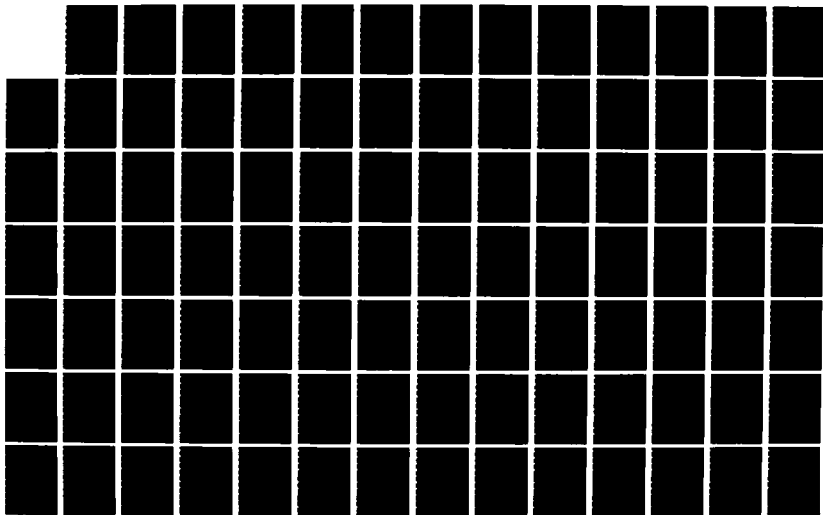
S LEIBOVICH ET AL 05 JAN 87 AFGL-TR-87-0011

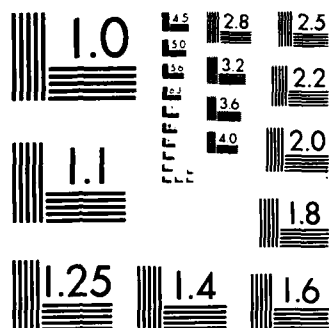
UNCLASSIFIED

F19628-83-C-0018

F/G 4/2

NL





MICROCOPY RESOLUTION TEST CHART
NATIONAL BUREAU OF STANDARDS-1963-A

Appendix B. Asymptotic analysis

The linear results obtained in this paper are here expressed in the standard formalism of asymptotic analysis, which facilitates comparison with other analyses developed in this way (e.g. Sykes 1980; Smith *et al.* 1981). We shall merely state the form of the leading terms of the asymptotic sequences and the results of the governing equations for the leading-order terms. It is assumed here that

$$h_m/L \gg l/L, \quad \text{and } h_m/L \gg H/L$$

so the neglected non-linear terms of $O(H/L)$ are of the same order as the small linear term of $O(l/L)$. Throughout this section, $X = x/L$, and we introduce the following stretched z variables appropriate to the various regions: in the outer region, we set

$$z = z/L,$$

and in the middle region, we set

$$\mu = z/h_m.$$

The inner region has already been treated by asymptotic methods in §3. In the outer region, the perturbation expansion is

$$\begin{aligned} (B.1) \quad u &= u^{(U)}(X, z) = (H/L) \{ u_0^{(U)} + (h_m/L) u_1^{(U)} + (h_m/L)^2 u_2^{(U)} + \dots \}, \\ w &= w^{(U)}(X, z) = (H/L) \{ w_0^{(U)} + (h_m/L) w_1^{(U)} + (h_m/L)^2 w_2^{(U)} + \dots \}, \\ p &= p^{(U)}(X, z) = (H/L) \{ p_0^{(U)} + (h_m/L) p_1^{(U)} + (h_m/L)^2 p_2^{(U)} + \dots \}, \end{aligned}$$

where

$$(B.2) \quad [u_0^{(U)}, w_0^{(U)}] = \frac{1}{\pi} \int_{-\infty}^{\infty} [(X - X'), z] \frac{f'(X')}{(X - X')^2 + z^2} dX',$$

$$(B.3) \quad [u_1^{(U)}, w_1^{(U)}] = \frac{1}{\pi} \int_{-\infty}^{\infty} [(X - X'), z] \frac{w_1^{(M)}(X', h_m)}{(X - X')^2 + z^2} dX',$$

with

$$(B.4) \quad w_1^{(M)}(X, h_m) = - \frac{d\sigma}{dX} U(h_m) \int_{\mu_1}^1 \frac{d\mu}{U^2(\mu)} ;$$

and

$$(B.5) \quad \begin{aligned} p_1^{(U)} &= -u_1^{(U)}, \quad p_2^{(U)} = -u_2^{(U)} \\ p_0^{(U)}(X, 0) &= -u_0^{(U)}(X, 0) = -\sigma(X) = -\frac{1}{\pi} \int_{-\infty}^{\infty} \frac{f'(X')}{X - X'} dX' \\ p_1^{(U)}(X, 0) &= -\sigma^{(1)}(X) U(h_m) \int_0^1 \frac{d\mu}{U^2(\mu)}, \end{aligned}$$

where

$$\sigma^{(1)}(X) = -\frac{1}{\pi} \int_{-\infty}^{\infty} \frac{\frac{d\sigma}{dX'}}{X - X'} dX', \quad \mu_1 = \frac{z_1}{h_m}.$$

In the middle layer, the perturbation expansion is

$$(B.6) \quad \begin{aligned} u &= (H/h_m) \{ u_0^{(M)} + (h_m/L) u_1^{(M)} + (h_m/L)^2 u_2^{(M)} + O((l/h_m)) \}, \\ w &= (H/h_m) \{ w_0^{(M)} + (h_m/L) w_1^{(M)} + (h_m/L)^2 w_2^{(M)} + O((l/h_m)) \}, \\ p &= (H/h_m) \{ p_0^{(M)} + (h_m/L) p_1^{(M)} + (h_m/L)^2 p_2^{(M)} + O((l/h_m)) \}, \end{aligned}$$

and these are functions of X and μ with

$$(B.7) \quad \begin{aligned} u_0^{(M)} &= -f(X) U'(\mu); \quad u_1^{(M)} = \frac{\sigma(X)}{U(\mu)}; \quad u_2^{(M)} = -\frac{p_2^{(M)}}{U(\mu)} + \sigma U' \int_{\mu_1}^{\mu} \frac{d\mu'}{U^2(\mu')} \\ w_0^{(M)} &= 0; \quad w_1^{(M)} = f'(X) U(\mu); \quad w_2^{(M)} = -\frac{d\sigma}{dX} U(\mu) \int_{\mu_1}^{\mu} \frac{d\mu'}{U^2(\mu')}, \end{aligned}$$

and

$$\begin{aligned}
p_0^{(M)} &= 0, & p_1^{(M)} &= p_0^{(U)}(X,0) = -\sigma(X), \\
\text{(B.8)} \quad p_2^{(M)} &= p_1^{(U)}(X,0) + \int_{\mu}^1 f''(X) U(\mu') d\mu'.
\end{aligned}$$

The term in $O(l/h_m)$ is caused by shear stresses in the middle layer. Note that $p_1^{(U)}$, $p_1^{(M)}$ are typically of opposite sign to $p_0^{(U)}$, and $p_0^{(M)}$ and are more peaked near the top of the hill, but the hill curvature term has the same sign as $p_0^{(U)}$ and is larger.

The asymptotic analysis of the inner region in §3 was matched with the expansion in the middle layer only to $O(H/L)$; but (B.6) and (B.7) show that the correction of $O(h_m/L)$ can easily be included in the middle layer and inner region results by correcting the pressure in the middle layer by using (B.8), so that in (M)

$$\text{(B.9)} \quad p = \frac{H}{L} \left\{ -\sigma(X) + \frac{h_m}{L} \sigma^{(1)}(X) U(h_m) \int_{\mu_1}^1 \frac{d\mu}{U^2(\mu)} + \frac{h_m}{L} f''(X) \int_{\mu}^1 U(\mu) d\mu \right\}.$$

This is equivalent to the expression discussed in §2.5 and plotted in fig. 4.

FIGURE CAPTIONS

1. Definition sketch of flow over a hill showing the two main regions of the flow and their subdivision. The height of the middle layer defines the reference velocity U_0 used in the analysis. Also shown is the range of upwind velocity profiles that are considered.

2. Profiles of velocity u_d and shear stress τ_d perturbations in and above the inner region.
 - (a) Sketch showing the zero-order solution ($\ln^{-1}L/z_0 \rightarrow 0$) ———
 first-order corrections of $O(\ln^{-1}(l/z_0))$ - - - -
 corrections of $O(h_m/L)$ ———
 (in this case a reduction - it may be an increase if the curvature is large).

 - (b) Profile of the new solution for the first-order correction $O(\ln^{-1}(l/z_0))$ to u_d in the shear stress layer of the inner region ———
 (the approximate solution of Jackson & Hunt (1975) - - - -).
 the simple form proposed by Jensen & Peterson (1978) ———.
 (This profile is found over the crests of sinusoidal hills with wave length $4L$ so that
 $k = \pi/2$)

 - (c) Profile of the new solution for the zero-order perturbation shear stress τ_d in the inner region, compared to the approximate JH solution.
 ——— Real part of $\tau_d^{(1)}$
 ······ Imaginary part of $\tau_d^{(1)}$
 x—x—x approximate solution of JH

 - (d) Profile of the gradient at the imaginary part of $\tau_d(Z)$, $\partial\tau_d/\partial Z$, in the inner region showing the transition between the (SS) and (IS) layers. ($\ln(l/z_0) = 7$).

3. Magnitude and phase of the maximum surface shear stress on a wavy wall.
 Comparisons between

- (i) computations using the methods of Richards (1980) (—) and
- (ii) the asymptotic limits ($kz_0 \rightarrow 0$) of Sykes (1980) (S) (—);

and

- (iii) the inner region solution for $\ln(l/z_0) \gg 1$ ($x \rightarrow x \rightarrow x$), and
- (iv) the approximate asymptotic solution of Jackson & Hunt (1975) (+—+—).

Note $k = 2\pi/\lambda$ where λ is the wavelength; z_0 is the roughness length.

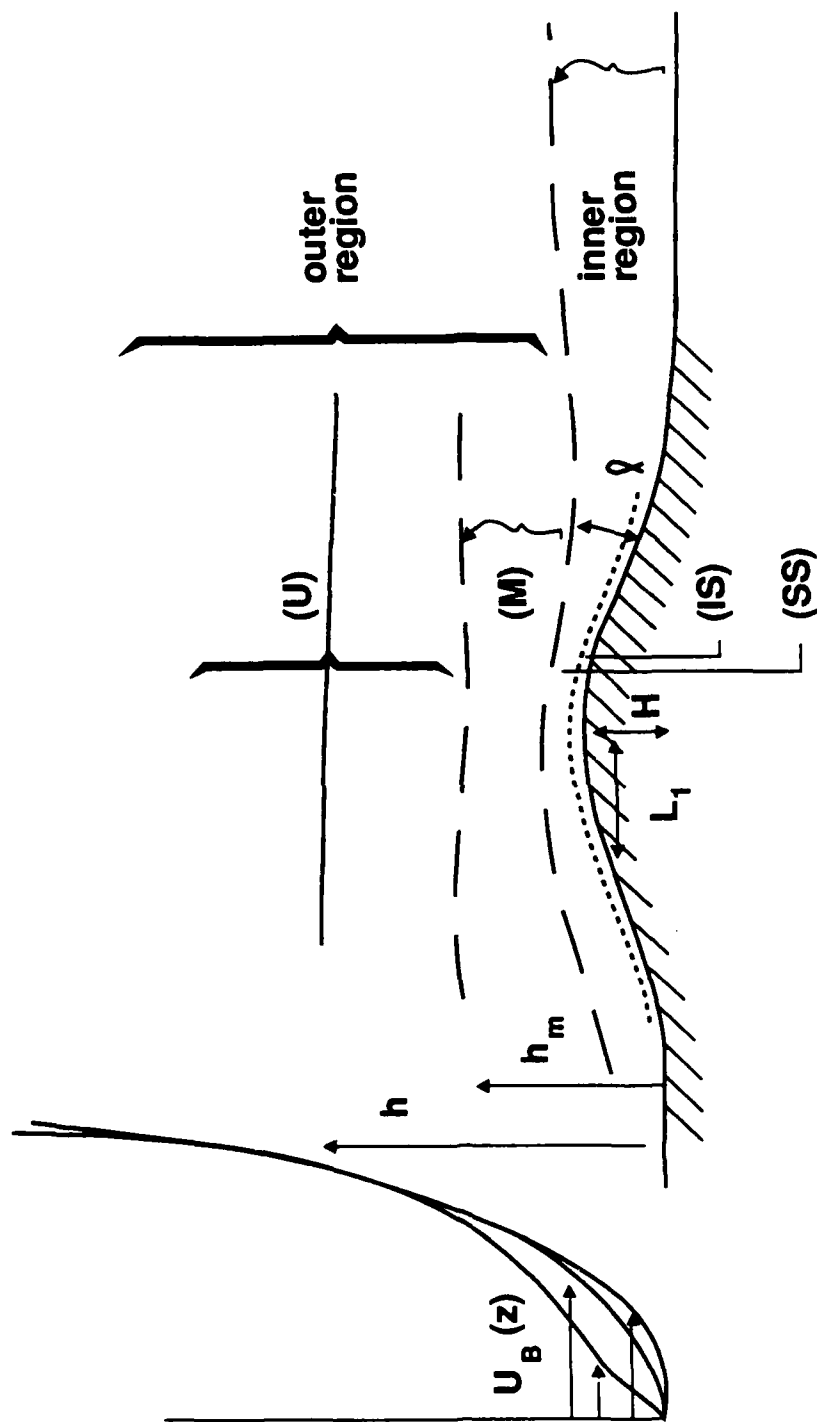
4. Vertical profile of the perturbation pressure for a logarithmic boundary layer profile over the crests of sinusoidal hills showing the $O(h_m/L)$ corrections to p_d in the middle layer for different (L/z_0) .
5. Aspects of the middle-layer structure and its matching with the upper layer.
 - (a) Typical profiles considered. Note the dotted line represents the actual form of $U(z)$ near the ground in stable conditions;
 - (b) The velocity perturbation u_d at the same displacement Z above the surface;
 - (c) The velocity perturbation at the same height z for different strengths of shear and relative scale of boundary layer depth to hill length;
 - (d) Streamline deflection for linear velocity profiles in the same two situations.
6. Various calculations of the increase in mean wind speed at the top of a bell-shaped hill.

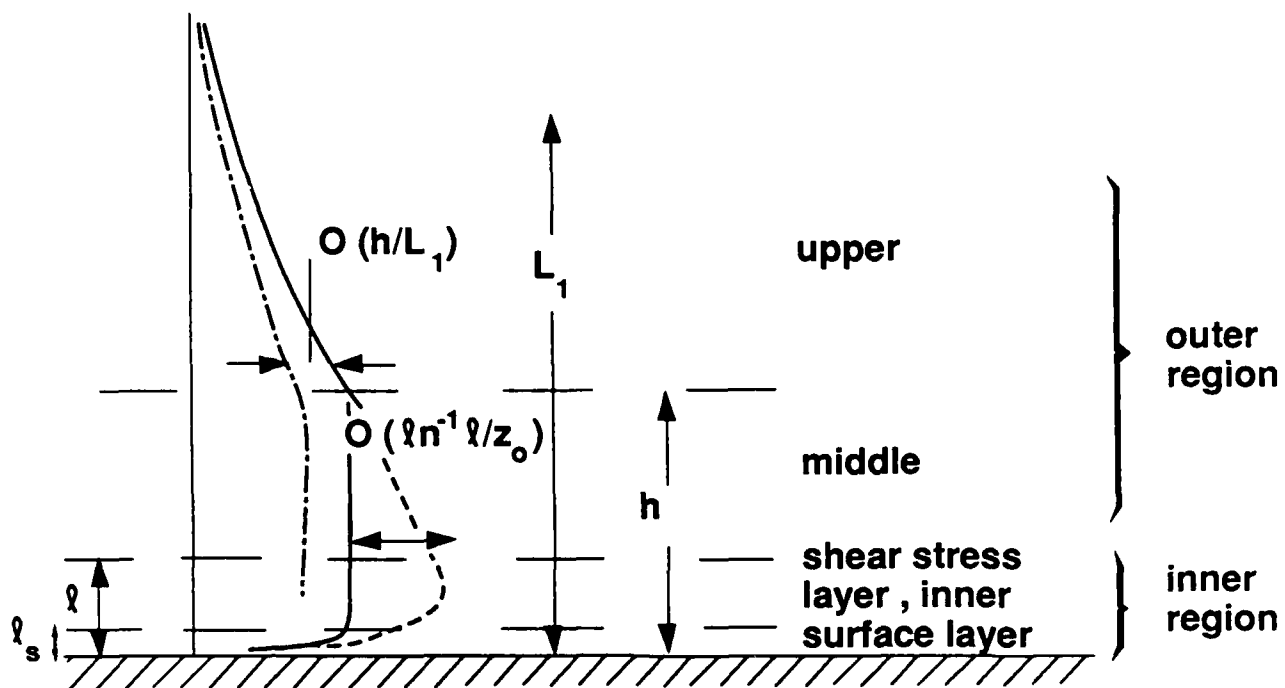
$$f = \frac{1}{1 + \left(\frac{x}{L}\right)^2}$$

at $Z \approx l$, for a case where $L/Z_0 = 1.25 \times 10^4$, $l/z_0 = 6.25$. [For the linear calculations it is assumed that $U(h_m)/U(l) \approx U(L)/U(l) = \ln(L/z_0)/\ln(l/z_0)$].

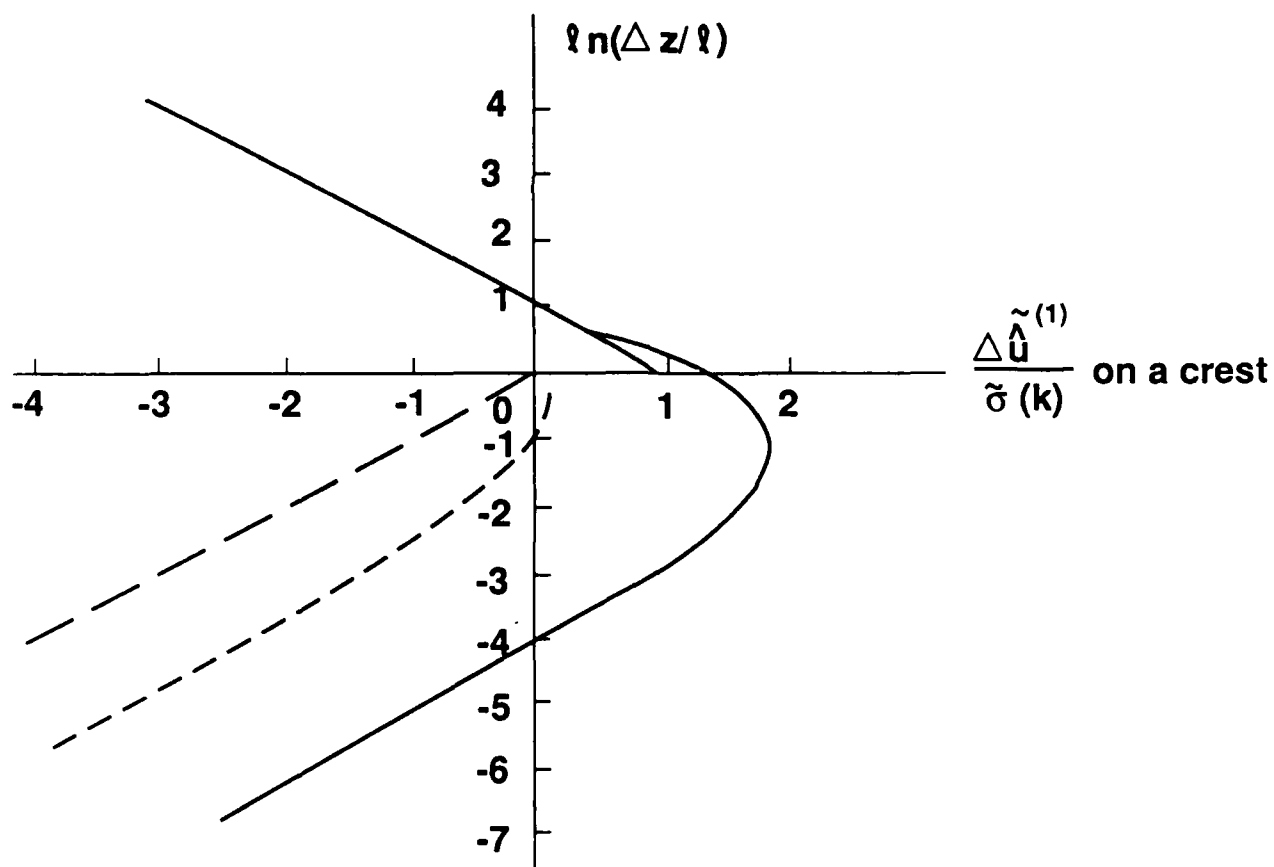
- linear model (5.10a) (also equation (2.4) of Britter, Hunt & Richards (1981));
- +— computation of nonlinear equation using same closure for a hump in the surface layer (Richards & Taylor 1980).
- — — Non-linear corrections using (5.5).

Figure 1

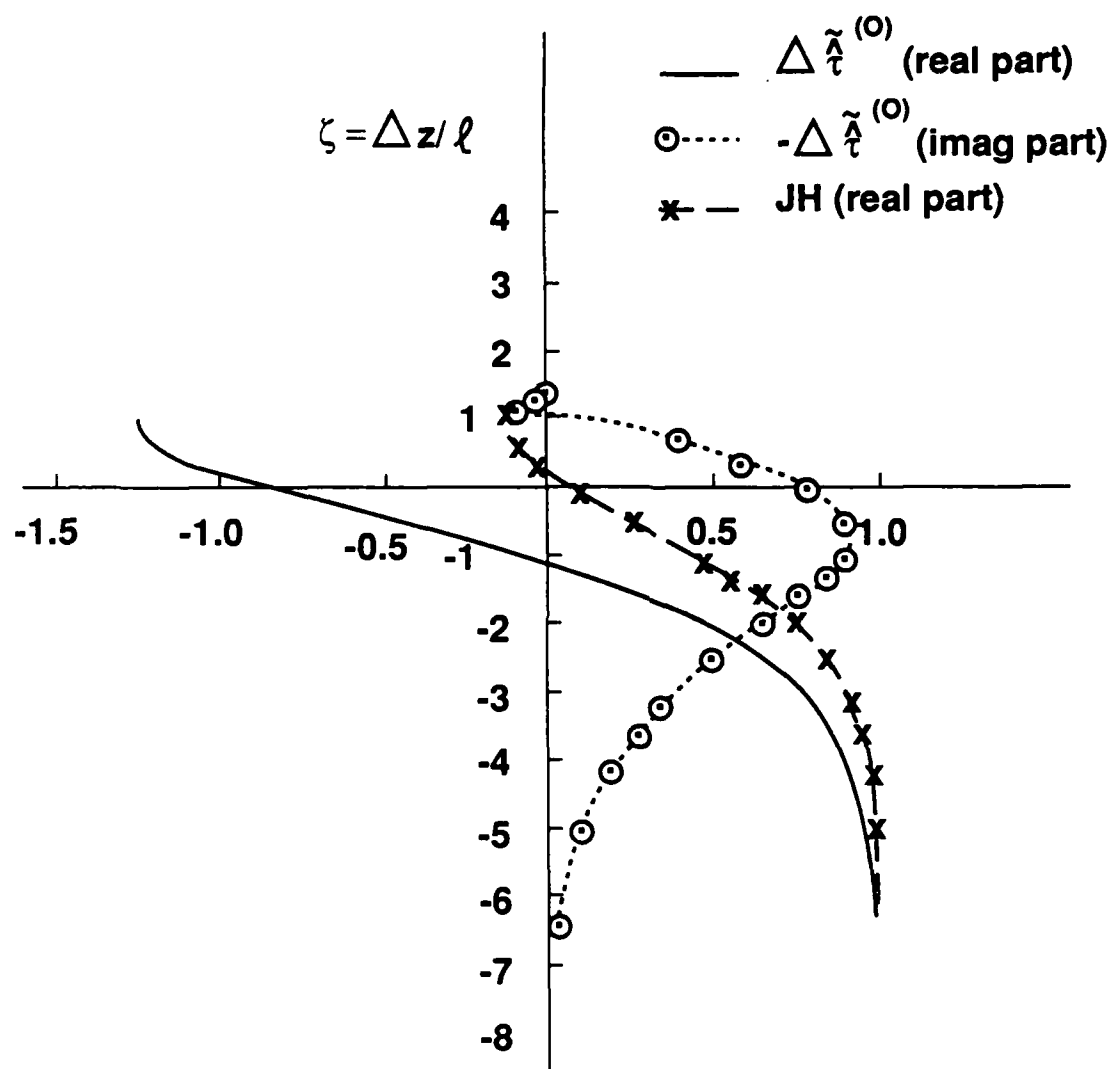




(2a)



(2b)



(2c)

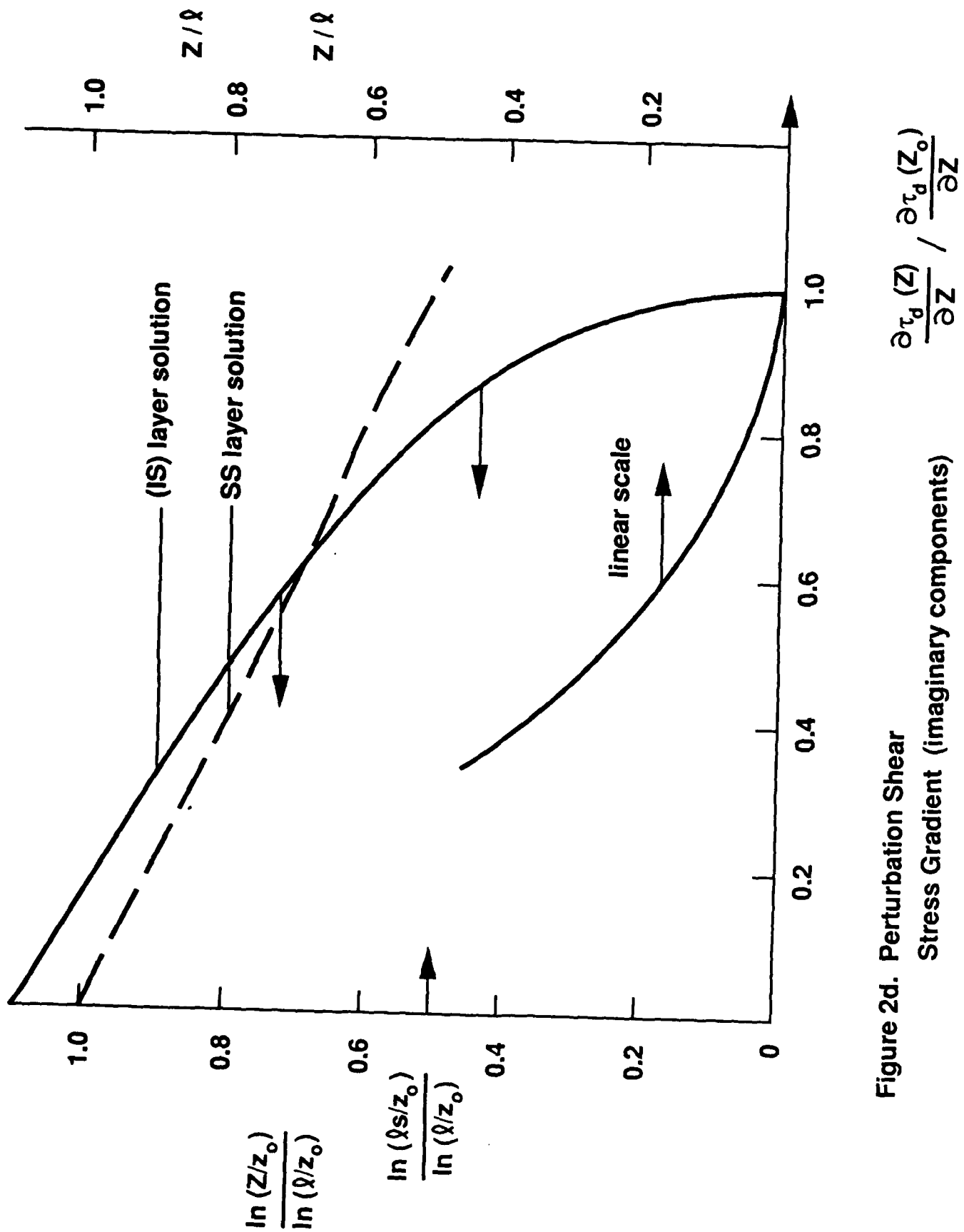


Figure 2d. Perturbation Shear Stress Gradient (imaginary components)

Figure 3

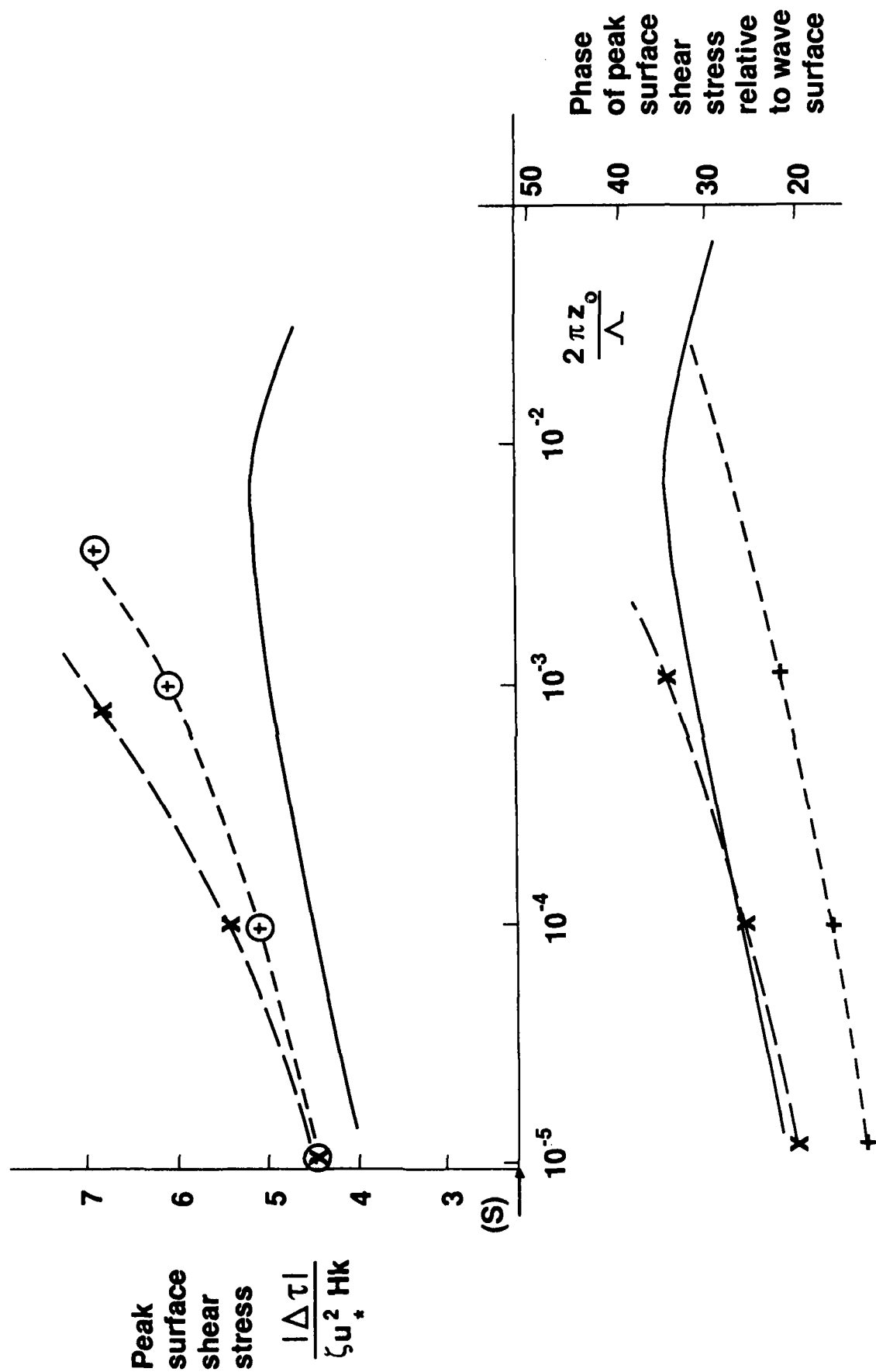


Figure 4

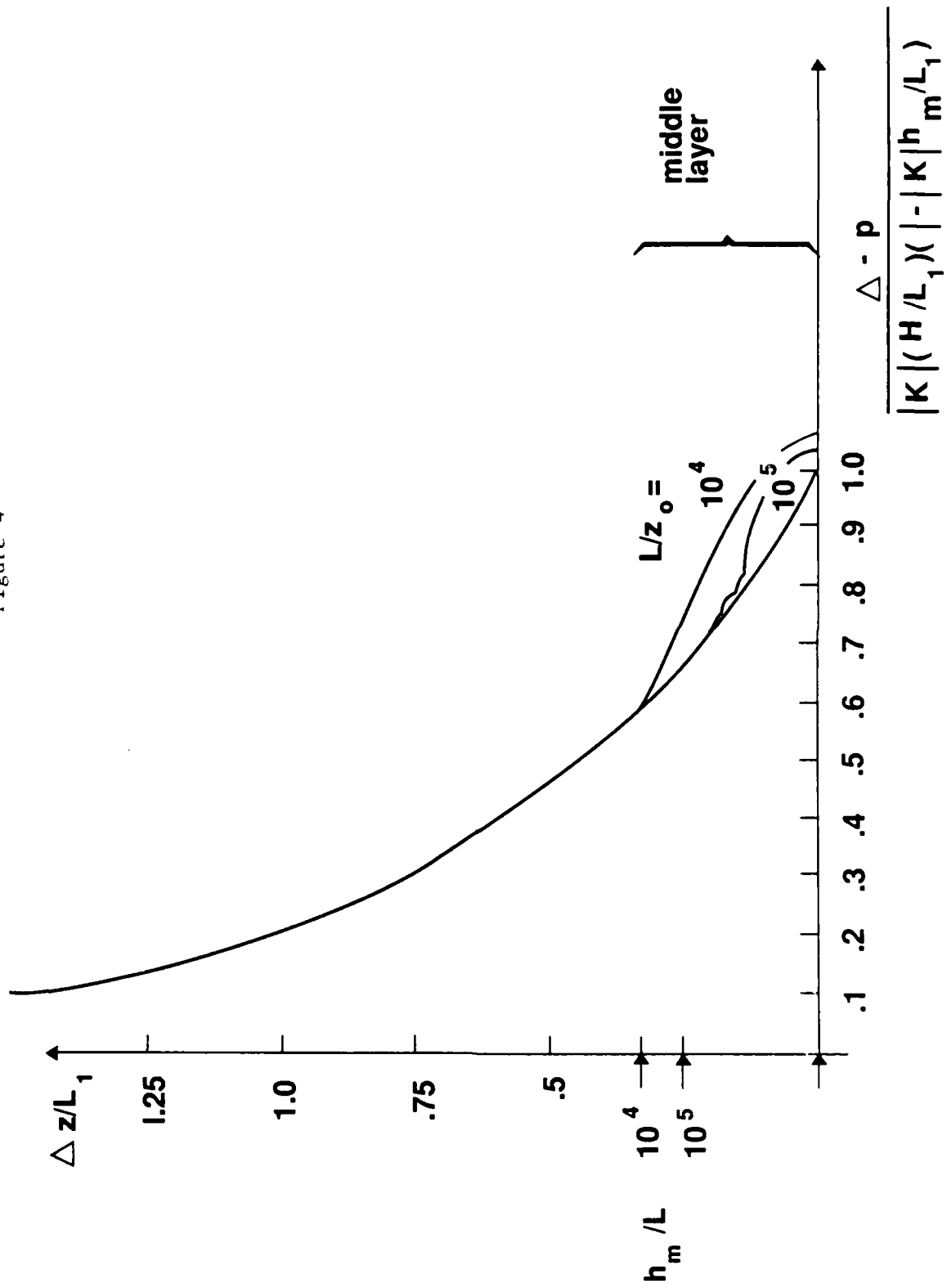


Figure 5

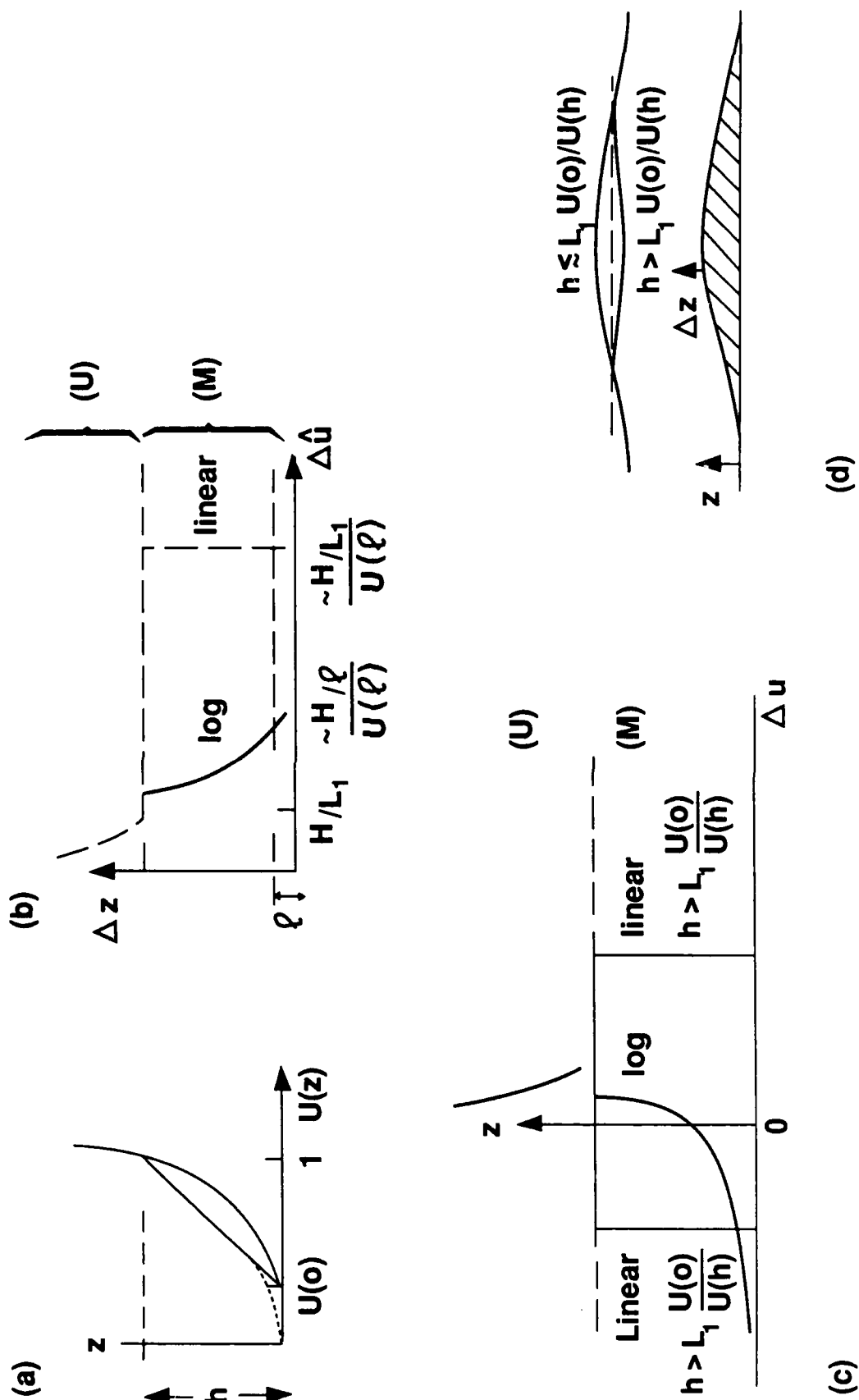
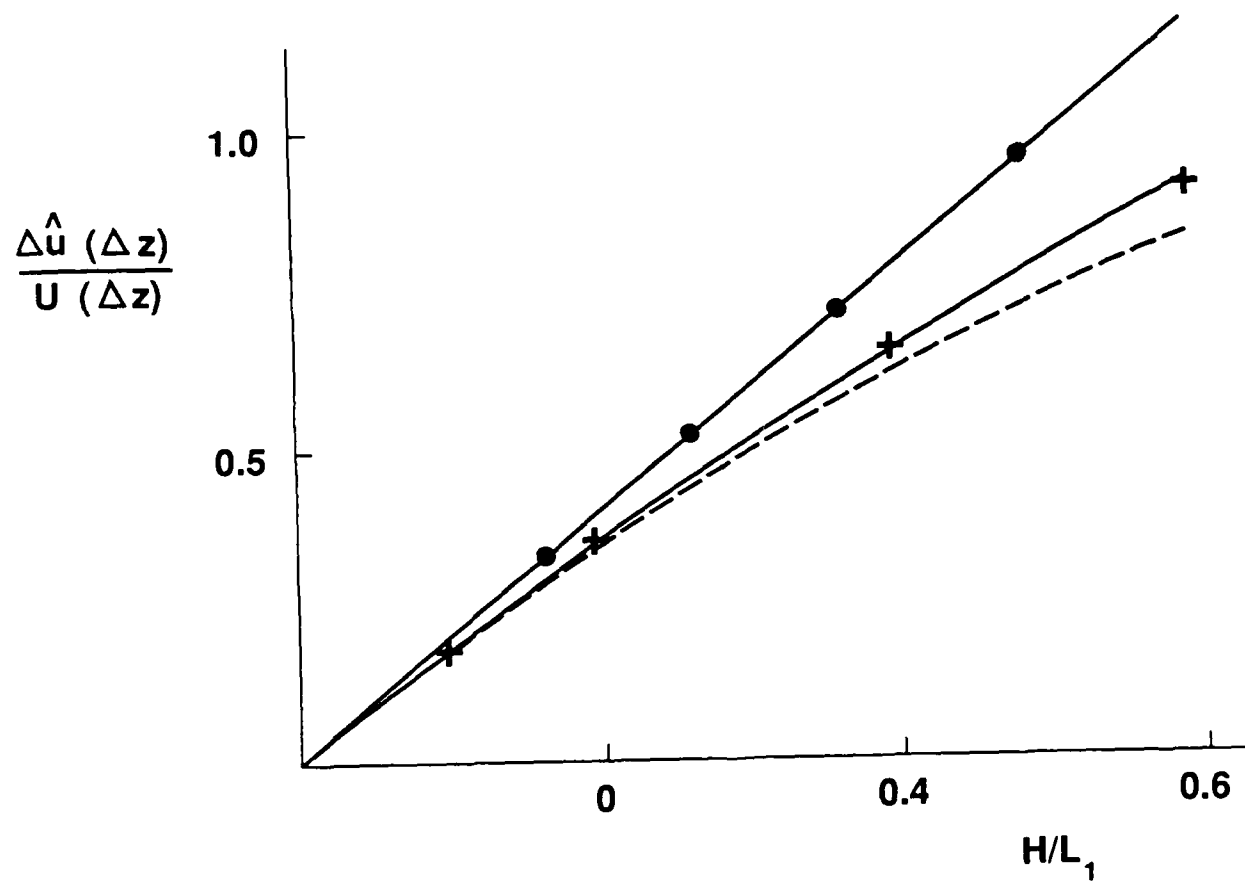


Figure 6



Chapter D

**Stratified shear flows over low hills
II. Stratification effects in the
outer flow region**

Prepared by
J.C.R. Hunt, K.J. Richards, and P.W.M. Brighton

II. Stratification effects in the outer flow region

J.C.R. Hunt

Department of Applied Mathematics and Theoretical Physics
University of Cambridge, Silver Street, Cambridge CB3 9EW

K.J. Richards

Institute of Oceanographic Sciences,
Wormley, Godalming, Surrey GU8 5UB

P.W.M. Brighton

Safety & Reliability Directorate
Wigshaw Lane, Culcheth, Warrington WA3 4NE.

Summary

In this paper the analysis of Part I is applied to flow over hills with low slopes, for various kinds of stable and unstable stratification in the approach flow. (The Froude number F based on the height is always greater than unity.) We concentrate on the flow in the inviscid outer region of the flow. It is shown that in the lower part of the outer region, the middle layer, where the shear is large, the upwind velocity profile and the shape of the hill largely determines the vertical perturbation velocity rather than the upwind density profile. In the 'upper layer' the structure of the flow depends largely on the form of the upwind density profile. For example, this largely determines the

location of maximum surface wind. New solutions for stable conditions are obtained when there is a constant density gradient, when $(N/U_B)^2 = z^{-2}$ and when there is an elevated inversion layer. In the first and third of these cases, we compare the results with the hydrostatic approximation, and also obtain new general formulae for the near-surface winds. An approximate formula is developed for surface winds at arbitrary values of $F(> 1)$ for uniform stable stratification. In weakly unstable or convective conditions over a hill, we show that there is a regular perturbation to the approach flow and find that the mean surface wind speeds are slightly increased.

In an appendix it is shown how the new solutions for stable flow over hills when $F > 1$ can be applied to the flow over hills of arbitrary slope in certain specified (but frequent) conditions when $F < 1$.

1. Introduction

Despite the extensive computational work and measurement of air flow over hills, a number of the main qualitative effects of upwind temperature and velocity gradients on such flows have yet to be firmly established, at least in the lowest 1 km of the atmosphere. Some typical questions that might reasonably be asked, in the context of air pollution dispersion, or the siting of wind-energy devices on hills, or the estimation of wind loads, are

- (i) How does the location and intensity of the maximum wind speed vary with upwind stable or unstable stratification?
-

- (ii) Does the shape of the hill have a similar affect on the wind speed in stratified or in neutral conditions?
- (iii) Where do streamlines come closest to the hill surface, and where is there the greatest lateral deflection of the flow?

These are a few of the general questions that arise in practical problems concerning airflow over hills and this paper is an attempt to help answer them for flow over low hills by drawing together some previous research and developing new solutions where appropriate.

As Scorer (1949) and many others have shown, even the qualitative features of these flows differ considerably with different profiles of the upwind temperature and velocity gradients. Over level terrain in the lowest 300m, these two gradients depend on each other. So we first consider in §2.1 which of the two are more important for the air flow over a hill, as these gradients vary relative to each other, using recent measurements of temperature and velocity from the 300m tower at Boulder, Colorado.

We show theoretically that a weak temperature gradient can increase the upwind velocity gradient sufficiently to magnify significantly the mean velocity over the hill, while being too weak to affect the dynamics of the flow. (A phenomenon observed in wind-tunnel studies by Boumeester 1978.)

When the dynamics of the flow over a hill are affected by sufficiently stable upwind temperature gradients, we show how different temperature profiles can have quite different

qualitative effects by deriving some general formulae for the mean flow over hills with different upwind temperature and velocity profiles. (Some rather general mathematical properties of the Scorer equation governing the outer flow have recently been derived by Bois, (1984).)

When the upwind stratification is strong or is confined to a shallow layer on or above the ground, a useful approach is to assume that vertical accelerations are negligible; this is called the 'hydrostatic' approximation (e.g. Houghton & Kasahara 1968; Lamb & Britter 1983). In the latter case, the flow is similar to that of a shallow layer of water over surface obstructions, and hydraulic methods of analysis can be appropriate.

We show in §2.3 how, when the hydrostatic approximation is valid, some new and simple formulae can be derived for flow over two- and three-dimensional hills, extending the results of Drazin & Su (1975) and R.B. Smith (1980). We provide some estimates and calculations for the errors, associated with the hydrostatic approximation. When a deep layer with a weak stable temperature gradient lies above an elevated inversion layer, the hydrostatic approximation should be used with care, as is shown by the same general analysis developed in §2.3.1. These are compared with the recent computations and field measurements of Carruthers & Choularton (1982).

The analysis here of stable flows over hills is mainly restricted to two- and three-dimensional hills of low slope, where the stratification is weak enough that the perturbations to the velocity are small. (Lilly & Klemp (1979) have

shown how non-linear effects can be estimated.)

This means that the Froude number F based on the hill height H must be somewhat greater than 1.0. Drazin (1961), Brighton (1978) and Hunt & Snyder (1980), and recent field experiments reported by Egan (1984) have shown how, when $F < 1$, around three-dimensional hills, the flow moves in nearly horizontal planes below the summit of the hill, but that near the summit in a layer of thickness (FH) the flow passes over the top of the hill. This is a region of some importance because of the high surface concentrations that are found when the heights of the upwind sources are, as is often the case, nearly equal to that of the hill. In an appendix we use the analysis for the low hills and show that the flow in this layer can be calculated, to first order, when the temperature profile decreases near the hill top. It can also be estimated when the temperature gradient is uniform (as has been suggested by Egan et al. (1981), and by Rowe et al. (1982)). (This 'summit layer' can be analysed exactly when the obstacle is 'porous', which is a model of a collection of hills (Pearson, Newley & Hunt 1985)).

Most previous theoretical papers on stratified flow over hills have been concentrated on stable conditions. However, the results of field experiments on flows over a hill by Bradley (1980, 1983) as well as previous experiments by Frenkiel (1965) have shown how an air flow across a hill is also affected by weakly unstable stratification. In strong convective conditions, cumulus clouds and local circulation over hills are a well-known phenomena (e.g. Scorer (1972), pp.84-84). We are concerned here with a different

situation, where all the convection 'cells' and turbulence are advected over the hill, and where the main effects are caused by the mean temperature gradient and by the elevated inversion at the top of the mixed layer.

In this paper we concentrate on the inviscid flow above the linear inner region. This means that the changes in shear stresses can be neglected in these analyses; (see Pt. I by Hunt, Leibovich & Richards (1985)). The inner region has been discussed in detail in Pt. I and in the general review of airflow over hills by Hunt & Richards (1984).

2.1 Structure of the middle layer

2.1.1 Shear-dominated middle layer

The linearised governing equation for a weak mean vertical velocity Δw in the inviscid outer region in a upwind flow over a hill with small slope is, following Scorer (1949),

$$\left[\frac{\partial^2}{\partial x^2} \left(\nabla^2 - \frac{d^2 U_B / dz^2}{U_B} \right) + \left[\frac{N^2}{U_B^2} \right] \nabla_H^2 \right] \Delta w = 0 \quad (2.1a)$$

where

$$\nabla^2 = \frac{\partial^2}{\partial z^2} + \nabla_H^2, \quad \nabla_H^2 = \left[\frac{\partial^2}{\partial x^2} + \frac{\partial^2}{\partial y^2} \right],$$

the buoyancy frequency $N^2(z) = -g \frac{d^2 \theta_B / dz^2}{\theta_B(z=0)}$ is defined in terms of the gradient of potential temperature θ_B in the upwind boundary layer, and $U_B(z)$ is the mean velocity of the upwind boundary layer which extends up to a height h (see figure 1).

The middle layer M extends up to a height h_m and is defined as the lower part of the outer region where the velocity shear has a dominant effect on the velocity perturbations and therefore is the dominant term in (2.1a). This implies that

$$U_B^{-1} d^2 U_B / dz^2 \gg N^2 / U_B^2 \quad (2.1b)$$

and

$$U_B \frac{d^2 U_B}{dz^2} > L_1^{-2} \quad (2.1c)$$

But the (M) layer is bounded below by the inner region of thickness l where shear stresses significantly affect the flow. Thus in (M) over a hill defined by $z = Hf(x/L_1)$ the vertical distance of a point from the hill surface $\Delta z = z - Hf(x)$, satisfies the inequality

$$h_m > \Delta z > l \quad (2.1d)$$

and Δw is governed by

$$\left[\frac{\partial^2}{\partial z^2} + U_B^{-1} \frac{d^2 U_B}{dz^2} \right] \Delta w = 0 \quad (2.1e)$$

If the height of the hill is large enough that H is of the order of h_m , (but still has a small slope), (2.1e) can be expressed in terms of the vertical distance from the hill surface Δz ,

$$\left[\frac{\partial^2}{\partial \Delta z^2} + U_B^{-1} \frac{d^2 U_B}{d \Delta z^2} \right] \Delta w = 0, \quad (2.1f)$$

with an error term of $O(h_m/L_1)$. The assumption that the hill has a small slope implies $H/L_1 < 1$. The thickness h_m of (M) is estimated by assuming that the conditions (2.1b) and (2.1c) are just satisfied for $z < h_m$. For example, if the form of the velocity profile $U_B(z)$ is approximately logarithmic, $h_m = L_1 \ln^{-1/2}(L_1/z_0)$. Thus h_m depends on the length of the hill and on the forms of the upwind profiles of velocity (for (2.1c)) and both temperature and velocity for (2.1b). (Note that if the hill has a range of scales

(kL_1) (where k varies from say 1 to 10), because the analysis is linear each component scale can be considered as a separate hill, with its own length scale kL_1 and its own value of $h_m(k)$. This technique was first developed by Walmsley et al. (1982).)

In turbulent flows, stable stratification generally increases the shear dU_B/dz , but decreases d^2U_B/dz^2 , (relative to $U_B(z)$ at the same height). Surface layer similarity arguments and field experiments (Monin & Yaglom 1971) show that

$$\frac{dU_B}{dz} = \frac{u_*}{kz} (1 + \alpha z/L_{Mo}) .$$

Here L_{Mo} is the Monin-Obukhov length and the constant α is found to be about 5 ± 1 . When $z/L_{Mo} \gg 1$, it is found that $L_{Mo} = 5(\sigma_w^2/N)$, where N is the local Brunt-Vaisala frequency and σ_w^2 is the variance of the vertical turbulence (Hunt 1982). Thence, since $\sigma_w = 1.3u_*$,

$$U_B''/U_B / (N/U_B)^2 = \frac{4(\sigma_w^2/N)}{z} \left[1 + \frac{\sigma_w}{zN} \ln \left(\frac{z}{z_0} \right) \right] \quad (2.2a)$$

Thus the condition (2.1b) is satisfied over level ground if $z < 4(\sigma_w^2/N)$, which implies that the thickness of (M) is given by

$$h_m = (\sigma_w^2/N) . \quad (2.2b)$$

In the most stable conditions, when $\sigma_w^2/N \leq 10m$, or $L_{Mo} \leq 50m$, this implies that $h_m = 10m$. (In such conditions

the thickness of the whole boundary layer $h = 50\text{m}$ according to the Minnesota measurements of Caughey et al.(1979.) However in such stable conditions the thickness of the inner region l may be of the same order as h_m , in which case the intermediate middle layer, as defined by the conditions (2.1b), (2.1c), does not exist.

However, the value for h_m which satisfies (2.1b) often exceeds the value given by (2.2a), especially in undulating or rough terrain. In recent field measurements on the 300m tower over rolling terrain at Boulder, Colorado, it was found that over a wide range of stable conditions, with L_{Mo} varying from 30m to 300m, when $z \leq 300\text{m}$ that

$$\left[\frac{d^2 U_B}{dz^2} \right] > 5 (N/U_B)^2 . \quad (2.2c)$$

(See figs. 2a,b for typical profiles of U_B, N and U_B''/U_N , and $(N/U_0)^2$ reported by Hunt, Kaimal & Gaynor (1985).) The data quoted by Foldvik (1962) also showed a similar result for z below about 1km.

Consequently we conclude that a middle layer can and often does exist in stable atmospheric flows. In this layer the solution for the vertical and horizontal velocity perturbations and pressure perturbations Δw and Δu and Δp are given by (2.9a) and (2.9b) of Part I. Normalising the velocity field by the upwind mean velocity U_0 at height h_m , so that

$$U_B(z) = U_0 \cdot U(z) ,$$

we obtain

$$\Delta w^{(M)} = A'(x)U_z(z) + \Delta p_0 \cdot \sigma(x)U(z) \int_1^z U^{-2}(z')dz' \quad (2.3a)$$

$$\Delta u^{(M)} = A(x)U'(z) - \Delta p_0 \cdot \sigma(x)J(z)/U(z) \quad (2.3b)$$

where

$$J(z) = [1 + UU' \int_0^z U^{-2}(z')dz'] \quad (2.3c)$$

To first order in h_m/L_1 , $\Delta p^{(M)} = \Delta p_0 \cdot \sigma(x)$ where Δp_0 is the characteristic magnitude of the normalised pressure perturbation. $\sigma(x)$ is a function of order 1 which is a function of the shape (for given slope or ratio H/L_1) and of the stratification. It is determined by the solution of the upper layer.

Matching the flow between the inner and outer regions requires that

$$A(x) = Hf(x/L_1) \quad ,$$

which implies that the displacement of the flow in the outer region is produced by the hill itself and not by the perturbations to the flow in the inner region.

The velocity profile function $J(z)$ is defined by (2.9c) of Pt. I. The correction to $\Delta p^{(M)}/(x,z)$ to first order in h_m/L_1 is given in Part I (Section 4 and Appendix B).

Essentially in the middle layer, the streamwise

perturbation is the sum of the displacement term $-Hf U'_0(z)$ and the pressure-driven term $\Delta p_0 \sigma(x)/U_0(z)$. Over the top of a hill in near-neutral conditions, the first term is negative and the second term is positive. A detailed discussion of these two terms for turbulent and laminar boundary layers is given in Pt.I.

Note that the condition (2.1b) can be satisfied by laminar stratified flow if $U_0/(hN) \gg 1$. Then the solutions of the form of (2.3) are also applicable (Sykes 1978; Brighton 1977).

2.1.2 Strong stratification in the middle layer

The vertical profiles of $N(z)$ and $\theta(z)$ in Figs.2 and 3 show that the temperature gradient or N^2 may increase by a factor of 20 or more in the 50 metres nearest the ground. Let the difference between the temperature in this surface layer and the top of the middle layer (extrapolated downwards) be $\Delta\theta_s$ (Fig.3d). This situation is typically found in the morning or the evening when unstable surface layers or surface stable layers develop, yet the main outer flow over the hill is largely unaffected. In such a condition N^2/U^2 may be significant but still smaller than U''/U for a depth h_{SI} of the order of 5 to 50m over typical hills.

Then if $N^2/U^2 \ll U''/U$, the solution in the shallow stratified layer (lying within the middle layer) is obtained by using equations (2.3a,b,c) as the first-order solution and then correcting for the stratification effects by using (2.1a) (Appendix 1). Denoting the corrected solutions for this stratified middle layer by (M,S), we obtain for $l < z < h_{SI}$,

$$\Delta w^{(MS)} = \Delta w^{(M)} - \frac{Hf'}{L_1} \frac{U(z)}{U_0^2} \int_0^z \frac{g \Delta\theta_s(z') dz'}{\theta(z=0) U^2(z)} \quad (2.3d)$$

$$\Delta u^{(MS)} = \Delta u^{(M)} - \frac{Hfg}{-U_0^2 \theta(z=0)} \left[\frac{\Delta\theta_s(z)}{U(z)} + U'(z) \int_0^z \frac{\Delta\theta_s(z') dz'}{U^2(z')} \right] \quad (2.3e)$$

In other words the correction to Δu is similar to the velocity in a high Froude number shallow-water flow over a hump

in that it decreases over the top of the hill in a stable surface inversion layer. Note too that the change in $\Delta u^{(M)}$ is independent of the thickness of the layer, provided it is shallow. The effects of stratification in the upper layer are incorporated in the expressions for $\Delta w^{(M)}$, $\Delta u^{(M)}$.

2.2 Structure of the upper layer (U)

In the upper layer (U) of the inviscid outer region, the shear effects are assumed to be negligible, so that

$$\left[U_B^{-1} d^2 U_B / dz^2 \right] \ll \min \left[L_1^{-2}, N^2 / U_B^2 \right]$$

where min. denotes whichever is the smaller of the terms. The governing equation, following from (2.1a), is

$$\text{two-dimensional hills: } \left[\frac{\partial^2}{\partial x^2} + \frac{\partial^2}{\partial z^2} + S^2(z) \right] \Delta w = 0 \quad (2.4a)$$

$$\text{three-dimensional hills: } \left[\frac{\partial^2}{\partial x^2} \nabla^2 + S^2 \nabla_H^2 \right] \Delta w = 0, \quad (2.4b)$$

where $S = N^2 / U_B^2(z)$.

To match with the middle layer, the boundary condition as $z/L_1 \rightarrow 0$, is that

$$\Delta w = (H/L_1) U_0 f'(x/L_1) \quad (2.5)$$

The term neglected is $O(h_m/L_1)$ and is given in Appendix B of Part 1.

When $z/L_1 \rightarrow \infty$, the usual radiation condition (e.g. Smith 1980) has to be applied to ensure the energy of the gravity waves is radiated away upwards. The profile of $S = (N/U_B)$ in or above the upper part of the planetary boundary layer typically has three forms (Fig.3):

- (1) S is constant;

(ii) S decreases with height z , either exponentially in the form examined by Foldvick (1962),

$$S = S_e^{-z/h_i} \quad (2.6a)$$

or algebraically:

$$S = S_o (h_m/z)^{\alpha_i}$$

where N_o and U_o are the values at the height h_m of the middle layer, and h_i is the vertical scale of the stably stratified region;

(iii) (N/U_B) is effectively zero below a height h_i and then has a significant value for a finite depth $h_{i1} < z < h_{i2}$.

This situation occurs when there are high winds and a strong elevated inversion and, for example, has been investigated over mountains in Wyoming by Marwitz et al. (and compared with wind-tunnel observations (see Kitabayashi, Orgil & Cermak 1971), and in northern England (Carruthers & Choularton 1982). In some cases, as Kitabayashi et al. and Houghton & Kasahara (1968) have noted, it is appropriate to approximate the elevated inversion layer by a step change in density or potential temperature $\Delta\theta_i$, i.e.

$$N^2 = \frac{g \Delta\theta_i}{\theta} \delta(z - h_i) \quad (2.7)$$

where $\delta(\)$ is a Dirac delta function (see Fig.3c). This may also be associated with a step change in strength and direction of wind velocity.

For purposes of dispersion, the aspects of flow of hills that are important to know are;

- (i) where the streamlines pass closest to the surface, i.e. where n , the distance from a mean streamline to the surface, is minimum, denoted by the point (x_{\min}, y_{\min}) ;
- (ii) how close the streamlines are to the surface, i.e. n_{\min} , as a function of the approach wind speed and stratification and slope of the hill,
- (iii) the change in the horizontal wind speed Δu over the hill.

Over two-dimensional hills, n is directly related to Δu by

$$\int_0^n (\Delta u + U) dz = \text{constant} \quad (2.8a)$$

whereas over three-dimensional hills, n has to be calculated from the vertical velocity perturbation Δw

$$z - z_{\infty} = Hf + n - n_{\infty} = \int_{-\infty}^x \left[\frac{\Delta w}{U + \Delta u} \right] dx \quad (2.8b)$$

where $z_{\infty} = n_{\infty}$ is the upwind height of a fluid element reaching (x, z) over the hill.

2.3 Upper-layer solutions

2.3.1 Constant N/U_B

The solutions to (2.4) for a two-dimensional hill subject to the boundary condition (2.5) and the radiation condition, can be expressed most generally by using Fourier transforms,

$$\Delta w = \frac{1}{2\pi} \int_{-\infty}^{\infty} e^{i\kappa_1 x} \Delta \bar{w}(\kappa_1, z) d\kappa_1 \quad (2.8c)$$

where $\Delta \bar{w}$ satisfies equation (2.4a) of Section 2.2, namely

$$\frac{\partial^2 \Delta \bar{w}}{\partial z^2} + (S^2(z) - \kappa_1^2) \Delta \bar{w} = 0, \quad (2.9a)$$

where we have shown $S(z) = N^2/U_B^2$, and $\Delta \bar{w}$ is subject to the boundary condition

$$\Delta \bar{w} = i \kappa_1 H/L_1 \bar{f}(\kappa_1) \quad \text{as } z/L_1 \rightarrow 0. \quad (2.9b)$$

If $S(z)$ in (2.9) is a constant, then

$$\Delta \bar{w} = i \kappa_1 H \bar{f}(\kappa_1) e^{-Mz}$$

where

$$M = \sqrt{(\kappa_1^2 - S^2)} \quad , \quad |\kappa_1| > S \quad (2.10)$$

$$= -i(\text{sgn } \kappa_1) \sqrt{(S^2 - \kappa_1^2)} \quad , \quad |\kappa_1| < S$$

and

$$\Delta \bar{u} = H \bar{f}(\kappa_1) E(\kappa_1)$$

$$\text{where } E(\kappa_1) = Me^{-Mz} \quad (2.11)$$

The inverse transform yields

$$\Delta u = (H/L_1) \int_{-\infty}^{\infty} E(\kappa_1, z) \bar{f}(\kappa_1) e^{i\kappa_1 x} d\kappa_1 \quad (2.12a)$$

$$\text{When } z/L_1 \rightarrow 0, \quad \Delta u(x) = (H/L_1) \sigma(x/L_1)$$

$$\text{where } \sigma = \int_{-\infty}^{\infty} E(\kappa_1, 0) \bar{f}(\kappa_1) e^{i\kappa_1 x} d\kappa_1 \quad (2.12b)$$

Using convolution theorem it can be shown that at the bottom of the upper layer ($z/L_1 \ll 1$), in limiting cases Δu can be expressed in terms of integrals involving only the hill shape $f(x/L_1)$. The limits correspond to very weak (neutral) and very strong stratification (the 'hydrostatic' limit), which are defined by the inverse Froude number based on the length of the hill $F_L^{-1} = N_0 L_1 / U_0$.

When

$$(N_0 L_1 / U_0) \ll 1, \text{ and } z/L_1 \rightarrow 0, \quad \Delta u = (H/L_1) \sigma_0(x/L_1) \quad (2.13)$$

and when

$$(N_0 L_1 / U_0) \gg 1 \text{ and } \frac{z N_0}{U_0} \rightarrow 0, \quad \Delta u = \frac{H}{L_1} \frac{N_0 L_1}{U_0} \sigma_{\infty}(x/L_1) \quad (2.14)$$

where

$$[\sigma_0, \sigma_\infty] = \frac{1}{\pi} \int_{-\infty}^{\infty} \frac{[df/d(x'/L_1), f(x'/L_1)]dx}{x - x'} \quad (2.15)$$

The results (2.13) and (2.14) can be generalised to three-dimensional hills with low slopes

$$[\sigma_0(x/L_1, y/L_1), \sigma_\infty(x/L_1, y/L_1)] = \frac{1}{2\pi} \int_{-\infty}^{\infty} \int_{-\infty}^{\infty} \frac{[\frac{\partial f}{\partial x}(\frac{x'y'}{L_1}), f(\frac{x'y'}{L_1})](x-x')dx'dy'}{[(x-x')^2 + (y-y')^2]^{3/2}} \quad (2.16)$$

This is a generalisation of Drazin & Su's (1975) result for two-dimensional flows quoted in (2.15). Thus in the middle layer and inner region, the perturbation velocity can be expressed in terms of straightforward integrals of the hill shape and in terms of the stratification.

For the particular case of the bell-shaped hills,

$$f(\frac{x}{L_1}) = \frac{1}{1 + (x/L_1)^2} \quad (a) \quad f\left(\frac{x}{L_1}, \frac{y}{L_1}\right) = \frac{1}{\left[1 + \left[\frac{x^2 + y^2}{L_1^2}\right]\right]^{3/2}} \quad (b) \quad (2.17)$$

the maximum value of $\Delta u(z=0)$, Δu_{\max} , has been computed and compared with the asymptotic solutions and is shown in Fig.4b. The variation of $\Delta u(z/L_1=0)$ is shown in Fig.4a. Streamlines are shown in Fig.4c. In neutral and strong stratified flows, $\Delta u(x,z)$ can be derived explicitly for the bell-shaped hills defined by (2.17b). For two-dimensional

hills, for very weak stratification

$$\frac{N_0 L_1}{U_0} \ll 1, \Delta u = \frac{(H/L_1) [(z/L_1 + 1)^2 - (x/L_1)^2]}{((z/L_1) + 1)^2 + (x/L_1)^2} \quad (2.18a)$$

To understand how surface winds change with a small change in stratification, it is interesting to expand the integral (2.12) as an asymptotic expansion when $N_0 L_1 / U_0 \ll 1$ and $|x|/L_1 \ll 1$. The near-surface wind perturbation can be derived from

$$\begin{aligned} \Delta u(x/L_1, z/L_1 \rightarrow 0) = (H/L_1) & \left[1 - 3x^2/L_1^2 + \frac{1}{2} \frac{N_0^2 L_1^2}{U_0^2} \ln \left[\frac{N_0 L_1}{U_0} \right] \right. \\ & \left. + o(N_0^2 L_1^2 / U_0^2) + \frac{1}{6} \left[\frac{N_0^3 L_1^3}{U_0^3} \right] x/L_1 \dots \right] \quad (2.18b) \end{aligned}$$

So, due to its dynamical effect on the flow over the hill, a small amount of stable stratification leads to a reduction in Δu of order $(N_0^2 L_1^2 / U_0^2) \ln(N_0 L_1 / U_0)$ and to a small movement of the maximum to the leeside. This surprisingly large (logarithmic) reduction can be understood by considering the first-order correction to Δu due to stratification which is

$$(g/(H/L_1)) \int_0^\infty [\hat{\delta}_2(z) d\theta_0/dz / (U_0^2 \theta_0)] dz$$

where $\hat{\delta}_2(z)$ is the vertical streamline deflection. Since $\hat{\delta}_2(z) \approx HL_1/z$ for $L_1 \ll z \ll \frac{U_0}{N_0}$, and since $\hat{\delta}_2(z)$ has a wave-

like form for $z \gg U_0/N_0$, the correction has the form

$$\frac{N^2}{(H/L_1)U_0^2} (H/L_1) (\ln N/U_0 - \ln L_1)$$

in agreement with (2.18b). (Thus if there is a non-uniform stratification where $d\theta_0/dz = \frac{1}{z^p}$ where $p > 0$, or if the hill is three-dimensional, the correction to Δu is of order R_{1L} where

$$R_{1L} = \frac{g(\theta_0(L_1) - \theta_0(l))L_1}{\theta_0(l)U_0^2(L_1)} \quad (2.18c)$$

For strong stratification

$$\frac{NL_1}{U_0} \gg 1, \quad \Delta u = \frac{NL_1}{U_0} \cdot \frac{H/L_1}{1 + (x/L_1)^2} \left[1 + O\left(\frac{NL_1}{U_0}\right)^{-1} \right] \quad (2.18d)$$

For three-dimensional weak stratification

$$\frac{N_0 L_1}{U_0} \ll 1, \quad \Delta u = \frac{-(3(x/L_1)^2 - c^2 H/L_1)}{c^5}$$

$$\delta_z = \frac{1}{U} \int_{-\infty}^x \Delta w dx = \frac{(1 + z/L_1) H/L_1}{c^3} \quad (2.19a)$$

and the vertical and horizontal deflections are given by

$$\delta_y = \int_{U=-\infty}^x \Delta v dx = \frac{(y/L_1) H/L_1}{c^3}$$

For strong stratification, the equivalent results were first obtained by Smith (1980), (though independently by us)

$NL_1/U_0 \gg 1$, $zN/U_0 \ll 1$ (note $NH/U_0 \ll 1$), $z/L_1 \ll 1$,

$$\Delta u = (x/L_1) (NL_1/U_0) (H/L_1)/c^3$$

$$\delta_z = \frac{NL_1}{U_0} H/L_1 \cdot \left[\frac{-(z/L_1)}{1 + (y/L_1)^2} \right] \\ \times \left[1 + \frac{(x/L_1)(1 - (y/L_1)^2)}{(1 + (y/L_1)^2)c} - \frac{2(y/L_1)^2}{1 + (y/L_1)^2} + \frac{(x/L_1)}{c^3} \right] + \frac{(H/L_1)}{c^3} \quad (2.19b)$$

$$\delta_y = \frac{y/L_1}{1 + (y/L_1)^2} \cdot \frac{NL_1}{U_0} \cdot H/L_1 \cdot \left[1 + \frac{x/L_1}{c} \right] \quad (2.19c)$$

where

$$c^2 = (x/L_1)^2 + (y/L_1)^2 + (1 + z/L_1)^2$$

Eq. (2.19) is used in the appendix for stratified flow over three-dimensional hills when $NH/U_0 < 1$. Fig.4b shows that when $NL_1 < 1$ or $F_L > 1$, the deviation from the solution for $NL_1/U_0 = 0$ for the maximum value of Δu or minimum value of n is small, but Fig.4a shows that the distribution of Δu or n varies considerably. However, a closer inspection of Fig.4a suggests that over a hill the variation of Δu and therefore the streamline height n is essentially a weighted mean of the variations when $F_L = \infty$ and $F_L = 0$. This means that we can use, over a wide variety of hills, a

simple form for Δu , namely

$$\sigma = \frac{\Delta u}{(H/L_1)} = \left[\frac{\sigma_o (x/L_1)}{(1 + (NL_1/U_o)^2)} + \frac{NL_1}{U_o} \sigma_{\infty} (x/L_1) \right] \quad (2.20)$$

where σ_o and σ_{∞} are given in (2.15) and (2.16). This interpolation function is plotted in Fig.4b; it is accurate to about 20% at the places where (Δu) is greatest. σ_o and σ_{∞} can be easily calculated for arbitrary hill shapes using (2.15) and (2.16). We have not tried this approximation out for three-dimensional hills using (2.16), but it might also be adequate.

Formally, (2.20) does not have the correct variation of Δu with $N_o L_1/U_o$ when $N_o L_1/U_o \ll 1$, because as shown in (2.18b), the variation of Δu is proportional to $(NL_1/U_o)^2 \ln(NL_1/U_o)$. But when $N_o L_1/U_o \approx 1$, this difference is not be significant.

2.3.2 (N/U_B) decreases with height

The graphs of N and U_B shown in Fig.2 indicate that for hills of limited length, it is quite possible to find (N/U_B) decreasing with height when $z = h_m$. To investigate this possibility, we calculate flow in the upper layer (U) over a sinusoidal range of hills. This brief analysis shows some of the major differences between uniform and decreasing vertical profiles of $N^2/U_B^2 = S(z)$.

First let $S(z) = \hat{S}_0 / z^2$, where $S = S_0 = \hat{S}_0 / h_m^2$ at $z = h_m$. Then from (2.9a) Δw satisfies

$$\left[\frac{\partial^2}{\partial z^2} + \left[\frac{\hat{S}_0}{z^2} - \kappa_1^2 \right] \right] \Delta \tilde{w} = 0 \quad (2.21)$$

Secondly, let \hat{S}_0 lie between 0 and $1/4$, so that we can write $\hat{S}_0 = 1/4 - \nu$, where $1/2 > \nu > 0$ (- a physically realistic assumption when $N_0 h_m / U_0 \leq 1/2$). Then the solution to (2.21), subject to (2.9b) is

$$\Delta \tilde{w} = i \kappa_1 H / L_1 \tilde{E}(\kappa_1) \frac{(h_m / L_1)^{-(1/2-\nu)}}{2\nu} \left[\frac{\Gamma(\nu)}{2} \right]^{-1} (z / L_1)^{1/2} K_\nu(\kappa_1 z / L_1) \quad (2.22)$$

If at the interface of the (U) and (M) layers $dN/dz = \text{constant}$, at $z = h_m$,

$$\frac{d}{dz} (N/U) = N_0 \frac{d}{dz} (1/U) \quad (2.23)$$

If $U(z)$ increases with z in proportion to $z^{1/2 - \nu}$, where $(1/2 - \nu) \ll 1$, it follows from (2.22) that

$$\Delta \tilde{w} \approx z^{(1/2 - \nu)} \approx U(z) \text{ as } z/L \rightarrow 0. \quad (2.24)$$

Thus in this special case Δw matches smoothly with the leading term for $\Delta \tilde{w}$ at the top of the middle layer (2.3a). In general, there would have to be a local matching solution at the interface of the (M) and (U) layers.

Given (2.22) it follows that

$$\Delta \tilde{u} = -H/L_1 \tilde{f}(\kappa_1) \frac{(h_m/L_1)^{-(1/2 - \nu)}}{z^\nu} \left[\frac{(\Gamma(\nu))}{2} \right]^{-1} \frac{d}{d(z/L_1)} \left[(z/L_1)^{1/2} K_\nu(\kappa_1 z/L_1) \right] \quad (2.25)$$

and when $\kappa_1 z/L_1 \ll 1$

$$\Delta \tilde{u} \approx - (H/L_1) \tilde{f}(\kappa_1) (h_m/L_1)^{-(1/2 - \nu)} (z/L_1)^{-(1/2 + \nu)}. \quad (2.26)$$

In Fig. 5a the forms of the vertical profiles of $|\Delta \tilde{w}|$ and $|\Delta \tilde{u}|$ are shown, and in Fig. 5b the form of the streamlines over a range of hills when $(h_m/L_1) < S_0^{1/2}$. Note that the effect of stable stratification in this case is to locate the maximum perturbation velocity and minimum n in the valleys, whereas the effect of a uniform profile of N/U is to locate u_{\max} and n_{\min} on the downwind slopes. We

should also expect to see the same effect on a single hill. We should also expect to see the same effect if the decrease of $\langle N/U_B \rangle$ with z is so abrupt that the $\langle N/U_B \rangle$ profile can be represented as a step change. We consider that possibility next.

2.3.3 Elevated inversion

The essential features of the effects on flow over hills of abrupt changes in potential temperature or wind speed can be studied by assuming that S has a delta function form. In the case of an elevated inversion

$$(N/U_B)^2 = U_B^{-2} \Delta S \delta(z - h_1) = \frac{F_1^{-2}}{h_1} \delta(z - h_1) \quad (2.27)$$

where $\Delta S = \frac{-g \Delta \rho_1}{\rho} = \frac{g \Delta \theta_1}{\theta}$, and $\Delta \rho_1$, $\Delta \theta_1$ are the discontinuities in density ρ or temperature θ across the inversion. It is also convenient mathematically, and appropriate physically, to assume

$$h_m < h_1 < L_1 \quad \text{and} \quad H < h_1. \quad (2.28)$$

This would be appropriate where $h_1 \approx 300\text{m}$, and $L_1 > 500\text{m}$. If the length of the hill is less than the inversion height, i.e. $L_1 < h_1$, then solutions can also be obtained analytically. They exhibit behaviour intermediate between that of neutral flow and that of quasi-hydraulic flow found here. By assuming that H/h_1 is small, nonlinear effects such as waves on the inversion layer can be ignored (Forbes & Schwartz 1982).

Given (2.27) and (2.28) it follows that the solution to (2.4a) below the inversion where $h_m < z < h_1$ is

$$\Delta w = (H/L_1) f'(x/L_1) + \zeta_1 \left[\frac{d \Delta h_1}{d(x/L_1)} - (H/L_1) f'(x/L_1) \right]$$

where $\zeta_i = z/h_i$ if $h_i \gg h_m$, but in many circumstances where inversions are within the middle layer, then

$$\zeta_i = U(z) \int_{z_0}^z dz' / U^2(z') / \int_{z_0}^{h_i} dz' / U^2(z'),$$

Then by continuity

$$\Delta u = \frac{Hf - \Delta h_i}{h_i} + \frac{h_i}{L_1} \left[\left(\frac{\zeta_i^2}{2} - \frac{1}{6} \right) \Delta h_i''(x/L_1) + \frac{\zeta_i - \zeta_1}{2} - \frac{1}{3} \frac{H}{L_1} f''(x/L_1) \right] \quad (2.29a)$$

Equation (2.4) can be integrated vertically across the temperature discontinuity at the elevated inversion at $z = h_i$. We obtain at $z = h_i$

$$\left[\frac{\partial \Delta w}{\partial z} \right]_{h_i} = -F_i^{-2} \frac{\Delta w}{h_i} (z = h_i) = -\frac{F_i^{-2}}{h_i} \frac{d\Delta h_i}{dx},$$

which from continuity and by integration w.r.t. x becomes at $z = h_i$

$$[\Delta u]_{h_i} / U = F_i^{-2} \Delta h_i / h_i \quad (2.29b)$$

where $[]_{h_i}$ denotes the change across $z = h_i$.

To calculate Δu in the uniformly stratified layer above the inversion where $(N/U_B)^2 = (N_O/U_O)^2$ is constant, we solve (2.4a) subject to the condition

$$\text{at } z = h_i, \Delta w = U_O dh_i / dx \quad (2.29c)$$

Hence at $z = h_i$, Δu is proportional to $U \Delta h_i / L_1$ where

" Δh_i " is the maximum perturbation of the inversion layer, and also Δu depends on $N_0 L_1 / U_0$. In particular from (2.13), (2.14) and (2.15), we can express Δu just above the inversion as

$$\Delta u(x, z = h_i) = \left[\frac{H}{L_1} \right] U \Sigma \quad (2.29d)$$

where, by analogy with (2.15), Σ can be expressed in terms of integrals involving the deflection of the inversion for weak and strong stratification above the inversion layer, viz.

$$\Sigma = \frac{1}{\pi} \int_{-\infty}^{\infty} \frac{\left[(d(\frac{\Delta h_i}{H})/d(x'/L_1)) \cdot (N_0 L_1 / U_0)^{-\frac{1}{2}} (\frac{\Delta h_i}{H})(x'/L_1) \right]}{(x/L_1 - x'/L_1)} dx'/L_1 \quad (2.29e)$$

when $F_L^{-1} = N_0 L_1 / U_0 \ll 1$ and $F_L^{-1} = N_0 L_1 / U_0 \gg 1$ respectively.

We can now calculate how the height n_1 of the inversion layer above the hill surface and the wind fields change with variation of the strengths of the inversion layer, and the upper layer stratification, measured by F_1^{-1} and F_L^{-1} respectively. (We are still assuming $\Delta u/U \ll 1$ and $H/L_1 \ll 1$, $h_1/L_1 \ll 1$).

By expressing n_1 in terms of the change of the inversion height Δh_i , and then combining (2.29a,b,d), n_1 is given by

$$n_1 = h_1 + \frac{Hf}{F_1^2 - 1} - \frac{h_1 F_1^2}{F_1^2 - 1} \left\{ \frac{H}{L_1} \Sigma(x/L_1) - h_1/L_1 \left[\frac{H}{L_1} \frac{f''}{6} + \frac{1}{3} \frac{\Delta h_i''}{L_1} \right] \right\} \quad (2.30)$$

From (2.30) and the previous discussion of $\Delta u^{(u)}$, many of the qualitative features of these kind of flows can be deduced by considering some limiting cases of (2.30) for various combinations of weak and strong inversion strengths and upper-layer stratification. We derive explicit expressions for the case of a two-dimensional bell-shaped hill defined by (2.17a).

For a weak elevated inversion, when $F_1 \gg 1$, (2.30) becomes

$$n_1 = h_i - \frac{h_i H}{L_1} \left[\Sigma(x/L_1) - \frac{h_i}{2L_1} f''(x/L_1) \right] + F_1^{-2} \left\{ Hf - \frac{h_i H}{L_1} \left[\Sigma - \frac{h_i}{2L_1} f'' \right] \right\} . \quad (2.31a)$$

Then if the upper stratification is weak,

$$F_L \gg 1 \quad \text{and} \quad \Sigma = \sigma_0 = \frac{1}{\pi} \int_{-\infty}^{\infty} \frac{df/d(x'/L_1)}{x - x'} dx' \left[1 + o(F_L^{-2} \ln F_L) \right] . \quad (2.31b)$$

For a bell-shaped hill, where

$$F_L \gg 1, \quad \sigma_0 = (H/L_1) (1 - (x/L_1)^2)/(1 + (x/L_1)^2)^2 \quad (2.31c)$$

and

$$f'' = -2(1 - 3(x/L_1)^2)/(1 + (x/L_1)^2)^3 . \quad (2.31d)$$

For a weak elevated inversion and a strong upper-layer stratification, where $F_1 \gg 1$ and $F_L \ll 1$, n_1 is still given

by (2.31a), but now

$$\Sigma = \sigma_{\infty} \frac{NL_1}{U} = \frac{NL_1}{U} \cdot \frac{1}{\pi} \int_{-\infty}^{\infty} \frac{f(x')}{x - x'} dx' (1 + o(F_L)) \quad (2.31e)$$

For a bell-shaped hill,

$$\sigma_{\infty} = \left[\frac{NL_1}{U} \right] \frac{x/L_1}{(1 + (x/L_1)^2)} \quad (2.31f)$$

and f'' is given by (2.31d).

Summarising these results, shows that an elevated inversion only affects the flow if the Froude number of the inversion is small enough that

$$F_i^{-2} > (h_i/L_1) \Sigma \quad \text{where} \quad 1 > F_i^{-2} \quad (2.32)$$

Since Σ is a function of upper-layer stratification, this means that if the upper layer stratification is weak ($F_L > 1$), there is an effect of the weak inversion if $F_1^2 < (L_1/h_1)$, and if the upper layer stratification is strong ($F_L < 1$) there is an effect of the inversion if $F_1^2 < (L_1/h_1)F_L$. Thus surprisingly the greater the upper-layer stratification, the greater the effect is of an elevated inversion. So for a weak elevated inversion in either case the height of the inversion increases over the hill top (i.e. an increase in n_{\min}), the well-known supercritical behaviour of a water surface. If the inversion is just strong enough for (2.32) to be satisfied, it can make the hill top a position of maximum n_1 and minimum velocity rather than minimum n_1 and maximum velocity.

another case like that in § 2.3.2. Note how when the upper layer is stratified, i.e. $F_L < \infty$, an elevated inversion does not affect the movement of the position of velocity maximum down the lee slope.

The physical explanation for these results is that, as the strength of a weak elevated inversion or uniform stratification increases, the increase in potential energy associated with the raising of the inversion over the hill has to be balanced by a reduction in kinetic energy over the hill top, so Δu is reduced. An alternative explanation is that since Δp increases at a given height z as the inversion is raised over the hill, Δu must decrease.

For a strong elevated inversion, when $F_1^2 \ll 1$, the streamline deflection n_1 can be expressed as

$$n_1 = h_1 - Hf - F_1^2 Hf \left[1 - \frac{1}{6} \frac{h_1^2}{L_1^2} f'' \right] - F_1^4 \left(Hf + \frac{h_1 H}{L_1} \left[\Sigma - \frac{1}{3} \frac{h_1}{L_1} f'' \right] \right). \quad (2.33)$$

Note that the magnitude of the upper layer velocity field only affects h_1 at $O(F_1^4)$ because to zero order $\Delta h_1 = 0$; so the effect of the hill on the upper-layer velocity is $O(F_1^2)$. The reason for the negative sign in front of Σ is because when $F_1^2 \ll 1$, the inversion height is deflected downwards and therefore Δu is negative (see Fig.5b) (the familiar subcritical behaviour of a water surface). Thus if the upper layer is weakly stratified, ($F_L \gg 1$), Σ is given by (2.31b), and if it is strongly stratified, ($F_L \ll 1$), Σ

is given by (2.31e) and the values of Σ and f'' for bell-shaped hills are given by (2.31c-f) respectively. Note that the neglect of the upper-layer motion underestimates the downwards deflection and so overestimates n_{\min} . For example, if $F_L = 0.5$, the downward deflection Δh_1 is increased by a factor $0.25 h_1/L_1$ when $P > 1$, and by more when F_L is smaller.

When the Froude number for the elevated inversion F_1 is of the order of unity, then, as may be seen from (2.30), large changes occur in the height of the inversion. It behaves like the surface of a stream and hydraulic theory may be appropriate. In fact, if $H \ll L_1$ and $h_1 \ll L_1$, a nonlinear theory can be developed along the lines of the foregoing linear theory to allow for changes in h_1 which are large compared with h_i . Then (2.29a) becomes

$$(U + \Delta u) + U/(n_i/h_i) \quad (2.34a)$$

and (2.29b) becomes

$$\frac{1}{2U^2} [(u + \Delta u)^2 - U^2]_{h_i} = F_1^2 \Delta h_i/h_i \quad (2.34b)$$

and (2.30) becomes

$$\frac{n_1 - h_1}{h_1} + \frac{Hf}{h_1} + \frac{F_1^2}{2} \left[\frac{1}{(n_i/h_i)^2} - 1 \right] = F_1^2 \left[\frac{\Delta u^{(U)}}{U} \right] (z = h_1) \quad (2.34c)$$

were it is assumed $\Delta u^{(U)}/U \ll 1$ and terms of $o(h_1/L_1)$ are negligible. Note that when $(n_1 - h_1)/L_1 \ll 1$ and $h_1/L_1 \ll 1$,

(2.34c) reduces to (2.30). Eq. (2.34b) combined with (2.29d,e) shows that when $H/L_1 \ll 1$ and $n_1 \ll L_1$, the upper layer motions only produce a perturbation on $(n_1 - h_1)/n_1$ of $O(H/L_1)$ if the upper layer is weakly stratified, but a perturbation of $O(N_0 H/U_0)$ if it is strongly stratified. On over most hills, if $F_1 \neq 1$, nonlinear hydraulic theory can be used as a first approximation and (2.34c) (with (2.34b) for calculating $h_1^{(U)}$) can be used to correct for the upper-layer motions.

For completeness we note that the salient results of this theory when $F_1 = 1$, namely that if $1 > F_1$, the flow becomes locally supercritical over the hill top (where $n_1 = n_1 F_1^{2/3}$), and h_1 continues to decrease on the downslope side to a minimum value n_{\min} given by the smallest root of

$$n_{\min} - n_1 = \frac{n_1 F_1^2}{2} \left[\frac{1}{(n_{\min}/h_1)^2} - 1 \right].$$

Hydraulic (or hydrostatic) theory has been used by several authors to study stratified flow over hills, notably by Houghton & Kasanara (1968), Marwitz et al. (whose published work was described by Kirapayoglu, Orfili & Germal (1971)), and more recently by Lamb & Britter (1984). In the second of these reports, the theory was compared qualitatively with laboratory and field experiments and in the third with a careful laboratory study in a water channel of stratified flow over three-dimensional hills with an elevated inversion and a neutral upper layer.

Without correcting for upper-layer accelerations, the

hydrostatic theory agreed well with observations, as our analysis here shows should be the case.

The effects of stable stratification above a relatively thin layer (thickness δ_1) of strong stable stratification in flow over a hill have recently been computed and measured by Carruthers & Choularton (1982). In their studies the length scales were $\delta_1 = 400\text{m}$, $h_1 = 600\text{m}$, $L_1 = 2000\text{m}$ and $H = 665\text{m}$. The stratification across the inversion was such that

$$\int_{h_1 - \delta_1/2}^{h_1 + \delta_1/2} (N/U_B)^2 dz = \frac{F_1^2}{h_1} \text{ lay in the range } 9 \times 10^{-4} \text{ m}^{-1} \text{ to } 2.25 \times 10^{-4} \text{ m}^{-1} .$$

so that $2 < F_1^2 < 8$.

For the upper layer, the stratification was such that $0.4 < F_L < 0.7$. Therefore we would expect the inversion displacement as given by Carruthers & Choularton (1982) in their Figs.8,9 to be described by Figs.6b (i) and (ii), and the magnitude of h_1 to be given approximately by (2.31a,b).

We present here a number of calculations from our formulae which can compare with Carruthers & Choularton's (C) which are in brackets.

In neutral conditions at $x/L_1 = 0$, $n_1/L_1 = 0.20;(0.24)$.

When

$$F_1^2 = 2, F_L = 0.4, x/L_1 = 1.0, n_1/L_1 = 0.28 \quad (0.23)$$

$$F_1^2 = 2, F_L = 0.7, x/L_1 = 1.0, n_1/L_1 = 0.36 \quad (0.27)$$

$$F_1^2 = 2, F_L = 0.7, x/L_1 = 1.0, n_1/L_1 = 0.44 \quad (0.42)$$

$$F_1^2 = 8, F_L = 0.7, x/L_1 = 1.0, n_1/L_1 = 0.38 \quad (0.36) \text{ (inferred)}$$

From the approximate agreement with the computations, it appears that useful estimates as well as general understanding of the effects of elevated inversions can be obtained from the idealised theory presented here. However where large wave motions occur in the upper layer, they may strongly affect the inversion layer, and then an analysis is required that studies strong interactions between the inversion layer and the upper layer.

2.3.4 Stable stratification below a strong elevated inversion

One of the kinds of stable stratification that has caused much interest has been when lee waves are produced by a uniform stratification and are trapped and amplified by a strong elevated inversion. Klemp & Lilly (1975) have shown that this situation can give rise to severe wind storms. Inviscid computations for this situation are presented here which have been compared with the laboratory experiments by Brighton (1977). We assume that the strength ΔS of the elevated inversion is such that

$$\Delta w / (H/L_1) \ll 1 \quad \text{at} \quad z = h_i$$

and that $h_i > h_m$, so Δw satisfies (2.9), subject to

$$\begin{aligned} \Delta \tilde{w} &= 0 \quad \text{at} \quad z = h_i \\ \Delta \tilde{w} &= ik_1 H/L_1 \tilde{f}(k_1) \quad \text{as} \quad z/L_1 \rightarrow 0 \end{aligned} \tag{2.35}$$

The solution is

$$\Delta \tilde{w} = ik_1 (H/L_1) \tilde{f} \frac{\sinh((h_i - z)M)}{\sinh h_i M} \tag{2.36}$$

where M is given by (2.10); then when

$$z/L_1 \ll 1, \quad -\Delta \tilde{p}^{(U)} = \Delta \tilde{u}^{(U)} = \frac{-H}{L_1} \tilde{f} \coth(Mh_i). \tag{2.37}$$

This solution has poles at

$$h_1 \sqrt{(S^2 - k_1^2)} = m\pi$$

and to produce no upstream influence, the contour of integration has to be deformed below these poles.

Consider the first-wave mode $m = 1$, for which

$$\pi > Sh_1 > 2\pi \quad \text{or} \quad \pi > F_L^{-1}(h_1/L_1) > 2\pi.$$

(For $Sh_1 < \pi$ no wave modes exist and the flow is said to be supercritical.) There are then two poles at $k = \pm k_p$, where $k_p = \sqrt{(S^2 - \pi^2/h_1^2)}$. In order to evaluate the integrals numerically, we split the pressure into its wave and non-wave components, i.e.

$$\Delta \tilde{p}^{(U)} = \Delta \tilde{p}_w + \Delta \tilde{p}_{nw} \quad (2.38)$$

where

$$\Delta \tilde{p}_w = \frac{\pi^2}{D^3 k_p} \left[\frac{\tilde{f}(k_p)}{k_1 - k_p} - \frac{\tilde{f}(-k_p)}{k_1 - k_p} \right].$$

The inverse transformation $\tilde{p}_w^{(1)}$ is then

$$\begin{aligned} \Delta \tilde{p}_w &= 0 & x < 0 \\ &= \frac{-2\pi^2}{D^3 k_p} \operatorname{fm} \left[\tilde{f}(k_p) e^{ik_p x} \right] & x > 0 \end{aligned} \quad (2.39)$$

and the inverse transform of $\Delta \tilde{p}_{nw} = \Delta \tilde{p}^{(U)} - \tilde{p}_w^{(0)}$ is evaluated numerically using an FFT algorithm.

The negative perturbation surface pressure $\frac{-\Delta p^{(U)}}{(H/L_1)}$ ($z/L_1=0$) is shown in Figs. 7a and 7b as a function of x/L_1 with $h_1/L_1=3$ for supercritical and subcritical ($m=1$) flows, respectively. The hill shape is taken to be Gaussian, i.e.

$$f(x/L_1) = e^{-(x/L_1)^2/2} \quad (2.40)$$

For $S < \pi/h_1$ (supercritical), the pressure distribution is symmetrical about the hill crest with the pressure minimum at the crest decreasing for increasing S . For $S > \pi/h_1$ (subcritical), the wave modes are allowed. Due to the reflection of energy from the upper boundary, the amplitude of the lee waves is greatly increased over that of the unbounded crest. The wave length of the lee waves is now given by

$$\Lambda = \left[\frac{2\pi U_0}{N} \right] \left[1 - \frac{\pi^2}{h_1^2 S^2} \right]^{-1/2} \quad (2.41)$$

Thus an upper estimate of the maximum near-surface velocity is

$$\begin{aligned} \Delta u^{(U)}(z/L_1=0) &= \frac{\Delta w(z/L_1=0)}{h_1} \Lambda \\ &= \frac{H/L_1}{S h_1} 2\pi \frac{1}{(1 - \pi^2/(h_1^2 S^2))^{1/2}} \quad (2.42) \end{aligned}$$

In the example given in Fig.7b, where $h_i = 3L_1$, it would be expected that $\Delta u^{(U)}$ would be singular when $SL_1 = \pi/3$. The calculations show the increasing value of Δu as $SL_1 \rightarrow 1$.

When $Sh_i = \pi$ large deflections of the elevated inversions are generated and nonlinear inertial effects below h_i become significant. If $|\Delta u^{(U)}/U| \ll 1$, but the shear flow amplification in (M) is large, then the nonlinear correction in §6.2 of Pt.I is applicable. Both effects limit the magnitude of Δu .

3. Unstable stratification

Observations (e.g. Frenkiel 1965; Bradley 1980, 1983) indicate that in moderate windspeeds over hills ($U_0 > 4\text{ms}^{-1}$), even when the mean temperature distribution of the approach flow is unstable (i.e. $d\theta_B/dz > 0$) where θ_B is the mean potential temperature, the turbulence and the mean velocity over a hill do not exhibit any singular behaviour and, downwind of the hill, casual observations suggest that the flow returns to its upwind form.

There are two main reasons why there might be a large change in the flow with a small degree of unstable stratification:

- (1) If the hill slope is great enough, and the approach wind speed is weak enough, a local convective cell could be formed. An approximate criterion for significant convection motions in the inner region is that

$$g\Delta\theta_1 L_1 / (2\theta_B(z=0)U_B^2(l)) < 1,$$

and for the outer region is that

$$g\Delta\theta_1 l / (2\theta_B(z=0)U_B^2) < 1,$$

where $\Delta\theta_1$ is the potential temperature across the inner layer thickness l). So if $L_1 = 300\text{m}$, ($l = 20\text{m}$), $\Delta\theta_1 = 1^\circ\text{C}$, the wind speed should be greater than 3m^{-1} for no thermal effects in the inner region.) In general, unstable buoyancy force effects make a large effect close to the surface and a smaller one in the outer flow, as qualitative observations of anabatic

winds show (e.g. Scorer 1972), and also katabatic downslope wind studies make clear (e.g. Manins & Sawford 1979).

- (ii) A stronger unsteady convective turbulence might be triggered by the presence of the hill. This does not appear to be observed. Since turbulent convection has some gross features in common with the predictions of linear stability analysis, linear analysis might provide some insight into the problem. Such an analysis shows that the only modes which are travelling relative to the flow and which can remain stationary relative to the hill are decaying rather than growing modes. Therefore the turbulence over a hill mainly consists of convective turbulence generated upwind.

We surmise therefore that in convective conditions, the air flow over a hill with low slope can be considered as a small perturbation to a flow with a mean velocity profile $U_B(z)$, and a mean potential temperature profile $\theta_B(z)$. The outer region turbulence, which is weak compared with $U_B(z)$ in the limit considered here, consists of the convective motions travelling with the mean flow, but distorted by the mean flow over the hill (as for examples discussed by Britter, Hunt & Richards 1981). In the inner region, the turbulence is in part generated (mechanically and thermally) locally over the hill, but the flow is still a small perturbation to the incident flow. Consequently the same boundary conditions at $z = 1$ can be applied in this case as in the stable and neutral flows.

Even these assumptions, the governing equation for the

outer region follows from equation (2.3), Pt.I. For a two-dimensional hill

$$\left[\frac{\partial^2}{\partial x^2} + \frac{\partial^2}{\partial z^2} - Sc^2 \right] \Delta w = 0 \quad (3.1)$$

where

$$Sc^2 = -g \frac{\partial \theta_B}{\partial z} / \left[\theta_B(z=0) U_B^2 \right] + \frac{d^2 U_B}{dz^2} / U_B.$$

In slightly unstable conditions, U_0'' is large enough for there to be a middle layer. The solutions for $\Delta w^{(M)}$, $\Delta u^{(M)}$, $\Delta p^{(M)}$ have the same form as for stable conditions viz. (2.3a), (2.3b), (2.3c).

Thus to leading order Δw in the upper layer must satisfy (3.1) subject to the boundary-layer condition

$$\Delta w = (H/L_1) f'(x/L_1) U_B(h_m) \text{ as } z/L_1 \rightarrow 0 \quad (3.2) \\ (\text{or } z = h_m)$$

In most unstable, and also neutral conditions, Δw is likely to be limited by an elevated stable inversion at $z = h_1$. It would be possible to combine an analysis of unstable conditions below $z = h_1$ with an analysis across the inversion, using the results of §2. But here we shall restrict ourselves to the case where the deflection Δh_1 to h_1 caused by the hill is small. We assume

$$\text{at } z = h_1, \quad \frac{\Delta w/U}{H/L_1} \ll 1 \quad \text{and} \quad \frac{\Delta h_1}{H} \ll 1 \quad (3.3)$$

For a hill where $L_1 < h_1$, this requires that

$$\frac{\Delta h_1}{H} = \frac{\frac{U_B^2}{g \Delta \theta_1 H}}{\theta_3} \cdot \left[\frac{H}{L_1} \right]^2 \cdot \frac{1}{h_1^2/L_1^2} \ll 1 \quad (3.4a)$$

and where $L_1 \gg h_1$, requires that (from (2.32a))

$$\frac{\Delta h_1}{H} = \frac{U_B^2}{(g \Delta \theta_1 / \theta_3) H} \cdot \frac{H}{h_1} \ll 1 \quad (3.4b)$$

Typically for $U_0 = 3 \text{ ms}^{-1}$, $\Delta \theta_1 = 3^\circ \text{K}$, $h_1 = 10^3 \text{ m}$, $H = 100 \text{ m}$,
 $\Delta h_1/H_1 = 10^{-2}$, 10^{-1} , respectively.

Uniform unstable stratification

On some occasions, the stratification parameter S_c decreases from its maximum value at $z = 0$ to a small, nearly constant value over the central mixed layer. So if the hill length L_1 is much greater than $(h_1/10)$, say 100 - 300m, Δw in the upper region may be estimated by assuming that in (3.1) S_c is a positive constant, subject to (3.2) and (3.3). As $z/L_1 \rightarrow 0$ and, if the conditions of (3.3) and (3.4) are valid, subject to

$$\Delta w = 0 \quad \text{at} \quad z = h_1. \quad (3.5)$$

Thence the Fourier transform solution is

$$\Delta w = H \int_{-\infty}^{\infty} i k_1 \bar{f}(k_1) \frac{\sinh \left[(h_1 - z) \sqrt{(k_1^2 + S_c^2)} \right] e^{i k_1 x}}{\sinh (h_1 \sqrt{(k_1^2 + S_c^2)})} dk_1. \quad (3.6)$$

If the hill's length is small compared with the inversion height, i.e. $z_1 \gg L_1$, then

$$\Delta u = H \int_{-\infty}^{\infty} \sqrt{(k_1^2 + S_c^2)} \bar{f}(k_1) e^{-z \sqrt{(k_1^2 + S_c^2)}} e^{-i k_1 x} dk_1. \quad (3.7)$$

Thus the phase of the horizontal velocity variation over the hill is not changed by unstable stratification, i.e. the maximum is still located on the summit.

The effect on $\Delta u(z/L_1 \rightarrow 0)$ of small values of S_c , from asymptotic analysis of the integral (3.7), is given by

as $S \rightarrow 0$

$$\Delta u = \frac{H}{L_1} \left[\frac{1}{\pi} \int_{-\infty}^{\infty} \frac{f'(x') dx'}{x - x'} - \frac{S_c^2 \ln S_c}{2\pi} \int_{-\infty}^{\infty} f(x') dx' + O(S_c^2) \right].$$

For a bell-shaped hill, $f = (1 + (x/L_1)^2)^{-1}$, we find on the hill top

$$\Delta u = H/L_1 \left[1 - \frac{S_c^2 \ln |S_c|}{2} \right]. \quad (3.8)$$

Nonuniform unstable stratification

For cases where $L_1 \leq h_i/10$, the perturbed flow mainly occurs in the lower part of the mixed layer where we can approximate S_c by

$$S_c(z) = S_0 e^{-z/\delta}.$$

Then (3.1) becomes

$$\left[\frac{\partial^2}{\partial x^2} + \frac{\partial^2}{\partial z^2} - S_0^2 e^{-2z/\delta} \right] \Delta w = 0. \quad (3.9)$$

Adapting Foldvik's (1962) analysis for a nonuniform stable flow over a hill, let

$$\Delta \bar{w} = \Delta \bar{w}(\eta, k_1), \quad \text{where } \eta = S_0 \delta e^{-z/\delta}$$

in which case (3.9) becomes

$$\frac{d^2 \Delta \bar{w}}{d\eta^2} + \frac{d \Delta \bar{w}}{d\eta} - \left[\frac{k^2 \delta^2}{\eta^2} + 1 \right] \Delta \bar{w} = 0 \quad , \quad (3.10)$$

with boundary conditions

$$\Delta \bar{w} = ik H U_0 (L_1) \hat{f}(k) \quad \text{at } \eta = S_0 \delta \quad (3.11a)$$

$$= 0 \quad \eta = S_0 \delta e^{-z_1/\delta} \quad (3.11b)$$

$$\text{or } \Delta \bar{w} = 0 \quad \text{as } \eta \rightarrow 0 \quad . \quad (3.11c)$$

The solution subject to (3.11a,c) is

$$\Delta \bar{w} = \frac{I_{k\delta}(\delta S_0 e^{-z/\delta})}{I_{k\delta}(\delta S_0)} ik \hat{f} H U_0 (L_1) \quad , \quad (3.12)$$

where $I_{k\delta}(\quad)$ is the modified Bessel function of order $k\delta$.

The solution to (3.12) has the correct limiting form as the stratification vanishes, i.e. as

$$S_0 \delta \rightarrow 0, \quad \Delta \bar{w} = H ik \hat{f} U_0 e^{-kz} \quad (3.13)$$

since as $z \rightarrow 0$

$$I_\nu(z) = (z/2)^\nu / \Gamma(\nu + 1) \quad .$$

The Fourier transform of the horizontal velocity perturbation

$$\Delta \bar{u} = H \bar{f} U_0 S_0 e^{-z/\delta} \left[\frac{I_{k\delta+1}(\eta) + \frac{\delta |k|}{\eta} I_{k\delta}(\eta)}{I_{k\delta}(\eta = 0)} \right]$$

so as $(z/\delta) \rightarrow 0$ and $S_0 \delta \rightarrow 0$

$$\Delta \bar{u} = H k \bar{f} U_0 \left[\frac{k}{|k|} + \frac{\delta S_0^2}{2k(1 + \delta |k|)} \right]$$

For a bell-shaped hill at $x = 0$, when $S_0 \delta \ll 1$

$$\frac{\Delta u}{U_0} = \frac{H}{L_1} \left[1 + \frac{S_0^2 L_1^2}{2} e^{L_1/\delta} E_1(L_1/\delta) \right] \quad (3.14)$$

where E_1 is the exponential function. So if

$$L_1/\delta \ll 1, \quad \Delta u/U_0 = H/L_1 \left[1 + \frac{S_0^2 L_1^2}{2} \left[-\ln(L_1/\delta) + 0.58 \right] \right] \quad (3.15a)$$

$$L_1/\delta \gg 1, \quad \frac{\Delta u}{U_0} = H/L_1 \left[1 + \frac{S_0^2 L_1^2}{2(1 + L_1/\delta)} \right] \quad (3.15b)$$

These results indicate how $\Delta u/U_0$, $\hat{\Delta p}/U_0^2$, and $\hat{\Delta \theta}/U_0$ in the inner layer vary with unstable stratification in a similar way to the analysis of §3.1.

Effects of the inversion layer

The height, z_1 , of the inversion layer above the mixed layer is usually much greater than the layer where the temperature changes rapidly. Typically

$$\delta \approx z_1/10, \text{ so that } z_1 \gg \delta.$$

Also in many convective situations the length scale of hills is comparable with the inversion depth ($z_1 \approx L_1$), so, as Bradley (1980) suggested, the effects of the inversion ought to be considered. Over most of the mixed layer, $\delta < z < z_1$, the P.T. of the vertical velocity is, if $S_0 \ll 1$,

$$\Delta \bar{w} = ikf U_0 H e^{-|k|z} \left[1 - \frac{\delta^2 S_0^2}{1 + \delta |k|} \right]$$

if the boundary condition that $\Delta \bar{w} = 0$ on $z = z_1$ is ignored. Note that $\Delta \bar{w}$ is less than it would be in neutral flow! To rectify this omission, the above expression has to be corrected so that, if $S_0 \delta \ll 1$, $z_1 \gg z > \delta$,

$$\Delta \bar{w} = ikf U_0 H \left[1 - \frac{S_0^2 \delta^2}{1 + \delta |k|} \right] \left[e^{-|k|z} - e^{-|k|(2z_1 - z)} \right]$$

and

$$\Delta \hat{u} = -|k| \bar{f} U_0 H \left[1 - \frac{S_0^2 \delta^2}{1 + \delta |k|} \right] \left[e^{-|k|z} + e^{-|k|(2z_1 - z)} \right].$$

Thus, when z/δ is $O(1)$

$$\Delta \bar{u} = |k| f' U_0 H \left[\frac{I_{\delta k+1}(\eta) + \frac{\delta |k|}{\eta} I_{\delta k}(\eta)}{I_{\delta k}(\eta) = 0} + \left[1 - \frac{\delta^2 S_0^2}{1 + \delta |k|} \right] e^{-|k|(2z_1 - z)} \right]$$

so as $z/L_1 \rightarrow 0$

$$\frac{\Delta \bar{u}}{U_0} = H f' \left[|k| + \frac{\delta S_0^2}{1(1 + \delta |k|)} + \left[1 - \frac{\delta^2 S_0^2}{1 + \delta |k|} \right] e^{-2z_1 |k|} \right] \quad (3.17)$$

For a bell-shaped hill we find the inverse transform on $x = 0$ to be

$$\frac{\Delta u}{U_0} = \frac{H}{L_1} \left[1 + \frac{S_0^2 L_1^2}{2} \left[e^{\frac{L_1}{\delta}} E_1(L_1/\delta) - e^{(L_1 + 2z_1)/\delta} E_1\left(\frac{L_1 + 1z_1}{\delta}\right) \right] + \frac{1}{1 + 2z_1/L_1} \right] \quad (3.18a)$$

In the usual limit where $L_1 \gg \delta$, (3.18a) reduces to

$$\frac{\Delta u}{U_0} = H/L_1 \left[1 + \frac{S_0^2 L_1^2}{2} \left[\frac{1}{1 + L_1/\delta} - \frac{1}{1 + (L_1 + 2z_1)/\delta} \right] \right]$$

$$\left. + \frac{1}{1 + 2h_i/L_1} \right\} \quad (3.18b)$$

Thus if $h_i = L_1$, the correction of the term proportional to $S_o^2 L_1^2$ due to unstable stratification is slightly reduced. There is, of course, a significant increase by 30% in $\Delta u/U$ when a strong elevated inversion exists, irrespective of the unstable stratification below the inversion.

The physical reason for the slight increase in the upper layer with unstable stratification is the following. The upward deflection over the hill locally increases θ and $\partial p/\partial z$. This reduces p and increases Δu at the bottom of the upper layer. Of course with unstable stratification, the shear in the middle layer is reduced, so the net effect of unstable stratification on Δu in the inner region can be reduced to $\Delta u/U(1)$.

4. Summary of outer region results

In this section we summarise the results of the analysis in Parts I and II for the general effect of stratification on flow over low hills, when effects of buoyancy forces are weak within the inner region. The effects of upwind temperature and velocity gradients on changes in the flow over a given hill are characterised by the way wind

speed in the middle layer $\hat{\Delta u}$ changes at a given displacement Δz above the surface just above the inner layer. In this section all variables are dimensional. Note that

$u = U_B(\Delta z) + \hat{\Delta u} = U_B(z) + \Delta u$. From the results of this paper and Part I, the dimensional value of Δu can be written schematically in terms of the hill slope, two amplification factors, and the velocity of the upwind flow at height h_m ,

$$\hat{\Delta u} = U_B(h_m) H/L_1 \cdot A_{VP} \left[\frac{u_*}{h_m N} \right] \cdot A_D(F_0)$$

upwind x	slope x	effects of	dynamic
velocity		stratification on the	effects of
		upwind velocity profile	stratification

The linear analysis clearly shows that $\hat{\Delta u}$ (or Δw or Δn_1 etc.) is proportional to the slope of the hill. The next factor shows how, since $\hat{\Delta u}(\Delta z) = [U_B^2(h_m)/U_B(\Delta z)]J(\Delta z)$ where $J(\Delta z)$ is defined by (2.3c), the surface wind amplification may be strongly affected by the dependence of the upwind velocity gradient or shear on stratification. The shear also affects the depth h_m of the middle layer if the

hill's length scale is less than the boundary layer depth. (The dependence of the shear on stratification is a function of the ratio of buoyancy to inertia' forces affecting the turbulence in the upwind flow and not those affecting the mean flow, e.g. $h_m N(h_m)/u_*$ or h_m/L_{MO} , where h_m is the scale of the middle layer, and $N(h_m)$ is the buoyancy frequency in the middle layer.) (For a short hill where $L < h$, the parameter is $h_m N(h_m)/u_*$.) The third factor determines $\Delta u^{(U)}$ or $\Delta p(x)$ and indicates the dependence of the flow on the ratio of the buoyancy forces over the hill to the inertial forces of the mean flow. Consequently a strong stratification is required for this effect to become important, as can be seen in the wind-tunnel studies of Bouwmeester (1978), and the atmospheric measurements of Bradley (1983), reviewed by Hunt & Richards (1984). These showed how Δu over an escarpment increased rapidly as the stratification increased from neutral, but with a further increase did not change much, as buoyancy forces reduced the amplification.

A suitable parameter, which includes the buoyancy effects of both uniform stratification and elevated inversions, is an overall Froude number F_0 where

$$F_0^2 = \frac{U_0^2}{\frac{g}{\theta_B(0)} \int_0^{L_1 \sqrt{2}} z \left[\frac{\partial \theta_B}{\partial z} \right] dz}$$

If $h_1 \ll L_1$, $F_0^{-2} = (F_1^{-2} + F_L^{-2})$ for an elevated inversion with uniform stratification above the inversion and $F_0^2 = F_L^2$ for uniform stratification.

Note how the velocity profile factor is a measure of the buoyancy acting on the turbulence over a long distance of the upwind flow, while the third factor is a measure of the buoyancy acting over the hill.

Other factors of the same order are the shape of the hill (see Table 1 in Part I), and also the form of the upwind temperature and velocity profiles which determine $N^2/U_B^2(z)$ in the upper layer.

It is useful to identify four main classes of stratified flow in the outer region over a hill. The stratification in the inner region (briefly discussed by Hunt & Richards 1984), can be quite different, e.g. neutral or slightly convective conditions may be found in the inner regions with a stable outer region, or conversely a neutral outer region and a local ground-level inversion in the inner region. That is why it is important to consider the regions differently, if possible. (We shall mainly consider hills which are long compared with the height of the middle layer ($L_1 > h_m$) in the criteria for the different classes.)

Neutral flow ($u_* / (h_m N(h_m)) \gg 1$, $h_m / L_{MO} \ll .1$)

Any stratification is too weak to affect the incident velocity profile and certainly too weak to affect the dynamics of the flow over the hill. A unique feature of neutral flow over the hill is that the displacement, δ_z , of the streamline and the proportional changes in the wind speed Δu are independent of the upwind windspeed.

Flow with weak stratification
($u_* / h_m N(h_m) \ll 1$; $h_m / |L_{MO}| > 0.1$)

In this case the stratification (stable or unstable) is strong enough to affect the turbulence and thence the velocity profile in the middle layer. (It may also be strong enough to affect the wake of the hill over a long distance downwind.) δ_z and Δu are dependent on windspeed in this case. But the stratification is too weak to affect the dynamics of the mean flow over the hill.

A typical situation where this might occur would be when

$N(z = 100m) = .0035 \text{ s}^{-1}$, $L_1 = 300m$, $L_{MO} = 300m$, $u_* = 0.1 \text{ ms}^{-1}$
 $U_B(z = 300m) = 3 \text{ ms}^{-1}$. Then $h_m = 100m$ and $l = 20m$.
 $U_0 / (NL_1) = 3.0$ but the ratio $U_B^2(L_1) / U_B^2(\Delta z)$ just above the inner region, where $\Delta z = l$, is increased by about 40% by estimating the profile from surface similarity - an unreliable estimate. It is by $O\left[\frac{zh_m}{L_{MO} \ln(h_m/z_0)}\right]^2$. Further examples of flow in stable and unstable stratification were given by Hunt (1981) and Hunt & Richards (1984).

Moderate stratification $F_0 < 1$

When the temperature gradient in the approach flow is large enough and extends at least over a depth of the order of L_1 (which may take the form of an elevated inversion at the height of the order of L_1), such that $F_0 < 3$ or for convective conditions $S_c L_1 > 3$, then the buoyancy forces significantly affect the mean flow over the hill. The analysis shows that, if $1.0 < F_0$, the changes in maximum windspeed are less than 20%.

However, in stable conditions the forms of the flow patterns change quite markedly, even when F_0 is about 2, with the flow speeding up, the streamlines approaching the surface on the lee slopes and, in three dimensions, spreading laterally, while the flow begins to stagnate on the upwind side. In unstable conditions there does not appear to be any major change in the pattern of the perturbation flow.

When a stable stratification is strong enough that $F_0 < 1.0$, the maximum flow speed up near the surface can be rather accurately estimated by the hydrostatic approximation, provided the stratification is not so strong that the Froude number based on the hill height $F = U_B / NH$ becomes less than 1.0. The proportional change in surface windspeed for a uniform stratification is $O(NH/U_B h_m)$ which is $O(F_0^{-1})$ or $O(NL_1/U_B(h_m))$ times as great as the change in neutral conditions.

We have also seen how the form of the change in windspeed or streamline deflection depends on the profile of $(N/U_B)^2$. If $(N/U_B)^2$ decreases fast enough with height (e.g. in proportion to z^{-2}), or if the stratification is

confined to an elevated inversion where $U_0^2 / (h_1 g \Delta \theta_3 / \theta_3) > 1$, then the maximum velocity occurs downwind of the hill, not over the point of maximum leeside slope, as in uniform stratification. The effects of an elevated inversion and a uniform stratification below it changes the position of Δu_{mx} yet again, and also provides a mechanism for even greater horizontal and vertical perturbation to the flow.

Strong stratification

When the upwind flow below or near the height of the hill is sufficiently stable that $F = U_0 / (NH) < 1$, then irrespective of whether the hill is two- or three-dimensional, there is effectively a region of blocked or horizontally-confined flow below the hill top for which $z < H (1 - F)$ (Brighton 1978; Hunt & Snyder 1980). Above this height, i.e. $z > H (1 - F)$ the flow approximately behaves as if it is travelling over a hill of height FH , (as discussed in the Appendix.) Then the analysis of the flow for moderate stratification provides an approximate model.

Acknowledgements

JCRH acknowledges support from Flow Analysis Associates of Ithaca, N.Y. He began some of this work while on a visit to the Cooperative Institute for Research in Environmental Sciences at the University of Colorado. KJR was supported at Cambridge by an Ernest Cook Fellowship of the Royal Society. PWB was supported at Cambridge by an SERC research student's grant.

Appendix 1 Solution for the vertical perturbation velocity in the middle layer, with a correction caused by surface stratification

In the middle layer, where $\frac{\partial^2 \Delta w}{\partial z^2} \gg \frac{\partial^2 \Delta w}{\partial x^2}$, if $L_1 \gg h_m \gg H$, and if buoyancy forces cannot be ignored, the governing equation for Δw is

$$\left[\frac{\partial^2}{\partial z^2} - \frac{U''}{U} + \left[\frac{N}{U} \right]^2 \right] \Delta w = 0.$$

(If $h_m = H$, we substitute Δz for z .)

Then, if we assume that $(N/U)^2 \ll (U''/U)$, and denote the solution ignoring buoyancy forces as $\Delta w^{(M)}$, given in (2.3)), then the first-order correction to Δw , $\Delta w^{(1)}$ must satisfy

$$\left[\frac{\partial^2}{\partial z^2} - \frac{U''}{U} \right] \Delta w^{(1)} = - \left[\frac{\Delta N^2}{U^2} \right] \Delta w^{(M)},$$

where (ΔN^2) is the increase in N^2 within the middle layer.

Since $\Delta w^{(M)}$ satisfies the lower boundary condition,

$$\Delta w^{(1)} = - \frac{H}{L_1} f(x/L_1) \left\{ -U \int \frac{dz}{U^2} \int_0^z \left[\frac{N^2}{U^2} \right] U \cdot U dz + U \int \frac{\Delta N^2}{U^2} U \cdot \left[U \int \frac{dz}{U^2} \right] dz \right\}$$

Thence integrating by parts and using the definition

$$\Delta N^2 = g \frac{d\Delta\theta_S/dz}{\theta_B(z=0)},$$

$$\Delta w^{(1)} = - \frac{H}{L_1} f(x/L_1) U \int_0^z \frac{\Delta\theta_S dz}{U^2(z)}.$$

By continuity

$$\Delta u^{(1)} = \frac{+H}{L_1} f(x/L_1) \left\{ \frac{\Delta \theta_s}{U(z)} + U'(z) \int \frac{\Delta \theta_s}{U^2} dz' \right\} .$$

These are the corrections in (2.3d) and (2.3e) of §2.1.2.

Appendix 2 Use of linearised analysis to describe flow over the top of hills in very stable flows

Consider a stably-stratified flow with a potential temperature profile $\theta_B(z)$ and velocity profile $U_B(z)$ which impinges on a single hill of height H . When inertial forces are generally much less than buoyancy forces, but much greater than viscous effects, except in thin boundary layers on the hill, then the Froude number

$$F_H = \frac{U_0}{NH} < 1, \quad \text{where } N = \sqrt{\left| \frac{g d\theta_B/dz}{\theta_B(H)} \right|}$$

where $Re = U_0(H)/\nu \gg 1$, where ν is the kinematic viscosity, and $U_0 = U_B(H)$.

The analyses of Drazin (1961) and Brighen (1976) showed how the flows around a three-dimensional hill divide into three main regions, as shown in Fig. A1(a).

There are two regions $[H_1]$ and $[H_2]$ where the flow is largely horizontal. $[H_1]$ lies between the top or summit region $[T]$, straddling the top of the hill and a thin region $[B]$ at the base of the hill. In this region the flow round the hill separates and a largely horizontal recirculating wake flow develops on the downwind side. $[H_2]$

lies above the hill. In the region [T] the flow has just enough kinetic energy ($\frac{1}{2}\rho_0 U_0^2$) to develop the potential energy $\frac{1}{2}\rho N^2 \delta_z^2$ to rise by an amount δ_z over the top. Consequently at a height $\delta = U_0/N$ from the hilltop or $H_c = (1 - \beta)H$ above the ground, there is a critical streamline ψ_c dividing the flow over the hill, approximately horizontal. The vertical displacements in [T] produce weak lee waves with displacements of the order of U_0/N in regions $[H_1], [H_2]$. This order-of-magnitude analysis has been confirmed by many laboratory tests (e.g. Snyder, Britter & Hunt 1979; Snyder et al. 1985), and the recent field test organised by Environmental Research and Technology for the Environmental Protection Agency (Egan 1984). In region [B] the streamlines move up the hill a short distance ($\frac{1}{2}U_0/N$) before travelling round horizontally. (Since U_0 is small and N is largest in this region, [B] is thinner than [T].)

The largely horizontal flow and diffusion in region $[H_1]$ was analysed by Hunt, Puttock & Snyder (1979) and has been tested in the laboratory (Snyder et al. 1979; Snyder & Hunt 1983) and now in the field (Egan 1984). However, there is still no proper theory for the flow in region [T]. Clearly this region is of practical importance because many sources of pollution are located in valleys at regions almost equal to that of nearby hills. Some attempts have been made to model the flow in this region as potential flow over a level surface of height H_1 and that part of the hill higher than H_1 as the divided streamline. But A. (1984) has shown that this does not correctly describe the highly asymmetric flow patterns in region [T] in which the streamlines

descend close to the hill surface on the lee side and develop waves downwind (Hunt & Snyder 1980). Nor do they account for the fact that the dividing streamline ψ_c is not horizontal; its vertical displacements are smaller than, but of the same order as, the height H^* of the 'cut-off' hill.

The first of these limitations can be overcome by modelling the flow in region [T] as stratified flow over a cut-off hill with low slope. The rounded shape of most hills means that the semi-length is greater than about twice the height H^* of the cut-off hill $L_c > 2H^*$. Since (see Fig.A1(b)) $H^* = H - H_c = FH$, the Froude number based on $H^* = (H - H_c)$, the height of the 'cut-off' hill is unity

$$\frac{U_o}{H^* N} = \frac{FH}{H^*} = 1.$$

(If the stratification weakens at the hill top, which is quite common, then U/H^*N may be greater than 1 (Fig.A1(c)).) Consequently, the Froude number based on L_c ,

$F_{Lc} = \frac{U_o}{L_c N} < 1/2$. Therefore the linearised analysis of inviscid stably-stratified flow over a hill with low slope when $F_{Lc} < 1$ can be applied.

Since upwind shear can be neglected over the depth of the cut-off hills, the problem is to solve the following shear-free equation for the vertical velocity, Δw , (normalised on the approach velocity U_o , at the hill top),

$$\left[\frac{\partial^2}{\partial x^2} \left[\frac{\partial^2}{\partial x^2} + \frac{\partial}{\partial y^2} + \frac{\partial^2}{\partial z^2} \right] + \frac{N^2 L_c^2}{U_o^2} \left[\frac{\partial^2}{\partial x^2} + \frac{\partial^2}{\partial y^2} \right] \right] \Delta w = 0 \quad (A1a)$$

where x, y, z are normalised on L_c , the hill's semi-length, and subject to

$$\Delta w = \frac{\partial f}{\partial x}(x, y) \quad \text{on } z = Hf, \quad \text{for } (x, y) \text{ within the region } H,$$

defined by $f(x, y) > H_c/H$ and denoted by $(x, y) \in H$,

$$\text{or } \Delta w = \frac{\partial \Delta f^*}{\partial x}(x, y) \quad \text{on } (z - H_c) = H^* \Delta f^*, \quad \text{where the cut-off hill profile}$$

$$\Delta f^* = \frac{H}{H^*} (f - H_c/H), \quad (x, y) \in H,$$

$$\text{and } \Delta w = 0 \quad \text{on } z = H_c/L_c \quad \text{for } (x, y) \text{ outside } H \quad ((A1))$$

(see Fig. A 2(a)).

We need to calculate the streamline vertical and horizontal deflections $\int_{x_s}^x \frac{(\Delta w, \Delta v)}{U_0} dz$, and the velocity u over the hill, using the continuity equation $\partial \Delta u / \partial x + \partial \Delta v / \partial y + \partial \Delta w / \partial z = 0$ and the fact that $\partial \Delta v / \partial x - \partial \Delta u / \partial y = 0$. Over a two-dimensional hill (or one where the lateral dimension of the hill at the dividing streamline height is much larger than L_c , i.e. $b_0 \gg L_c$) the solution of (A1) when $L_c \gg H$, $U_0 NL \gg 1$ but $U_0 NH \ll 1$, for the perturbation in the normalised streamwise velocity near the surface is from (2.15)

$$\Delta u = \frac{NL}{U_0} \frac{H^*}{L_c} \frac{1}{\pi} \int_{x \in H} \frac{\Delta f^*(x) dx}{x - x_s} \quad (A2)$$

The streamline height over the surface is given by

$$z_s - Hf = (H_s - H_c) (1 + \Delta u) \quad (A3)$$

Over a three-dimensional hill, the general solution (2.15) for Δu is

$$\Delta u = \frac{NL_c}{U_0} \frac{H^*}{L_c} + \frac{1}{2\pi} \iint_{x',y' \in H} \frac{\Delta f^*(x',y')(x-x')dx'dy'}{[(x-x')^2 + (y-y')^2]^{3/2}} \quad (A4)$$

and

$$z_s - Hf = H_s - H_0 = \frac{NL_c}{U_0} \frac{H^*}{L_c} + \frac{1}{2\pi} \iint_{x',y' \in H} \left[\frac{\Delta f^*}{(y-y')^2} \frac{(x-x')(x-x')^2 + (y-y')^2}{[(x-x')^2 + (y-y')^2]^{3/2}} \right] dx'dy' \quad (A5a)$$

and

$$y(x,y;x_s) - y - y_s = \frac{NL_c}{U_0} \frac{H^*}{L_c} + \frac{1}{2\pi} \iint_{x',y' \in H} \left[\frac{\Delta f^*}{(y-y')^2} \frac{(x-x')(x-x')^2 + (y-y')^2}{[(x-x')^2 + (y-y')^2]^{3/2}} \right] dx'dy' \quad (A5b)$$

For the particular case of a rounded hill with shape defined by $f = 1/(1+x^2+y^2)^{3/2}$ which cannot be appropriate for a cut-off hill, analytical expressions can be derived. (See §2.3 and Smith 1980).

In Fig.3 it was shown how these asymptotic formulas for $NL_c/U_0 \gg 1$ agree to 10% with the exact solutions to the linearised equation (A1). When $NL_c/U_0 \approx 2$. This graph also shows how the streamlines come closest to the hill surface on the lee side when the Froude number is small. This can lead to the highest concentration from upwind sources being

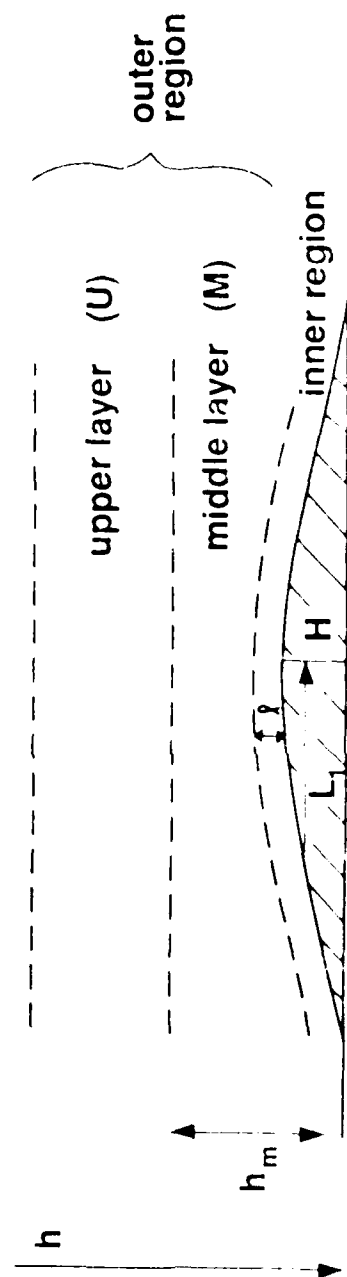


Figure 1. Rotation of the regions of the flow and their length scales.

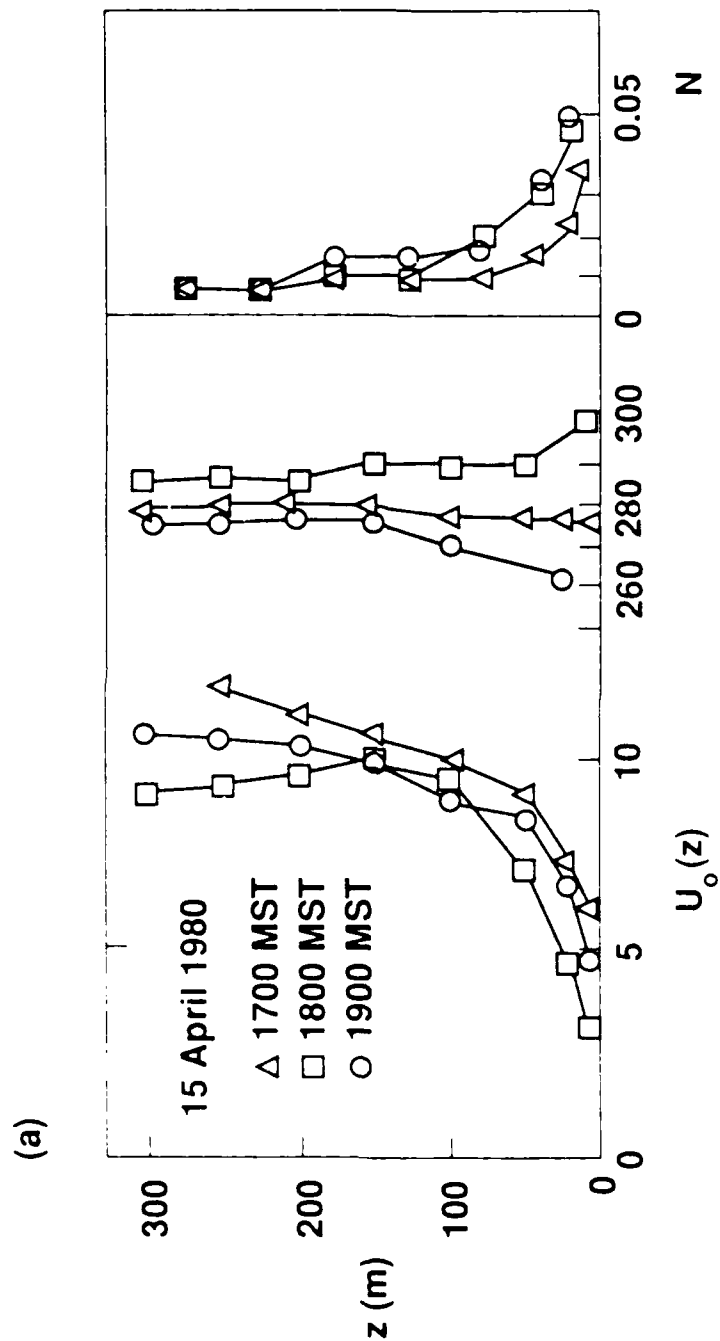


Figure 2. Typical vertical profiles in stable conditions over rolling terrain at Boulder, Colorado (Chen *et al.*, 1983; Forcel, 1983).

Figure 2 shows typical vertical profiles in stable conditions over rolling terrain at Boulder, Colorado (Chen *et al.*, 1983; Forcel, 1983).

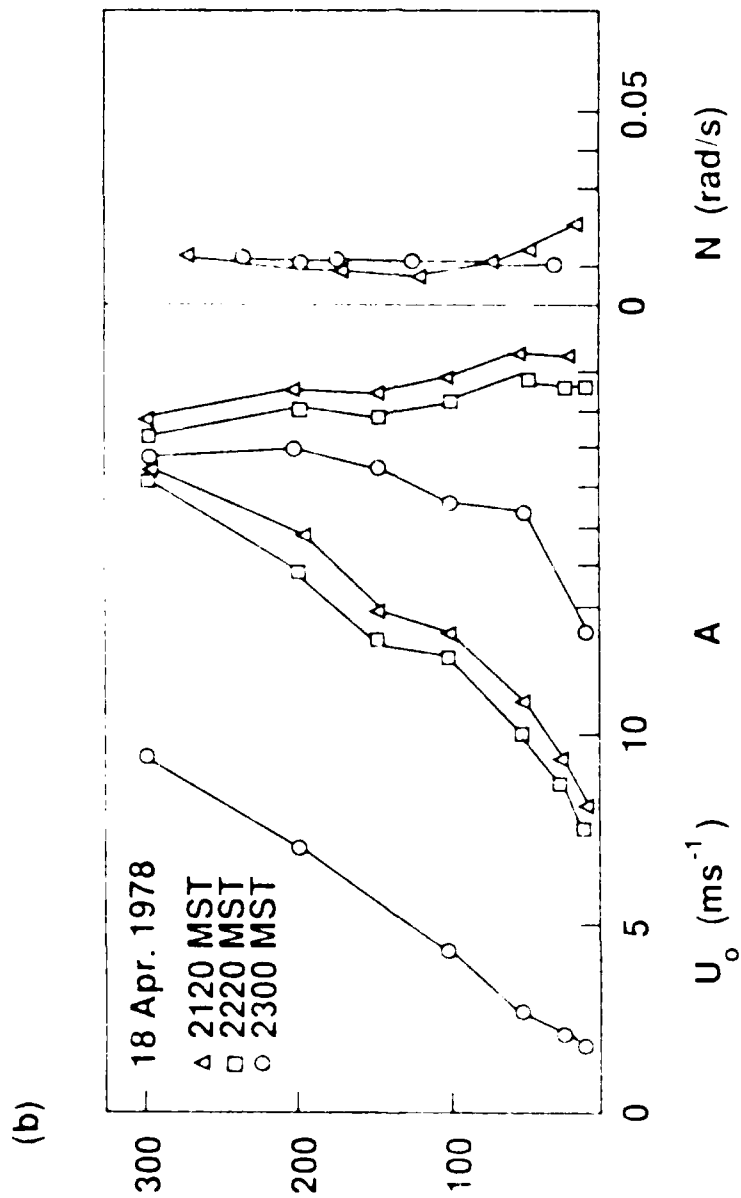


Figure 7a) (ii)

Mean velocity U_0 , direction A , and lag frequency N .

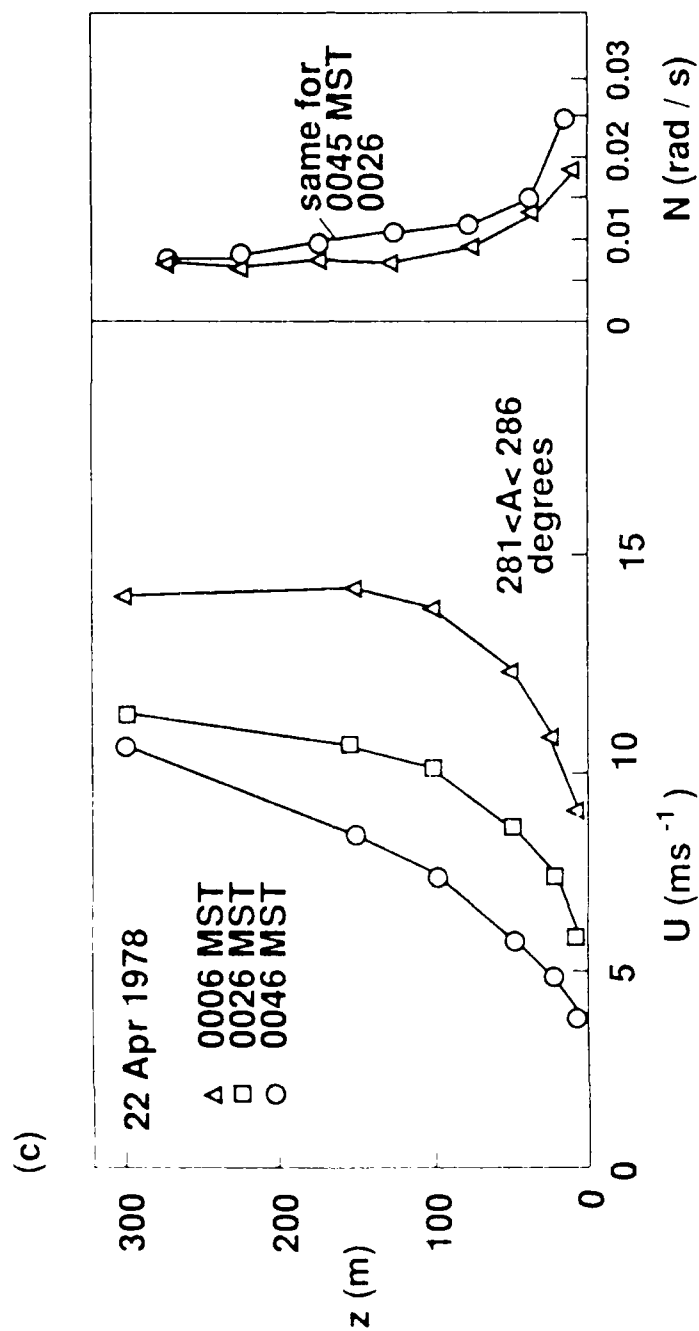


Figure 2 a) (iii)

Mean velocity \bar{u}_0 , direction A , and buoyancy frequency N .

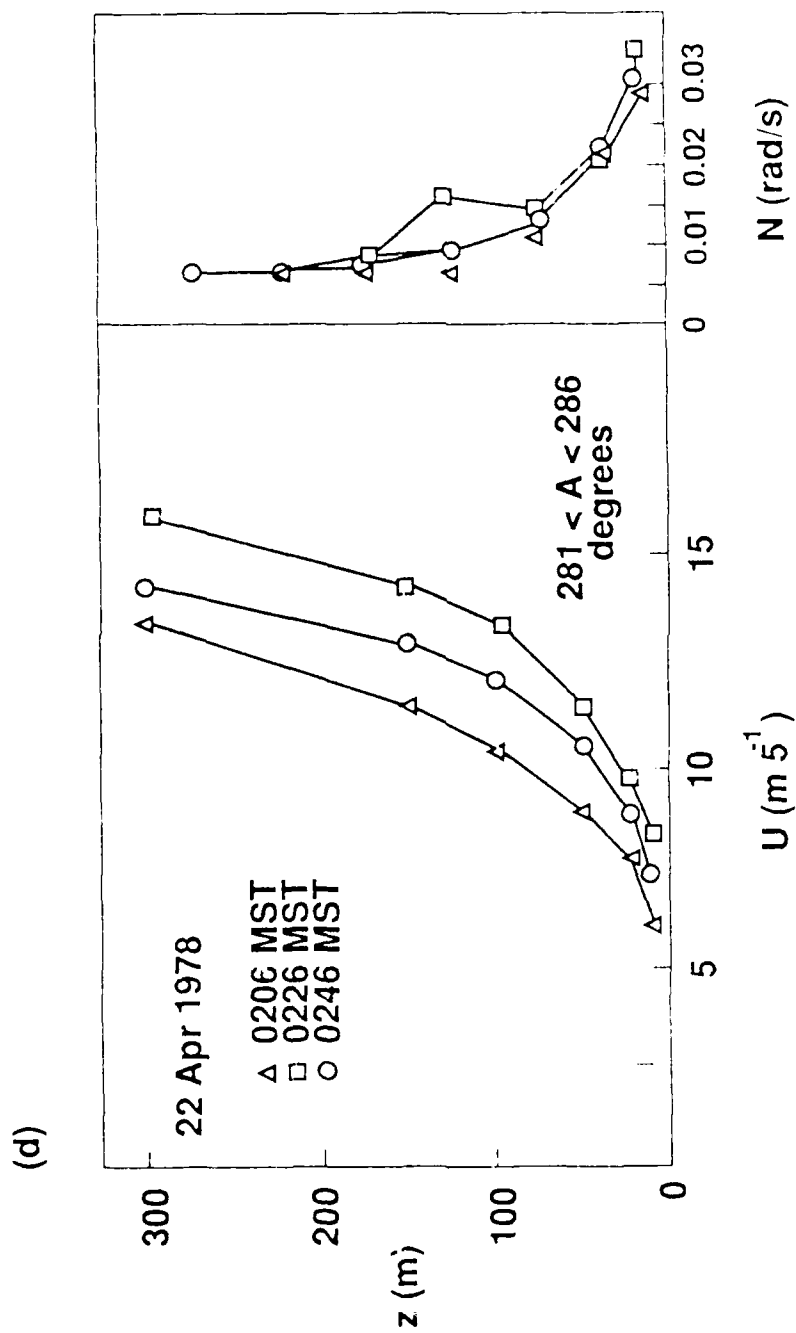


Figure 2(a)(iv)

Mean velocity U_0 , direction θ_0 , and buoyancy frequency N .

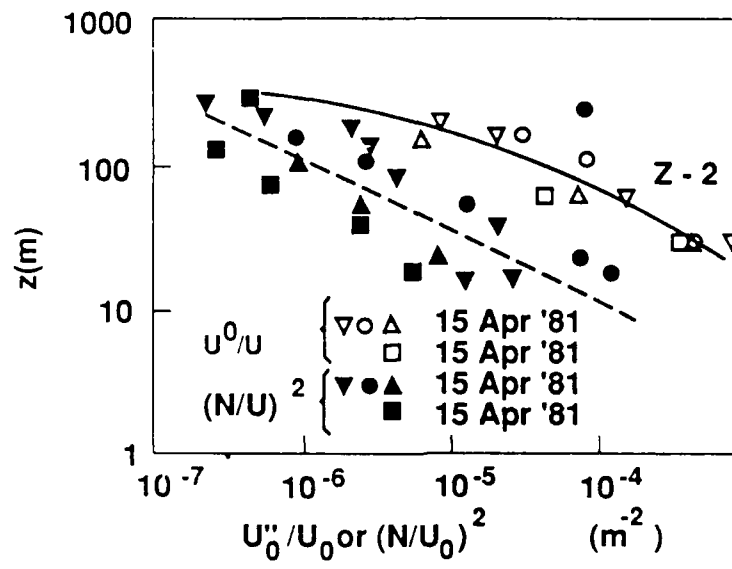


Figure 2 b)
 $(d^2U_0/dx^2)/U_0(z)$ and $(N/U_0(z))^2$.

(3)

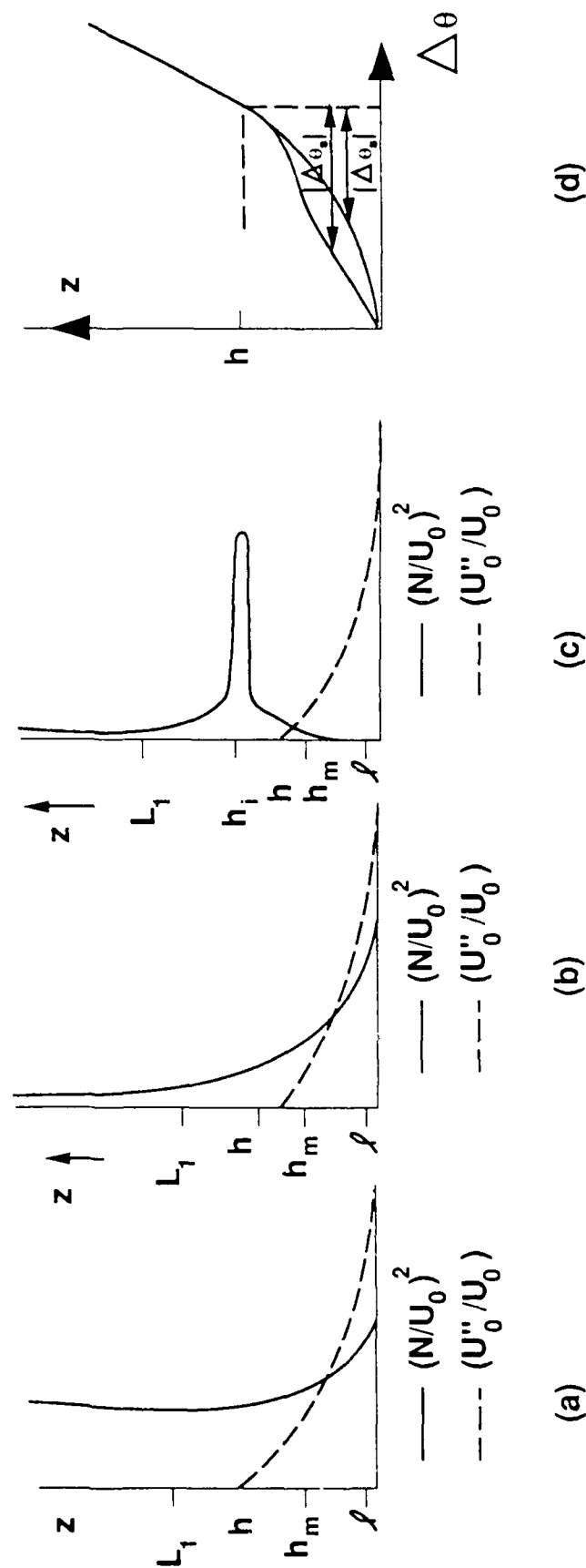


Figure 3. Idealized forms of stratification and velocity gradient profiles for the various regions of the flow over a hill.

$(N/U)^2$; - - - U''/U

a) N/U_0 constant in the upper layer.

b) N/U_0 decreases with z .

c) Elevated inversion at $z = h_i$.

d) Typical profiles of mean temperature relative to ground level $A\theta(z)$ in the middle layer. $\Delta\theta$ denotes the modulus of the difference $A\theta_s$ between $A\theta$ at h_m and at z .

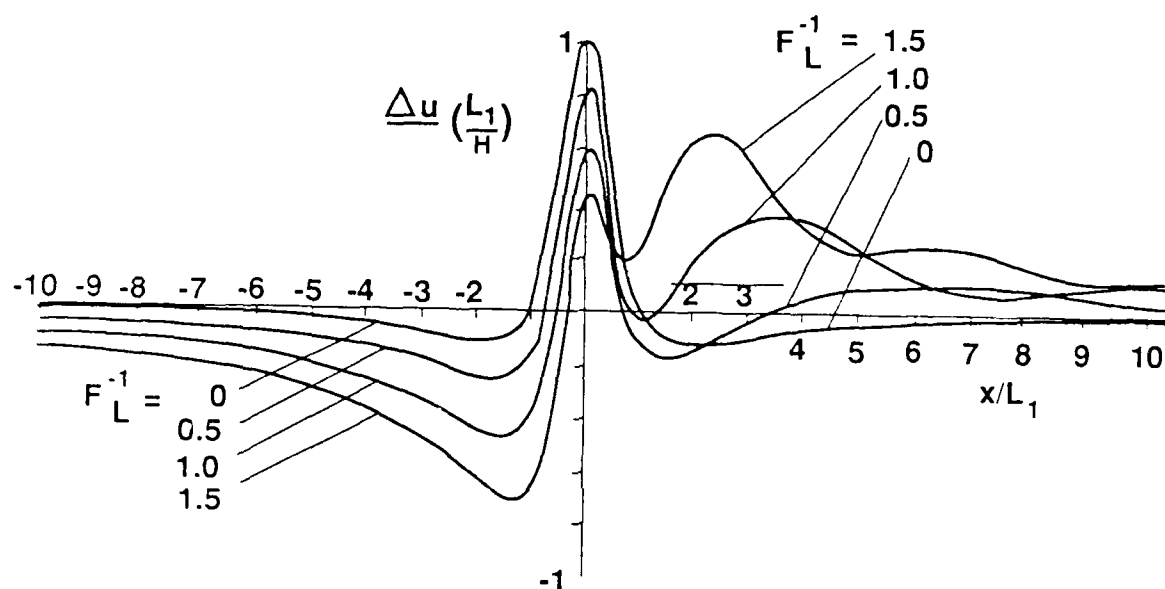


Figure 4. Uniformly stratified flow over two- and three-dimensional hills, with a constant velocity upwind.

- a) graph of the normalized horizontal surface velocity $\Delta u \cdot (L_1/H)$ over a two-dimensional bell-shaped hill as a function of Froude number $F_L = U/(NL_1)$.

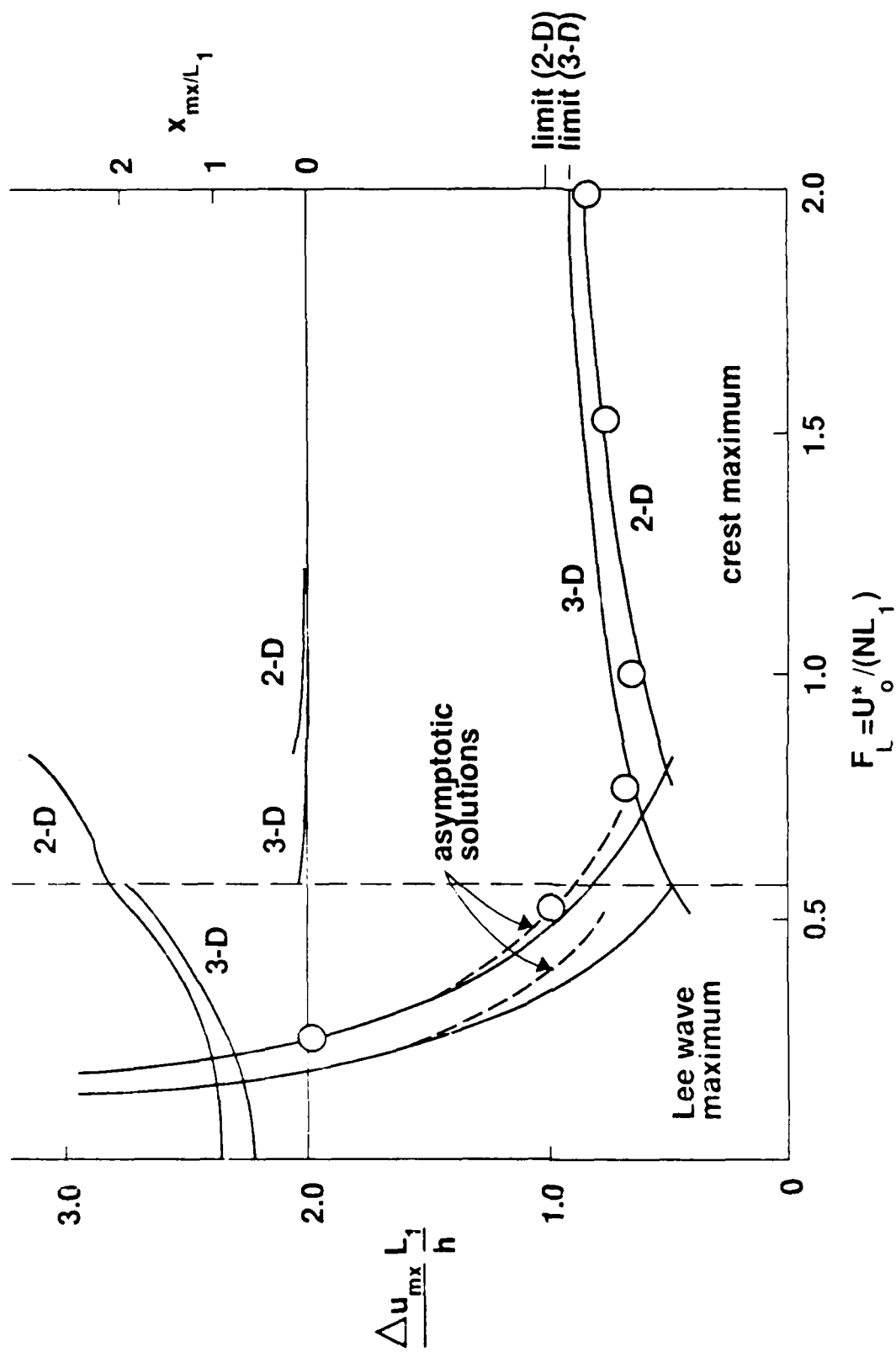


Figure 4b) The value and location of maximum surface velocity $\Delta u_{\max}(L_1/H)$ and x_{\max}/L_1 for two- and three dimensional bell-shaped hills. \circ approximate interpolation function (2.20).

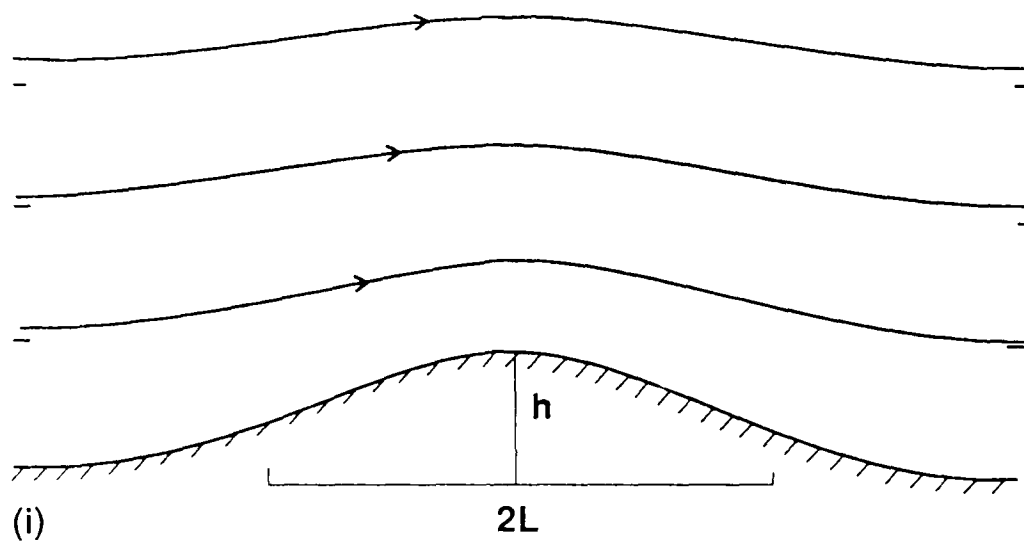


Figure 4 c) Computed (linear analysis) streamlines of the upper layer flow over a 3-dimensional bell-shaped hill. $H/L_1 = 1.2$.

(i) Neutral flow, (ii) Stable flow $F_1 = 0.2$.

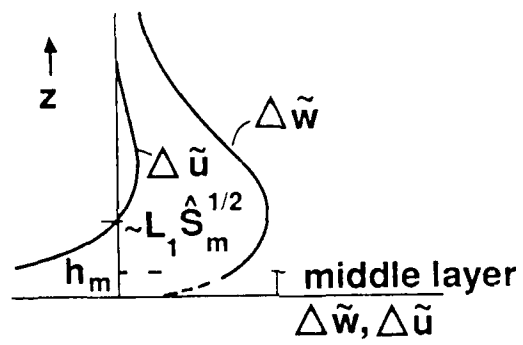


Figure 5.

- a) Vertical profiles of $|\Delta \mathbf{w}|$ and $|\Delta \mathbf{u}|$ when N/U_0 decreases with height.

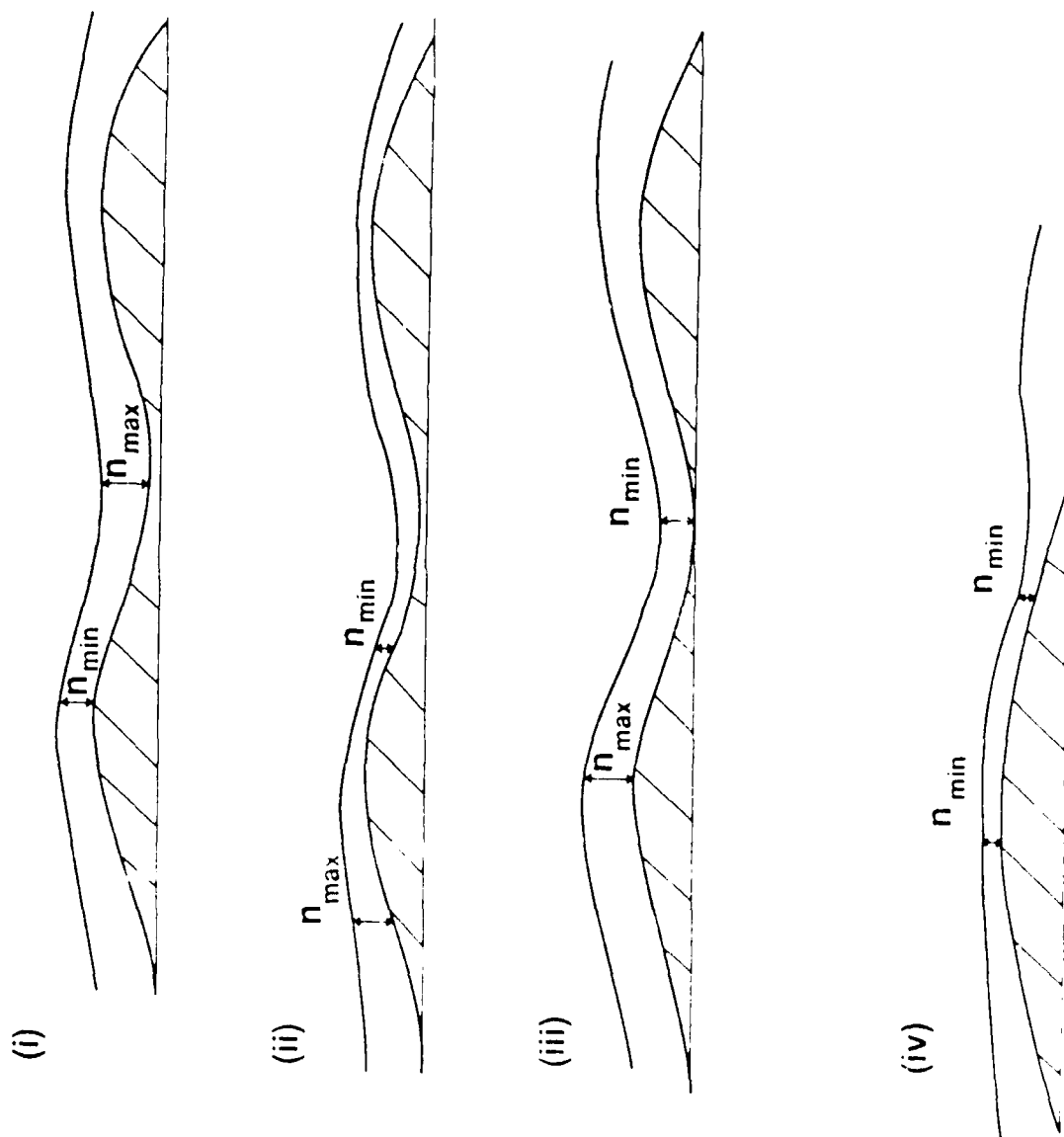


Figure 5b) Streamlines over a range of hills when $h_r/L_r <$

5.000.

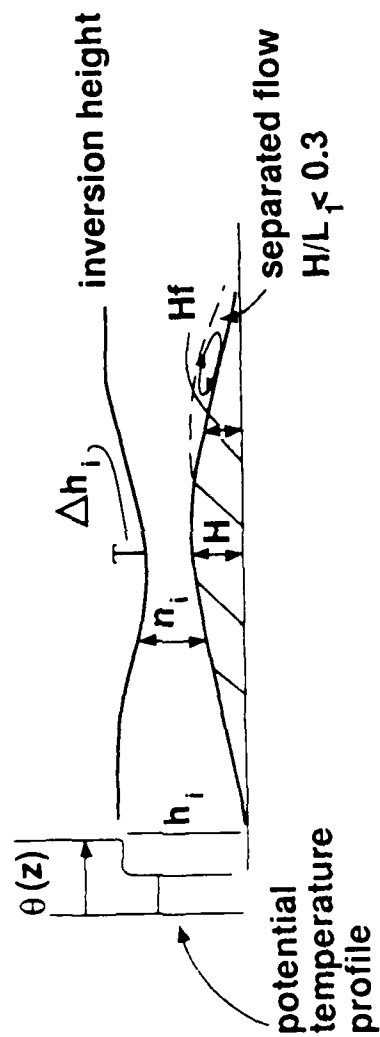
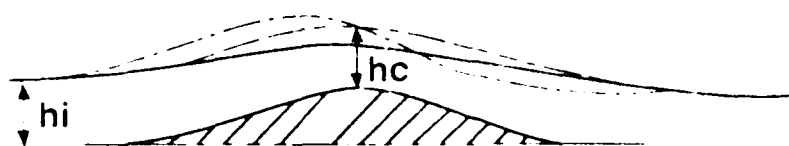


Figure 6.

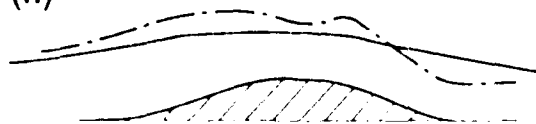
- a) Illustrating the problem of flow over a hill with an elevated upwind inversion, with $F_i < 1$.

(i)



— $F_i \rightarrow \infty$ $F_L \gg 1$
 - - $F_i > 1$ $F_L \gg 1$
 - · - $F_i > 1$ $F_L < 1$

(ii)



— $F_i \rightarrow \infty$ $F_L \gg 1$
 - - $F_i > 1$ $F_L \sim 1$

(iii)



— $F_i \ll 1$ (ignoring upper layer motions) $H/L_1 \rightarrow 0$
 - - $F_i \ll 1$, $F_L \gg 1$, $(H/L_1 \ll 1)$,
 - · - $F_i \ll 1$, $F_L < 1$

(iv)



— $F_i \sim 1$ ($H/L_1 \rightarrow 0$, ignoring upper layer motions)
 - - $F_i \sim 1$, $F_L \gg 1$ ($H/L_1 \ll 1$)
 - · - $F_i \sim 1$, $F_L < 1$ ($H/L_1 \ll 1$)

Figure 6.3) Inverted: displacement, and surface calculated for bottom profiles.

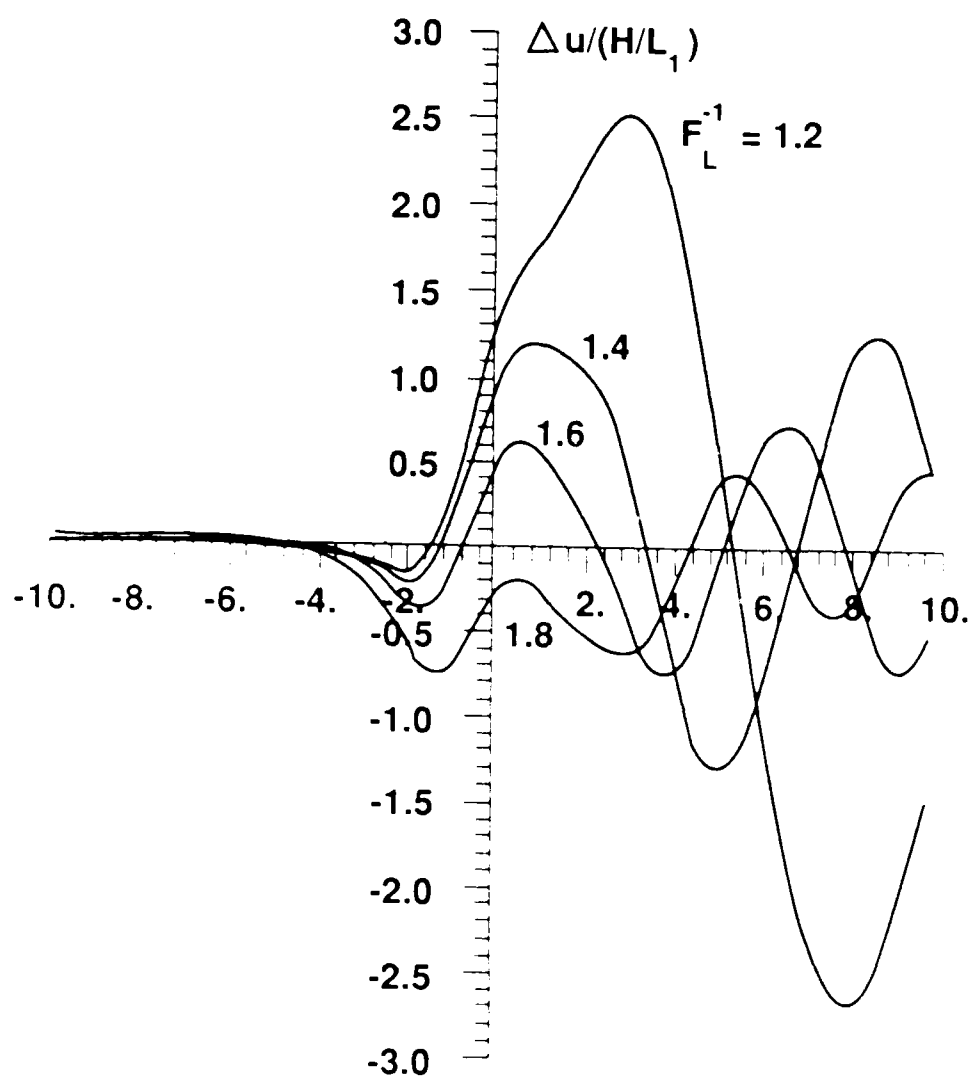


Figure 7. Distribution of Δu over channel width.

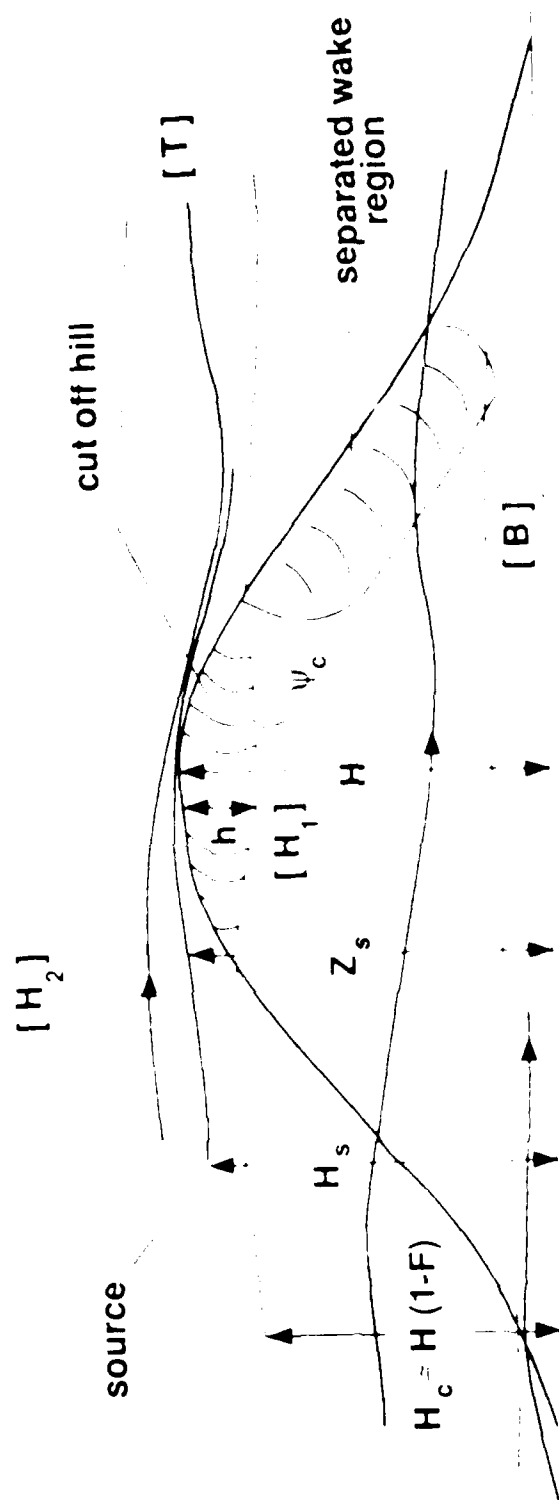


Figure 10

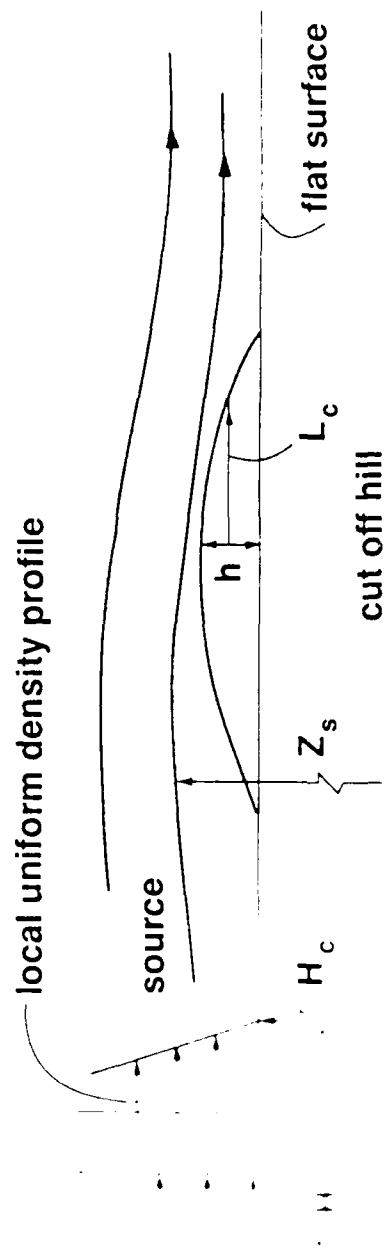


Fig. 1. Hill for studying flow in region (T)

AD-A184 222

HEAT AND MOISTURE TRANSPORT IN THE ATMOSPHERIC BOUNDARY 3/3

LAYER(U) FLOW ANALYSIS ASSOCIATES ITHACA NY

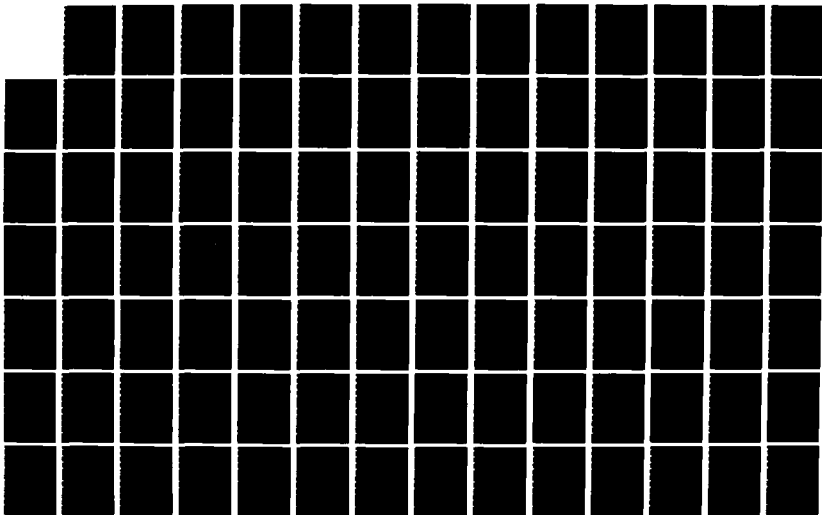
S LEIBOVICH ET AL 05 JAN 87 AFGL-TR-87-0011

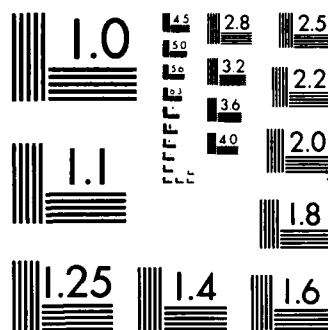
UNCLASSIFIED

F19628-83-C-0018

F/G 4/2

NL





MICROCOPY RESOLUTION TEST CHART
NATIONAL BUREAU OF STANDARDS-1963-A

Figure A2 (a)

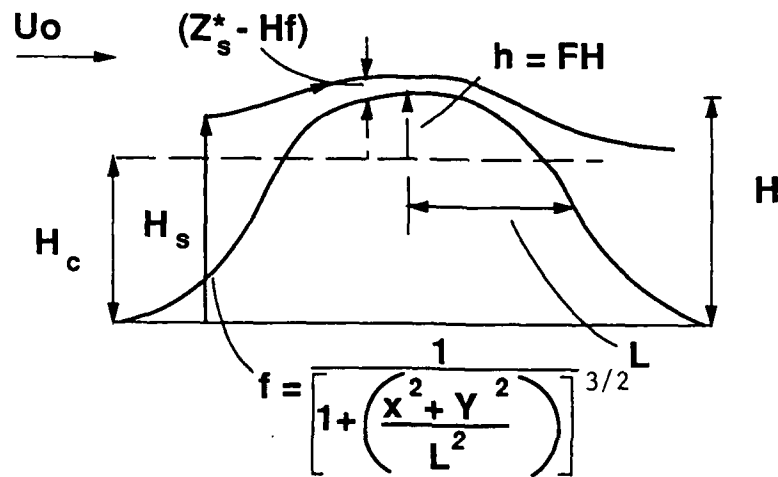
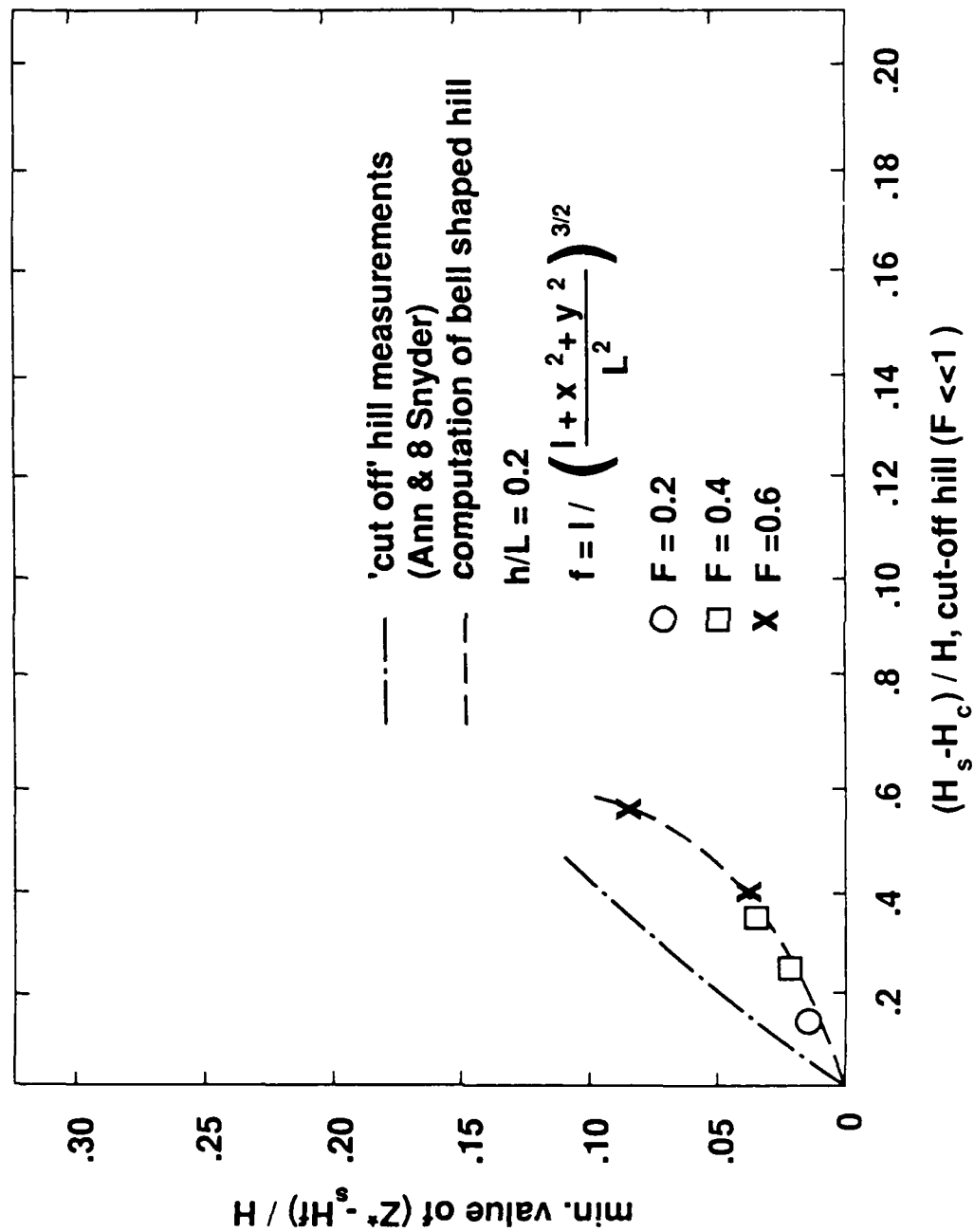


Figure A2 (a) Definition sketch for bell-shaped hill

Fig. A 2.(b) H_s/h , bell shaped hill ($F \gtrsim 1$)



Chapter E

**Temperature field in turbulent
flow over hills**

Prepared by
J.C.R. Hunt

Summary

A brief review is given in the first two sections of the general physical processes governing the temperature field in the earth's boundary layer and the way it changes over hills, with particular emphasis on the time scales and length scales that determine these changes. The changes over the surface are quite different to those in the bulk of the boundary layer.

Next, different models are developed for these two regions of the flow. Near the surface, the turbulence is close to equilibrium and an eddy diffusivity model enables the temperature field to be computed in terms of the upwind temperature, the mean and turbulent wind field and the changes in surface fluxes over the hill. Some surprising results emerge about the different trends of these processes. From the calculated distribution of temperature fluxes and mean temperature gradients over the hill, it is possible to estimate the change in the dissipation and structure function of temperature and humidity fluctuations, ϵ_θ and C_T^{-2} , E_q and C_q^{-2} .

In the flow above the inner region, we provide an estimate for the changes in temperature spectra which should be of practical value for the propagation of electromagnetic waves.

1. Introduction

To analyse the problem of how the temperature field changes over hills, it is first necessary to describe the broad features of the atmospheric boundary layer over level ground. The temperature field in the atmospheric boundary layer is closely linked to the velocity field. Both are strongly affected by the local diurnal heating and cooling of the ground by radiation to the ground by day and from the ground by night. But also they are affected by the advection from elsewhere of air with different temperature and velocity field; for example by large-scale frontal systems, sea breezes, or localized thunderstorm outflows. Because these individual temperature and velocity fields are less frequent and have special characteristics, we concentrate on slowly-varying conditions driven largely by the diurnal cycle. (For a general review see Nieuwstadt & Van Dop 1982).

The atmosphere is largely heated and cooled by the turbulent transport of heat from and to the ground. This transfer of heat to the atmosphere F_θ (Wm^{-2}), then determines the temperature difference between the ground $\Theta(0)$ and the air $\Theta(z)$ above it. The temperature of the ground Θ_g depends on the balance between the radiant heat from or to the sky R_n , the heat flux upwards from the soil $F_G + R_n$. In the presence of vegetation, the heat flux to or from the air flow above the vegetation F_θ can be significantly different from $(F_G + R_n)$ because of latent heat being absorbed or released by the wet vegetation. Clearly the water vapour flux F_q is therefore intimately linked to F_G (see Thom 1975 and the discussion in §2).

When there is a net upwards heat flux, $F_\theta(>0)$, buoyancy forces drive large eddying motions whose vertical extent is limited by the stably stratified air above the boundary layer. (The lower atmosphere in the absence of motion tends to be isothermal because of radiative heat transfer between different layers, and is therefore slightly hydrostatically stable). The *convective* boundary layer thickness h typically grows during the day to its maximum (say 1-2km) in mid-afternoon. The structure (from Kaimal et al. 1976 - see fig. 1), shows a *uniform* potential temperature θ_m^* through the bulk of the layer

($0 \leq z/h \leq 1$), and only a thin surface layer ($z/h \leq 0.1$) where there is unstable temperature gradient, and the temperature may rise to its surface value as much as 30°C above the mid-layer value. The mean wind velocity $U_B(z)$ is usually approximately constant within the mixed layer, but also has a large gradient in the surface layer.

In this surface layer, the turbulence is generated both by the buoyancy forces which depend on the surface flux F_θ , and by the mean velocity gradient which depends on the shear stress ($\tau_* = \rho U_*^2$). So the structure of the mean temperature Θ and velocity U_B fields are determined by the height (L - the Monin-Obukhov length) at which the buoyancy forces dominate over the shear stresses. Its definition is

$$(1.1) \quad L_{MO} = -u_*^3 \rho C_p \Theta_0 / (g k F_\theta),$$

where ρ is the density, C_p the specific heat, k the van-Karman constant, Θ_0 is the mean temperature at a reference height (typically 10m above the ground).

Dimensional arguments (substantiated by experiment and computation) show that Θ and U_B can be expressed in terms of F_θ and u_*

$$(1.2a) \quad \frac{d\Theta}{dz}(z) = \frac{T_*}{kz} f_\theta(z/L_{MO}), \quad \frac{dU_B}{dz} = \frac{u_*}{kz} f_u(z/L_{MO}),$$

where $f_H(z/L_{MO})$ and $f_u(z/L_{MO}) \rightarrow 1$ when $z/L_{MO} \rightarrow 0$. When these are integrated, special constants appear. When $z/L_{MO} \rightarrow 0$,

$$(1.2b) \quad (\Theta(z) - \Theta(0))/k = T_* \{ \ln(z/z_0) + B^{-1} \}, \text{ and } U_B = (u_*/k) \ln(z/z_0)$$

where B^{-1} is a thermal parameter dependent on u_* , and z_0 is the roughness length. Over rough surfaces B has been found empirically to be given by $B^{-1} \approx 8u_*^{1/3}$, where u_* is measured in ms^{-1} .

When $L_{MO} < 0$,

$$(1.3a) \quad f_\theta(z/L_{MO}) = (1 - 16z/L_{MO})^{-1/2}$$

$$(1.3b) \quad f_u(z/L_{MO}) = (1 - 16z/L_{MO})^{-1/4}.$$

These formulae are approximately valid for $z/h \leq 0.1$.

The key features of the turbulence structure are these. When $z \leq L_{MO}$ the vertical turbulence, σ_w , scales on u_* , and when $z \geq L_{MO}$, it scales on the buoyancy velocity scale

$$(1.4a) \quad w_* = \{ (gF_\theta h)/(\rho C_p \Theta_0) \}^{1/3},$$

and increases to a maximum value in the mixed layer. In fact,

$$(1.4b) \quad \sigma_w = 1.4(z/h)^{1/3} w_* \text{ for } z/h \leq 0.2,$$

$$(1.4c) \quad \sigma_w = 0.6 w_* \text{ for } z/h \geq 0.2.$$

The horizontal turbulence scales on w_* throughout the layer. The scale of vertical turbulence increases in proportion to z for $z/h \leq 0.1$ and is about $0.2h$ for $z/h \geq 0.1$. The energy dissipation ϵ is approximately constant through the mixed layer. But in the surface layer, where the rate of production of turbulent kinetic energy ($u_*^2 dU/dz$) by shear plus the rate of production by buoyancy forces

$$F_\theta g/(\rho C_p \Theta_0) = u_*^3/kL$$

is approximately balanced by the rate of dissipation of kinetic energy, so

$$(1.5) \quad \epsilon_B = \frac{u_*^3}{kz} [f_u - z/L].$$

The variance of the temperature fluctuations σ_θ^2 in the convective boundary layer decreases from its maximum value near the surface

$$(1.6) \quad \sigma_\theta^2 \approx \frac{1}{2} T_*^2 (z/L)^{-2/3}.$$

The integral scale of these fluctuations L_θ are about 5 times that of the vertical fluctuations $L_x^{(w)}$ at all heights. The distribution of the rate of dissipation of temperature fluctuations, ϵ_θ in the surface layer is determined by an approximate balance between the production of temperature fluctuations - $(F_\theta/\rho C_p) d\theta/dz$ and ϵ_θ , so $\epsilon_{\theta B} = -(T_*^2 u_*/kz) f_\theta(z/L)$.

In a stably stratified boundary layer the heat is transferred to the ground, so all the turbulence energy comes from the shear near the surface. The thickness h of these layers is much less -- as low as 30m. in some extreme cases. In the surface layer Θ and U are given

by equations (1.2) and (1.3a), (1.3b). The profiles throughout the layer are given in figure 2. Note that the temperature gradient $\partial\Theta/\partial z$ remains positive right through the layer. In fact, the Richardson number $Ri = (N/dU/dz)^2$ is often found to be constant through the main part of the layer, ($N^2 = g[d\Theta/dz]/\Theta(0)$) showing how the turbulence exists in a form of local equilibrium (Brost & Wyngaard 1978).

The vertical turbulence decreases to near zero at the top of the stratified boundary layer, but σ_θ remains large, due partly to wave-like motions. In the surface layer, $\sigma_\theta \approx T_*$. The scale of temperature fluctuations L_θ is larger than that of the velocity fluctuations - the latter being controlled by the large shear, so

$$(1.7a) \quad \epsilon \propto \sigma_w^2 dU/dz \quad ,$$

(Caughey et al (1979) Hunt, Kaimal & Gaynor (1985). It is more usual, though arguably less physically correct, to suggest

$$(1.7b) \quad \epsilon \propto \sigma_w^2 N \quad .$$

When the heat flux from or to the ground becomes small, or the wind speed (driven by horizontal pressure gradients) is large enough that $L_{MO}/h \rightarrow \infty$, the buoyancy forces are negligible throughout the layer. In rare cases the thickness and the structure is determined by Coriolis forces, (so that $h \approx 1/2u_* / f$); more usually, h is determined by the period over which the boundary layer has been developing by u_* , and by the value of N above the layer. There is usually some weak temperature field $\theta(z)$, and therefore the temperature fluctuates even in this situation. Typically in the surface layer

$$\sigma_w \approx u_*$$

$$L_x^{(w)} \approx \frac{1}{2} z.$$

$$L_x^{(\theta)} \approx 15 z \quad .$$

(1.8a-e)

$$\sigma_\theta \approx T_*$$

$$\epsilon_{\theta_B} = \frac{T_*^2 u_*}{kz} ; \quad \epsilon_B = \frac{u_*^3}{kz}$$

For the transmission of electromagnetic radiation through the atmosphere, it is important to know the correlation and spectrum of the small scales of temperature and humidity fluctuations (i.e. in the *inertial* subrange). This was recently reviewed by Wyngaard & Lemone 1980. It is customary to express this small scale structure using the structure function

$$(1.9) \quad \overline{(\theta(x+r) - \theta(x))^2} = C_T^2 r^{2/3}$$

where $C_T^2 \approx 3 \epsilon_\theta \epsilon^{-1/3}$. In this report we discuss how C_T^2 is changed in air flow over hills on the basis of calculations of the temperature field. It is found that for $z/h \leq 0.5$, in the convective boundary layer ($L_{MO} < 0$),

$$(1.10) \quad C_T^2 = \frac{4.9 T_*^2}{z^{2/3}} [1 - 7z/L_{MO}]^{2/3} ,$$

and in the stable boundary layer

$$C_T^2 = \frac{4.9 T_*^2}{z^{2/3}} [1 + 2.4(z/L_{MO})^{2/3}] .$$

The refractive index fluctuations are also affected by water vapor fluctuation and correlation between the water vapor and temperature fluctuations. (see Wyngaard & Lemone 1980).

2. Overall structure of the mean and fluctuating temperature field over hills

The mean and fluctuating velocity field over a hill say $z = Hf(x/L_1)$ naturally divides itself into two regions (figure 3). In the inner region within a distance of order l from the surface (typically $1/10$ of the hill length), the changes of the mean flow U_0 are strongly affected by the shear stress generated over the surface of the hill and therefore by the changes in the shear stresses. Also the turbulence increases and decreases in proportion to the local surface shear stress, defined in terms of the upwind shear stress as $u_*^2(1+\tau)$, where $\tau(x,y)$ is the local dimensionless perturbation. The reason is that the timescale for the turbulence $T_L (= L_x^{(w)}/\sigma_w)$ is less than the time to travel over the hill ($\approx L/U(l)$) within this layer., and so the turbulence adjusts to the local conditions for $z \leq l$. (Britter, Hunt & Richards, 1981).

Above this layer the airflow travels too fast over the hill for the effects of the surface to diffuse upwards. So the changes in the mean flow are caused by the air flow having to pass over the hill and the internal adjustments within the flow are controlled by the inertial forces (of which the pressure gradient is an important manifestation; Hunt & Richards 1984; Hunt, Leibovich & Richards (1986)).

The maximum mean vertical velocity w in this outer region occurs at a height h_m which is typically about $1/3 L$ ($h_m = L/l^{1/2}(L/z_0)$), where L is a characteristic hill length. This height defines the mean velocity scales $U_0 = U_B(z = h_m)$, and the mean horizontal and vertical perturbation velocity components uU_0 and wU_0 are scaled on this value. The perturbation pressure Δp is of order of $\rho(H/L)U_0^2$, where H/L is the slope. This is the pressure that controls the flow near the surface. (Hunt, Leibovich & Richards 1986).

A similar division into regions is appropriate for determining the measured fluctuating temperature field. Within the inner region, where the flow and turbulence adjusts to the local condition, the mean temperature is controlled by the local surface heat flux $F_0(1+g(x))$ and the local shear stress $\rho u_*^2(1+\tau)$, and the changes in the local mean wind speed uU_0 and the changes in the turbulent diffusion coefficient K_z to $K_z + \Delta K_z$).

The time scale for temperature fluctuations in the surface layer is $T_\theta \sim \theta^2/\epsilon_\theta \sim kz/u_*$ while the travel time T is $L/U(z) = Lk/(u_* l \ln(z/z_0))$. Consequently, T_θ is less than T when $z \leq l_\theta$ where $l_\theta \sim L/\ln(l_\theta/z_0)$ (so l_θ has about the same thickness as that of the inner region). In the inner region, the temperature spectrum can adjust to the local flow and surface conditions for wavelengths less than about λ_l

$$\lambda_l \sim \epsilon^{1/2} T^{3/2} \approx l \ln^{3/2}(l/z_0)$$

(since time scale for adjustment of a wavelength λ is of order $\epsilon^{-1/3}(2\pi/\lambda)^{-2/3}$, Panofsky et al 1982). Typically $l \approx 10\text{-}30\text{m}$; so the small-scale spectrum of practical interest (of scales much less than l) is expected to have a local structure and be determined by the local values of ϵ_θ and ϵ .

Above the inner region the large-scale temperature fluctuations are not determined by the local conditions because their time scale T_θ is *larger* than the travel time over the hill. They have been generated in the air flow upwind of the hill and are distorted by the change in the mean flow, the turbulence and the mean temperature gradient over the hill. The small scales of temperature are likely to be affected by changes in local small-scale turbulence, rather than by changes in the whole turbulence field, since only the small scales can adjust fast enough. There is some evidence from wind-tunnel studies that the temperature spectrum may be significantly distorted.

3. The temperature structure in the inner region

3.1 *Changes in surface heat and water vapor fluxes over a hill*

In this region the temperature, θ , and humidity, q , are determined by the local heat flux F_θ or water vapor flux F_q from or to the ground, the vertical diffusion of heat and water vapor, and by the advection of heat and water vapor from upwind. Over uniform flat terrain the advection has a negligible affect on the distribution of θ and q . But over non-uniform terrain such as a hill, where the surface fluxes vary with downwind distance, and advection of θ and q affects the vertical distribution of θ and q . Furthermore, the convergence and divergence of streamlines and the change in the turbulence over the hill can have comparable effects on $\theta(z)$ and $q(z)$.

A widely accepted model for the 'sensible' heat flux and the water fluxes at the ground, when covered with vegetation, is that developed by Monteith. Its mathematical derivation and implications were nicely discussed by Thom (1975); its use in dispersion modelling was developed by Smith & Blackall (1979). It is convenient to express F_θ and F_q in terms of net in-coming radiation heat flux R_n and the net heat flux arriving at the surface from the soil G , the Bowen-ratio β , and the latent heat of water λ , as

$$(3.1a,b) \quad F_\theta = \frac{R\beta}{1+\beta}, \quad F_q = \frac{R}{\lambda(1+\beta)}.$$

where the net heat flux from the radiation and soil is $R = R_n + G$. Thus, the relation between F_θ and F_q is

$$(3.2) \quad F_q/F_\theta = 1/(\beta\lambda)$$

The ratio β depends on the shear stress at the ground τ_* , the roughness z_0 , the local mean temperature θ and water vapor concentration q , and also the *nature* of the vegetation. The lowest value of this ratio is zero, when the winds are moderate, the air is dry and all the energy is used to evaporate water from the vegetation. There is no upper limit of this ratio, if there are few plants or they have a high 'stomatal' resistance.

The changes in F_θ and F_q , denoted by ΔF_θ , ΔF_q , can be expressed in terms of the upwind value of F_θ and F_q , and in terms of the changes in β and R thus

$$(3.3) \quad \Delta F_\theta / F_{\theta 0} = \Delta R / R + \delta \beta / [\beta(1 + \beta)]$$

and

$$(3.4) \quad \Delta F_q / F_{q0} = \Delta R / R - \delta \beta / (1 + \beta).$$

This result reveals the sensitivity of the changes in F_θ and F_q to the value of β .

On more or less sunny days any changes in $(R_n + G)$ are mainly caused by changes in the *direct* solar radiation R_s reaching the surface. Then we can assume that the net radiation and ground heat flux is related to the changes R_s by a relation like

$$(3.5) \quad \frac{\Delta R}{R} \approx \chi_R \Delta R_s / R_s$$

where the coefficient χ_R is not equal to 1.0 as supposed by Smith & Blackall (1979), because R_n , the net radiation, is only about 1/3 of the solar radiation reaching a surface. Of course the diffused radiation tends to be concentrated at angles near to the solar elevation ϕ . (Fig. 3) From data quoted by Geiger (1965, p. 376) it appears that $\chi_R \approx 0.7$.

For a slope equal to $(H/L) f'(x/L)$, the proportional change

$$(3.6) \quad \Delta R_s / R_s \approx (\cot \phi)(H/L)f'$$

Note that $\cot \phi$ is smaller in summer than winter. Geiger's data shows that on a south facing slope of 10° , $\Delta R/R = 0.13$ averaged over the whole year, but 0.4 in winter and 0.06 in summer. At $48^\circ N$, $\cot \phi \approx 2.9$ in winter and .47 in summer, so the predicted variation in $\Delta R/R$ from (2.6) would be .5 in winter and .04 in winter. At night or in foggy or overcast conditions R does not depend on the slope (for small slopes).

From Monteith's formula in the appendix we can derive the changes in β caused by changes in θ , q , and τ : β is also changed by variations in the surface vegetation or roughness. We are assuming here that the form of the vegetation remains fixed over the hill. These expressions are

$$(3.7) \quad \Delta F_{\theta}/F_{\theta 0} = \Delta R/R + \chi_{\tau} |\Delta \tau|/\tau + \chi_{\theta} \Delta \theta/\theta_0 + \chi_q \Delta q/q_0$$

$$(3.8) \quad \Delta F_q/F_{q0} = \Delta R/R + \psi_{\tau} |\Delta \tau|/\tau + \psi_{\theta} \Delta \theta/\theta_0 + \psi_q \Delta q/q_0.$$

In sunny conditions (3.5) and (3.6) can be used for the first terms.

As is shown in the appendix χ_{τ} and ψ_{τ} can range between about -1/2 and 1/2 in most kinds of condition, when the heat flux is radiation controlled. This is consistent with recent data that gives χ_{τ} equal to about -1/2 in stable conditions, when the heat flux is *downwards* and the heat transfer is controlled by forced advection over the ground. This is based on a correlation of measurements by Venkatram, (1980). In the former case generally χ_{τ} depends on the nature and state of the vegetation and the humidity of the air.

A range of examples is given in the Appendix.

The parameters χ_{θ} and χ_q depend on the humidity, i.e. the ratio of q to its saturated value at the temperature θ . If the air is saturated, $\chi_{\theta} = \chi_q = 0$. But for typical air flow over vegetation in mid-latitudes, a change of -1°C for given q or a doubling of q for given θ produces a similar order of magnitude of increase in F_{θ} as 1 ms^{-1} change in wind speed, i.e. $|\chi_{\theta}| \approx (1/3)10^{-2}$, $\chi_q \sim 1$.

This provides some framework for considering how the surface heat and water fluxes can change over a hill. Some results were reported by Hunt & Richards (1984).

There is some laboratory evidence for the validity of (3.8), when the upwind flow is unsaturated. Dawkins & Davis (1981) measured the change in flux of vapors from a small region on a surface located on a model hill in a wind tunnel. They found that the flux increased by about 50% of the increase in $\Delta \tau/\tau$. (That is not how they expressed their result - that is our interpretation.) A similar result was found by Verma & Cermak (1974) in their study of mass transfer over wavy surfaces.

3.2 Analysis of the mean temperature field

In the inner region the vertical gradients of temperature and velocity are large compared with horizontal gradients, and the relevant small scales of turbulence are close to local equilibrium. Consequently, the change in perturbation temperature (which we scale with the upwind parameter T_*), θ^* , can be calculated by assuming that the perturbation in vertical heat flux ΔF_θ can be estimated with an eddy diffusivity $(K_z + \Delta K_z)$, which is perturbed by the change in turbulence. (We assume that its distribution with height is not changed; this is probably not a good approximation over steeper hills because K_z appears to be a function of the local mean shear (Newley 1986)).

The conservation equation for heat leads to the usual 'advective-diffusive' equation for temperature over hilly surface (which we take to be two dimensional for simplicity)

$$(3.9) \quad \rho c_p \left[u_d^* \frac{\partial \theta^*}{\partial x} + w_d^* \frac{\partial \theta^*}{\partial Z} \right] = \frac{\partial (F_\theta + \Delta F_\theta)}{\partial Z}.$$

The vertical displacement co-ordinate Z is defined in terms of the height $Hf(x/L)$ of the hill

$$(3.10) \quad Z = z - Hf(x/L),$$

where it is assumed that H/L is small. Terms of $O((H/L)^2)$ are neglected. The velocity components u_d^* and w_d^* are defined in terms of x and Z . Equation (3.9) is now written in terms of perturbation quantities and normalized in terms of $U_0 (=U_B(h_m))$ and T_* .

$$(3.11a,b,c) \quad \begin{aligned} u_d^* &= U_0 [U(Z) + u_d(x,Z)] \\ w_d^* &= U_0 w_d(x,Z) \\ \theta^* &= \theta(Z) + \frac{T_*}{k} \theta(x,Z), \end{aligned}$$

so that using (1.3)

$$(3.12) \quad \frac{\partial \theta^*}{\partial Z} = \frac{T_*}{k} \left[\frac{1}{Z} f(Z/L_{MO}) + \frac{\partial \theta}{\partial Z} \right],$$

where $f_\theta(Z/L_{MO})$ is the local Monin-Obukhov function over the hill surface. Using the eddy diffusivity hypothesis, the heat flux is given by

$$(3.13) \quad \frac{F_{\theta} + \Delta F_{\theta}}{\rho C_p} = ku_* \left[1 + \frac{\tau}{2} \frac{Z \partial \theta^*}{\partial Z} / f_{\theta}(Z/L_{MO}) \right],$$

where $\rho \tau u_*^2$ is the perturbation Reynolds stress. Thence, using (3.12) the calculations for l/L_{MO} is small (say less than 0.1),

$$(3.14) \quad \frac{\Delta F_{\theta}}{\rho C_p} = u_* T_* \left\{ \frac{\tau}{2} + \frac{\partial \theta / \partial Z}{f_{\theta}(Z/L_{MO})} - \frac{\Delta f}{f_{\theta}(Z/L_{MO})} \right\},$$

where $f_{\theta} = f_{\theta} + \Delta f$, and Δf is the change in the Monin-Obukhov function. The flow is near neutral in the inner layer if its thickness l is less than about 1/20 of the Monin-Obukhov length L_{MO} (or the Richardson number is less than about 0.1). Then $f_{\theta} \approx 1$ and $\Delta f = 0$.

The boundary conditions on the temperature in the inner region are

- (i) that the heat flux is equal to the mean surface heat F_{θ}^* at the ground, where $F_{\theta}^* = F_{\theta} + \Delta F_{\theta}$. From (1.3) this means that

$$\frac{\partial \theta^*}{\partial Z} = \frac{(F_{\theta} + \Delta F_{\theta})/\rho C_p}{k \sqrt{(\tau^*/\rho)}}$$

where τ^* is the local shear stress. Since $\tau^* = \rho u_*^2(1 + \tau)$, the non-dimensional perturbation temperature satisfies

$$(3.15a) \quad \frac{\partial \theta}{\partial z} = G(x) \Delta F_{\theta} / F_{\theta}$$

where

$$G(x) = \Delta F_{\theta} F_{\theta} - \tau/2 ;$$

- (ii) that very close to the surface the temperature should have the same relations to the local heat flux F_{θ}^* and shear stress τ^* as over level ground, so from (1.2),

$$(3.15b) \quad \theta^*(z) - \theta^*(0) = \frac{F_{\theta}^*}{k \rho C_p} \left[\ln \frac{Z}{z_0} + B^{-1} \right]$$

where $B^{-1} = B_0^{-1} + \Delta B^{-1}$. For typical vegetation, $B^{-1} = 8 (\tau_*/\rho)^{1/6}$ so

$B_0^{-1} = 8 u_*^{1/3}$ and $\Delta B^{-1} = \frac{8}{6} \tau(x) u_*^{1/3}$; (u_* is in ms^{-1}); therefore from (3.5b)

$$(3.15c) \quad \theta(Z) - \theta(0) = G(x) \left[\ln \frac{Z}{z_0} + B_0^{-1} \right] + \Delta B^{-1} .$$

- (iii) Upwind and downwind the perturbation temperature tends to zero. We now derive the normalized governing equation for θ . Substituting (3.12) and (3.14) into (3.9), and scaling x in terms of L , and Z in terms of l , we obtain

$$\left[\frac{U(y)}{U(l)} \frac{\partial \theta}{\partial (X)} + \frac{(w_d/U(l)) L}{\zeta} \frac{1}{l} \right] = \left[\frac{\partial}{\partial \zeta} \left[\zeta \frac{\partial \theta}{\partial \zeta} \right] + \frac{1}{2} \frac{\partial \tau}{\partial \zeta} \right] \frac{k^2 L}{l \ln \frac{l}{z_0}} .$$

But from the definition of l for the mean flow

$$\ln (l/z_0) = 2k^2 L .$$

and the use of the continuity equation simplifies this to

$$L(\theta) \equiv \left[1 + \frac{\ln \zeta}{\ln \left(\frac{l}{z_0} \right)} \right] \frac{\partial \theta^*}{\partial X} - \frac{1}{2} \frac{\partial}{\partial \zeta} \left[\zeta \frac{\partial \theta}{\partial \zeta} \right] = \frac{1}{U(l)} \frac{1}{\zeta} \int \frac{\partial u_d}{\partial X} d\zeta + \frac{1}{2} \frac{\partial \tau}{\partial \zeta}$$

At this stage it is convenient to separate the factors that determine θ , the perturbation temperature, corresponding to the 'source' terms on the right and to the change in surface flux $\Delta F_\theta(0)$.

We let

$$(3.17a) \quad \theta = \theta^{(a)} + \theta^{(b)} + \theta^{(c)}$$

where

$$(3.17b) \quad L(\theta^{(a)}) = \frac{1}{\zeta} \int_0^\zeta \frac{\partial u_d(\zeta')}{\partial X} d\zeta' \text{ subject to } \zeta \frac{\partial \theta^{(a)}}{\partial \zeta} \rightarrow 0 \text{ as } \zeta \rightarrow 0 ,$$

$$(3.17c) \quad L(\theta^{(b)}) = \frac{1}{2} \frac{\partial \tau}{\partial \zeta} \text{ subject to } \zeta \frac{\partial \theta^{(b)}}{\partial \zeta} \rightarrow 0 \text{ as } \zeta \rightarrow 0$$

and

$$(3.17d) \quad L(\theta^{(c)}) = 0, \text{ subject to } \theta^{(c)} \rightarrow 0 \text{ as } \zeta \rightarrow \infty \quad \zeta \frac{\partial \theta^{(c)}}{\partial \zeta} \rightarrow G(x) \text{ as } \zeta \rightarrow 0 .$$

Using Fourier transforms and the results of the analysis of the mean flow by Hunt, Leibovich & Richards (1986), the perturbations $\theta^{(a)}$ are expressed as asymptotic expansions in $\ln(l/z_0)$. Thus

$$(3.18) \quad \theta^{(a)} = \frac{H/L}{U^2(l)} \left[\theta^{(a,0)} + \frac{1}{\ln(l/z_0)} \theta^{(a,1)} + \dots \right] .$$

We only need to consider the bulk of the inner region where $\ln \zeta / \ln(l/z_0) \gg 1$ because there is no discontinuity in θ or $\zeta \partial\theta/\partial\zeta$ across the inner stress layer where this approximation is not valid. Then the equation (3.17b) reduces to

$$(3.19a) \quad i\kappa_1 \theta^{(a,0)} - \frac{1}{2} \frac{\partial}{\partial \zeta} \left[\zeta \frac{\partial \theta^{(Ba,0)}}{\partial \zeta} \right] = i\kappa_1 \sigma$$

$$(3.19b) \quad i\kappa_1 \theta^{(a,0)} - \frac{1}{2} \frac{\partial}{\partial \zeta} \left[\zeta \frac{\partial \theta^{(a,1)}}{\partial \zeta} \right] = \sigma h(\zeta) - i\kappa_1 \ln \zeta \theta^{(a,0)}$$

where

$$h(\zeta) = - \left[\frac{4}{\zeta} \int_0^\zeta K_0(p') d\zeta' + \ln \zeta - 2 \right]$$

where $p' = \sqrt{i\kappa_1 \zeta}$.

Since $\zeta \leq 1$ in the inner region, we approximate $h(\zeta)$ (to within 10%) by the expression

$$(3.19c) \quad h(\zeta) = - \left[4K_0(p) - \frac{5}{2} + \ln \zeta \right] .$$

The solution to (3.19a) is obtained by noting from HRL that

$$\left(i\kappa_1 - \frac{\partial}{\partial \zeta} \left[\zeta \frac{\partial}{\partial \zeta} \right] \right) (K_0(p)) = 0 .$$

so

$$L(K_0(p)) = \frac{1}{2} i\kappa_1 K_0(p) .$$

and that the complementary function to (3.19) is $K_0(q)$ where $q = 2\sqrt{i\kappa_1 \zeta}$.

Therefore

$$(3.20a) \quad \theta^{(a)} = \frac{(H/L)\sigma(\kappa_1)}{U^2(l)} \left[1 - \frac{1}{\ln(\frac{l}{z_0})} \left[8K_0(p) - 4K_0(q) - \frac{5}{2} + 2 \ln \zeta \right] \right] .$$

At the surface (as $\zeta \rightarrow 0$),

$$(3.20b) \quad \theta^{(a)} \approx H/L \frac{\sigma(\kappa_1)}{U^2(l)} \left[1 - \frac{5/2 + 2 \ln 2 + 2 \ln \kappa_1 + i\pi}{\ln(\frac{l}{z_0})} \right] .$$

Note that

$$(3.21a) \quad \frac{\partial \theta^{(a)}}{\partial \zeta} = - \frac{(H/L)\sigma(\kappa_1)}{U^2(l) \ln(\frac{l}{z_0})} \left[\frac{2}{\zeta} + \frac{4\sqrt{\kappa_1}}{\sqrt{\zeta}} \left[2(\ker'_0(p) + i \operatorname{kei}'_0(p)) \right. \right. \\ \left. \left. - [\ker'_0(q) + i \operatorname{kei}'_0(q)] \right] \right] .$$

As $\zeta \rightarrow 0$,

$$(3.21b) \quad \partial \theta^{(a)} / \partial \zeta \propto - (\partial / \partial \zeta) [p^2 \ln p] \sim - \ln \zeta = O[(H/L)\sigma U^{-2}(l) \ln^{-1}(l/z_0) \ln \zeta] .$$

For the effect of the perturbation in shear stress, (3.19c) leads to

$$(3.22a) \quad i\kappa_1 \theta^{(b,0)} - \frac{1}{2} \frac{\partial}{\partial \zeta} \left[\zeta \frac{\partial \theta^{(b,0)}}{\partial \zeta} \right] = \frac{-H}{L} \sigma \cdot \frac{1}{2U^2(l)} \lambda(\zeta) ,$$

where

$$\lambda(\zeta) = \frac{\partial}{\partial \zeta} \left[\zeta \frac{\partial}{\partial \zeta} [4K_0(p) + \ln \zeta - 1] \right] .$$

The integral which satisfies (3.17c) (or 3.22a) is

$$(3.22b) \quad \theta^{(b,0)} = -\sigma \cdot 4 [K_0(p) - K_0(q)] .$$

Thus as $\zeta \rightarrow 0$, since

$$(3.22c) \quad K_0(p) \sim -\frac{1}{2} \ln \zeta - \ln 2 - \ln i, \quad K_0(q) \sim -\frac{1}{2} \ln \zeta - \frac{3}{2} \ln 2 - \ln i, \quad \theta^{(b)} = -\frac{H}{L} \frac{\sigma}{U^2(l)} \cdot 2 \ln 2 .$$

and

$$(3.23a) \quad \frac{\partial \theta^{(b)}}{\partial \zeta} = - \frac{\frac{H}{L} \sigma}{U^2(l)} \frac{4\sqrt{\kappa}}{\sqrt{\zeta}} \times \\ [\ker_1(p) - \sqrt{2} \ker_1(q))(1-i) + (\operatorname{kei}_1(p) - \sqrt{2} \operatorname{kei}_1(q))(1+i)] .$$

Again, $\partial \theta^{(b)} / \partial \zeta \propto \ln \zeta$ as $\zeta \rightarrow 0$, but the order of magnitude is great.

$$\frac{\partial \theta^{(b)}}{\partial \zeta} = 0 \left[\frac{\frac{H}{L} \sigma}{U^2(l)} \ln \zeta \right] .$$

The solution for the third component $\theta^{(c)}$ is given by

$$(3.24a) \quad \theta^{(c)}(\kappa_1, \zeta) = -2G(\kappa_1) K_0(p) .$$

This satisfies the surface flux condition (3.19d), because as $\zeta \rightarrow 0$,

$$(3.24b) \quad \theta^{(c)} = -2G(\kappa_1) \left[-\frac{1}{2} \ln \zeta - \gamma - \frac{1}{2} \ln i \right]$$

where γ is Euler's constant, and therefore

$$\zeta \frac{\partial \theta^{(c)}}{\partial \zeta} = G(\kappa_1) ,$$

but (3.24) must also satisfy the condition for $\theta^{(c)}$ at the surface specified by (3.15c). By expressing (3.15c) in terms of ζ and substituting the limiting form of $\theta^{(c)}$ given by (3.24b) into (3.15c), it follows that

$$(3.25a) \quad -\theta^{(c)}(\kappa_1, 0) = G(\kappa_1) \left[B_0^{-1} - 2\gamma - i\pi + \ln \left(\frac{l}{z_0} \right) \right] + \Delta B^{-1} ,$$

where

$$G(\kappa_1) = g(\kappa_1) - \frac{1}{2} \tau(\kappa_1, 0) ,$$

where ΔB^{-1} depends on the distribution of τ over the surface. An approximate form is

$$\Delta B^{-1} \sim 4.3 \tau(\kappa_1) u_*^{-1/3} \text{ where } u_* \text{ is in ms}^{-1} .$$

The vertical gradient of $\theta^{(c)}$ obtained by differentiating (3.24a) is

$$(3.25b) \quad \frac{\partial \theta^{(c)}}{\partial \zeta} = - G(\kappa_1) \frac{2\sqrt{\kappa_1}}{\sqrt{\zeta}} \left[\ker_1(p)(1-i) + \operatorname{kei}_1(p)(1+i) \right] .$$

Near the surface $\partial \theta^{(c)} / \partial \zeta \sim G(\kappa_1) [1/\zeta + i4\kappa_1 \ln \zeta]$.

3.3 Discussion of analysis of inner region mean temperature distribution

The order of magnitude and phase of the different components at the mean temperature perturbation on the surface can be compared using solutions (3.20a), (3.22b) and (3.24a).

The perturbation $\theta^{(a)}$ caused by the convergence and divergence of the streamlines brings warm air near the ground when the streamlines converge. Therefore $\theta^{(a)}$ is in phase with the surface mean speed and mean elevation at the surface (when the hill is large enough or the surface smooth enough that $\ln l/z_0 \gg 1$). From (3.20) it follows that

$$(3.26a) \quad \theta^{(a)} \approx \left(\frac{H}{L_1} \right) \frac{U^2(h_m)}{U^2(l)} \left[1 + \frac{5}{\ln \left(\frac{l}{z_0} \right)} \right] .$$

(In this expression the second-order term has been retained because typically it is of the same order as the first-order term.) Since the greater the shear in the upwind flow (i.e. the ratio of $U(h_m)$ to $U(l)$), the greater is the speed up and rate of convergence of streamlines over the hill, so it is not surprising that $\theta^{(a)}$ is also proportional to the upwind shear.

The vertical profile of $\theta^{(a)}$ in figure (a) shows that the perturbation is maximum above the surface and just below the height where the horizontal velocity perturbation of u_d is maximum. Therefore the gradient of $\theta^{(a)}$, $\partial\theta^{(a)}/\partial\zeta$, is positive below about $l/4$ and negative above $l/4$. We note that to first order $\theta^{(a)}$ is constant with height in the inner region. This is because the rate of convergence (or vertical velocity) to the first order increases with z and the mean velocity gradient $\partial\theta/\partial z$ decreases in proportion to l/z and the product of these two effects is constant with height. Thus the gradient of $\theta^{(a)}$ is determined by the second-order term in (3.11a), and its magnitude from (3.10b) is

$$(3.26b) \quad \partial\theta^{(a)}/\partial\zeta \approx (H/L) U^2(h_m)/(U^2(l) \ln(l/z_0)) .$$

The perturbation component $\theta^{(b)}$ caused by the change in the vertical diffusivity, which is proportional to τ , leads to a change in vertical heat flux gradient proportional to

$\partial\tau/\partial Z$ Since $\partial\tau/\partial Z$ increases rapidly toward the bottom of the inner region (in proportion to $-\ln(l/Z)$) the change in $\partial F_\theta/\partial Z$ is greatest close to the surface, where

$$\frac{\partial F_\theta}{\partial Z} \propto \left[\frac{H}{L} \frac{U^2(h_m)}{U^2(l)} (-\ln(l/Z)) \right] .$$

This is of the same order and has approximately the opposite phase as the convergence effect, because although, $-\tau/(0)$, is in phase with the surface, $\partial\tau/\partial z$ (as $Z/l \rightarrow 0$) is about 90° out of phase with the surface elevation.

This explains why $\theta^{(b)}(0)$ is about 180° out of phase with $\theta^{(a)}$ but of the same order of magnitude, thus (from (3.22)),

$$(3.27a) \quad \theta^{(b)} \approx \frac{H}{L} \frac{U^2(h_m)}{U^2(l)} .$$

The rapid variation in $\partial\tau/\partial\zeta$ near the surface leads, however, to a rapid decrease in $\theta^{(b)}$ over a scale l and therefore its vertical gradient has magnitude

$$(3.27b) \quad \frac{\partial\theta^{(b)}}{\partial\zeta} \approx \frac{H}{L} \frac{U^2(h_m)}{U^2(l)} ,$$

which is $O(\ln(l/z_0))$ greater than $\partial\theta^{(a)}/\partial\zeta$. (This would be a factor of five or six in practice.)

Graphs of $\theta^{(b)}(\zeta)$ and $\partial\theta^{(b)}/\partial\zeta$ are shown in Figure 00.

The perturbation component $\theta^{(c)}$ caused by the changes in surface heat flux and shear stress is such that its gradient is in phase with these components at the surface, the surface temperature itself (given by (3.15a)) slightly lags the phase of the combined surface flux G by (3.15a)) $\pi/\ln(l/z_0)$. HLR showed that the surface shear stress is in phase with the surface elevation but slightly leads its phase by $\pi/(\ln(l/z_0))$. Therefore, to first order, the phase of the surface temperature depends on the relative magnitude of the surface heat flux and shear stress, which depend on the kind of heating occurring over the terrain.

The order of magnitude of this surface component follows from (3.15a). If the normalized change in heat flux is proportional to the slope (e.g. by the effects of solar radiation),

$$(3.28) \quad \theta^{(c)}(0) \approx H/L \ln(l/z_0) .$$

This is greater than the other components $\theta^{(a)}$ and $\theta^{(b)}$, but the numerical factor may not be very large (e.g. $2 \ln 2 U^2(h_m)/U^2(l)$ is typically about three, while $\ln(l/z_0)$ is about five or six).

If the change in heat flux is proportional to the changes in surface shear stress (so that there is a net change in $F_\theta/\sqrt{\tau}$), then the relative change in $\theta^{(c)}$ is greater than (3.28).

3.4 Typical changes in surface flux over terrain

We can now calculate the changes in temperature caused by different changes in surface heat flux $g(x)$ over a hill, using the approximate formula developed in §3.1

$$(3.29) \quad g(x) = \frac{\Delta F_{\theta}(0)}{F_{\theta}(0)} \approx \chi_T \frac{\Delta \tau}{t} + \chi_R \frac{\Delta R_n}{R} + \chi_q \frac{\Delta q}{q} .$$

Case (i)

$$\Delta R_n = 0, \chi_T = \frac{1}{2}, \Delta q/q = 0$$

Here is no change in radiant heat to the ground (e.g. cloudy conditions), and any heat flux is being caused by the heat flux to the surface from below the surface. There is no change in humidity. The change in $g(x)$ is just caused by the change in shear stress. In this case the change in the combined flux term $G(x)$ is zero, so that effectively T_* is constant over the hill. Therefore the changes to $\theta^{(c)}$ are at the surface where $\theta^{(c)}$ is changed by the constant term $\Delta B^{-1} = 4/3\tau u_*^{1/3}$. The perturbation contributions to $\theta^{(a)}$ and $\theta^{(b)}$ are independent of these changes in surface conditions.

Case (ii)

$$\text{Here } \Delta R_n/R = H/L f(x/L), \chi_T = 1/2, \Delta = 0.$$

The primary change is caused by changes in incident radiation which are proportional to the slope. We have chosen the constant for multiplying the slope to be unity, corresponding to a latitude of about 50°N.

3.5 Estimation of the changes in turbulence structures

The turbulence is close to equilibrium at the bottom of the inner region because its time scale T_L is small compared with the travel time T . We have made the assumption that the turbulence is local equilibrium right through the layer in order to be able to use the simplification of the 'mixing length' model for the heat flux.

In the same vein is the assumption that in the inner region the temperature fluctuation and their dissipations are determined by the local heat flux $F_\theta(z)$ based on the local mean temperature gradients and the local sheart stress. From (1.8d), this implies that if

$l/|L_{MO}| \ll 1$, the variance over the hill is given by

$$\overline{\theta_B^2} + \overline{\Delta\theta^2} = \frac{(F_\theta + \Delta F_\theta / \rho C_p)^2}{u_*^2 (1 + t(z))} .$$

Therefore the fractional change is

$$(3.30) \quad \overline{\Delta\theta^2} / \overline{\theta_B^2} = [2\Delta F_\theta(z) / F_\theta(z) - t] = 2\zeta \partial\theta / \partial\zeta .$$

In local equilibrium the rate of generation of temperature fluctuations is equal to its rate of dissipation. Therefore the fractal change in dissipation is

$$\frac{\Delta\epsilon_\theta}{\epsilon_\theta} = \frac{[-\Delta F_\theta \frac{\partial\theta}{\partial Z} - \frac{\partial\Delta\theta}{\partial Z} \cdot F_\theta] / C_p}{-F_\theta \partial\theta / \partial Z} ,$$

$$(3.31) \quad \frac{\Delta\epsilon_\theta}{\epsilon_\theta} = \left[2\zeta \frac{\partial\theta}{\partial\zeta} + \frac{T}{2} \right] ,$$

where

$$t = \frac{(H/L) U^2(h_m)}{U^2(l)} \left[1 + \frac{5}{\ln(l/z_0)} \right] ,$$

and

$$\theta = \theta^{(a)} + \theta^{(b)} + \theta^{(c)} .$$

We note that (3.30) and (3.31) are consistent with the usual similarity hypothesis of turbulence that

$$\epsilon_{\theta} \propto \sigma_w^2 \overline{\theta^2} / L_x^{(w)} .$$

Since $w \propto u_*$ in the inner regions where $l / |L_{MO}| \ll 1$, and since $L_x^{(w)}$ is proportional to distance above the surface Z , it follows that

$$(3.32) \quad \epsilon_{\theta} \propto u_* \left(1 + \frac{t}{2}\right) \overline{\theta^2}, \quad \text{and} \quad \frac{\Delta \epsilon_{\theta}}{\epsilon_{\theta_B}} = \frac{\Delta \overline{\theta^2}}{\overline{\theta_B^2}} + \frac{t}{2} .$$

The change in the rate of energy dissipation ϵ in the inner region is given approximately by

$$(3.33) \quad \frac{\Delta \epsilon}{\epsilon_B} = \frac{3}{2} t .$$

Therefore

$$\frac{\Delta \epsilon}{\epsilon_B} = \frac{3}{2} 2 \frac{H}{L} \sigma(x) \frac{U^2(h_m)}{U^2(l)} \left[\zeta \frac{\partial u^{(1)}}{\partial \zeta} \right] ,$$

where the Fourier transform of $u^{(1)}$ is given by

$$- (4K_0(p) + \ln \zeta - 1) \quad \text{and} \quad p = 2\sqrt{i\kappa_1 \zeta} .$$

Therefore the relative change in the structure function parameter C_T^2 over hills for temperature fluctuations is given in terms of its value in the upwind boundary layer $(C_T^2)_B$ by

$$(3.24) \quad \frac{C_T^2}{(C_T^2)_B} = \left[1 + \frac{\Delta \epsilon_{\theta}}{\epsilon_{\theta_B}} \right] \left[1 + \frac{\Delta \epsilon}{\epsilon} \right]^{-1/3} ,$$

where $\Delta \epsilon_{\theta}$ is given by (3.22) and $\Delta \epsilon$ by (3.23). If the changes in ϵ_{θ} and ϵ are small enough, (3.24) reduces to

$$\frac{C_T^2}{(C_T^2)_B} = \left[1 + 2\zeta \frac{\partial \theta}{\partial y} + \frac{t}{2} - \frac{t}{2} \right] = \left[1 + 2\zeta \frac{\partial \theta}{\partial y} \right] .$$

Thus it is only the change in temperature (when normalized on the upwind values of T_*) that determines the first-order change in C_T^2 near the surface. Of course, as we saw in §3.2, the change in θ is significantly affected by the change in shear stress.

4. The change in the temperature spectra in the outer region

4.1 Governing equations and approximations

In the outer region the mean temperature gradient is changed by the convergence and divergence of the mean streamlines. The changes in the velocity and temperature fluctuations, however, are not just determined by the local changes in the mean velocity and temperature fields, because, unlike in the inner region, the memory time or turnover or Lagrangian time-scale T_L is longer than the travel time T . Thus the changes in the fluctuations are determined by the nature of the upwind fluctuations and by the changes in the mean field along the whole trajectory from upwind to the measuring point.

There is a well-established theory for the changes of the velocity fluctuations in the outer region, based on a linear theory for the distortion of the vorticity of the upwind turbulence by the convergence and divergence of the streamlines. This rapid distortion theory enables the changes in the velocity spectra to be predicted, with the results for the changes that are correct to within about 25% (Britter, Hunt & Richards 1981; Panofsky et al. 1982). There has been no corresponding theory for the changes in the temperature spectra.

Warhaft (1980) has measured the changes in spectra of temperature fluctuations in a wind-tunnel contraction. These measurements have not previously been analyzed; they provide a valuable set of data for beginning to construct a model for these temperature fluctuations.

In this section we consider three effects:

- (i) The effect of the change in the mean velocity and the turbulence on the change in the mean temperature field, $\Delta\theta$. We show that in the outer region (unlike the inner region) the turbulence has little effect on $\Delta\theta$.
- (ii) The effect of $\Delta\theta$ on the fluctuating temperature θ' . For most purposes it is a small effect.

(iii) The direct effect on θ' of the convergence and divergence of the streamlines and the changes in the turbulence. We look particularly at how the spectrum of θ' changes, as the wave numbers change. The leading-order effect is that caused by the mean flow. However the distortions to the spectra caused by non-linear pressures associated with the changes in u are unexpected and possibly important. The theoretical suggestions are largely in agreement with Warhaft's measurements. Fig. 5.

We first derive the equations for the mean and fluctuating temperature field θ^* , θ' in terms of the mean and fluctuating velocity field U , u' . (We shall only be concerned with length scales larger than the Kolmogorov microscales so that molecular diffusion can be neglected.)

From the full equations

$$(4.1) \quad \left(\frac{\partial}{\partial t} + (U + u') \cdot \nabla \right) (\theta^* + \theta') = 0$$

it follows that θ^* satisfies:

$$(4.2) \quad \frac{\partial \theta^*}{\partial t} + (u' \cdot \nabla) \theta^* = - \nabla \cdot (\overline{u' \theta'})$$

In the outer region the right-hand side can be neglected. For a two-dimensional steady flow the mean velocity and temperature can be expressed in terms of the displaced coordinates as

$$(4.3a) \quad \begin{aligned} U(x,z) &= (U_B(x,Z), 0) + (u_d^*, w_d^*)(x,Z) \\ \theta^*(x,z) &= \Theta(x,Z) + \Delta\theta(x,Z) \end{aligned}$$

where

$$(4.3b) \quad Z = z - Hf(x/L) \quad \text{and} \quad \partial u_d^* / \partial x + \partial w_d^* / \partial Z = 0.$$

The mean temperature can also be expressed in terms of the upwind mean temperature profile plus a mean perturbation $\Delta\theta$. Then (4.2) reduces to

$$(4.4) \quad U_B \frac{\partial \Delta\theta}{\partial x} + w_d^* \frac{\partial \Theta}{\partial Z} = 0$$

whence, from (4.3b) and using the fact that U_B varies slowly with height,

$$(4.5) \quad \frac{\partial \Delta \theta}{\partial Z} \equiv \frac{u_d^*}{U_B} \frac{\partial \Theta}{\partial Z} \left[1 + O\left(\frac{u_*}{U_B}\right) \right].$$

The equation for the fluctuating velocity θ' is given by

$$(4.6) \quad \frac{\partial \theta'}{\partial t} + (U \cdot \nabla) \theta' = - \nabla \cdot (u' \theta' - \overline{u' \theta'})$$

The left-hand side of (4.6) shows the effects of linear distortions on the fluctuating temperature and the right-hand side the effects of non-linear distortions. The change in the term $(U \cdot \nabla) \theta'$ in the accelerating flow is $O(u_d^* \theta' / L_\theta)$ or $O(H/L U_0 \theta' / L_\theta)$. The change in the term $(u' \cdot \nabla) \theta'$ is $O(u_0 \partial \Delta \theta / \partial Z)$ or $O(\Delta u' / U_0 \partial \Theta / \partial Z)$, whichever is the larger, where $\Delta u'$ is the order of magnitude of the change in u' over the hill.

Since $\frac{\Delta u'}{u'} \sim |u_d^*| U_B \sim H/L$ and since $\frac{\partial \Delta \theta}{\partial Z} = O\left(\frac{|u_d^*|}{U_B}\right) \partial \Theta / \partial Z$ it follows that $u_0 \frac{\partial \Delta \theta}{\partial Z}$ is of the

same order as $\frac{\Delta w}{U_0} \partial \Theta / \partial Z$.

For typical boundary-layer flows $U_0 \theta' / L_\theta \sim U_0 T_* / z$, while

$$u_0 \frac{\partial \Delta \theta}{\partial Z} \leq \frac{H}{L} \frac{u_* T_*}{Z}$$

in near neutral flows. Consequently the change in $(U \cdot \nabla) \theta'$ is much greater (by $O(U_0 / u_*)$) than the change in $(u' \cdot \nabla) \theta'$ in the outer region, and is the most significant linear term.

In stably stratified flows, using the theory of Pearson, Puttock & Hunt (1983), and the measurements of Hunt, Kaimal and Gaynor (1985), the estimates for these terms are:

$$L_\theta \sim \sigma_w / N \text{ and } \theta' \sim \left(\frac{\sigma_w}{N}\right) \partial \frac{\Theta}{\partial Z} \text{ so } \left(\frac{H}{L}\right) U_0 \frac{\theta'}{L_\theta} \sim \frac{H}{L} U_0 \frac{\partial \Theta}{\partial Z}.$$

Then $u_0 \partial \Delta \theta / \partial Z \sim \sigma_w H / L \partial \Theta / \partial Z$.

Thus stable conditions are similar to neutral ones in that the change in $\partial \theta' / \partial Z$ also has a smaller effect on θ' than the change in U .

The order of magnitude of the non-linear term on the right-hand side of (4.6) for eddies of scale L_θ is $u_0'\theta'/L_\theta$. Thus the ratio of the right-hand side to the largest term on the left-hand side is u_0'/U_0 . Since $u_0'/U_0 \ll 1$ (typically less than 0.1 in the outer region), this suggests that to first order the non-linear terms can be neglected. However a better understanding of how the non-linear term distorts the spectrum is obtained by analyzing how the wavenumbers of the temperature fluctuations are distorted. This also leads us to our desired result for the change in the spectra.

4.2 Fourier analysis and estimates of non-linear corrections

In the outer region the length scales of the temperature and velocity fluctuations of interest are small compared with the depth of the boundary layer (h) or the length of the hill (if $L \sim h$). Therefore θ' and u' can be expressed in terms of a local co-ordinate frame at a position $\mathbf{x}_0(t) = \int \mathbf{U} dt$ moving with the mean flow, viz: $\mathbf{X} = \mathbf{x} - \int \mathbf{U} dt$; and thence taking Fourier transforms S_θ, S_i with a local wavenumber $\chi(t)$ (see Fig. 6)

$$(4.7) \quad (\theta'(\mathbf{x}, t), u_i(\mathbf{x}, t)) = \iiint (S_\theta(\mathbf{X}, t), S_i(\mathbf{X}, t)) \exp i(\chi \mathbf{X}) d\chi$$

The equation θ' in local co-ordinates is

$$(4.8) \quad \frac{\partial S_\theta}{\partial t} + X_j \frac{\partial U_j}{\partial x_j} \frac{\partial \theta'}{\partial x_i} = -u_k(x_0) \frac{\partial \theta'}{\partial x_k} - X_j \frac{\partial u_k}{\partial x_j} \frac{\partial \theta'}{\partial x_k}$$

Substituting (4.7) into (4.8) leads to an equation for S_θ :

$$\frac{\partial S_\theta}{\partial t} + S_\theta \left(i X_k \frac{d\chi_k}{dt} \right) + i X_j \frac{\partial U_j}{\partial x_j} \chi_i S_\theta = -u_k(x_0) \chi_k S_\theta + \int X_j \chi_j \chi_k S_\theta(\chi') S_k(\chi - \chi') d\chi'$$

These equations are only satisfied by matching coefficients of S_θ and $X_j S_\theta$.

$$(4.9) \quad \frac{\partial S_\theta}{\partial t} = u_k \chi_k S_\theta$$

and

$$(4.10) \quad S_\theta \left[\frac{d\chi_k}{dt} + \frac{\partial U_j}{\partial x_k} \chi_j \right] = \int \chi_j \chi_k S_\theta(\chi') S_k(\chi - \chi') d\chi'$$

Thus the error in the magnitude of S_θ caused by neglecting the non-linear terms in (4.8) increases with the travel time T ; its order of magnitude is apparently of $O(\Delta u_0 \chi T)$ where Δu_0 is the change in the turbulence over the hill.

The error in the magnitude of the wavenumber χ is also apparently $O(\Delta u_0 \chi T)$. These naive estimates are far too large if they are used to estimate the errors in the spectra because they do not allow for the fact that the error terms are random and contain products that have weak correlation (e.g. $u_k S_\theta$). One way to estimate the error term, analytically, is to divide the velocity and temperature spectra into two halves, and assume that the fluctuations in the two halves are approximately uncorrelated, and to use the fact that small scale fluctuations (χ) have a correlation time scale of order $\epsilon^{-1/3} \chi^{-2/3}$.

If $\chi > L_x^{-1}$, where L_x is the scale of the velocity fluctuations, then the rate of change of the temperature spectrum $\Phi_\theta(\chi)$ ($\propto |S_\theta|^2$) depends on the amplification $A(\chi)$ of the small-scale velocity fluctuations. A two scale analysis suggests

$$(4.11a) \quad \frac{d\Phi_\theta}{dt}(\chi) \sim \Phi_\theta(k) \chi^{2/3} \epsilon^{1/3} A(\chi).$$

$$(4.11b) \quad \text{for } 2\pi L_x^{-1} \leq \chi \leq \left(\frac{\epsilon}{\nu^3}\right)^{1/4}$$

where $\chi = |\chi|$.

Over a hill of slope H/L the amplification A of the turbulent energy by linear rapid distortion process is of the order of H/L . But for scales much smaller than a critical scale l_* , non-linear processes reduce this amplification where $\epsilon^{-1/3} l^{2/3} \sim T \sim U_0/L$. For $L \sim 10^3\text{m}$, $l_* \sim 1\text{m}$. Thus, the typical proportional change in Φ_θ over a hill of 100m for an eddy scale of the order of about 1 meter would be (from 4.11a) about

$$\frac{1}{l_*^{2/3}} \frac{u_0}{L_x^{1/3}} \cdot \frac{H}{L} \cdot \frac{L}{U_0} \sim \frac{.01 \cdot 100}{1 \cdot (100)^{1/3}} \sim \frac{1}{4}.$$

This would be negligible. But for higher hills the change might be significant. For smaller scales non-linear processes would reduce any amplification.

The most significant feature of (4.11) is that it indicates that the form of the inertial range of the spectrum changes in an accelerating flow, and most surprisingly that the departure of the spectrum from the (-5/3) inertial subrange spectrum increases as the wave number increases. In his wind-tunnel experiments, Warhaft (1980) found that the high wavenumber spectrum was indeed amplified, by an increasing amount as χ increased. The estimate (4.11) agrees qualitatively with his observations, including the criteria for its applicability. As (4.11b), implies he found that when L_θ/L_χ decreased a larger range of the temperature spectra was amplified. (In his case he compared $L_\theta/L_\chi \sim 1/2$ to $L_\theta/L_\chi \sim 1$).

Since there is no significant effect of mean temperature gradient, there is no net increase of $\langle \theta^2 \rangle$, so the increase in small-scale temperature fluctuations indicated by (4.11) has to be compensated by a reduction in the intensity of large-scale temperature fluctuations, (as Warhaft observed). This effect is only significant if L_θ is less than, approximately, L_χ . So in the atmosphere where $L_\theta > L_\chi$, there is likely to be little reduction in Θ_θ when $\chi_1 < L_\chi^{-1}$.

4.3 Change in temperature spectra by linear straining

We have shown that, for length scales of temperature fluctuations of interest, in the outer region of flow over hills, the change in the Fourier transform and thence the spectrum of temperature fluctuations are not affected, to first order, by the changes in the non-linear terms in (4.9) and (4.10).

From (4.9) it follows that on the trajectory of a fluid element on a mean streamline, for a given local wavenumber \mathbf{X} , $S_\theta(\mathbf{X})$ does not change, and therefore the three dimensional spectrum at a three dimensional wavenumber \mathbf{X} at a position \mathbf{x} over the hill is equal to the upwind spectrum with wavenumber \mathbf{K} , i.e.

$$(4.12) \quad \Theta_\theta(\mathbf{X}(\mathbf{x})) = \Theta_\theta(\mathbf{K})$$

Equations (4.10) gives the change in wavenumber along the same trajectory. Thus over a two dimensional hill

$$(4.13a) \quad \frac{dx_1}{dt} = -x_1 \frac{\partial U_1}{\partial x_1} - x_3 \frac{\partial U_3}{\partial x_3}$$

$$(4.13b) \quad \frac{dx_3}{dt} = -x_1 \frac{\partial U_1}{\partial x_3} - x_3 \frac{\partial U_3}{\partial x_3}$$

In general the solution of these coupled equations (4.13) require integration along the mean streamlines over the hill. But for hills with low slope, an analytical integration becomes possible; since

$$\frac{d\chi_1}{dt} = U_1 \frac{d\chi_1}{dx} = U_1 \frac{\partial \chi_1}{\partial x} \left(1 + O\left(\frac{H}{L_1}\right)\right)$$

Then (4.13) becomes

$$\frac{\partial}{\partial x} (U_1 \chi_1) = -\kappa_3 \frac{\partial U_3}{\partial x_1}; \quad U_B^2 \frac{\partial}{\partial x_1} \left(\frac{\chi_3}{U_1}\right) = -\kappa_1 \frac{\partial U_3}{\partial x_1}.$$

Note that in the outer region $\partial U_1 / \partial x_3 \sim \partial U_3 / \partial x_1$, to leading order in u_∞ / U_0 , and by continuity $\partial U_3 / \partial x_3 = -\partial U_1 / \partial x_1$.

Thus at a given distance x in the flow direction and given height z

$$\chi_1(x, z) = \frac{\kappa_1 U_B(z)}{U_1} - \kappa_3 \frac{U_3}{U_1}$$

while

$$\chi_3(x, z) = \kappa_3 \frac{U_1}{U_B} - \kappa_1 \frac{U_3}{U_B}$$

Using the previous notation for the perturbations of the mean velocity

$$\mathbf{U} = U_1 (U + u, 0, w)(x, z)$$

the components of χ can be expressed as

$$\chi_1 = \frac{\kappa_1}{1 + \frac{u}{U}} - \frac{\kappa_3 w}{U(z)}, \quad \chi_2 = \kappa_2$$

(4.14)

$$\text{and } \chi_3 = \kappa_3 \left(1 + \frac{u}{U}\right) - \frac{\kappa_1 w}{U(z)}$$

Therefore the local three-dimensional temperature spectrum $\Phi_\theta(\mathbf{X})$ over two-dimensional hills at high wavenumber can be derived from the upwind spectrum by:

$$(4.15) \quad \Phi_\theta(\chi) = \Phi_\theta(k) \propto \frac{\epsilon_\theta \epsilon^{-1/3}}{\kappa^{11/3}}$$

where $k = \kappa$ and κ_i is expressed in terms of χ_i by (4.14).

For example at the top of a hill where $w = 0$, (4.14) reduces to

$$\kappa_1 = \chi_1 \left(1 + \frac{u}{U}\right), \quad \kappa_2 = \chi_2, \quad \kappa_3 = \frac{\chi_3}{\left(1 + \frac{u}{U}\right)}$$

So from (4.15)

$$(4.16) \quad \Phi_\theta(\mathbf{X}) \propto \frac{\epsilon_\theta \epsilon^{-1/3}}{\left[\chi_1^2 \left(1 + \frac{u}{U}\right)^2 + \chi_2^2 + \frac{\chi_3^2}{\left(1 + \frac{u}{U}\right)^2}\right]^{11/3}}$$

Thence the one-dimensional spectrum can be derived by integrating (4.10): $\Phi_\theta(\chi_1)$
 $= \iint \Phi_\theta \chi_2 d\chi_2 d\chi_3$. So

$$\Phi_\theta(\chi_1) \propto \frac{\epsilon_\theta \epsilon^{-1/3}}{\left[\chi_1^{5/3} \left(1 + \frac{u}{U}\right)^{2/3}\right]}$$

Another way of expressing this result is in terms of the temperature structure function -, which is not now isotropic: For a displacement r_x in the x direction

$$(4.17a) \quad \overline{(\theta(x,y,z) - \theta(x+r,y,z))^2} \propto \left(1 + \frac{u}{U}\right)^{2/3} r_x^{2/3} \epsilon_\theta \epsilon^{-1/3}$$

Also the integral scale of the temperature fluctuations in the direction of flow, L_θ , is similarly distorted:

$$\text{Since } L_\theta = \frac{\pi \phi_\theta(0)}{\theta^2} = \frac{\pi}{\theta^2} \iint \Phi_\theta(0, \chi_2, \chi_3) d\chi_2 d\chi_3$$

$$(4.18) \quad \frac{L_\theta}{L_{\theta_B}} = 1 + \frac{u}{U} .$$

Warhaft (1980) expressed his measurements of the distortion of the spectrum in terms of the change in the wavenumber, χ_{mx} , at the maximum of the function $\chi\phi_\theta(\chi)$. For typical spectral it is generally found that $\chi_{mx} \propto 1/L_\theta$. He found that the proportional change in $\chi_{mx}-1$ from upwind, $\chi_{mx(B)}/\chi_{mx}$, was approximately equal to the amplification of the mean speed in the contraction of the wind tunnel, when $L_\theta \approx L_x$. (When $L_\theta < L_x$, the amplification was less.)

Thus, we conclude that the major effect on the temperature spectrum over hills even for scales as small as 0.1m is the linear distortion of the wave numbers. The non-linear effects lead to distortion of the form of the spectrum.

These effects summarized in the schematic diagram Fig. 6.).

Appendix

Variation of heat and water flux over a surface

From Monteith's formula, as explained by Thom (1975) and Smith & Blackall (1979), F_θ and F_q are given by:

$$F_\theta(z) = \beta R / (1 + \beta), F_q(z) = R / ((1 + \beta)\lambda)$$

where the Bowen-ratio $\beta(z) = (r_a + r_{st} - r_i) / ((\Delta/\gamma)r_a + r_i)$, R is the net surface heat flux. λ is the latent heat of vaporization of liquid water, and the resistances r_a, r_{st}, r_i have the following values:

The aerodynamic resistance $r_a(z) = [1/(ku^*)] \ln((z-d)/z_0/5)$, where d is the displacement height, which is at the order of the vegetation height. $r_a(z)$ is usually defined in terms of the velocity at a particular value of $(z-d)$, eg

$$\begin{aligned} r_a(z) &= 6.25/U(z) \ln((z-d)/z_0) \ln(5(z-d)/z_0) \\ &= 2 \times 10^2 / U(z) \text{ for } z_0 \approx 10^{-2} \text{ m.} \end{aligned}$$

For a typical wind speed at 5 ms^{-1} , $r_a \approx 40 \text{ s m}^{-1}$. the stomatal resistance r_{st} is the resistance by the vegetation to evaporation and transpiration. When the plant surfaces are wet $r_{st} \rightarrow 0$, but when the plants transpire very slowly $r_{st} \rightarrow \infty$. In most typical air flows over crops, $r_{st} \approx r_a \approx 40 \text{ s m}^{-1}$. Monteith called r_i the 'isothermal resistance' because if $r_a + r_{st} = r_i$, there can be isothermal flow. r_i is defined as:

$$r_i = (\rho c_p / (R\gamma)) (p_{sv} - p_v),$$

where γ is the psychrometric constant $\gamma = \rho c_p / (\lambda \epsilon)$ - usually in $\text{mb}^\circ\text{C}^{-1}$, and ζ, c_p, ϵ, p are the density, specific heat, ratio of molecular weights of water to air ($\approx 5/8$), pressure. p_{sv}, p_v are the saturated and local vapor pressure: P_{sv} is a function of the temperature θ , $p_v/p = 8/5 q$, where q is the water vapor concentration.

The parameter Δ in the expression for the Bowen ratio is related to r_i :

$$\Delta = 1/2 ((\partial p_{sv} / \partial \theta)(z) + (\partial p_{sv} / \partial \theta)(\theta = 0))$$

$\Delta/\gamma(\theta)$ is plotted in Fig. A.1 from Thom (1973).

In order to understand how β varies with perturbation of τ , θ and q , we have to consider various conditions of humidity and plant type.

- (i) In conditions at about 50% humidity over field crops in mid latitudes (Thom, p. 103, 1973) $r_a \approx r_{st} \approx r_i$, $\gamma \approx 0.66$ mb/°C, $R \approx 100$ W/m². So $\delta\beta \approx 0(-\delta r_a/r_a - \delta r_i/r_i)$.

Note that since $\partial\beta/\partial r_i < 0 < \Delta/\gamma < 6$ in these conditions $\partial\beta/\partial r_a < 0$,

Thence, since $\partial r_a/\partial \tau \propto -\delta\tau/\tau$, $\partial r_i/\partial q \propto -\delta q$, $\partial\beta/\partial r_i < 0$ and $\partial\beta/\partial r_a < 0$

$$\delta F_\theta/F_\theta \sim -\delta F_q/F_q = 0(1/2\delta\tau/\tau, (-pc_p/R)(\Delta/(r_a)\delta\theta, \delta q/q)$$

depending which term is most significant.

Since $1 \leq \Delta \leq 6$ mb/°C for $0 < \theta < 40^\circ\text{C}$, $pc_p\Delta/(Rr_a)$ is of the order $1\text{sm}^{-1}\text{C}^{-1}$

Then an increase in wind speed reduces the evaporation, and increases the heat flux from the ground.

- (ii) In conditions, where there is a strong, dry air flow over irrigated vegetation,

$$r_i \gg r_a, r_i \gg r_{st}, \text{ then } \beta \rightarrow -1$$

so that F_θ/R and F_q/R become indeterminate; but $F_\theta = -F_q$.

In other words there is a downward flux of sensible heat.

- (iii) Where there is a strong dry air flow over vegetation which is wet on the surface, then there is no stomatal resistance to transpiration so $r_i \gg r_a \gg r_{st}$. Then $F_q > 0$ and $F_\theta < 0$ because of the evaporation.

In that case

$$\beta \rightarrow -1 + (\Delta/\gamma + 1)r_a/r_i$$

So $F_\theta \approx -[R/((\Delta/\gamma) + 1)]r_i/r_a$, $F_q \approx [R/(\Delta/\gamma + 1)]r_i/r_a$, then $\delta F_q/F_q \approx -\delta F_\theta/F_\theta \approx$

$$\Delta R/R + (1/2)|\Delta\tau/\tau - \delta r_i/r_i|.$$

In the case, an increase in surface shear decreases the magnitude of F_θ .

- (iv) When the wind is strong, there is some humidity and some transpiration. So that

$$r_a \gg r_{st}, r_a \gg r_i,$$

and $\beta \rightarrow 1/(\Delta/\gamma) \approx 1/2$ at 20°C .

Then F_q is about twice F_θ ; both are positive if $R > 0$ and both are independent of wind speed.

- (v) When the (stomatal) resistance is high, and the wind speed is moderate so that

$$r_{st} \gg r_a, r_i,$$

Then $\beta \rightarrow r_{st}/((\Delta/\gamma)r_a + r_i) \gg 1$.

so that $F_\theta \approx R$ and $F_q \approx (R/r_{st}) ((\Delta/\gamma)r_a + r_i) \ll R$.

In this case the heat flux is approximately independent of wind speed, but note that F_q increases with r_a , or decreases with wind speed.

References

- Brost, R. & Wyngaard, J.C. 1978. A model study of the stably stratified planetary boundary layer. *J. Atmos. Sci.* 35, 1427-1440.
- Britter, R.E., Hunt, J.C.R. & Richards, K. 1981. *Q.J. Roy. Met. Soc.* 107, 91.
- Caughey, S., Wyngaard, J.C. & Kaimal, J.C. 1979. *J. Atmos. Sci.* 36, 1041.
- Dawkins, R.A. & Davies, D.R. 1981. *J. Fluid Mech.* 108, 423-442.
- Geiger, R. 1965. The climate near the ground. Harvard U.P.
- Hunt, J.C.R., Leibovich, S., Richards, K. 1986. Stratified shear flows over low hills. I. Effects of upwind shear. Submitted to *Q.J. Roy. Met. Soc.*
- Hunt, J.C.R., Kaimal, J.C. & Gaynor, J. 1985. Some observations of turbulence structure in stable layers. *Q.J. Roy. Met. Soc.* 111, 223-259.
- Hunt, J.C.R. & Richards, K.J. 1984. Boundary Layer Meteorology 30, 223-259.
- Kaimal, J.C., Wyngaard, J.C., Jaugen, D.N., Cote, O.R., Izumi, Y., Caughey, S.J. & Reading, J.C. 1976. Turbulence structure in the convective boundary layer. *J. Atmos. Sci.* 33, 2152.
- Nieuwstadt, F.T.M. & van Dop, H. 1982. Atmospheric turbulence and air pollution modelling. Riedel.
- Panofsky, H.A., Larks, D., Kipshutz, R., Stone, G., Bradley, E.F., Bowen, A.J. & Hogstrup, J. 1982. Spectra of velocity components over complex terrain. *Q.J. Roy. Met. Soc.* 108, 215.
- Smith, F.B. & Blackall, R.M. 1979. Proc. Symp. Math. Models & Turbulent Diffusion in the Environment. Academic Press.
- Thom, A. 1975. Vegetation and the Atmosphere. Ed. J.L. Monteith. p. 57-110. Academic Press.
- Venkatram, A. Heat flux at ground in stable conditions. *B.L. Met.* 19.
- Venkatram, A. 1980. Heat flux at ground in stable conditions. *B.L. Met.* 18, 481.
- Verma, S.B. & Cermak, J.E. 1974. Colo. State Univ. Rep. CER70-71 SBV-JEC-59.
- Wyngaard, J.C. & Lemone, M.A. 1980. Behavior of the refractive structure parameter in the entraining convective boundary layer. *J. Atmos. Sci.* 37, 1573.

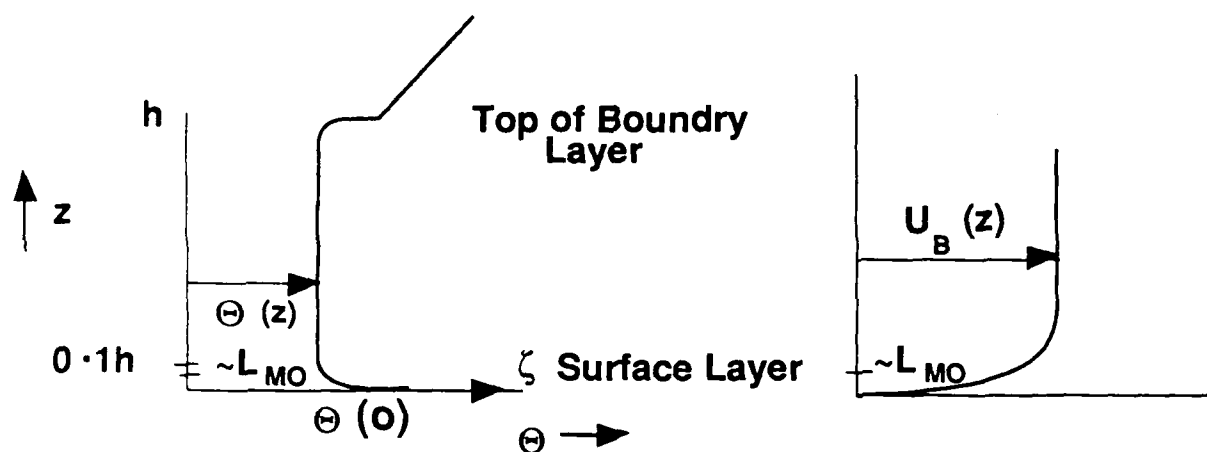


Figure 1. Mean potential temperature and velocity profiles in the convective boundary layer. ($L_{MO} < 0$)

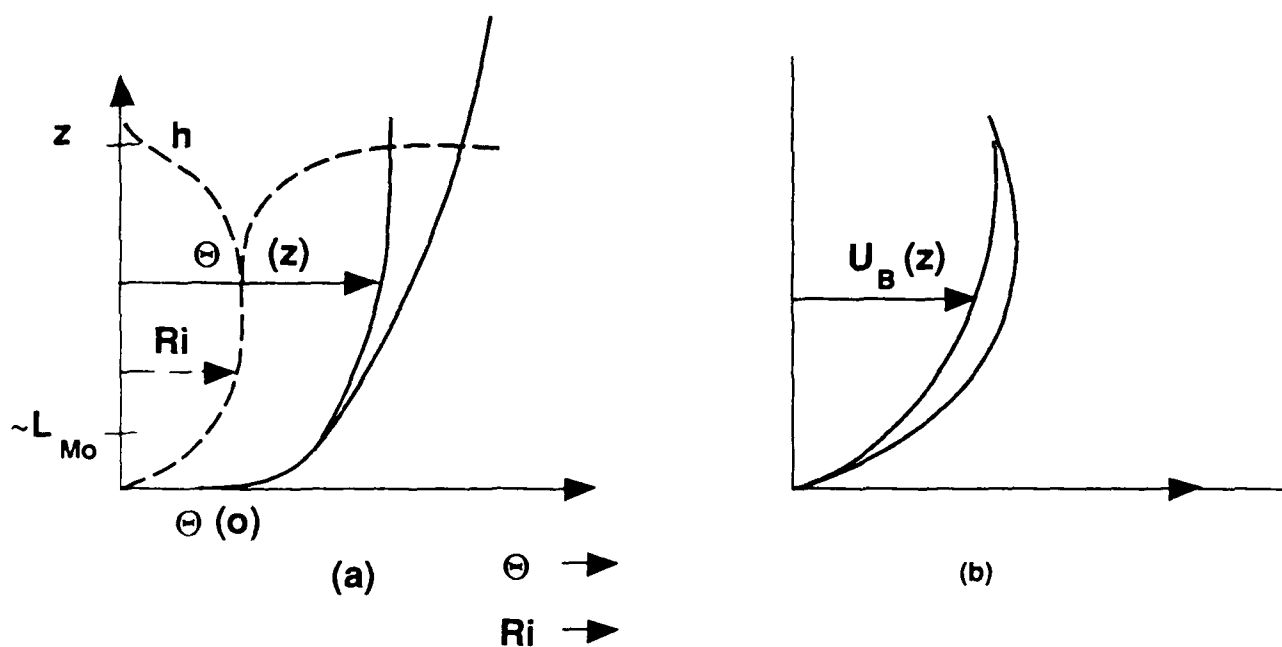


Figure 2. Typical profiles of mean potential temperature and mean velocity in the stable boundary layer. Figure 2a includes a profile of Richardson number. Its value at the top of the boundary layer tends to be indeterminate or very variable.

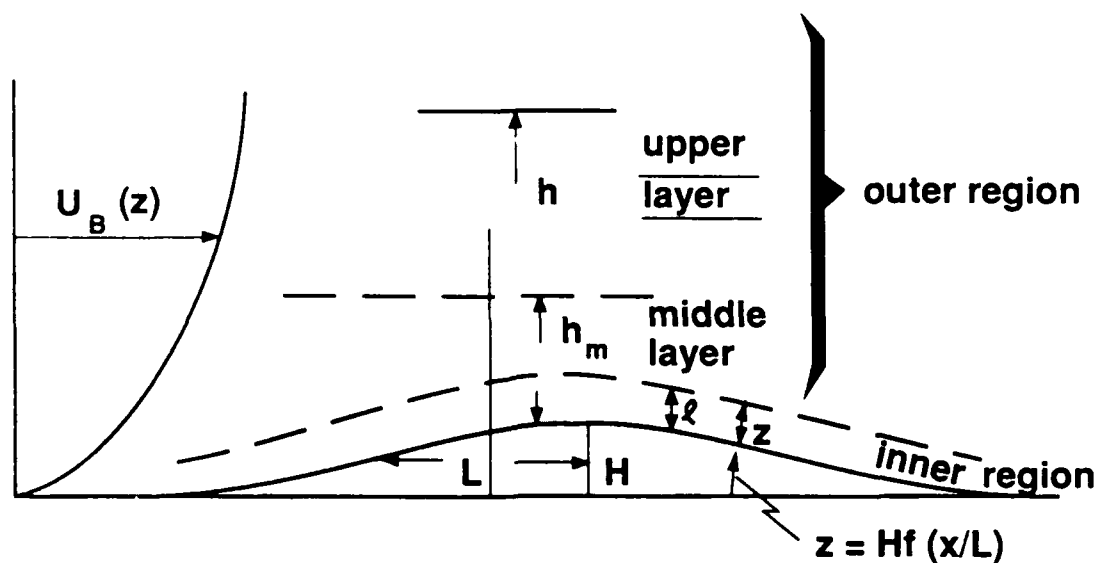


Figure 3. Region of different flow characteristics over a hill.

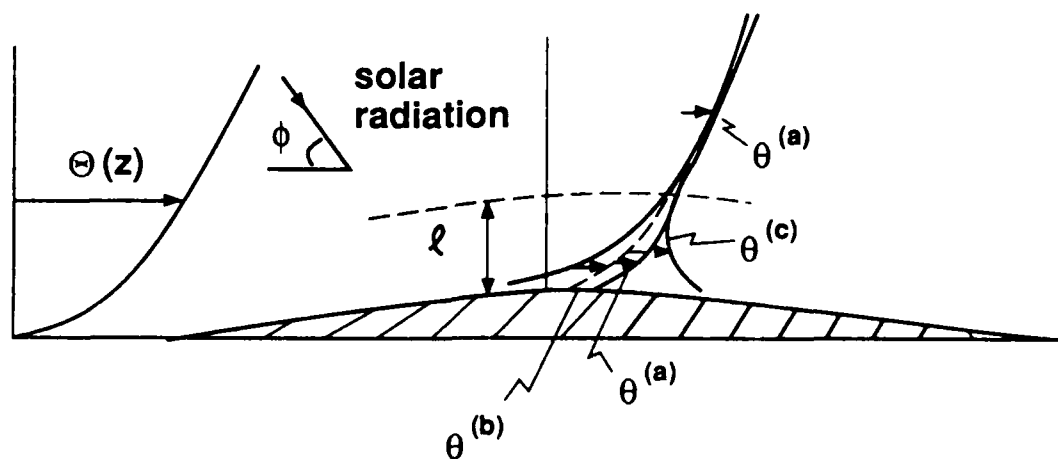
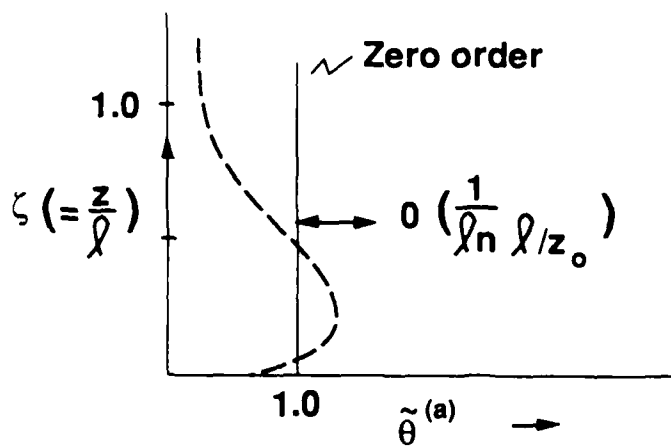


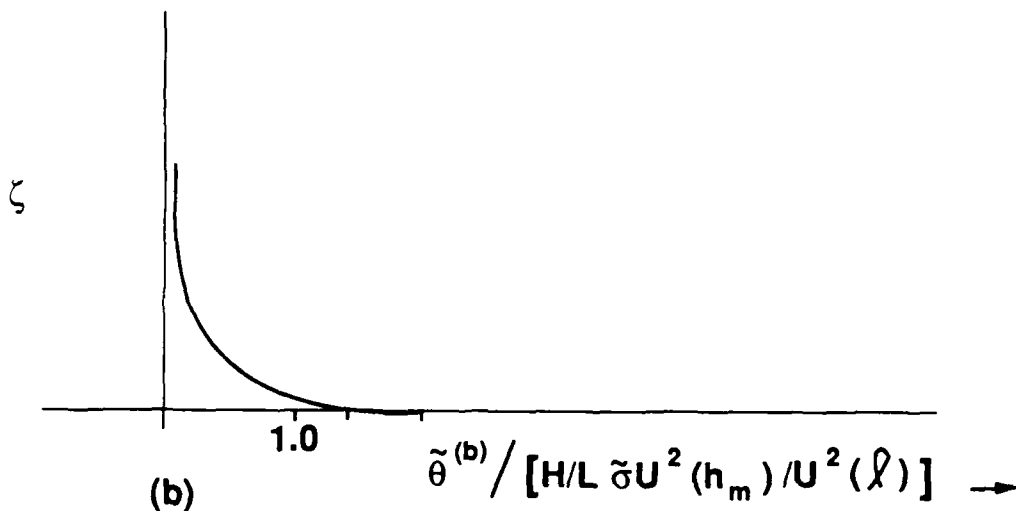
Figure 4. Different components of the perturbation to the mean temperature over the top of a hill. $\theta^{(a)}$ - convergence of mean streamlines. $\theta^{(b)}$ - increased diffusivity caused by excess turbulence $\theta^{(c)}$ - increased in heat flux from surface associated with increase in stream. (The sign of these components differ over the parts of the hill).

Figure 5

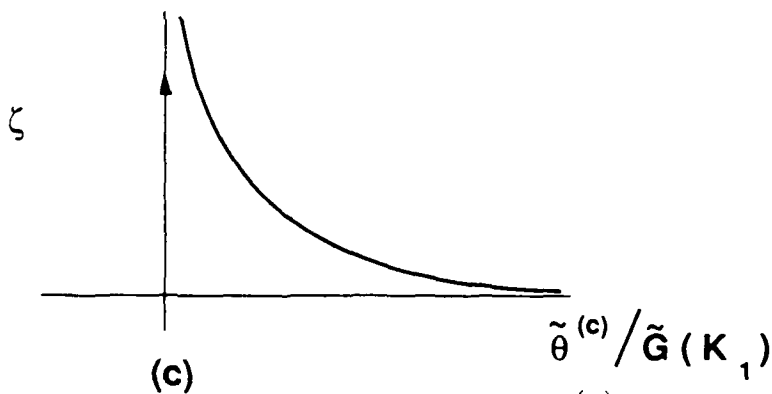


$$\left[\frac{H}{L} \tilde{\sigma} U^2(h_m) / U^2(l) \right]$$

(a) Fourier transform of $\theta^{(a)}$ (Real part).

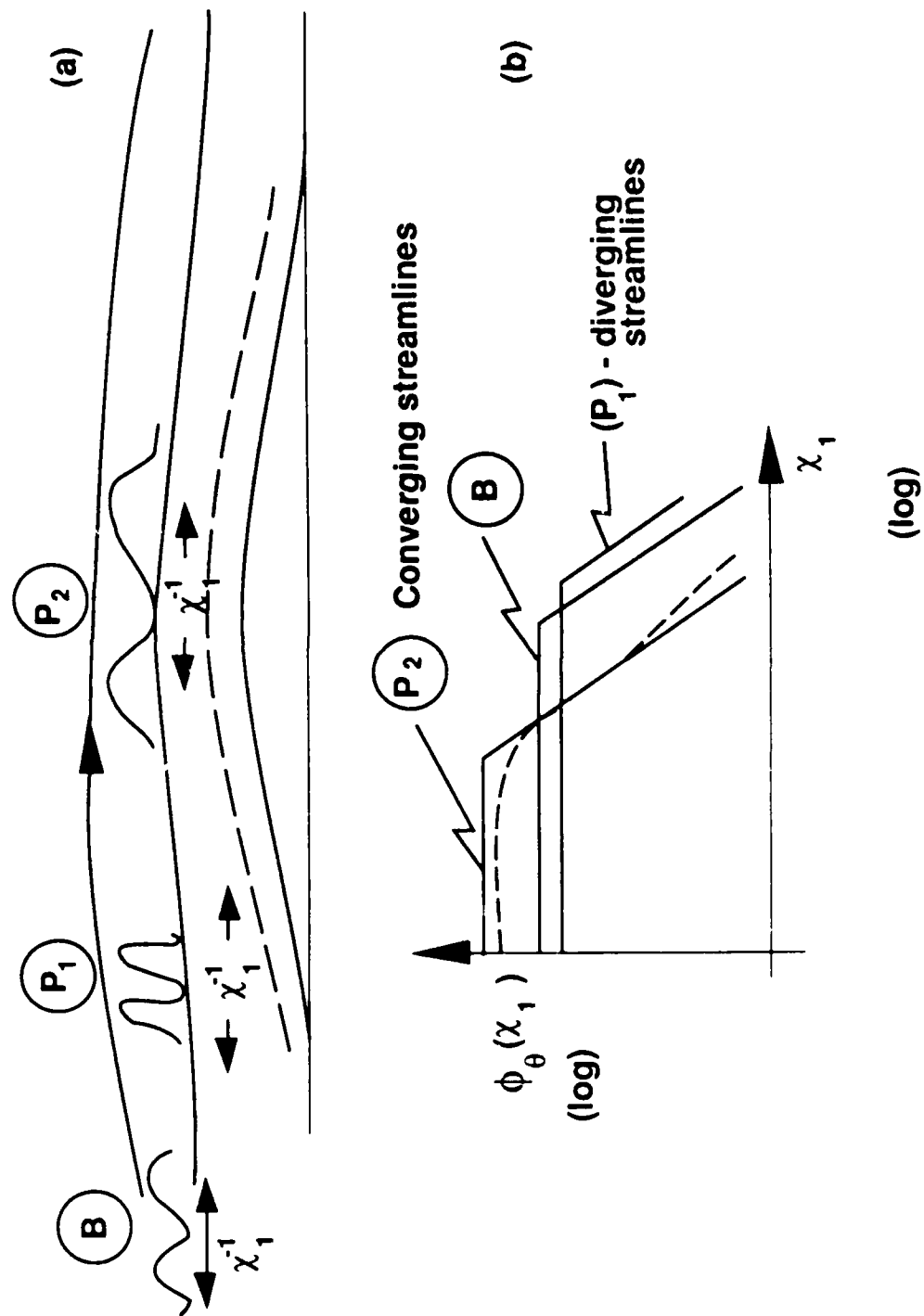


(b) Fourier transform of $\theta^{(b)}$. (Real part)



(c) Fourier transform of $\theta^{(c)}$ (normalized as perturbation in surface heat flux and shear stress). (Real part).

Figure 6



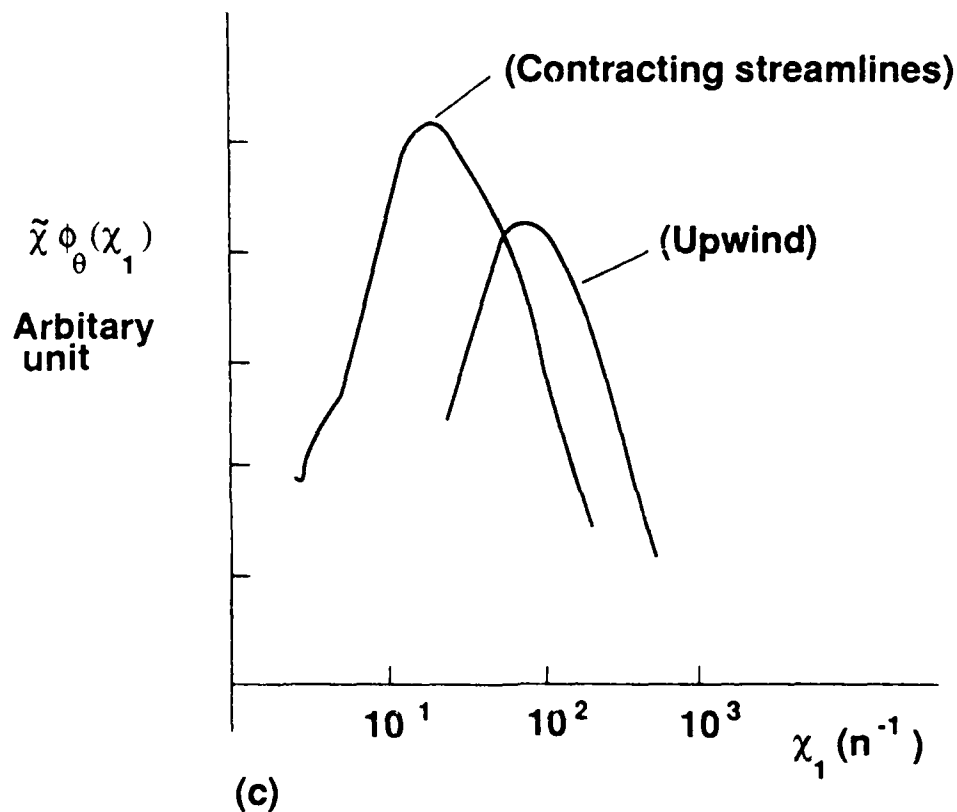


Figure 6

- (a) schematic diagram to show how diverging and converging streamlines of the mean flow affect the wave number.
- (b) change in the spectra of temperature caused by the mean streamlines' convergenced divergence. --- convection caused by non-linear processes (stronger when $L_g < L_x$).
- (c) Measurements of $\chi_1 \phi_\theta(\chi_1)$ before and after a contraction in a wind tunnel by Warhaft (1980) - in agreement with (b)

Chapter F

**Modelling of turbulent heat and moisture
transport in atmospheric flows**

Prepared by
J.L. Lumley

Modelling of Turbulent Heat and Moisture Transport in Atmospheric Flows

Construction of the model

The general construction of the model is described fully in Lumley & Mansfield (1984), to which the reader is referred for details. Briefly, it is a fully three dimensional second order model for the transport of latent and sensible heat in the atmospheric surface layer. The variables used are density anomaly and water vapor mixture fraction (specific humidity). An algebraic form for the third moments derived from first principles is used (as opposed to an *ad hoc* model). Every attempt has been made to make the model as realizable as possible, compatible with computational efficiency. That is, the modeled equations are constructed in such a way that all variances are automatically maintained non-negative, and all fluxes automatically satisfy Schwartz's inequality at all times. This is at least true in the continuum limit; the satisfaction of these various inequalities by the differenced forms of the equations is more delicate, and will be discussed later.

At the time of the *Interim Technical Report*, although the full model had been presented, it had been exercised only in a windless situation. This had the advantage of being vertically axisymmetric, and consequently having only five independent non-zero third moments. As will be discussed in greater detail later, the algebraic expressions for the third moments are cross-coupled, and the linear expressions for the moments must be solved at each grid point to obtain the required values. Solution of a 5×5 system does not present problems either by hand or by machine or by symbolic algebra program, such as MAKCYMA. Our first goal following the *Interim Technical Report* was the exercise of the program with wind. Unfortunately, when the wind is introduced, the system is no longer vertically axisymmetric, and there are now twelve independent third moments. Solution of this system at each grid point is roughly six times as costly in machine time. Thus, exercise of the model to resolve difficulties became a major undertaking.

When the wind was first introduced, we experienced serious instability at the inversion base. This instability did not appear until several hundred time steps had been

calculated. It was clear that it was not a customary numerical instability, but a non-linear instability introduced by the model. The instability appeared in the region near the inversion base where all the variables were tending to zero. Their values in this region were essentially negligible physically, but the way in which they all approached zero together was critical. The better part of a year was spent in seeking the source of this problem. (Recall that our effort during this year had been reduced to approximately one-third of that during the initial years of the contract).

The problem was caused by realizability violations near the inversion base, and by the way in which we tried to avoid them. The general technique of making the continuum version of the model fully realizable is not adequate in this region, where differencing errors can cause realizability violations even if the continuum model is fully realizable: it should be recalled that our model is not, in fact fully realizable. We find it essential at each time step to examine the values of all the fluxes and variances in this region for violations of Schwartz's inequality and negativity. Violations that are discovered are corrected by adjustment of the variables. The way in which the variables are adjusted is critical; it must be done smoothly, so that when the curves are differenced to determine the right hand side of the equations for the next time step, no unphysical terms are introduced. It must be done in the proper sequence. The correct variables must be adjusted. The problem usually arose near a zero of a flux, which usually did not occur at a grid point. Schwartz's inequality would be violated on one side or the other of the zero. There is a choice of three variables to adjust to correct the violation, the flux or one of the variances. The correction must be carried to at least two neighboring grid points on each side with a smooth weighting function, gradually reducing. If it is the flux that is adjusted, there is a problem. Suppose that the flux were positive at the point of violation, but negative at the neighboring point, and that the required adjustment at the point of violation were negative, should the adjustment at the neighboring point be positive or negative? Our inability to resolve this problem in any consistent manner lead us finally to adjust the variances, which did not

present this difficulty. Note, however, that we have to deal with $\langle \rho'u_1 \rangle$, $\langle \rho'u_3 \rangle$ and $\langle u_1u_3 \rangle$, with variances $\langle \rho'^2 \rangle$, $\langle u_1^2 \rangle$ and $\langle u_3^2 \rangle$; each variance appears in two of the fluxes. The required adjustment (possibly zero) in each of the products of standard deviations gives three equations in three unknowns, the adjustments required in each of the standard deviations. These are then smoothly distributed on each side of the point in question. Now, however, the values of the variances have been changed at points at which Schwartz's inequality had not previously been violated; it is necessary to make another sweep to check again for violations, and go through the same procedure again. Fortunately, this process converges. We monitored the number of violations and the number of iterations required as the run progressed; a rapid increase in the number of either required usually indicated the presence of an instability. Our final technique (combined with explicit calculation of the pressure transport, which improved the stability) proved satisfactory.

This phase of the work was completed by September 30, 1985. A one-dimensional tape with programmable boundary conditions and synoptic conditions was prepared, together with a user's manual, and forwarded to the contract manager. We include in this report figures (1 - 13) from the test calculation we carried out. This is the same physical situation we examined in the windless case: a dry boundary layer arrives over water; the radiant input remains the same, and the water temperature is the same as the air temperature; the input changes from sensible heat to latent heat, resulting in a sharp drop in the surface density anomaly flux; a stable region develops near the surface, and is gradually transported upward; finally the region is again fully mixed, with the new lower value of the surface density anomaly flux.

In Figures 1 - 13, the computer-generated call-outs are transparent acronyms: RPS, for example, is *Rho Prime Squared*, while DRB is *Derivative of Rho Bar*, or $\langle \rho' \rangle_3$. The notation is the same as that in Lumley & Mansfield (1984). \bar{F} and f are the mean and fluctuating water vapor mixture fraction, $\langle \epsilon_p \rangle$ is the dissipation of fluctuating water vapor

mixture fraction variance. C_f , C_1 and C_p are the relaxation coefficients (which multiply the pressure correlations) in respectively : the water vapor mixture fraction flux equation, the Reynolds stress equation, and the density anomaly flux equation.

During the final year of the contract we have concentrated on installing our program on Cornell's production supercomputer facility. This has involved writing a new code to handle our massive equation set, a new treatment of the boundary conditions, modifications to the way we handle the third moments, motivated by time considerations, a new treatment of the pressure, and testing of the new algorithms. Each of these is described in detail below. It should be borne in mind that we are hoping to solve 21 equations over an irregular boundary in three dimensions. The solution of four such equations in these circumstances (the "simple" test we use for our algorithms) is equivalent to ordinary computational fluid dynamics, i.e.- the solution of the Navier-Stokes equations. This is not generally regarded as an off-the-shelf item in three dimensions. Only in this way can one appreciate the magnitude of the problem we are attacking.

Computation of the pressure

In a three-dimensional computation it is necessary to determine the mean pressure from an equation; this was not necessary in our one-dimensional computations, in which the homogeneity assumption combined with the Boussinesq approximation made the pressure (anomaly) uniform.

The usual method for determining the pressure is to use the incompressibility assumption

$$u_{i,i} = 0$$

We take the divergence of the equation for the mean velocity, using the incompressibility assumption, to obtain a Poisson equation for the mean pressure:

$$-P_{,ii}/\rho = U_{i,j}U_{j,i} + \langle u_{i,j}u_{j,i} \rangle + g\langle \rho' \rangle_{,3}/\rho_0$$

This may now be solved by standard Poisson equation solvers, using the values of the mean velocity and the Reynolds stress determined at the last time step. On a regular grid,

in a box, the pseudo-spectral method is very fast: the products on the right hand side of the Poisson equation are calculated, and the Fast Fourier Transform is applied to both sides. The transform of the pressure is calculated in Fourier space, and the FFT used to return it to real space.

Unfortunately, solution of the Poisson equation in three dimensions on an irregular grid, in an irregular geometry (as required by terrain) is expensive in computational time. The FFT can no longer be used conveniently, and over-relaxation, or a similar technique must be used, requiring many iterations.

In order to avoid this difficulty, we have used an alternate scheme. The atmosphere is, after all, not an incompressible medium. It is a compressible gas, with a finite velocity of sound. It is therefore more realistic to use the equations for a compressible gas. Experimentally, it is known that the effects of compressibility on mean streamlines are negligible if the mean flow Mach number is below about 0.3. Of course, mean flow Mach numbers in typical flows in the atmospheric surface layer are more nearly of the order of 0.03, but between 0.3 and 0.03 we would expect to see negligible change in the mean flow. The use of the equations for a compressible gas has the advantage that the equations are predictive equations that can be solved by time stepping, like all the other equations that we are solving.

We begin with the equation for the instantaneous density and velocity:

$$\partial_t \rho + \rho_{,i} u_i + \rho u_{i,i} = 0$$

Using the isentropic relation between the pressure and density $dp/d\rho = a^2$, where a is the isentropic speed of sound, $a^2 = \gamma RT$, and the equation of state $P = \rho RT$, we have

$$\partial_t p + p_{,i} u_i + \gamma p u_{i,i} = 0$$

For a diatomic gas, $\gamma = 1.4$. This can be placed in conservative form as

$$\partial_t p + (p u_i)_{,i} + (\gamma - 1) p u_{i,i} = 0$$

We may now introduce the Reynolds decomposition $p = P + p'$ and average, to obtain

$$\partial_t P + (P U_i)_{,i} + \langle p' u_i \rangle_{,i} + (\gamma - 1) P U_{i,i} = 0$$

We have neglected a term $\langle p'u_{i,i} \rangle$, on the grounds that the Mach number of the fluctuating velocity is (in the atmospheric boundary layer) only about 4% of the mean flow Mach number; for this reason $u_{i,i}$ for the fluctuating velocity will be negligible, even if $U_{i,i}$ is not. The term $\langle p'u_i \rangle$ is one of those modeled, as $-0.2\langle q^2 u_i \rangle$, and this quantity is calculated. Note that all terms but the first ($\partial_t P$) are known at each time step.

In effect, setting the level of the absolute pressure, which appears nowhere else in the system of equations, determines the mean flow Mach number, and determines the strength of the feedback in the pressure equation. Note that $M^2 = a^2/U^2 = \gamma P/\rho U^2$. At each time step, $U_{i,i}$ is calculated. If it is not zero, it is multiplied by a fairly large number (P), and from this a new pressure field is determined which will tend to reduce the value of $U_{i,i}$.

As an aside, since the pressure always appears in the momentum equations divided by ρ_0 , it would be reasonable to work in terms of the kinematic pressure $P/\rho_0 = \Pi$, say. Since our pressure equation is homogeneous in the pressure, we can divide by ρ_0 and write a similar equation for Π .

Three dimensional test of numerical algorithm and pressure equation.

In order to test our general numerical algorithm, and to test our method of calculating the pressure, we have carried out a fully three dimensional laminar calculation, choosing as our problem one for which an exact solution of the Navier Stokes equations is known to exist. Our numerical algorithm is set up to handle an essentially arbitrary number of equations of the form

$$\partial_t f = (Df_{,i})_{,i} + (E_i f)_{,i} + Ff + G$$

We selected a laminar problem because the laminar Navier-Stokes equations are three equations of this form. In addition, it will be seen that the pressure equation is also of this form. Hence, by solving the laminar Navier-Stokes equations with the pressure determined by our compressible algorithm, we are effectively testing our algorithm on a four equation system, instead of the twenty-one equation system that we ultimately have in mind. In addition, the determination of the pressure using our compressible algorithm

can be done as well in a laminar situation. Finally, we have the advantage that exact solutions to the Navier Stokes equations exist for several problems, and we can hence determine the accuracy of our computation.

We took as our problem the impingement of an axisymmetric jet on a flat plate. This was studied by Homann (*Zeitschrift für Angewandte Mathematik und Mechanik* 16 (1936) 153-164). If the plate lies in the 1-2 plane, and the jet approaches along the 3-axis, the velocity field is given by

$$U_1 = (S/2)x_1f(\eta)$$

$$U_2 = (S/2)x_2f(\eta)$$

$$U_3 = -2(S\nu/2)^{1/2}f(\eta)$$

$$\eta = (S/2\nu)^{1/2}x_3$$

$$\Pi = \Pi_0 - (1/2)[(S/2)^2(x_1^2 + x_2^2) + u_3^2] + \nu u_{3,3}$$

where S is the strain rate of the approaching inviscid flow. The function F has been tabulated by Homann. We carry out the computation in a cubic box of side L , including one-quarter of the jet. That is, the sides of the box are the planes $x_1 = 0$, $x_1 = L$, $x_2 = 0$, $x_2 = L$, $x_3 = 0$, $x_3 = L$. The maximum velocity is roughly SL . We choose to normalize all velocities by SL , lengths by L , time by $1/S$. We indicate nondimensionalized quantities by italics. Thus,

$$U_i/SL = U_i$$

$$x_i/L = x_i$$

$$St = t$$

$$\nu/SL^2 = 1/Re$$

the inverse of the Reynolds number. The pressure normalization is

$$\Pi/S^2L^2 = \Pi$$

Our equations of motion now read

$$\partial_t \mu_i + (U_i U_j)_j = -\Pi_{,i} + Re^{-1} U_{i,jj}$$

$$\partial_t \Pi + (\Pi U_i)_{,i} = \Pi(1 - \gamma) U_{i,i}$$

To set the level of pressure, we take $SL/a = M_0 = 0.3$. Hence,

$$\Pi_0 = (\gamma M_0^2)^{-1}$$

The box is now a unit cube, and the exact solution becomes

$$U_1 = x_1 f/2$$

$$U_2 = x_2 f/2$$

$$U_3 = -(2/\text{Re})^{1/2} f$$

$$\eta = (\text{Re}/2)^{1/2} x_3$$

$$\Pi = \Pi_0 - (1/2)[(x_1^2 + x_2^2)/4 + U_3^2] + U_{3,3}/\text{Re}$$

To select a value for the Reynolds number we note that the boundary layer thickness is roughly $(2/\text{Re})^{1/2}$ in dimensionless form. To have an interesting calculation, i.e., one in which the effect of viscosity can be seen, we want the boundary layer thickness to be roughly 1/2. Hence, we take $\text{Re} = 8$.

So far as the boundary conditions are concerned, we use the exact solutions on the inflow face $x_3 = 1$, and on the outflow faces, $x_1 = 1$, $x_2 = 1$. On the bottom we use the no slip condition $U_1 = U_2 = U_3 = 0$, with the corresponding pressure condition

$$\Pi = \Pi_0 - (x_1^2 + x_2^2)/8$$

On the faces quartering the jet we use symmetry conditions. That is, on the face $x_1 = 0$ we use

$$U_1 = 0, U_{2,1} = 0, U_{3,1} = 0, \Pi_{,1} = 0$$

while on the face $x_2 = 0$ we use

$$U_2 = 0, U_{1,2} = 0, U_{3,2} = 0, \Pi_{,2} = 0$$

As initial conditions we begin with the exact solution. As might be expected, the solution converges quite rapidly, and is stable. Numerical values of the velocity divergence are nowhere more than roughly 0.1, and over most of the flow considerably less. In figures 14, 15 and 16 we show several views of the solution. It can be seen that the streamlines have generally the correct shape. Numerical values of the velocity field are

within a few percent of the correct values. We feel that the results can be interpreted as very positive for both the numerical algorithm and for the pressure equation.

Computation of the third moments

In the one dimensional computations we were able to use the our (essentially) exact form for the third moments. This is summarized in Lumley & Mansfield (1984). Briefly, this is an algebraic form for the third moments, obtained by perturbation expansion about a nearly homogeneous, nearly Gaussian state of near-equilibrium. The equations are seriously cross-coupled. In a general three-dimensional case there are nineteen independent third moments, ten including three velocities, six including two velocities and the density anomaly, and three including one velocity and the square of the density anomaly. Although the matrix of coefficients is relatively sparse, it is difficult to eliminate more than three of the variables, (reducing the system to 16×16), since the terms involving the density anomaly appear in all equations involving the vertical velocity, through the buoyancy. In our one-dimensional problem, things were much simpler; even with wind shear, there are only twelve independent non-zero third moments, while in the windless (vertically axisymmetric) case, there are only five. Inversion programs, including symbolic inversion, are relatively efficient up to 6×6 , and rapidly break down thereafter. We were able to obtain the values in the 12×12 case using Gaussian elimination. This was time consuming, but not insupportable, since the number of grid points was limited. In three dimensions, however, we will have probably 20^3 grid points instead of 20, for a factor of 400, while the solution of a 19×19 linear system by Gaussian elimination will take roughly 2.5 times as long as a 12×12 , for a net factor of 10^3 in the time required for this part of the calculation. Since in one dimension the calculation already ran of the order of tens of minutes (say, 20 minutes for a typical case) on the IBM 4341, this part of the calculation alone might be expected to run day and night for two weeks on the same machine. While we expect considerable increases in speed by running on a highly parallel supercomputer, they will probably not be enough to compensate for this problem.

The efficient solution of large, relatively sparse, systems like this is a current research area. Several members of Cornell's Department of Computer Science are currently working on this problem. It is quite possible that within a few years we will see considerable increases in efficiency for the solution of such systems. In the meantime, however, we must proceed.

This situation was clearly untenable. We were desperately in need of a way of simplifying the calculation of the third moments, but without discarding the benefits of the form. Wherever our form for the third moments has been used, it has given values of the third moments essentially within experimental error. Our form for the third moments is virtually unique in the annals of turbulence in being to a great extent the exact result of an asymptotic expansion, and hence being a genuine approximation, rather than an *ad hoc* model. Hence, it seemed desirable to preserve some part of it.

In the initial development of our third moment form, we had neglected gradients of the mean fields. This was done on the basis of the perturbation expansion, which indicated that these gradients were of lower order. In our development of the complete forms (see Lumley & Mansfield (1984) we kept these mean field gradients, since we felt that we might find sharp gradients in the mean fields at the inversion base, gradients large enough to upset the order of magnitude analysis, and raise these terms to the same order as those retained. In our extremity, however, this seems to be the least damaging place to introduce an approximation: we propose to neglect the mean field gradients in the three-dimensional case. It is not out of the question to consider the possibility of surveying the field computed with this reduced system for regions of large gradients, and solving the full system at a restricted number of points in the vicinity of the large gradients.

Elimination of the mean field gradients allows the system to be split into two essentially independent systems, a 9×9 and a 10×10 . Four of the 10×10 can be explicitly solved, leaving a 6×6 . The 9×9 can be further reduced without much difficulty to a 6×6 and a 3×3 . Computation of this system using Gaussian elimination should take only 56%

of the time required to compute the 12×12 used for the horizontally homogeneous case. Since MACSYMA is relatively efficient for 6×6 matrices, there are possible further savings by solving the system explicitly symbolically. In this way we have achieved a saving in time of between five and ten (five without symbolic reduction), and have reduced the expected running time on a supercomputer to something less than that for an exact simulation of a homogeneous isothermal turbulent flow. We include in this report a table of the coefficients of our reduced system.

Explanation of Table Markovianized Gen'l Matrix

This is the matrix of coefficients in the nineteen equations for the nineteen independent third moments involving velocity and density anomaly in the fully three-dimensional case, with mean field gradients eliminated by order of magnitude analysis. Since the mean field gradients arise from the substantial derivatives, their elimination is referred to as Markovianization (in a Markov process, the future state depends only on the present state, and not on the past; hence, does not depend on the present derivative in the continuum limit). Because of the limitations of the program EXCEL it was necessary to introduce some abbreviations in the matrix. We have designated C_1 by C, and $C_{\rho'}$ by C'; $\langle q^2 \rangle / \langle \epsilon \rangle$ by T, and $\langle \rho'^2 \rangle / \langle \epsilon_{\rho'} \rangle$ by T'; and finally β by b. All notation is the same as in Lumley & Mansfield (1984). The column designations A - S are as follows: A = $\langle u_1^3 \rangle$, B = $\langle u_2^3 \rangle$, C = $\langle u_3^3 \rangle$, D = $\langle u_1^2 u_2 \rangle$, E = $\langle u_1^2 u_3 \rangle$, F = $\langle u_2^2 u_1 \rangle$, G = $\langle u_2^2 u_3 \rangle$, H = $\langle u_3^2 u_1 \rangle$, I = $\langle u_3^2 u_2 \rangle$, J = $\langle u_1 u_2 u_3 \rangle$, K = $\langle \rho' u_1^2 \rangle$, L = $\langle \rho' u_1 u_2 \rangle$, M = $\langle \rho' u_1 u_3 \rangle$, N = $\langle \rho' u_2^2 \rangle$, O = $\langle \rho' u_2 u_3 \rangle$, P = $\langle \rho' u_3^2 \rangle$, Q = $\langle \rho' u_1 \rangle$, R = $\langle \rho' u_2 \rangle$, S = $\langle \rho' u_3 \rangle$. The matrix may be visualized as post-multiplied by a column matrix of these variables. Note that equations 12, 17, 18 and 19 have only one entry, and hence can be solved immediately. Note also that the matrix 10A - 19I is empty, so that the matrix 10J - 19S is independent of 1A - 9I. With the elimination of 12, 17, 18 and 19, this leaves a 6x6. Since the sub-matrix A1-C3 is diagonal, we may easily multiply each of rows 1-3 by the appropriate factor and subtract from rows 4-9 to eliminate all entries below the diagonal in columns A-C. This makes the sub-matrix D4-I9 independent of the first three terms, giving a 6x6. The right hand sides of the equations (i.e.- the column matrix appearing on the right hand side of the martical equation) are as follows:

$$\begin{aligned} 1 &= 3\langle u_1^2 \rangle_{,1} \langle u_1^2 \rangle + 3\langle u_1^2 \rangle_{,2} \langle u_2 u_1 \rangle + 3\langle u_1^2 \rangle_{,3} \langle u_3 u_1 \rangle \\ 2 &= 3\langle u_2^2 \rangle_{,1} \langle u_1 u_2 \rangle + 3\langle u_2^2 \rangle_{,2} \langle u_2^2 \rangle + 3\langle u_2^2 \rangle_{,3} \langle u_3 u_2 \rangle \\ 3 &= 3\langle u_3^2 \rangle_{,1} \langle u_1 u_3 \rangle + 3\langle u_3^2 \rangle_{,2} \langle u_2 u_3 \rangle + 3\langle u_3^2 \rangle_{,3} \langle u_3^2 \rangle \end{aligned}$$

$$\begin{aligned}
4 &= \langle u_1^2 \rangle, 1 \langle u_1 u_2 \rangle + \langle u_1^2 \rangle, 2 \langle u_2^2 \rangle + \langle u_1^2 \rangle, 3 \langle u_3 u_2 \rangle + 2 \langle u_1 u_2 \rangle, 1 \langle u_1^2 \rangle + \\
&2 \langle u_1 u_2 \rangle, 2 \langle u_2 u_1 \rangle + \langle u_1 u_2 \rangle, 3 \langle u_3 u_1 \rangle \\
5 &= \langle u_1^2 \rangle, 1 \langle u_1 u_3 \rangle + \langle u_1^2 \rangle, 2 \langle u_2 u_3 \rangle + \langle u_1^2 \rangle, 3 \langle u_3^2 \rangle + 2 \langle u_1 u_3 \rangle, 1 \langle u_1^2 \rangle + \\
&2 \langle u_1 u_3 \rangle, 2 \langle u_2 u_1 \rangle + 2 \langle u_1 u_3 \rangle, 3 \langle u_3 u_1 \rangle \\
6 &= \langle u_2^2 \rangle, 1 \langle u_1^2 \rangle + \langle u_2^2 \rangle, 2 \langle u_2 u_1 \rangle + \langle u_2^2 \rangle, 3 \langle u_3 u_1 \rangle + 2 \langle u_2 u_1 \rangle, 1 \langle u_1 u_2 \rangle + \\
&2 \langle u_2 u_1 \rangle, 2 \langle u_2^2 \rangle + 2 \langle u_2 u_1 \rangle, 3 \langle u_3 u_2 \rangle \\
7 &= \langle u_2^2 \rangle, 1 \langle u_1 u_3 \rangle + \langle u_2^2 \rangle, 2 \langle u_2 u_3 \rangle + \langle u_2^2 \rangle, 3 \langle u_3^2 \rangle + 2 \langle u_2 u_3 \rangle, 1 \langle u_1 u_2 \rangle + \\
&2 \langle u_2 u_3 \rangle, 2 \langle u_2^2 \rangle + 2 \langle u_2 u_3 \rangle, 3 \langle u_3 u_2 \rangle \\
8 &= \langle u_3^2 \rangle, 1 \langle u_1^2 \rangle + \langle u_3^2 \rangle, 2 \langle u_2 u_1 \rangle + \langle u_3^2 \rangle, 3 \langle u_3 u_1 \rangle + 2 \langle u_3 u_1 \rangle, 1 \langle u_1 u_3 \rangle + \\
&2 \langle u_3 u_1 \rangle, 2 \langle u_2 u_3 \rangle + 2 \langle u_3 u_1 \rangle, 3 \langle u_3^2 \rangle \\
9 &= \langle u_3^2 \rangle, 1 \langle u_1 u_2 \rangle + \langle u_3^2 \rangle, 2 \langle u_2^2 \rangle + \langle u_3^2 \rangle, 3 \langle u_3 u_2 \rangle + 2 \langle u_3 u_2 \rangle, 1 \langle u_1 u_3 \rangle + \\
&2 \langle u_3 u_2 \rangle, 2 \langle u_2 u_3 \rangle + 2 \langle u_3 u_2 \rangle, 3 \langle u_3^2 \rangle \\
10 &= \langle u_1 u_2 \rangle, 1 \langle u_1 u_3 \rangle + \langle u_1 u_2 \rangle, 2 \langle u_2 u_3 \rangle + \langle u_1 u_2 \rangle, 3 \langle u_3^2 \rangle + \langle u_1 u_3 \rangle, 1 \langle u_1 u_2 \rangle + \\
&\langle u_1 u_3 \rangle, 2 \langle u_2^2 \rangle + \langle u_1 u_3 \rangle, 3 \langle u_3 u_2 \rangle + \langle u_2 u_3 \rangle, 1 \langle u_1^2 \rangle + \langle u_2 u_3 \rangle, 2 \langle u_2 u_1 \rangle + \\
&\langle u_2 u_3 \rangle, 3 \langle u_3 u_1 \rangle \\
11 &= \langle u_1^2 \rangle, 1 \langle \rho' u_1 \rangle + \langle u_1^2 \rangle, 2 \langle \rho' u_2 \rangle + \langle u_1^2 \rangle, 3 \langle \rho' u_3 \rangle + 2 \langle \rho' u_1 \rangle, 1 \langle u_1^2 \rangle + \\
&2 \langle \rho' u_1 \rangle, 2 \langle u_2 u_1 \rangle + 2 \langle \rho' u_1 \rangle, 3 \langle u_3 u_1 \rangle \\
12 &= \langle \rho' u_1 \rangle, 1 \langle u_1 u_2 \rangle + \langle \rho' u_1 \rangle, 2 \langle u_2^2 \rangle + \langle \rho' u_1 \rangle, 3 \langle u_3 u_2 \rangle + \langle \rho' u_2 \rangle, 1 \langle u_1^2 \rangle + \\
&\langle \rho' u_2 \rangle, 2 \langle u_2 u_1 \rangle + \langle \rho' u_2 \rangle, 3 \langle u_3 u_1 \rangle + \langle u_1 u_2 \rangle, 1 \langle \rho' u_1 \rangle + \langle u_1 u_2 \rangle, 2 \langle \rho' u_2 \rangle + \\
&\langle u_1 u_2 \rangle, 3 \langle \rho' u_3 \rangle \\
13 &= \langle \rho' u_1 \rangle, 1 \langle u_1 u_3 \rangle + \langle \rho' u_1 \rangle, 2 \langle u_2 u_3 \rangle + \langle \rho' u_1 \rangle, 3 \langle u_3^2 \rangle + \langle \rho' u_3 \rangle, 1 \langle u_1^2 \rangle + \\
&\langle \rho' u_3 \rangle, 2 \langle u_2 u_1 \rangle + \langle \rho' u_3 \rangle, 3 \langle u_3 u_1 \rangle + \langle u_1 u_3 \rangle, 1 \langle \rho' u_1 \rangle + \langle u_1 u_3 \rangle, 2 \langle \rho' u_2 \rangle + \\
&\langle u_1 u_3 \rangle, 3 \langle \rho' u_3 \rangle \\
14 &= 2 \langle \rho' u_2 \rangle, 1 \langle u_1 u_2 \rangle + 2 \langle \rho' u_2 \rangle, 2 \langle u_2^2 \rangle + 2 \langle \rho' u_2 \rangle, 3 \langle u_3 u_2 \rangle + \langle u_2^2 \rangle, 1 \langle \rho' u_1 \rangle + \\
&\langle u_2^2 \rangle, 2 \langle \rho' u_2 \rangle + \langle u_2^2 \rangle, 3 \langle \rho' u_3 \rangle
\end{aligned}$$

SECTION II. PRESCRIBED LOAD ALLOWANCE (CONTINUED)

(1) FEDERAL STOCK NUMBER	(2) DESCRIPTION	USABLE ON CODE	(3) 15-DAY ORG. MAINT. ALLOWANCE			
			(a) 1-5	(b) 6-20	(c) 21-50	(d) 51-100
5930-729-1706	SWITCH, LEVER: (3 pos locking); SM-B-335465; 80063	1,2,3	*	*	*	2
5930-729-1709	SWITCH, LEVER: (2 pos locking); SM-B-335735; 80063	1,2,3	*	*	*	2
5930-734-5202	CIRCUIT BREAKER: F/heater; 10172H334A; 17465	2,3	*	*	*	2
5935-045-9830	CONNECTOR, PLUG, ELECTRICAL U-185B/G	1,2,3	*	*	*	2
5935-045-9831	CONNECTOR, RECEPTACLE, ELECTRICAL U-186/G, U-186A/G	1,2,3	2	2	4	8
	OR					
5935-926-7428	CONNECTOR, RECEPTACLE, ELECTRICAL U-186C/G	1,2,3	2	2	4	8
5935-162-6285	DUMMY PLUG, TELEPHONE: (red); 165D; 01401	1,2,3	2	4	11	20
5935-192-4826	JACK, TELEPHONE: JJ-086; 81349	1,2,3	11	39	92	179
5935-228-4038	JACK, TELEPHONE: JJ-085; 81349	1,2,3	11	19	92	179
5935-283-1269	JACK, TELEPHONE: JJ-034; 81349	1,2,3	*	*	*	2
5935-359-6025	CONNECTOR, RECEPTACLE, ELECTRICAL: F/heater; 9210; 74545	1,2,3	*	*	2	2
5935-577-8804	ADAPTER CONNECTOR UG-1312/U	1,2,3	*	*	*	2
5935-577-8781	JACK, TELEPHONE: JJ-024; 81349	1,2,3	2	2	4	8
5935-642-0743	DUMMY PLUG TELEPHONE: (Black); 165C; 01401	1,2,3	3	7	18	33
5935-682-1070	CLAMP, ELECTRICAL: KS-17; 09922	1,2,3	*	*	2	2
5935-775-2446	DUMMY PLUG: SM-B-370299; 80063	1,2,3	2	2	4	8
5935-892-9176	CONNECTOR, PLUG, ELECTRICAL: U/with cable assy CX-469A/U and CX-4693A/U; SC-B-76446-1; 80063	1,2,3	*	*	*	2
5940-049-8791	CLIP, SPRING, TENSION: U/ to retain tube extractor; 107002 Type XX; 75915	1,2,3	*	*	*	2
5940-223-5293	POST, BINDING: SC-DL-72398; 80063	1,2,3	2	2	4	7
5940-254-2244	CAP, ELECTRICAL: (F/binding post); SC-C-76202-1; 80063	1,2,3	2	2	4	7
5940-702-7256	TERMINAL LUG: KPA25/W; 09922	1,2,3	*	*	2	2
5940-802-3771	SPLICE, WIRE: PT60M; 59730	1,2,3	*	*	2	2
5950-815-6687	CIRCUIT BREAKER: 15 amp; Q01515; 08434	2,3	*	*	2	2
5975-702-9311	CAP, ELECTRICAL: PT6M; 59730	1,2,3	*	*	2	2
5975-711-1856	GASKET: U/on duplex outlet; 585; 73586	1,2	*	*	*	2

SECTION II PRESCRIBED LOAD ALLOWANCE (CONTINUED)

(1) FEDERAL STOCK NUMBER	(2) DESCRIPTION	USABLE ON CODE	(3) 15-DAY ORG. MAINT. ALLOWANCE			
			(a) 1-5	(b) 6-20	(c) 21-50	(d) 51-100
5975-682-0461	BUSHING, ELECTRICAL CONDUCTOR: 112; 04009	1,2,3	*	*	*	2
5975-682-0519	HANGER, CABLE: (U/to retain cables to side of shelter); SM-B-363104; 80063	1,2,3	*	*	*	2
5995-681-8427	CABLE ASSEMBLY, SPECIAL PURPOSE, ELECTRICAL CX-4768/U: (2 ft)	1,2,3	2	2	4	7
5995-681-8429	CABLE ASSEMBLY, SPECIAL PURPOSE, ELECTRICAL CX-4768/U: (4 ft)	1,2,3	2	2	4	7
5995-681-8430	CABLE ASSEMBLY, SPECIAL PURPOSE, ELECTRICAL CX-4768/U: (5 ft)	1,2,3	*	2	2	3
5995-681-8436	CABLE ASSEMBLY, SPECIAL PURPOSE, ELECTRICAL CX-4768/U: (3 ft)	1,2,3	2	2	4	7
5995-681-8441	CABLE ASSEMBLY, SPECIAL PURPOSE, ELECTRICAL CX-4766/U: (4 ft 8-1/4 in)	1,2,3	*	*	*	2
5995-681-8448	CABLE ASSEMBLY, SPECIAL PURPOSE, ELECTRICAL CX-4767/U: (4 ft 8-1/4 in)	1,2,3	*	*	*	2
5995-681-8450	CABLE ASSEMBLY, SPECIAL PURPOSE, ELECTRICAL CX-4774/U: (4 ft 8-1/2 in)	1,2,3	2	2	3	6
5995-681-8472	CABLE ASSEMBLY, SPECIAL PURPOSE, ELECTRICAL CX-4769/U: (4 ft)	1,2,3	2	2	4	7
5995-681-8473	CABLE ASSEMBLY, SPECIAL PURPOSE, ELECTRICAL CX-4769/U: (3 ft)	1,2,3	2	2	4	7
5995-681-8474	CABLE ASSEMBLY, SPECIAL PURPOSE, ELECTRICAL CX-4769/U: (5 ft)	1,2,3	*	2	2	3
5995-681-8475	CABLE ASSEMBLY, SPECIAL PURPOSE, ELECTRICAL CX-4769/U: (2 ft)	1,2,3	2	2	4	7
5995-688-5699	CORD ASSEMBLY, ELECTRICAL CX-4695/U: (5 ft 10 in)	1,2,3	*	*	*	2
5995-985-7569	CABLE ASSEMBLY, TELEPHONE CX-4566A/G: (250 ft)	1,2,3	*	*	*	2
6210-199-8633	LAMPHOLDER: (F/neon lamp); MS90287-20; 81349	1,2,3	*	*	*	2
6210-686-5568	SHIELD, ELECTRIC LIGHT: SM-B-335531; 80063	1,2,3	*	*	2	2
6240-143-3070	LAMP, INCANDESCENT: 50A/RS; 24455	1,2,3	*	2	2	3
6240-155-7786	LAMP, INCANDESCENT: FR-2; 24455	1,2,3	*	2	2	3
6240-223-9100	LAMP, GLOW: NE-51; 81349	1,2,3	*	2	2	3
6240-223-9104	LAMP, GLOW: NE-40; 81349	1,2,3	*	2	2	3
6240-270-4286	LAMP, GLOW: NE-21; 81349	1,2,3	2	3	4	16
6240-538-8447	LAMP, FLUORESCENT: F20T12/CW; 24455	1,2,3	2	3	7	13

SECTION II. PRESCRIBED LOAD ALLOWANCE (CONTINUED)

(1) FEDERAL STOCK NUMBER	(2) DESCRIPTION	USABLE OM CODE	(3) 15-DAY ORG. MAINT. ALLOWANCE			
			(a) 1-5	(b) 6-20	(c) 21-50	(d) 51-100
6250-174-4684	LAMPHOLDER: (F/fluorescent lamp and starter) 78X736; 24455	1,2,3	*	*	2	2
6250-299-2884	STARTER, FLUORESCENT LAMP: FS-2; 64959	1,2,3	*	*	*	2
6250-299-6093	LAMPHOLDER: (F/fluorescent lamp); 78X491; 24455	1,2,3	*	*	2	2
6250-582-3462	LAMPHOLDER: (Holds indicator glow lamps); 10-06; 952+3	1,2,3	*	*	2	2
6250-582-3463	LAMPHOLDER: (porcelain); 246; 73586	1,2,3	*	*	*	2
6250-804-3449	BALLAST LAMP: (F/fluorescent lamp); 89G457D; 24455	1,2,3	*	*	*	2
6680-793-9575	SWITCH, THERMOSTATIC: (P/o heater); 2727A; 65289	2,3	*	*	*	2

Rbc-PM 1117-48

SECTION III: REPAIR PARTS FOR ORGANIZATIONAL MAINTENANCE

(1) SAR CODE	(2) FEDERAL STOCK NUMBER	(3) DESCRIPTION Reference Number & Mfr Code	(4) UNIT OF MEAS	(5) QTY INC IN UNIT	(6) 15-DAY ORGANIZATIONAL MAINTENANCE ALLOW				(7) ILLUSTRATIONS	
					(a) 1-5	(b) 6-20	(c) 21-50	(d) 51-100	(a) FIG NO.	(b) ITEM NO. OR REFERENCE DESIGNATION
P-0 A000	5995-681-2474	CABLE, PATCHING, COMMUNICATION SB-411, MGR (This item is nonexpendable) SHEETER, ELECTRICAL EQUIPMENT S-171A/MGR, S-171A/B/MGR NOTE: Usable on code 1 refers to S-171 MGR, 2 refers to S-171A/MGR, 3 refers to S-171B/MGR.								
P-0 A001	5995-681-2475	ADAPTER, CONNECTOR UG-4312/U	1,2,3	ea	2	*	*	*	2 1-11	TP1, TP2
P-0 A002	5995-681-2476	AMMETER, MGR-650/SPEECH; 70347	1,2,3	ea	1	*	*	*	4-1	ME
P-0 A003	5995-681-2477	AXE, SINGLE BIT: 590-A-3085, Type 1, Design 21 2174	1,2,3	ea	1	*	*	*	1-4 4-1	
P-0 A004	5995-681-2478	BALLAST, LAMP: F fluorescent lamp; 24455	1,2,3	ea	6	*	*	*	2 4-1	
P-0 A005	5995-681-2479	BUSHING, ELECTRICAL CONDUCTOR: 110; 24456	1,2,3	ea	2	*	*	*	2	
P-0 A006	5995-681-2480	BUSHING, ELECTRICAL CONDUCTOR, U/W heater; 140; 24456	1	ea	1	*	*	*	4-1	
P-0 A007	5995-681-2481	BUSHING, ELECTRICAL CONDUCTOR: Tite-bite; 2445; 24455	1	ea	2	*	*	*		
P-0 A008	5995-681-2482	CABLE ASSEMBLY, TELEPHONE CX-4566A/G; (250 ft)	1,2,3	ea	1	*	*	*	2 1-11	
P-0 A009	5995-681-2483	CABLE ASSEMBLY, SPECIAL PURPOSE, ELECTRICAL CX-4767/U; (4 ft 8-1/4 in.)	1,2,3	ea	1	*	*	*	2 1-5	W218
P-0 A010	5995-681-2484	CABLE ASSEMBLY, SPECIAL PURPOSE, ELECTRICAL CX-4767/U; (4 ft 8-1/4 in.)	1,2,3	ea	1	*	*	*	2 1-5	W10
P-0 A011	5995-681-2485	CABLE ASSEMBLY, SPECIAL PURPOSE, ELECTRICAL CX-4768/U; (2 ft)	1,2,3	ea	27	2	2	4	7 1-5	W39 thru W65
P-0 A012	5995-681-2486	CABLE ASSEMBLY, SPECIAL PURPOSE, ELECTRICAL CX-4768/U; (3 ft)	1,2,3	ea	27	2	2	4	7 1-5	W120 thru W146
P-0 A013	5995-681-2487	CABLE ASSEMBLY, SPECIAL PURPOSE, ELECTRICAL CX-4768/U; (4 ft)	1,2,3	ea	27	2	2	4	7 1-5	W147 thru W173
P-0 A014	5995-681-2488	CABLE ASSEMBLY, SPECIAL PURPOSE, ELECTRICAL CX-4768/U; (5 ft)	1,2,3	ea	12	*	2	2	3 1-5	W186 thru W197
P-0 A015	5995-681-2489	CABLE ASSEMBLY, SPECIAL PURPOSE, ELECTRICAL CX-4769/U; (2 ft)	1,2,3	ea	27	2	2	4	7 1-5	W12 thru W38
P-0 A016	5995-681-2490	CABLE ASSEMBLY, SPECIAL PURPOSE, ELECTRICAL CX-4769/U; (3 ft)	1,2,3	ea	27	2	2	4	7 1-5	W66 thru W92
P-0 A017	5995-681-2491	CABLE ASSEMBLY, SPECIAL PURPOSE, ELECTRICAL CX-4769/U; (4 ft)	1,2,3	ea	27	2	2	4	7 1-5	W93 thru W119
P-0 A018	5995-681-2492	CABLE ASSEMBLY, SPECIAL PURPOSE, ELECTRICAL CX-4769/U; (5 ft)	1,2,3	ea	12	*	2	2	3 1-5	W174 thru W185
P-0 A019	5995-681-2493	CABLE ASSEMBLY, SPECIAL PURPOSE, ELECTRICAL CX-4774/U; (4 ft 8-1/2 in.)	1,2,3	ea	20	2	2	3	6 1-5	W198 thru W217
P-0 A020	6145-164-6948	CABLE, POWER, ELECTRICAL: Power cable for heater; 2 cond #16 awg; Type HPD; 80660	1	ft	6	*	*	*	4-1	
P-0 A021	6145-164-6949	CABLE, POWER, ELECTRICAL: F/heater; SI-5325, Type 65/.0063; 24455	2,3	ft	6	*	*	*	4-1	
P-0 A022	6145-164-6950	CABLE, POWER, ELECTRICAL: U/with CX-4693A/U and CX-4694A/U; 2 cond #6 1 cond #8; SC-A-46608B; 80063	1,2,3	ft	150	*	*	*	1-11	
P-0 A023	5975-702-9311	CAP, ELECTRICAL: P26M; 59730	1,2,3	ea	10	*	*	2	2	
P-0 A024	5940-254-2244	CAP, ELECTRICAL: (f/binding post); SC-C-76202-1; 80063	1,2,3	ea	40	2	2	4	7	
P-0 A025	5910-553-6006	CAPACITOR, FIXED, PAPER DIELECTRIC: U/with fluorescent lamp fixtures; SC-C-33033-4; 80063	1,2,3	ea	5	*	*	2	2	
P-0 A026	5910-553-6007	CHAIN, BRAD: Connects cable reel holder to wall; 43; 70692	1,2,3	ft	10	*	*	*		

SECTION III. REPAIR PARTS FOR ORGANIZATIONAL MAINTENANCE (CONTINUED)

(1) SNR CODE	(2) FEDERAL STOCK NUMBER	(3) DESCRIPTION	(4) UNIT OF MEAS	(5) QTY INC IN UNIT	(6) 15-DAY ORGANIZATIONAL MAINTENANCE ALLOW				(7) ILLUSTRATIONS	
					(a) 1-5	(b) 6-20	(c) 21-50	(d) 51-100	(a) FIG NO.	(b) ITEM NO. OR REFERENCE DESIGNATION
P-0 A040	4010-729-5951	CHAIN, WELDLESS: (U/on bulletin board); F26404; 96344	1,2,3	ea	14	*	*	*		
P-0 A042	5930-734-5202	CIRCUIT BREAKER: F/heater; 10172W334A; 17465	2,3	ea	1	*	*	*	2	4-5
P-0 A043	5925-682-1071	CIRCUIT BREAKER: 50 amps; Q0250; 88434	1,2,3	ea	1	*	*	2	2	4-5 CB7A, CB7B
P-0 A044	5925-818-4811	CIRCUIT BREAKER: 15 amps; Q0115; 88434	1 2,3	ea ea	6 2	*	*	2 2	2 2	4-13 CB1 thru CB6 4-13 CB3, CB4
P-0 A046	5950-815-6687	CIRCUIT BREAKER: 15 amps; Q01515; 88434	2,3	ea	4	*	*	2	2	4-13 CB1, CB2, CB5, CB6
P-0 A047	5935-682-1070	CLAMP, ELECTRICAL: RS-17; 09922	1,2,3	ea	3	*	*	2	2	
P-0 A048	5940-049-8791	CLIP, SPRING, TENSION: U/to retain tube extractor; 107002 type XI; 75915	1,2,3	ea	2	*	*	*	2	
P-0 A049	5940-727-7646	CLIP, SPRING, TENSION: Holds spare starters; 109002 type XI; 75915	1,2,3	ea	3	*	*	2	2	
P-0 A050	6645-973-0178	CLOCK, AIRCRAFT, MECHANICAL: SM-B-364789; 80063	1	ea	1	*	*	*	*	4-16
P-0 A051	6645-950-8590	CLOCK, AIRCRAFT, MECHANICAL: (Retain mtg bracket when replacing clock)	2,3	ea	1	*	*	*	*	4-16
P-0 A052	5935-359-6025	CONNECTOR, RECEPTACLE, ELECTRICAL: F/heater; 9210; 74545	1,2,3	ea	4	*	*	2	2	4-13 J35 thru J38
P-0 A053	5935-518-9653	CONNECTOR, PLUG, ELECTRICAL UP-120M	1,2,3	ea	1	*	*	*	*	
P-0 A054	5935-00-246-4515	CONNECTOR, PLUG, ELECTRICAL: U/with cable assy CX-4694A/U; SC-B-76446-2; 80063 U-228/U	1,2,3	ea	1	*	*	*	*	1-11
P-0 A055	5935-00-168-1145	CONNECTOR, PLUG, ELECTRICAL: U/with cable assy CX-4694A/U and CX-4693A/U; SC-B-76446-1; 80063 U-228/U	1,2,3	ea	2	*	*	*	2	1-11
P-0 A056	5935-549-3562	CONNECTOR, RECEPTACLE, ELECTRICAL: U/on conduit assy; 9200; 74545	1,2,3	ea	1	*	*	*	*	4-13 J40
P-0 A057	5935-537-4253	CONNECTOR, RECEPTACLE, ELECTRICAL: Power-in on power entrance box; SM-B-364595; 80063	1,2,3	ea	1	*	*	*	*	1-8 J34
P-0 A058	5935-666-4512	CONNECTOR, RECEPTACLE, ELECTRICAL: Power-out on power entrance box; SM-B-364594; 80063	1,2,3	ea	1	*	*	*	*	1-8 J33
P-0 A059	5935-045-9830	CONNECTOR, PLUG, ELECTRICAL U-185B/G	1,2,3	ea	2	*	*	*	2	
P-0 A060	5935-045-9831	CONNECTOR, RECEPTACLE, ELECTRICAL U-186/G, U-186A/G	1,2,3	ea	48	2	2	4	8	
		OR								
P-0 A061	5935-926-7428	CONNECTOR, RECEPTACLE, ELECTRICAL U-186C/G	1,2,3	ea	48	2	2	4	8	
P-0 A062	5120-694-1197	CONTACT, POSITIONER, ELECTRON TUBE SOCKET: 7 pin contact; 5191; 72653	1,2	ea	1	*	*	*	*	
P-0 A063	5120-293-0270	CONTACT POSITIONER, ELECTRON TUBE SOCKET: 9 pin contact; 8105; 72653	1,2	ea	1	*	*	*	*	
P-0 A065	5995-688-5699	CORD ASSEMBLY, ELECTRICAL CX-4695/U: (5 ft 10 in).	1,2,3	ea	1	*	*	*	2	1-5 W11
P-0 A066	4030-805-0068	COUPLING, BEAD CHAIN: 10A; 70892	1,2,3	ea	4	*	*	*	*	
P-0 A067	5935-729-0778	COVER, ELECTRICAL CONNECTOR: CE-9176; 96097	1,2	ea	2	*	*	*	*	
P-0 A070	5410-072-0992	CURTAIN, BLACKOUT: 51 in x 63 in lg; SM-C-478682; 80063	1,2,3	ea	2	*	*	*	*	1-4
P-0 A076	5935-642-0743	DUMMY PLUG, TELEPHONE: (Black); 1650; 01401	1,2,3	ea	150	3	7	18	33	1-6
P-0 A077	5935-162-6285	DUMMY PLUG, TELEPHONE: (Red); 1650; 01401	1,2,3	ea	75	2	4	11	20	1-6

SECTION III. REPAIR PARTS FOR ORGANIZATIONAL MAINTENANCE (CONTINUED)

(1) SMB CODE INDEX NO.	(2) FEDERAL STOCK NUMBER	(3) DESCRIPTION Reference Number & Mfr Code	(4) UNIT OF MEAS USABLE ON CODE	(5) QTY INC IN UNIT	(6) 15-DAY ORGANIZATIONAL MAINTENANCE ALLOW				(7) ILLUSTRATIONS	
					(a) 1-5	(b) 6-20	(c) 21-50	(d) 51-100	(a) FIG NO.	(b) ITEM NO. OR REFERENCE DESIGNATION
P-O A078	5935-775-2446	DUMMY PLUG: SM-B-370299; 80063	1,2,3	ea	38	2	2	4	8	1-6
P-O A085	5120-293-3603	EXTRACTOR, ELECTRON TUBE: (7 pin miniature); 7L13; 95344	1,2,3	ea	1	*	*	*	*	4-16
P-O A086	5120-293-2692	EXTRACTOR, ELECTRON TUBE: (9 pin miniature); 9L13; 95344	1,2,3	ea	1	*	*	*	*	4-16
P-O A096	5975-711-1856	GASKET: U/oa duplex outlet; 585; 73586	1,2	ea	1	*	*	*	2	
P-O A098	5120-776-9918	GRIP, CABLE, MOVER: (12 in lg); BQA265; 95344	1,2,3	ea	45	*	2	2	3	1-6 0510 thru 0554
P-O A099	5120-752-8859	GRIP, CABLE, MOVER: 8 in lg U/with CX-4694/U and CX-4694/U; ESR-9; 95344	1	ea	4	*	*	*	*	
P-O A100	5120-776-9917	GRIP, CABLE, MOVER: 16 in lg; BQA6-8P; 95344	1,2,3	ea	5	*	*	*	2	1-6
P-O A101	5325-248-7104	GROMMET, RUBBER: P/o control, tel line C-2894/PQ; 913; 73543	1,2,3	ea	1	*	*	*	*	1-13 8264
P-O A102	5120-251-14489	HAMMER, HAND: (8-lb lead); OGG-B-86; 81349	1,2,3	ea	1	*	*	*	*	4-16
P-O A103	5975-682-0519	RANGER, CABLE: (U/to retain cables to side of shelter); SM-B-363104; 80063	1,2,3	ea	2	*	*	*	2	1-6
P-O A105	5820-706-7185	HEATING, ELEMENT, ELECTRICAL: U/w heater RD-375/U; A22/5007/1; 63325	1	ea	1	*	*	*	*	4-1
P-O A106	4840-404- 9232	HEATING ELEMENT, ELECTRICAL: P/heater; 3954-0; 72143	2,3	ea	1	*	*	*	*	4-2
P-O A109	3895-766-8473	HOLDER, CABLE, REEL: Retains cable reel during transit; SM-B-363238; 80063	1,2,3	ea	2	*	*	*	*	1-4
P-O A110	4140-765-7748	IMPELLER, FAN, AXIAL: P/o heater RD-375/U; OU-720-5; 60399	1	ea	1	*	*	*	*	4-1
P-O A111	4520-792-8398	IMPELLER, FAN, AXIAL: 20; 60399	1,2	ea	1	*	*	*	*	4-2
P-O A112	4140-069-1952	IMPELLER, FAN, CENTRIFUGAL: P/exhaust blowers; 610-314-2; 60399	1,2	ea	2	*	*	*	*	
P-O A113	4140-073-3246	IMPELLER, FAN, CENTRIFUGAL: A16999; 60399	3	ea	2	*	*	*	*	
P-O A115	5935-577-2781	JACK, TELEPHONE: JJ-024; 81349	1,2,3	ea	48	2	2	4	8	
P-O A116	5935-283-1269	JACK, TELEPHONE: JJ-034; 81349	1,2,3	ea	2	*	*	*	2	
P-O A117	5935-228-4038	JACK, TELEPHONE: JJ-085; 81349	1,2,3	ea	1203	11	39	92	179	
P-O A118	5935-192-4038	JACK, TELEPHONE: JJ-086; 81349	1,2,3	ea	1207	11	39	92	179	
P-O A119	5355-682-6806	KNOB: On-off knob on heater; Mold type 1600; 72512	1	ea	1	*	*	*	*	4-1
P-O A120	2540-246-8483	LADDER, VEHICLE BOARDING ME-3543/0; 3C-01-147188; 80063	1,2,3	ea	1	*	*	*	*	4-16
P-O A121	5240-538-8447	LAMP, FLUORESCENT: F20T12/CW; 24455	1,2,3	ea	5	2	3	7	13	4-6 D87 thru D811
P-O A122	5240-270-4286	LAMP, GLOW: ME21; 81349	1,2,3	ea	6	2	3	9	16	1-7 D81 thru D86
P-O A123	5240-223-3104	LAMP, GLOW: ME40; 81349	1,2,3	ea	1	*	2	2	3	1-7 D812
P-O A125	5240-223-3100	LAMP, GLOW: ME51; 81349	1,2,3	ea	1	*	2	2	3	1-7 D813
P-O A126	5240-143-3070	LAMP, INCANDESCENT: 50A/MS; 24455	1,2,3	ea	1	*	2	2	3	1-7
P-O A127	5240-143-3076	LAMP, INCANDESCENT: PR-2; 24455	1,2,3	ea	1	*	2	2	3	1-7

SECTION III. REPAIR PARTS FOR ORGANIZATIONAL MAINTENANCE (CONTINUED)

(1) SHE CODE INDEX NO.	(2) FEDERAL STOCK NUMBER	(3) DESCRIPTION Reference Number & Mfr Code	(4) UNIT OF MEAS IN UNIT	(5) QTY INC IN UNIT	(6) 15-DAY ORGANIZATIONAL MAINTENANCE ALLOW				(7) ILLUSTRATIONS		
					(a) 1-5	(b) 6-20	(c) 21-50	(d) 51-100	(a) FIG NO.	(b) ITEM NO. OR REFERENCE DESIGNATION	
P-0 A130	6250-682-3462	LAMPHOLDER: (Holds indicator glow lamps); 95263; 10-06	1,2,3	ea	6	*	*	2	2	4-5	XD81 thru XD86
P-0 A131	6250-299-6093	LAMPHOLDER: (F/fluorescent lamp); 78X491; 24455	1,2,3	ea	5	*	*	2	2	4-6	
P-0 A132	6250-174-4684	LAMPHOLDER: (F/fluorescent lamp and starter); 78X736; 24455	1,2,3	ea	5	*	*	2	2	4-6	
P-0 A133	6210-722- 3781	LIGHT INDICATOR (F/NEON LAMP) MS90287-20 81349	1,2,3	ea	1	*	*	*	2		
P-0 A134	6250-682-3463	LAMPHOLDER: (porcelain); 246; 73586	1,2,3	ea	1	*	*	*	2		XD812
P-0 A135	6230-803-7063	LAMP, ELECTRIC: (6 V); 2106-7; 32572	1,2,3	ea	1	*	*	*	*	4-16	
P-0 A136	5410-732-2525	LEAD, ELECTRICAL: (F/grounding); 84-B-352166C; 80063	1,2,3	ea	1	*	*	*	*	1-6	
P-0 A137	6230-615-5384	LIGHT, EXTENSION: (25 ft); W-L-661, Type 1, Class 1; 81349	1,2,3	ea	1	*	*	*	*	1-6	
P-0 A138		LOCKSPRING, TURNLOCK, FASTENER: U/on ventilator covers; 85-225; 72794	1	ea	2	*	*	*	2		
P-0 A139	5325-290-4345	LOCKSPRING, TURNLOCK FASTENER: U/on distribution box terminal box, air filter covers and storage cabinet; 86-275; 72794	1,2,3	ea	8	*	*	2	2		
P-0 A140	5325-289-3371	LOCKSPRING, TURNLOCK, FASTENER: U/on holder for axe, hammer and flashlight; 84-225; 72794	1,2	ea	7	*	*	2	2		
P-0 A141	6105-561-6321	MOTOR, AC: (P/o exhaust blowers); A826590; 16748	1,2,3	ea	2	*	*	*	*	1-14	B1, B2
P-0 A142	6105-726-8684	MOTOR, AC: 5KSP51A124C; 24455	1,2,3	ea	1	*	*	*	*	4-1	B3
P-0 A143	5915-803-8110	NETWORK, HYBRID, CIRCUIT: 84-C-364673; 80063	1,2,3	ea	12	*	*	2	2	1-3	
P-0 A144	5340-682-1508	PADLOCK: 325A1B; 29823	1,2,3	ea	1	*	*	*	*		
P-0 A146	5315-844-5644	PIN, SPRING: U/w cable ree. holders; 79-012-062-0500; 72962	1,2	ea	6	*	*	*	2		
P-0 A147		PIN, STRAIGHTENER, ELECTRON TUBE: (P/7 and 9 pin); D-27988; 88065	3	ea	1	*	*	*	*		
P-0 A148	5975-682-0476	PLATE, WALL, ELECTRICAL: 5260; 74545	1	ea	1	*	*	*	*		
P-0 A149	5940-223-5293	POST, BINDING: 8C-DL-72398; 80063	1,2,3	ea	40	2	2	4	7		
P-0 A150	8130-656-1090	REEL, CABLE NC-435/U	1,2,3	ea	2	*	*	*	*		
P-0 A152	5410-783-6250	REPAIR KIT, ELECTRICAL EQUIPMENT SHELTER MK-680/G: (U/to repair punctures to shelter skin); NOTE: Item to be requisitioned for immediate use only, order direct from depot stock.	1,2,3	ea	1	*	*	*	*		
P-0 A153	5905-803-2908	RESISTOR, FIXED, COMPOSITION: (30,000 ohms 1/4 w ±5%); RC09GF303J; 81349	1,2,3	ea	6	*	*	2	2	4-5	R1 thru R6
P-0 A154	5905-583-5207	RESISTOR, FIXED, FILM: (6,490 ohms, 1/4 w); RM65B6491F; 81349	1,2,3	ea	1	*	*	*	*	4-9	R3
P-0 A155	5905-581-0098	RESISTOR, FIXED, FILM: (2,940 ohm 1/4 w); RM65B2941F; 81349	1,2,3	ea	2	*	*	*	2	4-9	R2, R4
P-0 A156	5905-801-8634	RESISTOR, FIXED, FILM: (665 ohm 1/4 w); RM65B6650F; 81349	1,2,3	ea	1	*	*	*	*	4-9	R1
P-0 A158	5975-224-5260	ROD, GROUND MK-148/G	1,2,3	ea	1	*	*	*	*	4-16	
P-0 A163	6210-686-5568	SHIELD, ELECTRIC LIGHT: 84-B-335531; 80063	1,2,3	ea	5	*	*	2	2	4-6	
P-0 A165	5310-682-5535	SPACER, SLEEVE: (U/on battery box terminal); F1170; 96344	1,2,3	ea	4	*	*	*	2		

SECTION III. REPAIR PARTS FOR ORGANIZATIONAL MAINTENANCE (CONTINUED)

(1) FEDERAL STOCK NUMBER	(2) DESCRIPTION	(3) USABLE ON CODE	(4) UNIT OF MEAS	(5) QTY INC IN UNIT	(6) 15-DAY ORGANIZATIONAL MAINTENANCE ALLOW				(7) ILLUSTRATIONS	
					(a) 1-5	(b) 6-20	(c) 21-50	(d) 51-100	(a) FIG NO.	(b) ITEM NO. OR REFERENCE DESIGNATION
P-0 AL66	5940-802-1771 SPLICE, WIRE: PT60M; 59730	1,2,3	ea	10	*	*	*	2	4-6	
P-0 AL67	6250-299-2684 STARTER, FLUORESCENT LAMP: P8-2; 64959	1,2,3	ea	5	*	*	*	2	1-7	
P-0 AL68	5124-230-2698 STUD, TURNLOCK FASTENER: 5-35-W/MILLOWING; 72794	1,2	ea	2	*	*	*	*		
P-0 AL69	5930-729-1709 SWITCH, LEVER: (2 pos; locking); 84-B-335735; 80063	1,2,3	ea	1	*	*	*	2	1-13	82
P-0 AL70	5930-729-1708 SWITCH, LEVER: (3 pos locking); 84-B-335465; 80063	1,2,3	ea	1	*	*	*	2	1-13	81
P-0 AL71	5930-705-9131 SWITCH, ROTARY: (P/o heater); 2800841; 70611	1	ea	1	*	*	*	2	4-1	
P-0 AL72	5930-669-7465 SWITCH, SENSITIVE: JARS-63; type 88021320; 81349	1,2,3	ea	1	*	*	*	2	4-16	
P-0 AL73	6680-793-9575 SWITCH, THERMOSTATIC: (P/o heater); 2727A; 65289	2,3	ea	1	*	*	*	2	4-1	
P-0 AL74	5930-682-0349 SWITCH, THERMOSTATIC: (P/o heater); 4142; 81349	1	ea	1	*	*	*	2	4-1	
P-0 AL75	5930-707-1313 SWITCH, THERMOSTATIC: (P/o heater); Type 884; 93410	1	ea	1	*	*	*	2	4-1	812
P-0 AL76	5930-504-9923 SWITCH, TOGGLE: (P/o heater); 756344; 17465	2,3	ea	1	*	*	*	2	4-3	
P-0 AL77	5930-636-4014 SWITCH, TOGGLE: 085521-1; 24455	1,2,3	ea	4	*	*	2	2		82 thru 85
P-0 AL78	5930-615-7896 SWITCH, TOGGLE: MB25098-22; 81349	1,2,3	ea	1	*	*	*	2		86
P-0 AL84	5940-702-7256 TERMINAL LUG: KPA25/W; 09922	1,2,3	ea	4	*	*	2	2		
P-0 AL85	5940-681-9807 TERMINAL STUD: P/grounding; 84-B-363337; 80063	1,2,3	ea	1	*	*	*	*		
P-0 AL87	5950-892-8224 TRANSFORMER, CURRENT: (U/v ammeter); 1623; 93993	1,2,3	ea	1	*	*	*	*	4-5	T1
P-0 AL88	6625-883-4272 VOLTMETER: MR364150ACVVR; 81349	1,2,3	ea	1	*	*	*	*	4-5	M3

SECTION IV. REPAIR PARTS FOR DIRECT SUPPORT, GENERAL SUPPORT, AND DEPOT MAINTENANCE

(1) SNR CODE	(2) FEDERAL STOCK NUMBER	(3) DESCRIPTION REFERENCE NUMBER & MFR. CODE	(4) UNIT OF MEAS	(5) QTY INC IN UNIT	(6) 30-DAY DS MAINT ALLOWANCE			(7) 30-DAY GS MAINT ALLOWANCE			(8) 1 YR ALW PER EQUIP CATGY	(9) DEPOT MAINT ALW PER 100 EQUIP	(10) ILLUSTRATIONS	
					(a) 1-20	(b) 21-50	(c) 51-100	(a) 1-20	(b) 21-50	(c) 51-100			(4) FIG NO.	(5) ITEM NO. ON REFERENCE DESIGNATION
P-C-R A001	5804-542-7274	PANEL, PATCHING, COMMUNICATION SB-611 MRC: (This item is nonexpendable) SHELTER, ELECTRICAL EQUIPMENT S-171/MRC, S-171A,B,MRC NOTE: Usable on code 1 refers to S-171/MRC; 2 refers to S-171A/MRC; 3 refers to S-171B/MRC												
P-O A006	5935-5-4804	ADAPTER, CONNECTOR UG-1312/U	1,2,3	ea	2	2	2	*	2	2	16	5	1-11	CP1, CP2
P-O A006	6025-890-5315	AMMETER, M936M001SPECR; 81349	1,2,3	ea	1	*	*	*	*	*	8	3	4-5	M2
P-O A007	4210-707-8111	AXE, SINGLE BIT: GGG-A-926B, Type 1, Design C; 81349	1,2,3	ea	1	*	*	*	*	*	4	1	1-4, 4-5	
P-O A009	6250-804-3449	BALLAST, LAMP: F/fluorescent lamp; 8045T; 24455	1,2,3	ea	5	*	2	*	2	2		5	4-6	
P-O A013	5975-681-4401	BUSHING, ELECTRICAL CONDUCTOR: 112; 24409	1,2,3	ea	2	*	2	*	2	2		6		
P-O A014	5975-681-4409	BUSHING, ELECTRICAL CONDUCTOR: U/w heater; 891; 44094	1	ea	1	*	*	*	*	*		1	4-1	
P-O A015	5975-681-4451	BUSHING, ELECTRICAL CONDUCTOR: Tite-Bite; 2210; 24455	1	ea	2	*	*	*	*	*		2		
P-O A016	5905-405-7569	CABLE ASSEMBLY, TELEPHONE CX-466A/G; (245 ft)	1,2,3	ea	1	*	2	*	2	2	12	5	1-11	
P-O A020	5995-681-8441	CABLE ASSEMBLY, SPECIAL PURPOSE ELECTRICAL CX-4766/U; (4 ft 8-1/4 in)	1,2,3	ea	1	*	2	*	2	2	12	5	1-5	W218
P-O A021	5995-681-8442	CABLE ASSEMBLY, SPECIAL PURPOSE ELECTRICAL CX-4767/U; (4 ft 8-1/4 in)	1,2,3	ea	1	*	2	*	2	2	12	5	1-5	W10
P-O A022	5995-681-8443	CABLE ASSEMBLY, SPECIAL PURPOSE ELECTRICAL CX-4768/U; (2 ft)	1,2,3	ea	27	3	7	2	3	3	158	125	1-5	W39 thru W65
P-O A023	5995-681-8436	CABLE ASSEMBLY, SPECIAL PURPOSE ELECTRICAL CX-4768/U; (3 ft)	1,2,3	ea	27	3	7	2	3	3	158	125	1-5	W120 thru W146
P-O A024	5995-681-8429	CABLE ASSEMBLY, SPECIAL PURPOSE ELECTRICAL CX-4768/U; (4 ft)	1,2,3	ea	27	3	7	2	3	3	158	125	1-5	W147 thru W173
P-O A025	5995-681-8430	CABLE ASSEMBLY, SPECIAL PURPOSE ELECTRICAL CX-4768/U; (5 ft)	1,2,3	ea	12	2	3	2	2	2	71	50	1-5	W186 thru W197
P-O A026	5995-681-8475	CABLE ASSEMBLY, SPECIAL PURPOSE ELECTRICAL CX-4769/U; (2 ft)	1,2,3	ea	27	3	7	2	3	3	158	125	1-5	W12 thru W38
P-O A027	5995-681-8473	CABLE ASSEMBLY, SPECIAL PURPOSE ELECTRICAL CX-4769/U; (3 ft)	1,2,3	ea	27	3	7	2	3	3	158	125	1-5	W66 thru W92
P-O A028	5995-681-8472	CABLE ASSEMBLY, SPECIAL PURPOSE ELECTRICAL CX-4769/U; (4 ft)	1,2,3	ea	27	3	7	2	3	3	158	125	1-5	W93 thru W119
P-O A029	5995-681-8474	CABLE ASSEMBLY, SPECIAL PURPOSE ELECTRICAL CX-4769/U; (5 ft)	1,2,3	ea	12	2	3	2	2	2	71	50	1-5	W174 thru W185
P-O A030	5995-681-8450	CABLE ASSEMBLY, SPECIAL PURPOSE ELECTRICAL CX-4774/U; (4 ft 8-1/2 in)	1,2,3	ea	20	2	6	2	2	3	130	100	1-5	W198 thru W217
P-O A031	6145-164-6946	CABLE, POWER, ELECTRICAL: Power cable for heater, 2 cond #16 avg; Type HFD; 80660	1	ft	6	*	*	*	*	*	30	60	4-1	
P-O A032	6145-752-2562	CABLE, POWER, ELECTRICAL: F/heater SI-5325, Type 65/0063; 24455	2,3	ft	6	*	*	*	*	*	30	60	4-1	
P-O A033	6145-752-2473	CABLE, POWER, ELECTRICAL: U/with CX-4693A/U and 4694A/U; 2 cond #6; 1 cond #8; SC-A-46608B; 80063	1,2,3	ft	150	*	*	*	*	*	750	1500	1-11	
P-H A035	6145-577-8480	CABLE, TELEPHONE WM-130A/G; U/with CX-4666A/G	1,2,3	ft	250			*	*	*	1250	2500		

SECTION IV. REPAIR PARTS FOR DIRECT SUPPORT, GENERAL SUPPORT, AND DEPOT MAINTENANCE (CONTINUED)

(1) SW CODE	(2) FEDERAL STOCK NUMBER	(3) DESCRIPTION	(4) UNIT OF MEAS	(5) QTY INC IN UNIT	(6) 30-DAY DS MAINT ALLOWANCE			(7) 30-DAY GS MAINT ALLOWANCE			(8) 1 YR ALW PER EQUIP CENCY	(9) DEPOT MAINT 100 PER EQUIP	(10) ILLUSTRATIONS	
					(a) 1-20	(b) 21-50	(c) 51-100	(a) 1-20	(b) 21-50	(c) 51-100			(a) FIG NO.	(b) ITEM NO. OR REFERENCE DESIGNATION
P-0 A030	5975-702-9311	CAP, ELECTRICAL: PTOM; 59730	1,2,3	ea	10	2	3	4	2	2	2	30		
P-0 A037	5940-254-3244	CAP, ELECTRICAL: (F/binding post) SC-C-76202-1; 80063	1,2,3	ea	40	3	7	13	2	3	3	158	125	
P-0 A038	5910-553-6096	CAPACITOR, FIXED, PAPER DIELECTRIC: U/with fluorescent lamp fixtures; SC-C-33033-4; 80063	1,2,3	ea	5	2	2	2	2	2	2	27	15	
P-0 A039	4110-171-4506	CHAIN, BEAD: Connects cable reel holder to wall; 70892	1,2,3	ft	10	*	*	*	*	*	*	100		
P-0 A040	4010-729-5951	CHAIN, WELDLESS: (U/on bulletin board); F28434; 46344	1,2,3	in	14	*	*	*	*	*	*	140		
P-0 A042	5930-734-5202	CIRCUIT BREAKER: F/heater; 10172H34A; 17465	2,3	ea	1	*	2	2	*	2	2	12	5	4-5
P-0 A043	5925-682-1071	CIRCUIT BREAKER: 50 amps; Q0250; 88434	1,2,3	ea	1	2	2	2	*	2	2	19	10	4-5 CB7A, CB7B
P-0 A044	5925-613-4811	CIRCUIT BREAKER: 15 amps; Q0115; 88434	1,2,3	ea	6	2	3	4	2	2	2	46	30	4-13 CB1 thru CB6
P-0 A046	5950-815-6627	CIRCUIT BREAKER: 15 amps; Q01515; 88434	2,3	ea	4	2	2	3	2	2	2	33	20	4-13 CB1, CB2, CB5, CB6
P-0 A047	5935-682-1070	CLAMP, ELECTRICAL: XS-17; 09922	1,2,3	ea	3	2	2	2	*	2	2	10		
P-0 A048	5940-049-2791	CLIP, SPRING, TENSION: U/to retain tube extractor; 107002 Type XX; 75915	1,2,3	ea	2	*	2	2	*	2	2	6		
P-0 A049	5340-727-7646	CLIP, SPRING TENSION: Holds spare starters; 109002 type XX; 75915	1,2,3	ea	3	2	2	2	*	2	2	10		
P-0 A050	6645-973-0178	CLOCK, AIRCRAFT, MECHANICAL: SM-B-364759; 80063	1	ea	1	*	*	*	*	*	*	4	1	4-16
P-0 A051	6645-950-0179	CLOCK, AIRCRAFT, MECHANICAL: (Retain mtg bracket when replacing clock)	2,3	ea	1	*	*	*	*	*	*	4	1	4-16
P-0 A052	5935-359-6025	CONNECTOR, RECEPTACLE, ELECTRICAL: F/heater; Q010; 74545	1,2,3	ea	4	2	2	2	*	2	2	19	10	4-13 J35 thru J38
P-0 A053	5935-518-9653	CONNECTOR, PLUG, ELECTRICAL UP-120M	1,2,3	ea	1	*	*	2	*	*	*	8	3	
P-0 A054		CONNECTOR, PLUG, ELECTRICAL: U/with cable assy CX-4694A/U; SC-B-76446-2; 80063	1,2,3	ea	1	*	*	2	*	*	*	8	3	1-11
P-0 A055	5935-892-9176	CONNECTOR, PLUG, ELECTRICAL: U/with cable assy CX-4694A/U and CX-4693A/U; SC-B-76446-1; 80063	1,2,3	ea	2	*	2	2	*	2	2	13	6	1-11
P-0 A056	5935-549-3562	CONNECTOR, PLUG, ELECTRICAL: U/on conduit assy; 9200; 74545	1,2,3	ea	1	*	*	2	*	*	*	8	3	4-13 J40
P-0 A057	5935-537-4253	CONNECTOR, RECEPTACLE, ELECTRICAL: Power-in on power entrance box; SM-B-364595; 80063	1,2,3	ea	1	*	*	2	*	*	*	8	3	1-8 J34
P-0 A058	5935-666-4512	CONNECTOR, RECEPTACLE, ELECTRICAL: Power-out on power entrance box; SM-B-364594; 80063	1,2,3	ea	1	*	*	2	*	*	*	8	3	1-8 J33
P-0 A059	5935-045-9830	CONNECTOR, PLUG, ELECTRICAL U-185B/G	1,2,3	ea	2	*	2	2	*	2	2	13	6	
P-0 A060	5935-045-9831	CONNECTOR, RECEPTACLE, ELECTRICAL U-186/G, U-186A/G	1,2,3	ea	48	3	9	16	2	3	4	187	150	
P-0 A061	5935-926-7428	OR CONNECTOR, RECEPTACLE, ELECTRICAL U-186C/G	1,2,3	ea	48	3	9	16	2	3	4	187	150	

SECTION IV. REPAIR PARTS FOR DIRECT SUPPORT, GENERAL SUPPORT, AND DEPOT MAINTENANCE (CONTINUED)

(1) S&C CODE	(2) FEDERAL STOCK NUMBER	(3) DESCRIPTION	(4) USABLE ON CODE	(5) UNIT OF MEAS	(6) QTY INC IN UNIT	(8) 30-DAY DS MAINT ALLOWANCE			(7) 30-DAY GS MAINT ALLOWANCE			(8) 1 YR ALW PER EQUIP CATEGORY	(9) DEPOT MAINT ALW PER 100 EQUIP	(10) ILLUSTRATIONS	
						(a) 1-20	(b) 21-60	(c) 61-100	(a) 1-20	(b) 21-60	(c) 61-100			(a) FIG NO.	(b) ITEM NO. OR REFERENCE DESIGNATION
P-O A062	5120-694-1197	CONTACT, POSITIONER, ELECTRON TUBE, SOCKET: 7 pin contact; 5191; 72653	1,2	ea	1	*	*	*	*	*	*	4	1		
P-O A063	5120-293-0270	CONTACT POSITIONER, ELECTRON TUBE SOCKET: 9 pin contact; 8104; 72653	1,2	ea	1	*	*	*	*	*	*	4	1		
P-C A065	5995-668-5699	YORK ASSEMBLY, ELECTRICAL CX-4695/U; (5 ft 10 in)	1,2,3	ea	1	*	2	2	*	2	2	12	5	1-5	W11
P-O A066	4030-805-0068	COUPLING, BEAD CHAIN: 13A; 70892	1,2,3	ea	4	*	*	2	*	*	2		4		
P-O A067	5935-729-0778	COVER, ELECTRICAL CONNECTOR: TE-9176; 96097	1,2	ea	2	*	*	*	*	*	*	5	2		
P-O A070	5410-072-0992	CURTAIN, BLACKOUT: 51 in W X 63 in lg; SM-C-476682; 80063	1,2,3	ea	2	*	*	*	*	*	*		2	1-4	
P-F A073	6110-777-8526	DOOR ASSEMBLY: (Cover for panel entrance box); SM-D-478773; 80063	1,2,3	ea	1	*	*	*	*	*	*		1	1-1	
P-F A074	6110-776-4542	DOOR ASSEMBLY: (Cover for signal entrance box; #714068; 96344	1,2	ea	2	*	*	*	*	*	*		2	1-1	
P-F A075	5410-072-0991	DOOR ASSEMBLY: SM-D-478725; 80063	3	ea	2	*	*	*	*	*	*		2	1-1	
P-O A076	5935-642-0743	DUMMY PLUG, TELEPHONE: (Black); 165C 01401	1,2,3	ea	150	15	35	68	9	13	17	479	700	1-6	
P-O A077	5935-162-6285	DUMMY PLUG, TELEPHONE: (red); 165D; 01401	1,2,3	ea	75	8	20	38	5	8	10	460	400	1-6	
P-O A078	5935-775-2446	DUMMY PLUG: SM-B-370299; 80063	1,2,3	ea	36	3	9	16	2	3	4	187	150	1-6	
P-C A085	5120-293-3603	EXTRACTOR, ELECTRON TUBE: (7 pin miniature); 7113; 95344	1,2,3	ea	1	*	*	*	*	*	*	4	1	4-16	
P-C A086	5120-293-2592	EXTRACTOR, ELECTRON TUBE: (9 pin miniature); MO. 9113; 95344	1,2,3	ea	1	*	*	*	*	*	*	4	1	4-16	
P-O A096	5975-711-1856	GASKET: U/on duplex outlet; 585; 73586	1,2	ea	1	*	2	2	*	2	2		5		
P-O A098	5120-776-9918	GRIP, CABLE, MOVIE: (12 in lg) BQA268; 95344	1,2,3	ea	45	2	3	5	2	2	2	59	40	1-6	0510 thru 0554
P-O A099	5120-752-8899	GRIP, CABLE MOVIE: 8 in lg U/with CX-4693/U and CX-4694/U; BHR-9; 95344	1	ea	4	*	*	2	*	*	2	10	4		
P-O A100	5120-776-9917	GRIP, CABLE, MOVIE: 16 in lg BQA6-8P; 95344	1,2,3	ea	5	*	2	2	*	2	2	12	5	1-6	
P-O A101	5325-248-7104	GRIMMERT, RUBBER: P/O control tel line C-2894/PQ; 913; 75943	1,2,3	ea	1	*	*	2	*	*	2	10	4	1-13	W26
P-O A102	5120-293-4489	HANDER, RARE: (816 lead); QOG-H-86; 81349	1,2,3	ea	1	*	*	*	*	*	*	4	1	4-16	
P-O A103	5975-682-0519	HANDER, CABLE: (U/to retain cables to side of shelter); SM-B-363104; 80063	1,2,3	ea	2	2	2	2	*	2	2		8	1-6	
P-O A105	5820-706-7185	HEATING ELEMENT ELECTRICAL: U/v heater MD-375/U; A22/5007/1; 61325	1	ea	1	*	*	2	*	*	*	8	3	4-1	
P-O A106	4840-404- 9232	HEATING ELEMENT, ELECTRICAL: P/heater; 3994-0; 72143	2,3	ea	1	*	*	2	*	*	*	8	3	4-2	
P-O A109	3895-766-8473	HOLDER, CABLE REEL: Retains cable reel during transit; SM-B-363238; 80063	1,2,3	ea	2	*	*	*	*	*	*		2	1-4	
P-O A110	4140-765-7748	IMPELLER, FAN, AXIAL: P/o heater MD-375/U; OU-720-5; 60399	1	ea	1	*	*	*	*	*	*	4	1	4-1	
P-O A111	4520-792-8398	IMPELLER, FAN, AXIAL: 20; 60399	2,3	ea	1	*	*	*	*	*	*	4	1	4-2	
P-O A112	4140-069-1952	IMPELLER, FAN CENTRIFUGAL: P/exhaust blowers; 610-314-2; 60399	1,2	ea	2	*	*	*	*	*	*	5	2		

SECTION IV. REPAIR PARTS FOR DIRECT SUPPORT, GENERAL SUPPORT, AND DEPOT MAINTENANCE (CONTINUED)

(1) P/N CODE	(2) FEDERAL STOCK NUMBER	(3) DESCRIPTION REFERENCE NUMBER & MFR. CODE	(4) UNIT OF MEAS	(5) QTY INC IN UNIT	(6) 30-DAY DS MAINT ALLOWANCE			(7) 30-DAY GS MAINT ALLOWANCE			(8) 1 YR ALW PER EQUIP CATGY	(9) DEPOT MAINT ALW PER EQUIP CATGY	(10) ILLUSTRATIONS	
					(a) 1-20	(b) 21-50	(c) 51-100	(a) 1-20	(b) 21-50	(c) 51-100			(a) FIG NO.	(b) ITEM NO. ON REFERENCE DESIGNATION
P-0 A113	4140-073-3240	IMPELLER, FAN, CENTRIFUGAL: A16353; 80339	EA	2	*	*	*	*	*	*	5	2		
P-0 A114	4935-577-0770	JACK, TELEPHONE: 02-024; 81349	EA	40	1	2	16	1	2	4	187	150		
P-0 A115	4935-283-1263	JACK, TELEPHONE: 02-014; 81349	EA	2	*	2	2	*	2	2	13	5		
P-0 A117	4935-228-4038	JACK, TELEPHONE: 02-085; 81349	EA	1203	75	177	144	44	66	87	4169	4000		
P-0 A118	4935-192-4820	JACK, TELEPHONE: 02-086; 81349	EA	1207	75	177	144	44	66		4,159	4000		
P-0 A119	5355-082-0806	KNOB: On-off knob on heater; Mold type 1600; 72512	EA	1	*	*	*	*	*	*		1	4-1	
P-0 A120	2540-946-9463	LADDER, VEHICLE BOARDING MX-1543; 31-30-01-14-1180; P-003	EA	1	*	*	*	*	*	*	4	1	4-16	
P-0 A121	6240-524-9447	LAMP, FLUORESCENT: FROTH LAMP, 24455	EA	5	5	14	15	4	6	8	197	150	4-6	DS1 thru DS12
P-0 A122	6240-223-9134	LAMP, GLOW: NE-51; 81349	EA	6	1	2	14	4	6	7	71	50	1-7	DS1 thru DS6
P-0 A123	6240-223-9134	LAMP, GLOW: NE-51; 81349	EA	1	2	3	6	2	3	4	71	50	1-7	DS1
P-0 A124	6240-223-9134	LAMP, GLOW: NE-51; 81349	EA	1	2	3	6	2	3	4	71	50	1-7	DS13
P-0 A126	6240-143-3070	LAMP, INCANDESCENT 50A; 80; 24455	EA	1	2	3	6	2	3	4	71	50	1-7	
P-0 A127	6240-155-7796	LAMP, INCANDESCENT: PR-2; 24455	EA	1	2	3	6	2	3	4	71	50	1-7	
P-0 A130	6250-682-3461	LAMPHOLDER: holds indicator glow lamp; 16-06; 72794	EA	6	2	3	4	2	2	2	46	40	4-5	DS1 thru DS4
P-0 A131	6250-299-6094	LAMPHOLDER: F fluorescent lamp; 78X491; 24455	EA	5	2	2	4	2	2	2	40	15	4-6	
P-0 A132	6250-174-4684	LAMPHOLDER: F fluorescent lamp and starter; 78X736; 24455	EA	5	2	2	4	2	2	2	40	15	4-6	
P-0 A133	6210-722-3781	LIGHT INDICATOR (F/NEON LAMP) MS-0027-10 81349	EA	1	*	2	2	*	2	2	12	5		
P-0 A134	6250-682-3461	LAMPHOLDER: (porcelain); 746; 73586	EA	1	*	2	2	*	2	2	12	5		DS1
P-0 A135	6230-803-7063	LAMP, ELECTRIC: 16 V; 2136-7; 32572	EA	1	*	*	*	*	*	*	4	1	4-16	
P-0 A136	5410-752-2525	LEAD, ELECTRICAL: (P grounding) SW-B-352; 560; 80063	EA	1	*	*	*	*	*	*	5	2	1-6	
P-0 A137	6230-615-5384	LIGHT, EXTENSION: (25 ft) W-1-661; Type 1; Class 1; 81349	EA	1	*	*	2	*	*	*	2	3	1-6	
P-0 A138		LOCKSPRING, TURNLOCK FASTENER: U/on ventilator covers, 35-225; 72794	EA	2	*	2	2	*	2	2		6		
P-0 A139	5325-290-4345	LOCKSPRING, TURNLOCK FASTENER: U/on distribution box terminal box, air filter covers and storage cabinet; 36-275; 72794	EA	8	2	2	3	2	2	2		25		
P-0 A140	5325-285-3371	LOCKSPRING, TURNLOCK FASTENER: U/on holder for axe, hammer and, 54-225; 72794	EA	7	2	2	3	2	2	2		20		
P-0 A141	6105-561-6321	MOTOR, AC: (P/o exhaust blower) AB26540; 16748	EA	2	*	*	2	*	*	2	10	4	1-14	B1, Bc
P-0 A142	6105-726-8684	MOTOR, AC: 5KBP51A240; 24455	EA	1	*	*	*	*	*	*	5	2	4-1	B3
P-0 A143	5915-803-8110	NETWORK, HYBRID, CIRCUIT: SW-C-364673; 80063	EA	12	2	2	2	*	2	2	19	10	1-3	

SECTION IV. REPAIR PARTS FOR DIRECT SUPPORT, GENERAL SUPPORT, AND DEPOT MAINTENANCE (CONTINUED)

(1) SIC CODE	(2) FEDERAL STOCK NUMBER	(3) DESCRIPTION		(4) UNIT OF MEAS	(5) QTY INC IN UNIT	(6) 30-DAY GS MAINT ALLOWANCE			(7) 30-DAY GS MAINT ALLOWANCE			(8) 1 YR ALW PER EQUIP CMTGY	(9) DEPOT MAINT ALW PER 100 EQUIP	(10) ILLUSTRATIONS	
		REFERENCE NUMBER & MFR. CODE	USABLE ON CODE			(a) 1-20	(b) 21-50	(c) 51-100	(a) 1-20	(b) 21-50	(c) 51-100			(a) FIG NO.	(b) ITEM NO. OR REFERENCE DESIGNATION
P-0 A178	5930-615-7896	SWITCH, TOGGLE; MS25098-22; 81349	1,2,3	ea	1	*	2	2	*	2	2	12	5		
P-0 A184	5940-702-7256	TERMINAL LUG; KP125/W; 09922	1,2,3	ea	4	*	*	3	2	2	2		20		
P-0 A185	5940-681-9607	TERMINAL STUD: F/grounding; SM-B-363337; 85063	1,2,3	ea	1	*	*	*	*	*	*	4	1		
P-0 A187	5950-892-8224	TRANSFORMER, CURRENT: (w/with ammeter); 1643; 93993	1,2,3	ea	1	*	*	2	*	*	*	8	1	4-5	T.
P-0 A188	5625-883-4272	VOLTMETER: MR36W150ACVTR; 81349	1,2,3	ea	1	*	*	2	*	*	2	10	4	4-5	M.

SECTION V. INDEX-FEDERAL STOCK NUMBER CROSS REFERENCE
TO INDEX NUMBER

FEDERAL STOCK NUMBER	INDEX NO.	FEDERAL STOCK NUMBER	INDEX NO.	FEDERAL STOCK NUMBER	INDEX NO.
2540-846-8483	A120	5820-706-7185	A105	5935-729-0778	A067
3895-766-8473	A109	5905-581-0098	A155	5935-775-7446	A078
4010-171-4506	A039	5905-583-5207	A154	5935-00-246-4515	A054
4010-729-5951	A040	5905-801-8634	A156	5935-00-168-1345	A055
4030-005-0068	A066	5905-803-2908	A153	5935-927-7428	A061
4140-069-1952	A112	5910-553-6096	A038	5940-049-8791	A046
4140-073-3246	A113	5915-803-8110	A143	5940-254-2244	A037
4140-765-7748	A110	5925-682-1071	A043	5940-254-2244	A037
4210-727-8111	A007	5925-818-4811	A044	5940-702-7256	A164
4340-404-0232	A106	5930-504-3923	A176	5940-802-3771	A166
4520-792-8398	A111	5930-615-7896	A178	5950-815-6687	A046
5120-251-4489	A102	5930-636-4014	A177	5950-892-8224	A187
5120-293-0270	A063	5930-669-7465	A172	5975-224-5260	A158
5120-293-2692	A086	5930-682-0349	A174	5975-682-0451	A015
5120-293-3603	A085	5930-705-9131	A171	5975-682-0461	A013
5120-694-1197	A062	5930-707-1313	A175	5975-682-0477	A148
5120-752-8859	A099	5930-729-1706	A170	5975-682-0519	A103
5120-775-9917	A100	5930-729-1709	A169	5975-688-4625	A014
5120-775-9918	A098	5930-734-5202	A042	5975-702-9311	A036
5310-782-5535	A165	5935-045-9830	A059	5975-711-1857	A096
5315-844-5644	A146	5935-045-9831	A060	5995-681-8427	A022
5325-248-7104	A101	5935-162-6285	A077	5995-681-8429	A024
5325-285-3371	A140	5935-192-4826	A118	5995-681-8430	A025
5325-290-2898	A168	5935-228-4038	A117	5995-681-8436	A023
5325-290-4345	A139	5935-283-1269	A116	5995-681-8441	A020
5340-682-1508	A144	5935-359-6025	A052	5995-681-8448	A021
5340-727-7646	A049	5935-518-9653	A053	5995-681-8450	A030
5355-682-6806	A119	5935-537-4253	A057	5995-681-8472	A028
5410-072-0991	A075	5935-549-3562	A056	5995-681-8473	A027
5410-072-0992	A070	5935-577-8781	A115	5995-681-8474	A029
5410-752-2525	A136	5935-577-8804	A005	5995-681-8475	A026
5410-783-6250	A152	5935-642-0743	A076	5995-688-5699	A065
5805-542-7274	A001	5935-666-4512	A058	5995-985-7569	A016
		5935-682-1070	A047	6105-561-1321	A141
				6105-727-4684	A142

SECTION V. INDEX-FEDERAL STOCK NUMBER CROSS REFERENCE
TO INDEX NUMBER (CONTINUED)

FEDERAL STOCK NUMBER	INDEX NO.	FEDERAL STOCK NUMBER	INDEX NO.	FEDERAL STOCK NUMBER	INDEX NO.
6110-776-4542	A074				
6110-777-8526	A073				
6135-120-1020	A008				
6145-164-6948	A031				
6145-577-8480	A035				
6145-752-2473	A033				
6145-752-2562	A032				
6210-722-3781	A133				
6210-686-5568	A163				
6230-615-5384	A137				
6230-803-7063	A135				
6240-143-3070	A126				
6240-155-7786	A127				
6240-223-9100	A125				
6240-223-9104	A123				
6240-270-4286	A122				
6240-538-8447	A121				
6250-174-4684	A132				
6250-299-2884	A167				
6250-299-6093	A131				
6250-682-3462	A130				
6250-682-3463	A134				
6250-804-3449	A009				
6625-883-4272	A168				
6625-892-5325	A006				
6645-350-3590	A051				
6645-973-0178	A050				
6680-793-9575	A173				
8130-656-1090	A150				
REFERENCE NO. MFG'S PART NO.		INDEX NO.			
D-2738W		A117			
3-5-225		A135			

SECTION VI. INDEX-FIGURE AND ITEM NUMBER CROSS REFERENCE TO INDEX NUMBER

FIG. NO.	ITEM NO. OR REFERENCE DESIGNATION	INDEX NO.	FIG. NO.	ITEM NO. OR REFERENCE DESIGNATION	INDEX NO.
1-4	B1, B2	A141	4-13	CB1--1	A044
				CB1--2,3	A046
				CB2--1	A044
1-5	W10	A021		CB2--2,3	A046
	W11	A065		CB3--1	A044
	W12 thru	A026		CB3--2,3	A044
	W38			CB4--1	A044
	W39 thru	A022		CB4--2,3	A044
	W65			CB5--1	A044
	W66 thru	A027		CB5--2,3	A046
	W92			CB6--1	A044
	W93 thru	A028		CB6--2,3	A046
	W119			J35 thru	A052
	W120 thru	A023		J38	
	W146			J40	A056
	W147 thru	A024			
	W173				
	W174 thru	A029			
	W185				
	W186 thru	A025			
	W197				
	W198 thru	A030			
	W217				
	W218	A020			
1-6	O510 thru	A098			
	O554				
1-7	DS1 thru	A120			
	DS6				
	DS12	A123			
	DS13	A125			
1-8	J33	A050			
	J34	A052			
1-12	HR64	A101			
	S1	A170			
	S2	A169			
4-1	B3	A142			
	S12	A175			
4-5	CB7A,	A043			
	CB7B				
	M2	A006			
	M3	A158			
	R1 thru	A153			
	R5				
	T1	A187			
	XCS1 thru	A171			
	XDS6				
4-6	DS7 thru	A121			
	DS11				
4-9	R1	A154			
	R2	A155			
	R3	A156			
	R4	A157			

SECTION VII. INDEX-REFERENCE DESIGNATION CROSS REFERENCE
TO INDEX NUMBER

REFERENCE DESIGNATION	INDEX NO.	REFERENCE DESIGNATION	INDEX NO.	REFERENCE DESIGNATION	INDEX NO.
B1, B2	A141	T1	A187		
B3	A142	W10	A021		
CB1--1	A044	W11	A065		
CB1--2,3	A046	W12 thru W38	A026		
CB2--1	A044	W39 thru W65	A022		
CB2--2,3	A046	W66 thru W92	A027		
CB3--1	A044	W93 thru W119	A028		
CB3--2,3	A044	W120 thru W146	A023		
CB4--1	A044	W147 thru W173	A024		
CB4--2,3	A044	W174 thru W185	A029		
CB5--1	A044	W186 thru W197	A025		
CB5--2,3	A046	W198 thru W217	A030		
CB6--1	A044	W218	A020		
CB6--2,3	A046	XDS1 thru XDS6	A130		
CB7A, CB7B	A043	XDS12	A134		
CP1, CP2	A005				
DS1 thru DS6	A122				
DS7 thru DS11	A121				
DS12	A123				
DS13	A125				
H264	A101				
J33	A058				
J34	A057				
J35 thru J38	A052				
J40	A056				
M2	A006				
M3	A188				
OS10 thru OS54	A098				
R1 thru R6	A153				
S1	A177				
S2 thru S6	A177				
S6	A178				

By Order of the Secretary of the Army:

HAROLD K. JOHNSON,
General, United States Army,
Chief of Staff.

Official:

J. C. LAMBERT,
Major General, United States Army,
The Adjutant General.

Distribution:

Active Army:

USASA (2)	USAAMS (5)	7-52
CNGB (1)	USASTC (2)	11-5
CC-E (7)	USATC AD (2)	11-8
Dir of Trans (1)	USATC Armor (2)	11-15
Cof Engrs (1)	USATC Engr (2)	11-18
TSG (1)	USATC Inf (2)	11-35
Cof Spts (1)	WRAMC (1)	11-37
USACDCEA (1)	Army Pic Cen (2)	11-38
USACDCCBRA (1)	Instl (2) except	11-39
USACDCCEA (1)	Ft. Monmouth (70)	11-55
USACDCOA (1)	Ft. Hancock (4)	11-57
USACDCQMA (1)	Ft. Gordon (10)	11-58
USACDCTA (1)	Ft. Huachuca (10)	11-95
USACDCADA (1)	Ft. Carson (25)	11-97
USACDCARMA (1)	WSMR (50)	11-98
USACDCAVNA (1)	GENDEP (2)	11-117
USACDCARYTA (1)	Sig Sec GENDEP (5)	11-137
USACDCSWA (1)	Sig Dep (12)	11-155
USACDCCEA:	USASETAF (5)	11-157
Ft. Huachuca (1)	A Dep (2) except	11-215
USAMC (5)	SAAD (30)	11-217
USCONARC (5)	TOAD (14)	11-237
ARADCOM (5)	FTWOAD (10)	11-337
ARADCOM Rgn (2)	LEAD (7)	11-500 (AA-AE) (4)
OS Maj Comd (4)	SHAD (3)	11-555
LOGCOMD (2)	NAAD (5)	11-557
USAMICOM (4)	SVAD (5)	11-558
USASMC (2)	CHAD (3)	11-587
USASCC (4)	ATAD (10)	11-592
MDW (1)	LBAD (14)	11-597
Armies (2) except	Sig Fld Maint Shops (2)	11-608
Seventh (5)	AMS (1)	17
Corps (2)	USAERDAA (2)	29-56
USAC (3)	USAERDAW (13)	37
11th Air Aslt Div (3)	Units org under fol TOE:	39-51
Svc Colleges (2)	(2 copies each UNOINDC)	54-2
Br Svc Sch (2) except	5-600	57
USASCS (25)	5-605	54-102
USASESCS (100)	7	54-202

NG: State AG (3); units—same as Active Army except allowance is one copy to each unit.

USAR: None.

For explanation of abbreviations used, see AR 320-50.

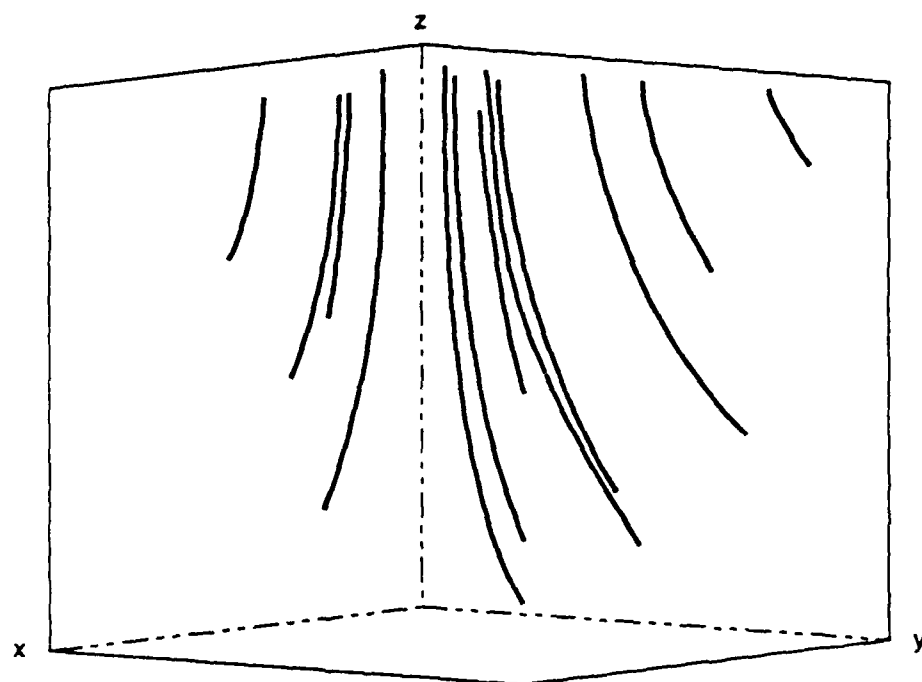


Figure 14

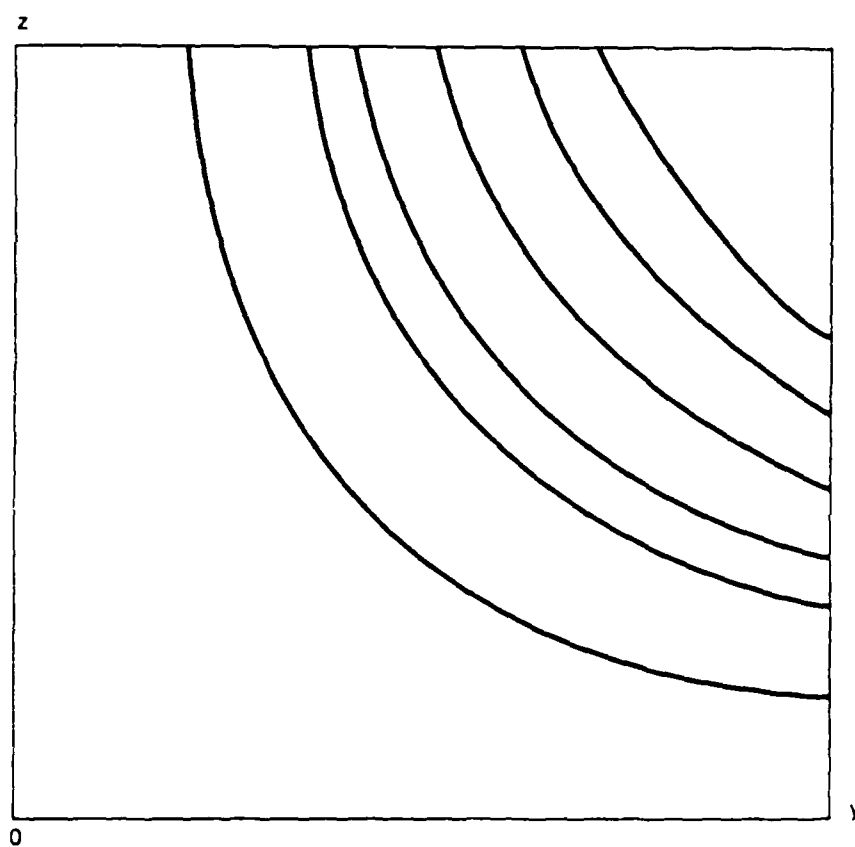


Figure 15

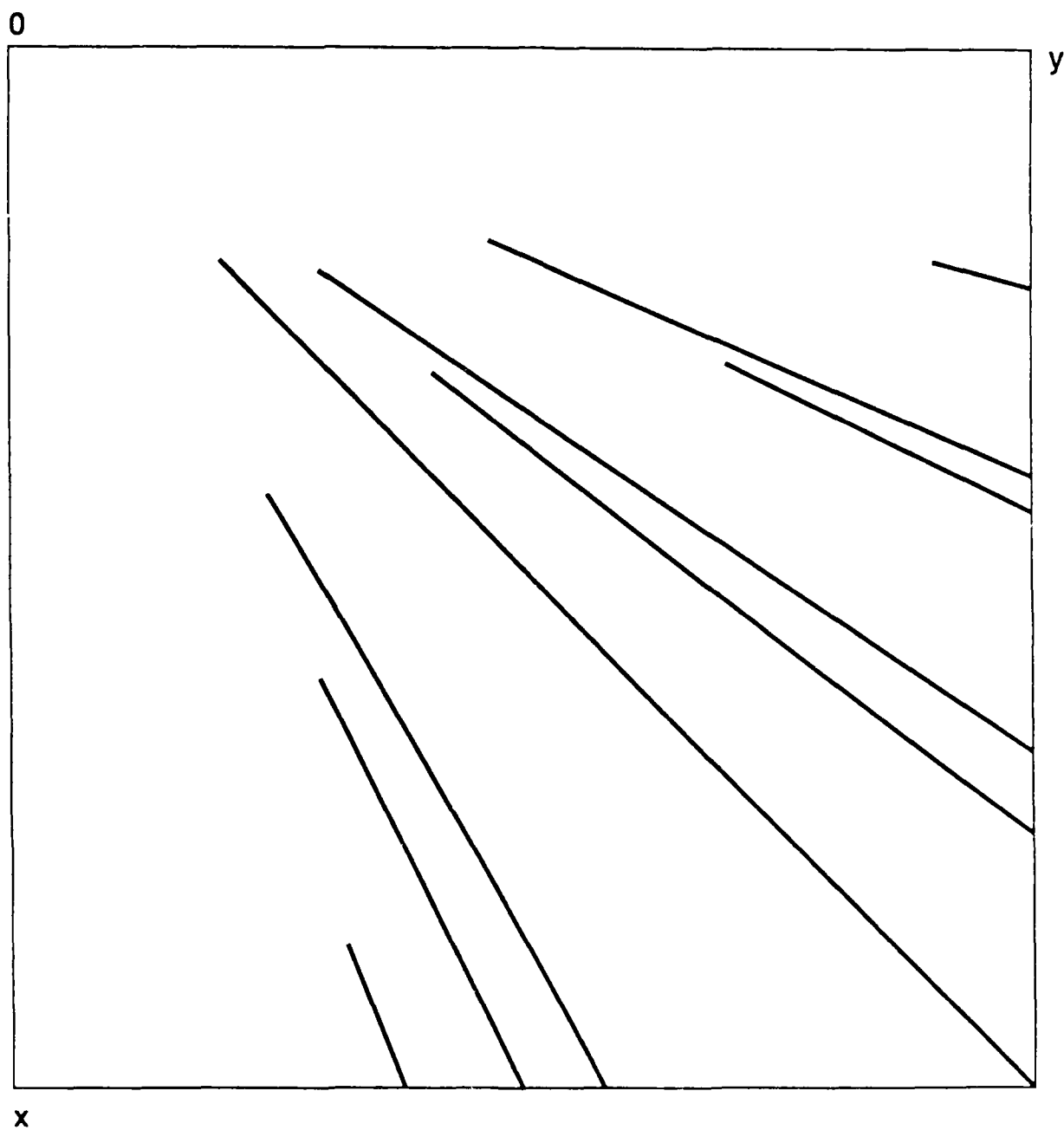


Figure 16

Chapter G

Algorithm development for three-dimensional second order turbulence model computations of flow over terrain

Prepared by
J.L. Lumley and P. Mansfield

We would like to construct and implement a numerical algorithm capable of solving rather general evolution equations on a finite three dimensional volume. Our interests in particular include applications to meteorological turbulent boundary layer problems in which wind shear, surface heating, and water vapor transport all appear. We have in the past implemented a one dimensional algorithm in which spatial homogeneity is assumed in the x and y directions; we now remove this assumption, with the ultimate goal of considering the domain to be the volume above a varied-terrain patch of the earth's surface.

The particular equations we wish to solve are derived from a second-order closure of the full three dimensional Navier-Stokes equations; see <1> for a full listing of the 21 equations of interest. The solution of these equations in 3-D presents a formidable task even for present-day large-scale computers. Here at Cornell there is an on-going movement towards parallel processing; in this spirit we have developed an algorithm (the "hopscotch process"; see below) which should prove compatible with parallel architecture as it becomes available - this parallelism appears in our method in two distinct manners.

The first aspect of parallelism to be exploited is the fact that each of our 21 equations can be solved (for one time step) independently of all the rest. While 21 simultaneous processes does not take full advantage of the several hundred (thousand?) processors envisioned for Cornell's experimental supercomputer, nevertheless there is no reason to ignore any possible advantages; any additional "bookkeeping" that comes with parallel processing should be more than compensated for by this (rather low) level of parallelism.

The more important aspect of our algorithm that exploits a parallel architecture is its "grid-point near-independence." Unlike our 1-D algorithm, which required in the calculation of third moments the inversion of a tri-diagonal matrix across the entire grid, our new (3-D) algorithm uses known values only at neighboring points in its time advancement. There is an uncertainty here - thinking as we are of each processor representing a (physical space) grid point, it is not yet clear whether our (minimal) shared memory requirements across "adjacent" processors will be met by the experimental machine - in any case, if a suitable computer does appear, our algorithm will be easily adaptable to it. If implemented, this level of parallelism will afford a most significant reduction in real-time calculation.

In preparation for the full 3-D algorithm, we have modified our existing 1-D code so that the integration subroutine incorporates the hopscotch process. We found the resulting profiles of the dependent variables to be substantially similar to those calculated by our former method, with a corresponding reduction in computer time needed of about 30% (in higher dimensions, we will obtain a larger savings). We have recently constructed

a 3-D hopscotch algorithm and tested it for very simple equations, building the numerical code in a modular fashion so that the desired future implementation of the full 21 equations is as straight-forward as possible; additionally, the passage to a fully parallel machine should not be too difficult. Because the integration technique plays a central role in our development we present a detailed description of it.

The algorithm we are using is based upon the so called "hopscotch process" outlined by Gourlay in <2>. Little attention is given in that article to the implementation of boundary conditions; we take care here to describe our particular implementation, diagramming the technique in two spatial dimensions - the passage to three is straight-forward.

Here is a brief overview:

The algorithm consists of two sweeps of the spatial grid for each time step (the fact that there are two sweeps is independent of spatial dimension). The first sweep is an explicit integration of the equation at every other grid point. Once this sweep is complete, the new values of the dependent variable are used to evaluate spatial derivatives at the other set of grid points. This evaluation is followed by (what is now) an implicit time integration on this set. For the following time step, the roles of the two sets of grid points are reversed. As Gourlay points out, "the algorithm is referred to as the 'hopscotch' process because its progress through the space-time grid resembles this game."

We now present further details, paying particular attention to the handling of boundary conditions.

Assume for the moment that the equation we wish to solve takes the simple form:

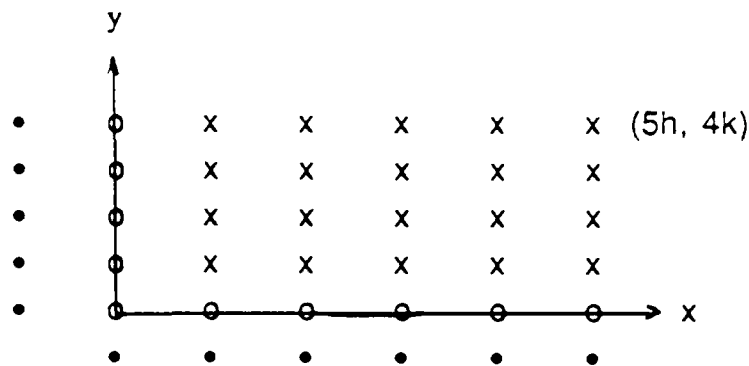
$$(1) \quad \frac{\partial U}{\partial t} = \kappa \left(\frac{\partial^2 U}{\partial x^2} + \frac{\partial^2 U}{\partial y^2} \right) + g(x,y,t)$$

Assume further that the solution is required on a rectangular region R for time $0 \leq t \leq T$. $g = g(x,y,t)$ is given, as is the initial condition $U(x,y,0)$. The boundary conditions are taken to have the form

$$(2) \quad A(x,y) \frac{\partial U}{\partial n}(x,y) + B(x,y) U(x,y) = C(x,y)$$

where $\partial U / \partial n$ is the normal derivative of U . A , B , and C are known functions of position (and time, if desired).

Let us take the rectangular region R to be the set of points enclosed by the x -axis, the y -axis, and the two lines $x = XL$, $y = YL$. We superimpose a grid on R partially consisting of the points (ih, jk) , where $i = 0, 1, 2, \dots, XL/h$, and $j = 0, 1, 2, \dots, YL/k$. There is an additional set of "helper" or "auxiliary" grid points needed just outside the region R ; without loss of generality we diagram the choice of grid near the origin - in this diagram x denotes an interior grid point, o a boundary point, and \bullet an auxiliary point.



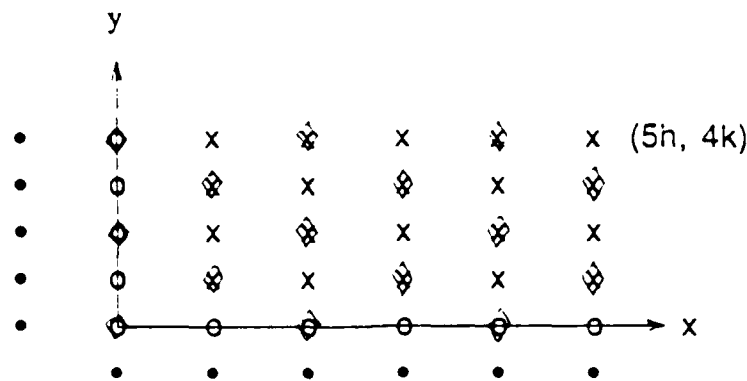
The point $(-h, -k)$ is NOT part of the grid.

Assume that the dependent variable U is known at time step n at all grid points. We proceed with the first (spatial) sweep to find U at time step $n+1$, the time step being Δt . For convenience, let $U^n(i, j) = U$ at (ih, jk) at time $n \Delta t$.

(1) For interior and boundary points (ih, jk) with $i + j$ even we use the forward in time, centered in space form of (1):

$$\begin{aligned}
 U^{n+1}(i, j) = & U^n(i, j) + \Delta t \bullet [\\
 (3) \quad & \kappa \left\{ \frac{U^n(i+1, j) + U^n(i-1, j) - 2U^n(i, j)}{h^2} + \frac{(U^n(i, j+1) + U^n(i, j-1) - 2U^n(i, j))}{k^2} \right\} \\
 & + g^n(i, j)]
 \end{aligned}$$

Superimposing a \diamond over those grid points at which U at time step $n + 1$ is now known, we have



To complete the first sweep, we must obtain U for time step $n + 1$ at those auxiliary points for which $i + j$ is even; to do so, we apply the boundary conditions at those boundary points for which $i + j$ is ODD. Furthermore, we use centered approximations, so that for example on the x-axis (where $j = 0$) the equation

$$A \frac{\partial u}{\partial y} + BU = C$$

becomes:

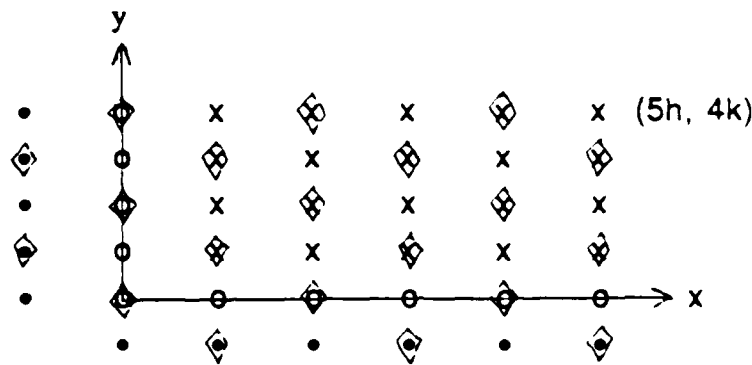
$$A(i,0) * \left\{ \frac{U^{n+1}(i,1) - U^{n+1}(i,-1)}{2k} \right\} + B(i,0) * \left\{ \frac{U^{n+1}(i-1,0) + U^{n+1}(i,1) + U^{n+1}(i+1,0) + U^{n+1}(i,-1)}{4} \right\} = C(i,0)$$

(4) $1-j$ odd i.e. i odd ($j=0$). (To evaluate $U^{n+1}(i,-1)$).

(Observe that the up-dated values of U are used.)

We can readily solve this equation for the only unknown, $U^{n+1}(i,-1)$.

The first sweep is now complete - we have obtained U for time step $n + 1$ at ALL grid points for which $i + j$ is even:



Second sweep:

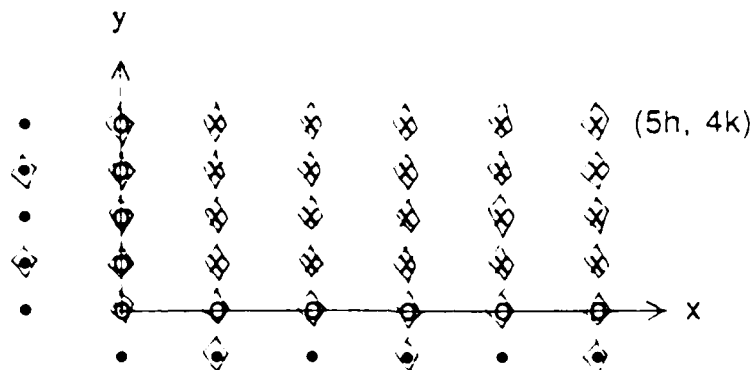
We are now ready to evaluate U at those interior and boundary points for which $i + j$ is odd; this time, instead of evaluating the right hand side of (1) at time step n , we evaluate it at time step $n + 1$:

$$(5) \quad \frac{U^{n+1}(i,j) - U^n(i,j)}{\Delta t} = \kappa \left\{ \frac{U^{n+1}(i+1,j) + U^{n+1}(i-1,j) - 2U^{n+1}(i,j)}{h^2} \right. \\ \left. + \frac{U^{n+1}(i,j+1) + U^{n+1}(i,j-1) - 2U^{n+1}(i,j)}{k^2} \right\} + g^{n+1}(i,j)$$

Solving this equation for $U^{n+1}(i,j)$ yields

$$(6) \quad U^{n+1}(i,j) = \left[U^n(i,j) + \kappa \Delta t \left\{ \frac{1}{h^2} (U^{n+1}(i+1,j) + U^{n+1}(i-1,j)) \right. \right. \\ \left. \left. + \frac{1}{k^2} (U^{n+1}(i,j+1) + U^{n+1}(i,j-1)) \right\} + \Delta t g^{n+1}(i,j) \right] / \\ \left[1 + 2 \kappa \Delta t \left(\frac{1}{h^2} + \frac{1}{k^2} \right) \right]$$

We have now obtained U for time step $n + 1$ at all of the points marked \diamond :



We find U at the remaining auxiliary points by applying the boundary conditions at the neighboring boundary points - we note that to find $U^{n+1}(-1,0)$, the boundary condition along the edge $x = 0$ is applied at $(0,0)$, and that to find $U^{n+1}(0,-1)$, the boundary condition along the edge $y = 0$ is applied at the same point $(0,0)$.

U at time step $n + 1$ is now completely specified. The procedure to find U at time step $n + 2$ is exactly the same, except that the roles of the "even" and "odd" grids are interchanged; the first sweep updates U (explicitly) at those points (i,j) for which $i + j$ is odd, etc.

Some observations:

- (1) At the interior points, we alternatingly use both explicit and implicit calculations.
- (2) At boundary points, we alternatingly apply the evolution equation and the boundary conditions.
- (3) The application of a boundary condition at a boundary point is used to obtain the value of U at the neighboring auxiliary point.

We note here that we have only written the algorithm for linear equations, a restriction which allows the implicit formula (6) to be obtained exactly. In the case of non-linear evolution equations, we have two options available to us in the calculation of the second sweep values - we can either numerically (approximately) solve the analogue to (5), or else we can replace the non-linear terms by centered approximations, e.g. $(U^{n+1}(i,j))^{**2}$ becomes

$$(7) \quad (U^{n+1}(i,j))^2 \rightarrow \left\{ \frac{1}{4} (U^{n+1}(i+1,j) + U^{n+1}(i-1,j) + U^{n+1}(i,j+1) + U^{n+1}(i,j-1)) \right\}^2$$

(all of the terms in this replacement would already be known from the first sweep.) This second option appears more attractive because it is analogous to the use of centered approximations used in the evaluation of boundary conditions (4); additionally, it should prove to be computationally less expensive.

The implementation of the 3-D algorithm for the simple forced heat equation is complete. Physically meaningful results have been obtained for a variety of both initial and boundary conditions. In the last paragraphs of this report we describe our current method of extracting and viewing any calculated scalar fields.

In keeping with our efforts to maintain at all times a modularized, flexible approach to code implementation, we output at desired intervals the full set of scalar fields. While this places some burden upon our physical computer memory, it has the following significant advantage: once a particular run has been made, a separate post-processing program is executed to analyze the results; the inputs to this post-processor include which variable is to be viewed, together with the particular slice on which the field's values are desired. An example might be "the values of the temperature at time t_1 on the plane $z = z_1$." An NCAR plotting subroutine is then called, outputting these temperature values on IMAP's 5080 terminals. Because the full 3-D output is available we can make further inquiries as desired through the post-processor.

It is of course our desire to have graphics output available in real-time, as the calculation is being performed, rather than having to wait until a particular run is complete. While we have yet to implement such capability, there is the prospect of eventually obtaining it as we begin to work with researchers of Cornell's Program of Computer Graphics: they have already completed some real-time graphics displays of simple dynamics and are expressly interested in moving towards the more challenging problems like the ones we have before us.

- (1) Lumley, J.L., and Mansfield, P.J. "Second order Modeling of Turbulent Transport in the Surface Mixed Layer", Boundary-Layer Meteorology 30 (1984) 139-142.
- (2) Gourlay, A.R., "Hopscotch a Fast Second-order Partial Differential Equation Solver", Inst. Maths. Applies 6 (1970), 375-390.

Current Three-Dimensional Code

This section contains a description of our current three dimensional code. This code has been designed in a modular fashion so that it may be expanded and modified in a relatively straight-forward manner. Additionally, the particular numerical algorithm used (the "hopscotch method") has been chosen so that at a future date a parallel implementation will be possible as the required underlying hardware and operating system become available.

Most of the variables we use appear in many different locations throughout the program. Because of this, we have a separate file dedicated to declarations. This file, TCOM, is compiled with each of our subroutines through the INCLUDE statement written near the top of each subroutine. As we expand the number of variables, we need only declare them in TCOM. Upon re-compilation of the program, all subroutines contain knowledge of any new variables through the INCLUDE statement.

The main program is called TOP ("Three-d OPerational"). We begin our description with it.

The nature of the problems we are attacking often leads to the appearance of instabilities of unknown origin. Because of the expense and time required for each computer run, it is helpful to periodically output the values of all dependent variables. The user controls when this is done through IVAR, IJN, and IJS; a description of the algebra of these variables is included below. For each requested output time, TOP writes (in loops 401, 402, and 403) the information needed for a re-started run. This information is written on Tape 11 the first time, Tape 12 the second,..., Tape 15 the fifth, and then back to Tape 11 the sixth, Tape 12 the seventh, etc.

The first subroutine called by TOP is TINIT ("Three-d INITialization"). TINIT is a short subroutine, calling TREAD, TCALC, and TU.

TREAD ("Three-d READ") reads five records from TAPE 4: Record:

1. NGX, NGY, NGZ, XL, YL, ZL
The number of interior grid points in the X, Y, and Z directions, followed by the (non-dimensional) lengths of the rectangular volume over which the integration is to be performed.
2. DELT, MTOT
The time step ("delta t"), and the maximum number of time steps allowed.
3. APPA1, APPA2, APPA3
Kappa1, Kappa2, and Kappa3: heat coefficients; see section ***.
4. T1, T2, T3, T4, T5, T6
Currently not used.
5. IVAR, (IJS(I), IJN(I), I = 1, IVAR)
These variables instruct the program at which time steps output should be produced. IVAR is the number of pairs that must follow. For each IJS, IJN pair, output is written every IJS steps for IJN times. Example:
2 5 1 1 3 - output would be written at time steps 5, 6, 7, and 8.

TCALC constructs some often used integers such as NGXP1 ("NGX plus 1", etc.) and NGXP2 (= NGX+2). DELX, DELY, and DELZ ("delta x, delta y, and delta z") are calculated from XL and NGX, YL and NGY, and ZL and NGZ, respectively.

Additionally, so are

$$AL1 = DELT / (DELX*DELX)$$

$$AL2 = DELT / (DELY*DELY)$$

$$AL3 = DELT / (DELZ*DELZ)$$

Finally, a coordinate system, X, Y, Z is constructed; the indices are chosen so that the eight vortices of the rectangular solid region are given by (0,0,0), (NGXP1,0,0), (NGXP1, NGYP1, 0), (0,NGYP1, 0), (0, 0, NGZP1), (NGXP1, 0, NGZP1), (NGXP1, NGYP1, NGZP1), and (0, NGYP1, NGZP1). Additionally, we note that points just outside the region ("auxilliary points";) are needed; examples of these are (-1, 0, 0) and (3, 2, NGZP2).

TU is the last subroutine called by TINIT. The initial conditions for all dependent variables are written here, inside the 100, 101, and 102 DO loops, TU then calls SURFI.

SURFI is a long subroutine which contains the boundary conditions on each of the six surfaces of the rectangular solid for all of the dependent variables. Each of these boundary conditions takes the form

$$A(X) * (D U(X) / D N(X)) + B(X) = C(X) ;$$

here $D N$ denotes the derivative in the direction normal to the surface.

It should be appreciated that there are six distinct surfaces, each a rectangle, on which boundary conditions of the form above must be specified. For convenience, we label these rectangles as follows:

Plane	Label
$z=0$	1
$y=0$	2
$x=XL$	3
$y=YL$	4
$x=0$	5
$z=ZL$	6

For each of our (arbitrarily) N variables, we are required to specify three functions (A , B , and C) on each of six surfaces, so that a total of 18 surface functions are needed for each and every dependent variable. These are specified in SURFI in the following way: there are three sets of double DO loops, and each set is dedicated to two of the six planes in which x , y , or z is fixed. As an example, the 101, 102 DO loop pair contains A , B , and C on the two planes 1 and 6, i.e. the planes $z=0$ and $z=ZL$. Let us concentrate on the specification for plane 6. The function A for the first dependent variable on this plane is $A6301$; here the 6 is for plane 6, the 3 is an aid to remind us that it is the third (z) direction that is normal to this plane, and the 01 is for the first dependent variable. In a similar vein, B and C for the first variable on plane 6 are $B601$ and $C601$, respectively.

To be sure, we demonstrate another example: in DO loop pair 103, 104, we might have $A4203 = 1.$, $B403 = \sin(3. * \pi * X(I)) * \sin(\pi * Z(I))$, and $C403 = 2.$; these inputs say that on the fourth plane ($y=YL$), the boundary condition for the third dependent variable $U3$ is given by $D U3 / D Y + U3 * \sin(3*\pi*X) * \sin(\pi*Z) = 2.$

This completes our description of SURFI, and hence of TU and TINT. We can now return to the main program TOP.

A prompt is now made to the user's screen asking for the value of ICONT - if 0 is entered, the program is configured to begin a new run; if 1, the user is indicating that a re-started run is desired. Subroutine FILL is called in either case, and is entered if a re-started run has been initiated.

Subroutine FILL is straight-forward - it queries the user (on his screen) for the number of the tape to be read, and then reads from that tape as it was previously written (by TOP) in the run to be re-started. FILL reads the FIRST set of fields on the designated tape, so that it is up to the user to have previously edited this tape if a set of output fields for more than one time have been written on it. Control is now returned to TOP.

The program has now been prepared and initiated for the time integration. Before it is begun, however, a call is made to TOUTR. This subroutine is essentially a diagnostic aid, and is often modified. It is used to output any desired segments of the calculated fields, adjunct variables, etc., for de-bugging purposes.

TOP is now ready to begin the time integration.

The sizes of the three outer DO loops in TOP (99, 100, 101) are specified by the output time control variables IVAR, IJN, and IJS. The innermost DO loop, 200, performs the time integration for each of the N dependent variables. In this loop, three subroutines are called - LOADIN, TINT, and LOADOU, each with the argument specifying which dependent variable is being integrated.

TINT (Three-d INTegration) contains the general numerical integration scheme detailed in the preceding section. The dependent variable in TINT is labeled U; in order to enter TINT, we must therefore load the dependent variable being integrated (one of U1, U2, ..., UN) into U, as well as all necessary boundary conditions - these tasks are accomplished in LOADIN.

Subroutine LOADIN is thus called for the i th time just before the integration of the i th variable. The loading of U_i and the corresponding boundary conditions is performed by four sets of DO loops, the first set for U_i and the next three sets for the boundary conditions. The set of three nested loops for U_i itself is straight forward. In the case of a (double) loop for a boundary condition, the precedure is as follows: recall that variables like A2403, B203, and C203 were initially specified in SURFI. These are down loaded (here $i = 3$) in LOADIN into the general forms A24, B2, and C2, respectively. After all six sets of boundary conditions (for $i = 3$) are loaded, LOADIN's task is complete, and control is returned to TOP.

TOP now makes a call to the heart of the program, TINT ("Three-d INTe-gration"):

TINT is a long subroutine which performs one complete time step march, using the 'hopscotch' method, of the general equation and its accompanying boundary conditions as specified in the preceding section. An understanding of the preceding section and of the hopscotch method should be sufficient to understand the (rather dense) code contained in TINT.

After TINT is executed, control is returned to TOP and the resulting field (U_i) is out-loaded in subroutine LOADOU into the particular variable being integrated - U_1 or U_2 or U_3 , etc.

Upon completion of the inner-most (200) DO loop in TOP, all of the dependent variables have been integrated. A call is then made to subroutine TRR in which the new values of the dependent variables are loaded into what now becomes their present values.

This completes the description of TOP and its associated subroutines.

The above section included a description of how program TOP outputs (at time intervals set by the user through IVAR, IJS, and IJN) the complete three dimensional fields of all dependent variables. These outputted fields can be used, as described above to re-start a given run. Additionally, through the use of a post-processor, TDPILOT, we may graphically view these 3-D fields. This section details the use of TDPILOT.

The essence of TDPLLOT is a call to the NCAR subroutine SRFACE. We assume here that the user has this NCAR routine available.

SRFACE plots functions of the form $Z = F(X,Y)$. Now our fields take the form $W = G(X,Y,Z)$. Therefore, in order to view them, it is necessary to slice our rectangular solid with a plane, and then examine W on this restricted, two dimensional surface. To keep matters relatively, simple, we require that the plane on which we desire to view W be normal to one of the axes X , Y , or Z .

TDPLLOT queries the user on this console for two integers, LX and LXV . LX must take the value 1, 2, or 3, depending upon the user's choice of cutting plane normal to the X , Y , or Z axis. For example, $LX = 2$, $LXV = 5$ instructs TDPLLOT to output the values of the desired field on the plane $y = 5$.

The exec which runs TDPLLOT, TDPLLOT EXEC, includes the line:

EXEC NCARPLOT SRFACE PLOT.

Thus, once the user enters LX and LXV , the desired plot is automatically generated and sent to his display device.

END
10-87
DTIC